Neutron Scattering Principal Investigators' Meeting

July 22-25, 2012

Gaithersburg Marriott Washingtonian Center

Gaithersburg, Maryland

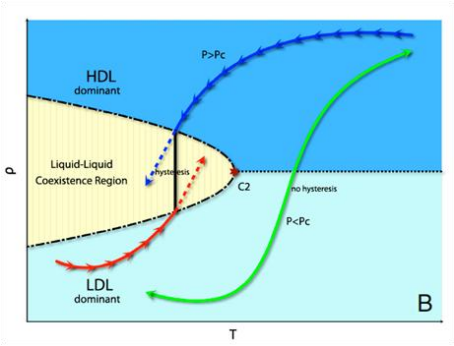

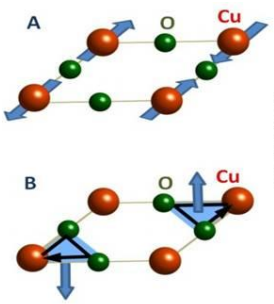

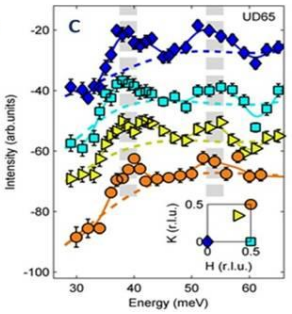

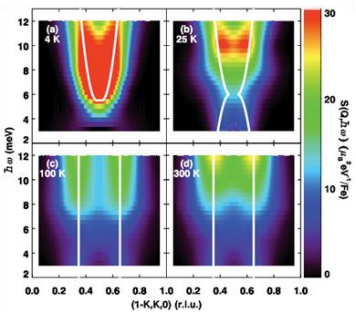

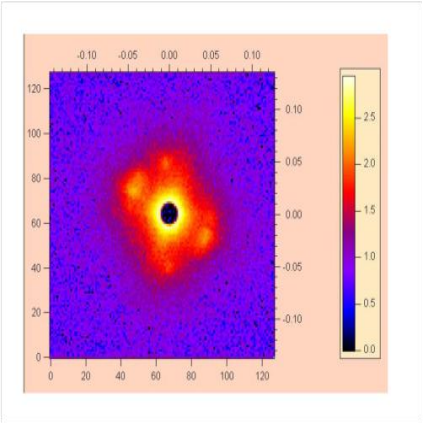

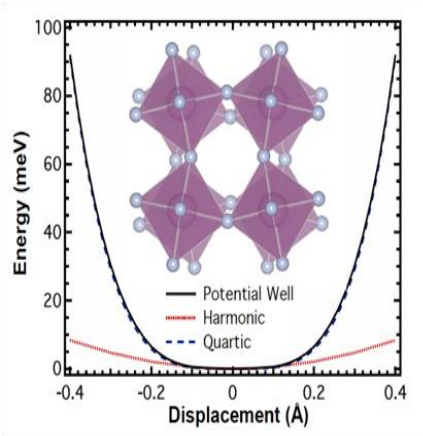

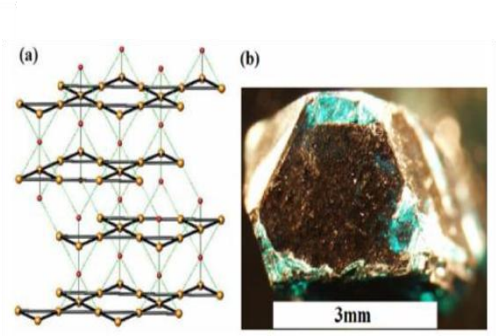

Office of Basic Energy Sciences
Division of Materials Sciences and Engineering

U.S. DEPARTMENT OF ENERGY | Office of Science

On the Cover

Top Left: Predicted density vs. temperature phase diagram of supercooled water in the presence of a first-order high density liquid (HDL) to low density liquid (LDL) phase transition based on the measured densities of confined water at high pressures during heating (the red curve connecting the points) and cooling (the blue curve connecting the points) cycles. The presence of significant hysteresis at high pressures in the measured densities during heating and cooling scans when crossing the transition line points to the putative first order liquid-liquid transition. However, at relatively low pressures, when no first-order line is crossed, there should be no hysteresis as shown with the green curve.
(Yang Zhang, Antonio Faraone, W. A. Kamitakahara, Kao-Hsiang Liu, Chung-Yuan Mou, Juscelino B. Leão, Sung Chang, and Sow-Hsin Chen, *Density hysteresis of heavy water confined in a nanoporous silica matrix*, Proc. National Academy of Sciences, **2011**, 108, 12206)

Top Middle: A) The fundamental building block of the copper-oxide superconductors is the Cu-O sheet. The well-studied conventional magnetism results from localized spin moments on the Cu atoms. B) Proposed novel magnetism due to circulating charge currents. C) Intensity of scattered neutrons at four wave vectors for the model material $HgBa_2CuO_{4+\delta}$. Two magnetic excitations (waves) can be discerned, one at about 40 meV and another at about 55 meV.
(Yuan Li, G. Yu, M. K. Chan, V. Balédent, Yangmu Li, N. Bariši´c, X. Zhao, K. Hradil, R. A. Mole, Y. Sidis, P. Steffens, P. Bourges, and M. Greven, Nature Physics, **2012**, 8, 404–410)

Top Right: The spectrum of low-energy magnetic excitations in an Fe-based superconductor is found to evolve in an unusual way. Contour intensity maps showing the fitted magnetic scattering intensity versus $\hbar\omega$ and Q at different temperatures for the superconducting FeTe0.35Se0.65: (a) 4 K, (b) 25 K, (c) 100 K, and (d) 300 K. The change in the distribution of spectral weight between 4 K and 25 K is due to the superconducting transition. The robust spectral weight at all temperatures cannot be explained by conduction electrons alone.
. (Zhijun Xu, Jinsheng Wen, Guangyong Xu, Songxue Chi, Wei Ku, Genda Gu, and J. M. Tranquada, Phys. Rev. B, **2011**, 84, 052506)

Bottom Left: Small-angle neutron scattering from a bulk sample of $Ni_{44}Co_6Mn_{40}Sn_{10}$, a precisely engineered off-stoichiometric Heusler alloy, showing the 2D q_x-q_y small angle scattering intensity map in a strained sample.
(Bhatti, El-Khatib, Srivastava, James, and Leighton, Phys. Rev. B, **2012**, 85, 134450)

Bottom Middle: Frozen phonon calculations evidencing that the most anomalous modes are quantum quartic oscillators, with transverse motions of fluorine atoms – a new mechanism for the negative thermal expansion coefficient of scandium fluoride.
(Chen W. Li, Xiaoli Tang, J. A. Muñoz, J. B. Keith, S. J. Tracy, D. L. Abernathy, and B. Fultz, Physical Review Letters, **2011**, 107, 195504)

Bottom Right: (a) Crystal structure of the ideal kagome lattice compound $ZnCu_3(OH)_6Cl_2$, also called herbertsmithite. (b) Single crystal synthesized for the magnetic measurements.
(T.H. Han, S. Chu, and Y.S. Lee, Physical Review Letters, **2012**, 108, 157202)

This document was produced under contract number DE-AC05-06OR23100 between the U.S. Department of Energy and Oak Ridge Associated Universities.

The research grants and contracts described in this document are supported by the U.S. DOE Office of Science, Office of Basic Energy Sciences, Materials Sciences and Engineering Division.

Foreword

This volume comprises the scientific content of the 2012 Neutron Scattering Principal Investigators' (PI) Meeting sponsored by the Division of Materials Sciences and Engineering (MSED) in the Office of Basic Energy Sciences (BES) of the U.S. Department of Energy (DOE). This meeting on July 22–25, 2012 at the Gaithersburg Marriott Washingtonian Center in Gaithersburg, Maryland, is the third in the series, covering the projects funded by the Neutron Scattering Program. BES MSED has a long tradition of supporting a comprehensive neutron scattering program in recognition of the high impact neutron scattering and spectroscopy tools have in discovery and use-inspired research.

The MSED Neutron Scattering Core Research Activity (CRA) supports basic research on the fundamental interactions of neutrons with matter to achieve an understanding of the atomic, electronic, and magnetic structures and excitations of materials and their relationship to materials' properties. Major emphasis is on the application of neutron scattering and spectroscopy for materials research, primarily at BES-supported user facilities. Development of next-generation instrumentation concepts, innovative optics for time-of-flight instruments and application of polarized neutrons are distinct aspects of this activity. The increasing complexity of DOE mission-relevant materials for various energy applications requires sophisticated scattering and computational tools to investigate the structure and dynamics at relevant length and time scales. Additionally, neutrons allow access to the behavior of matter in extreme environment such as high temperature, pressure and magnetic field. A continuing theme of this program is the integration of material synthesis, neutron scattering measurements and computational modeling as this is vital to obtain controlled samples for experiments and modeling for an in-depth understanding of the structure and dynamics of materials and their relationship to macroscopic properties.

The purpose of the BES biannual PI meetings is to bring together all the researchers funded by BES in the neutron scattering area to get a first-hand look at the range of research topics and ongoing activities in the program, to foster an awareness of the research of others in the program, to facilitate the exchange of new results and research highlights, to promote new ideas and collaborations among participants and BES scientific user facilities, and to identify and pursue new scientific opportunities and new frontiers. For BES the PI meetings provide an opportunity to see the entire portfolio/program at one time on a periodic basis, to assess the state of the program and chart new scientific directions, and to turn a 'collection of projects' into a visionary, forward-looking program.

We thank all the meeting participants for their active contributions in sharing their ideas and research accomplishments. Sincere thanks are also due to the speakers from other BES programs involved with neutron scattering in multidisciplinary research. We wish to thank Teresa Crockett in MSED and Lee-Ann Talley at the Oak Ridge Institute for Science and Education (ORISE) for their outstanding work in all aspects of the meeting organization.

Thiyaga P. Thiyagarajan and Helen Kerch
MSED, BES, Office of Science
U.S. Department of Energy

Table of Contents

AGENDA

2012 Neutron Scattering
Principal Investigators' Meeting
Materials Sciences and Engineering Division, Office of Basic Energy Sciences
U. S. Department of Energy

Program Chair: Thiyaga P. Thiyagarajan, Program Manager, Neutron Scattering

SUNDAY, JULY 22, 2012

6:00 – 8:00 pm Registration

******* Dinner on Your Own *******

MONDAY, JULY 23, 2012

7:00 – 8:00 am ***** Breakfast *****

8:00 – 8:05 am Helen Kerch, Team Lead, Scattering and Instrumentation Sciences
Welcome

8:05 – 8:45 am Linda Horton, Director, Division of Materials Sciences and Engineering
BES Program Updates and Processes

8:45 – 9:00 am Thiyaga P. Thiyagarajan,
Neutron Scattering Program Management

Session I **High Temperature Superconductors - Cuprates**
Chair: John Sarrao, Los Alamos National Laboratory

9:00 – 9:30 am John Tranquada, Brookhaven National Laboratory
Neutron Scattering Studies of Cuprate Superconductors

9:30 – 10:00 am Martin Greven, University of Minnesota
Crystal Growth and Scattering Studies of Model Cuprate Superconductors

10:00 – 10:30 am Dmitry Reznik, University of Colorado, Boulder
Neutron and X-ray Scattering Investigation of Electron-Phonon Effects in Cuprate Superconductors and Related Compounds

10:30 – 11:00 am ***** Break *****

Session II	**Correlated Electron Systems (I)** Chair: Zlatko Tesonavic, Johns Hopkins University
11:00 – 11:30 am	Collin Broholm, Johns Hopkins University *Quantum Correlated Materials and Phenomena*
11:30 – 12:00 noon	Robert McQueeney, Ames Laboratory *Correlations and Competition between the Lattice, Electrons, and Magnetism*
12:00 – 12:30 pm	Pengcheng Dai, University of Tennessee, Knoxville *Using Neutron as a Probe to Study Magnetic Excitations in Strongly Correlated Electron Materials*
12:30 – 1:00 pm	Raymond Osborn, Argonne National Laboratory *Phase Competition in Bulk Materials: Superconductivity vs Spin and Charge Density Waves*
1:00 – 2:00 pm	***** Working Lunch ***** Introduction of Poster Session I Presenters with Highlights **Thiyaga P. Thiyagarajan,** Program Manager, Neutron Scattering
2:00 – 3:30 pm	***Poster Session I***
3:30 – 4:00 pm	***** Coffee Break *****
Session III	**Correlated Electron Systems (II)** Chair: Stephan Rosenkranz, Argonne National Laboratory
4:00 – 4:30 pm	Joe Thompson, Los Alamos National Laboratory *Complex Electronic Materials*
4:30 – 5:00 pm	G. Y. Xu, I. A. Zaliznyak, G.D. Gu, and J. M. Tranquada, Brookhaven National Laboratory *Neutron Scattering Studies of Fe-Based Superconductors*
5:00 – 5:30 pm	Brent Fultz, Caltech *Vibrational Thermodynamics of Materials*
5:30 – 6:00 pm	Takeshi Egami, University of Tennessee, Knoxville *Neutron Scattering Study of Strongly Correlated Systems*
6:00 – 7:30 pm	***** Working Dinner ***** Scientific Highlights of the Day – Discussion and Input from Attendees **Thiyaga P. Thiyagarajan,** Program Manager, Neutron Scattering

Session IV	**Energy Materials** Chair: James Rhyne, Los Alamos National Laboratory
7:30 – 8:00 pm	Taner Yildirim, NIST/University of Pennsylvania *From Fundamental Understanding to Predicting New Nanomaterials for High-Capacity Hydrogen/Methane Storage and Carbon Capture*
8:00 – 8:30 pm	Alamgir Karim, University of Akron *In Situ Neutron Scattering Determination of 3D Phase-Morphology Correlations in Fullerene Block Copolymer Systems*
8:30 – 9:00 pm	Olivier Delaire, Oak Ridge National Laboratory *Inelastic Neutron Scattering Studies of Phonons in Thermoelectrics*
9:00 – 9:30 pm	***Continuation of Poster Session I***

TUESDAY, JULY 24, 2012

7:00 – 8:00 am	***** Breakfast *****
Session V	**Organic Photovoltaics and Soft Matter** Chair: Dvora Perahia, Clemson University
8:00 – 8:30 am	Dhandapani Venkataraman (Invited), University of Massachusetts *Polymer Based Materials for Harvesting Solar Energy: Design, Synthesis and Controlled Assemblies.*
8:30 – 9:00 am	Danilo Pozzo, University of Washington *Structure and Properties of Conjugated Polymer Networks for Organic Photovoltaics*
9:00 – 9:30 am	Wei-Ren Chen, Oak Ridge National Laboratory *Investigating Multiphasic Soft Colloids using Neutron Scattering, Simulations and Specific Tailored Synthesis*
9:30 – 10:00 am	Bradley Olsen, Massachusetts Institute of Technology *Thermodynamics of Self-Assembly in Globular Protein-Polymer Conjugates*
10:00 – 10:30 am	***** Break *****

Session VI	**Advanced Capabilities (I)** Chair: Raymond Osborn, Argonne National Laboratory
10:30 – 11:00 am	Robert McGreevy (Invited), Oak Ridge National Laboratory *Data and Analysis: Maximizing the Impact of Neutron Scattering at ORNL*
11:00 – 11:30 am	M.A.M. Bourke (Invited), Los Alamos National Laboratory *Neutron Scattering at Lujan Neutron Scattering Center (LANSCE): Capabilities and Scientific Highlights*
11:30 – 12:00 Noon	Dan Neumann (Invited), National Institute of Standards and Technology *The NIST Center for Neutron Research: Current and Future Capabilities*
12:00 – 12:30 PM	Boris Khaykovich, Massachusetts Institute of Technology *Optics for Advanced Neutron Imaging and Scattering*
12:30 – 1:30 pm	***** Working Lunch ***** Introduction of Poster Session II Presenters with Highlights **Thiyaga P. Thiyagarajan,** Program Manager, Neutron Scattering
1:30 – 3:00 pm	***Poster Session II***
3:00 – 3:30 pm	***** Coffee Break *****
Session VII	**Heterostructures** Chair: Alan Goldman, Ames Laboratory
3:30 – 4:00 pm	Chris Leighton, University of Minnesota *Neutron Scattering Studies of Cobaltite Crystals and Heterostructures*
4:00 – 4:30 pm	Eric Fullerton, University of California, San Diego *Neutron and X-ray Studies of Spin and Charge Manipulation in Magnetic Nanostructures*
4:30 – 5:00 pm	Suzanne te Velthuis, Argonne National Laboratory *Phase Competition in Interfacial Materials: Magnetic Heterostructures*
5:00 – 5:30 pm	Valery Kiryukhin, Rutgers University *Neutron and Ellipsometry Studies of Multiferroics: Magnetic Structure, Excitations, and Hybrid Modes*
5:30 – 6:00 pm	***** Break*****
6:00 – 7:30 pm	***** Working Dinner ***** Scientific Highlights of the Day – Discussion and Input from Attendees **Thiyaga P. Thiyagarajan,** Program Manager, Neutron Scattering

Session VIII	**Advanced Capabilities (II)** Chair: Igor Zaliznyak, Brookhaven National Laboratory
7:30 – 8:00 PM	W.M. Snow, Indiana University *Polarized ^{3}He in Neutron Scattering*
8:00 – 8:30 pm	Roger Pynn, Indiana University *Development of New Methods for Studying Nanostructures using Neutron Scattering*
8:30 – 9:30 pm	***Continuation of Poster Session II***

WEDNESDAY, JULY 25, 2012

7:00 – 8:00 am	***** Breakfast *****
Session IX	**Frustrated Magnetism** Chair: *Oleg Tchernyshyov, Johns Hopkins University*
8:00 – 8:30 am	Young Lee, Massachusetts Institute of Technology *A Unified Effort for Crystal Growth, Neutron Scattering, and X-ray Scattering Studies of Novel Correlated Electron Materials*
8:30 – 9:00 am	Seung-Hun Lee, University of Virginia *Neutron Scattering Study of Unconventional Superconductors*
9:00 – 9:30 am	Tyrel McQueen, Johns Hopkins University *Orbital Selective Magnetism in the Spin-Ladder Iron Selenides $Ba_{1-x}K_xFe_2Se_3$*
9:30 – 10:00 am	***** Break *****
Session X	**Dynamics** Chair: George Reiter, University of Houston
10:00 – 10:30 am	Morten Eskildsen, University of Notre Dame *Metastable Vortex Lattices – Properties and Applications*
10:30 – 11:00 am	Henry Glyde, University of Delaware *Neutron Scattering Studies of Classical and Quantum Fluids in Porous Media*
11:00 – 11:30 am	Christopher Bertrand, Massachusetts Institute of Technology *Neutron and X-ray Scattering Studies of the Liquid-Liquid Transition in Supercooled Confined Water and the Slow Dynamics in Biomolecular Assemblies*

11:30 – 11:45 am	Remarks – Discussion of Meeting Highlights **Helen Kerch (**Team Lead, Scattering and Instrumentation Team) and **Thiyaga P. Thiyagarajan**, Program Manager, Neutron Scattering
11:45 am - 1:00 pm	***** Working Lunch***** Meeting Feedback – Questionnaire, Suggestion for Future Meetings **Thiyaga P. Thiyagarajan,** Program Manager, Neutron Scattering
1:00 pm	***** Adjourn*****

Session I

High Temperature Superconductors – Cuprates

Neutron Scattering Studies of Cuprate Superconductors

J. M. Tranquada (jtran@bnl.gov), G. D. Gu, M. Hücker, G. Y. Xu, and I. A. Zaliznyak
Condensed Matter Physics & Materials Science Department
Brookhaven National Laboratory, Upton, NY 11973-5000

Program Scope

Superconductivity in hole-doped cuprates occurs in a regime such that the doped holes frustrate the antiferromagnetic correlations among copper moments while the local antiferromagnetism frustrates the kinetic energy of the holes. The observed behavior is too complicated to describe with ab initio calculations, thus requiring the application of effective models; however, there is no real consensus on the appropriate effective model necessary to describe the observed electronic and magnetic correlations. On the experimental side, the challenge is to establish the features that are universal among the superconducting cuprate families, which will provide essential guidance to theorists.

A major focus of our effort has been the application of neutron and hard-x-ray scattering techniques to the study of the spin and charge stripe correlations, especially on crystals grown in our lab. Past work has established the existence of spin and charge stripe order in certain cuprates and the approximate character of the associated spin dynamics. Much of the current work is aimed at testing the degree to which stripe correlations may be common among the cuprates and determining the relationship between stripes and superconductivity.

Recent Progress

Character of stripe order. Previous work on crystals of $La_{2-x}Ba_xCuO_4$ (LBCO) has established the temperature and doping dependence of the spin and charge order parameters. Current work addresses the detailed structure of the stripe-ordered phase at x = 1/8. Hücker and Zaliznyak have analyzed intensities of a few dozen spin-order superlattice peaks determined by neutron scattering. The analysis demonstrates that a quantitative description requires the use of a magnetic form factor that includes a substantial hybridization between Cu 3*d* and O 2*p* orbitals, as established in earlier work on Sr_2CuO_3 by Zaliznyak.

Hücker is also analyzing a few hundred charge-order intensities obtained by hard-x-ray scattering. Correcting the intensities for effects such as absorption, extinction and resolution is non-trivial as the crystals must be relatively thick in order to get sufficient scattered signal from the extremely weak superlattice peaks. The goal is to establish an improved model of the atomic displacements associated with charge order.

Stripes and superconductivity. It has been suggested that a spin gap and resonance peak are common features of all superconductors with proximate antiferromagnetism. Tranquada has found a counter example in LBCO with x = 0.095. The low-energy incommensurate magnetic excitations are effectively gapless, and there is no sign of a resonance peak; nevertheless, the sample exhibits robust superconductivity with T_c = 32 K. The coexistence may require a phase-

coupled spatial modulation of the superconducting and spin correlations in a fashion similar to that predicted for the pair-density-wave state.

Universality of stripe correlations. Evidence of spin-stripe correlations in $La_{2-x}Sr_xCuO_4$ was reported long ago, but evidence for charge-stripe order has been more difficult to obtain. Hücker has collaborated with N.B. Christensen (U. Copenhagen), J. Chang (PSI), and M. Fujita (Tohoku U.) on hard-x-ray diffraction searches for charge order induced by magnetic fields of up to 10 T. Success was recently obtained for samples with detectable traces of the low-temperature-tetragonal phase, associated with the twin domains of the dominant orthorhombic structure.

Tranquada has collaborated with M. Fujita and K. Yamada (Tohoku U.) on neutron scattering measurements of low-energy magnetic excitations in crystals of $Bi_{2+x}Sr_{2-x}CuO_{6+\delta}$. The results show incommensurate spin fluctuations corresponding to a stripe density that varies linearly with hole doping, just as in LBCO. The interpretation of charge modulations imaged on the surface of similar crystals by scanning tunneling microscopy will need some reconsideration.

Crystal preparation. We are presently completing commissioning of a new high-pressure furnace, capable of temperatures up to 1000°C and pressures up to 7000 bar with 20% oxygen. In a commissioning run, Gu annealed a crystal of $La_{1.9}Ca_{1.1}Cu_2O_{6+\delta}$, which had no bulk superconductivity before treatment but afterwards exhibited full bulk diamagnetism below 54 K. Eventually, larger crystals will be annealed with varying conditions and characterized by neutron scattering. Gu has also begun work on underdoping $Bi_2Sr_2CaCu_2O_{8+\delta}$ crystals with fluorine. One goal is to prepare large, uniformly underdoped crystals for inelastic neutron studies.

Future Plans

Direct determination of longer-range exchange interactions. Magnetic interactions between sites more distant than nearest neighbor can lead to frustration. The usual approach to determining these interactions involves fitting the measured spin-wave dispersion of an antiferromagnetically-ordered state. Other groups have already provided evidence for a finite 4-spin cyclic exchange. Zaliznyak proposes to directly measure magnetic bond energies in La_2CuO_4 by applying the single-mode approximation to excitation spectra. This approach is facilitated by the improved knowledge of the magnetic form factor, as mentioned above.

Charge stripes in other cuprate families. Hücker intends to use hard-x-ray diffraction in high magnetic fields to search for field-induced charge stripe order in cuprates beyond the 214 family. Candidate systems include Bi2201 and Bi2212.

Dynamic charge stripes. We would like to examine the impact of dynamic charge stripes on the superconductivity. The challenge is that no unique signature of dynamic charge stripes has yet been identified. Tranquada has collaborated with D. Reznik (U. Colorado) on experiments that have successfully detected low-energy lattice fluctuations associated with stripe order in $La_{1.67}Sr_{0.33}NiO_4$; the intensity is maximized at the charge-ordering transition. The next goal is to try such experiments on LBCO. If successful, the signature can be used to test for slowly fluctuating charge stripes in other cuprates.

Publications

1. A. A. Schafgans, C. C. Homes, G. D. Gu, Seiki Komiya, Yoichi Ando, and D. N. Basov.
Breakdown of the universal Josephson relation in spin-ordered cuprate superconductors.
Phys. Rev. B **82**, 100505 (2010).
2. S. Wakimoto, H. Hiraka, K. Kudo, D. Okamoto, T. Nishizaki, K. Kakurai, T. Hong, A. Zheludev, J. M. Tranquada, N. Kobayashi, and K. Yamada.
Magnetic field effect on Fe-induced short-range magnetic correlation and electrical conductivity in $Bi_{1.75}Pb_{0.35}Sr_{1.90}Cu_{0.91}Fe_{0.09}O_{6+y}$.
Phys. Rev. B **82**, 064507 (2010).
3. S. Blanc, Y. Gallais, M. Cazayous, M. A. Méasson, A. Sacuto, A. Georges, J. S. Wen, Z. J. Xu, G. D. Gu, and D. Colson.
Loss of antinodal coherence with a single d-wave superconducting gap leads to two energy scales for underdoped cuprate superconductors.
Phys. Rev. B **82**, 144516 (2010).
4. D. S. Ellis, Jungho Kim, Harry Zhang, J. P. Hill, G. D. Gu, S. Komiya, Y. Ando, D. Casa, T. Gog, and Y.-J. Kim.
Electronic structure of doped lanthanum cuprates studied with resonant inelastic x-ray scattering.
Phys. Rev. B **83**, 075120 (2011).
5. Grafe, H.-J., Curro, N.J., Young, B.L., Vyalikh, A., Vavilova, J., Gu, G.D., Hücker, M., and Büchner, B.
Charge order and low frequency spin dynamics in lanthanum cuprates revealed by Nuclear Magnetic Resonance.
Eur. Phys. J. Special Topics **188**, 89–101 (2010).
6. G.-H. Gweon, B. S. Shastry, and G. D. Gu.
Extremely Correlated Fermi-Liquid Description of Normal-State ARPES in Cuprates.
Phys. Rev. Lett. **107**, 056404 (2011).
7. M. Hücker, M. v. Zimmermann, G. D. Gu, Z. J. Xu, J. S. Wen, G. Y. Xu, H. J. Kang, A. Zheludev, and J. M. Tranquada.
Stripe order in superconducting $La_{2-x}Ba_xCuO_4$ ($0.095 \leq x \leq 0.155$).
Phys. Rev. B **83**, 104506 (2011).
8. M. Hücker, M. Zimmermann, Z. Xu, J. Wen, G. Gu, W. Tian, J. Zarestky, and J. Tranquada.
Zn-Doping Dependence of Stripe Order in $La_{1.905}Ba_{0.095}CuO_4$.
J. Supercond. Nov. Magn. **24**, 1229–1233 (2011).
9. T. Kondo, Y. Hamaya, A.D. Palczewski, T. Takeuchi, J.S. Wen, Z.J. Xu, G.D. Gu, J. Schmalian, and A. Kaminski.
Disentangling Cooper-pair formation above the transition temperature from the pseudogap state in the cuprates.
Nat. Phys. **7**, 21–25 (2011).
10. M. Matsuda, J. A. Fernandez-Baca, M. Fujita, K. Yamada, and J. M. Tranquada.
Detailed structure of the low-energy magnetic dispersion of the diagonal incommensurate phase in $La_{1.975}Sr_{0.025}CuO_4$.
Phys. Rev. B **84**, 104524 (2011).
11. J.-Q. Meng, M. Brunner, K.-H. Kim, H.-G. Lee, S.-I. Lee, J. S. Wen, Z. J. Xu, G. D. Gu, and G.-H. Gweon.
Momentum-space electronic structures and charge orders of the high-temperature superconductors $Ca_{2-x}Na_xCuO_2Cl_2$ and $Bi_2Sr_2CaCu_2O_{8+\delta}$.
Phys. Rev. B **84**, 060513 (2011).
12. C. V. Parker, P. Aynajian, E. H. da Silva Neto, A. Pushp, S. Ono, J. S. Wen, Z. J. Xu, G.D. Gu, and A. Yazdani.
Fluctuating stripes at the onset of the pseudogap in the high-T_c superconductor $Bi_2Sr_2CaCu_2O_{8+x}$.
Nature **468**, 677–680 (2010).
13. A. Sacuto, Y. Gallais, M. Cazayous, S. Blanc, M.-A. Méasson, J. S. Wen, Z. J. Xu, G. D. Gu, and D. Colson.
Electronic Raman scattering in copper oxide superconductors: Understanding the phase diagram.
C. R. Phys. **12**, 480–501 (2011).
14. H.-B. Yang, J. D. Rameau, Z.-H. Pan, G. D. Gu, P. D. Johnson, H. Claus, D. G. Hinks, and T. E. Kidd.
Reconstructed Fermi Surface of Underdoped $Bi_2Sr_2CaCu_2O_{8+\delta}$ Cuprate Superconductors. *Phys. Rev. Lett.* **107**, 047003 (2011).

15. J. Crocker, A.P. Dioguardi, N. apRoberts Warren, A.C. Shockley, H.-J. Grafe, Z. Xu, J. Wen, G. Gu, and N. J. Curro. NMR studies of pseudogap and electronic inhomogeneity in $Bi_2Sr_2CaCu_2O_{8+\delta}$.
Phys. Rev. B **84**, 224502 (2011).
16. E. H. da Silva Neto, C. V. Parker, P. Aynajian, A. Pushp, A. Yazdani, J. S. Wen, Z. J. Xu, and G. D. Gu.
Scattering from incipient stripe order in the high-temperature superconductor $Bi_2Sr_2CaCu_2O_{8+\delta}$.
Phys. Rev. B **85**, 104521 (2012).
17. M. Enoki, M. Fujita, S. Iikubo, J. M. Tranquada, and K. Yamada.
Incommensurate Magnetic Excitation in Spin-Glass Phase of Bi2201 Cuprate.
J. Phys. Soc. Jpn. **80**, SB026 (2011).
18. M. Fujita, H. Hiraka, M. Matsuda, M. Matsuura, J. M. Tranquada, S. Wakimoto, G. Y. Xu, and K. Yamada.
Progress in Neutron Scattering Studies of Spin Excitations in High-T_c Cuprates.
J. Phys. Soc. Jpn. **81**, 011007 (2012).
19. R. D. Gann, J. S. Wen, Z. J. Xu, G. D. Gu, and J. A. Yarmoff.
Surface restructuring in sputter-damaged $Bi_2Sr_2CaCu_2O_{8+\delta}$.
Phys. Rev. B **84**, 165411 (2011).
20. C. C. Homes, M. Hücker, Q. Li, Z. J. Xu, J. S. Wen, G. D. Gu, and J. M. Tranquada.
Determination of the optical properties of $La_{2-x}Ba_xCuO_4$ for several dopings, including the anomalous x=1/8 phase.
Phys. Rev. B **85**, 134510 (2012).
21. Lu Li, N. Alidoust, J. M. Tranquada, G. D. Gu, and N. P. Ong.
Unusual Nernst Effect Suggesting Time-Reversal Violation in the Striped Cuprate Superconductor $La_{2-x}Ba_xCuO_4$.
Phys. Rev. Lett. **107**, 277001 (2011).
22. S. R. Park, A. Hamann, L. Pintschovius, D. Lamago, G. Khaliullin, M. Fujita, K. Yamada, G. D. Gu, J. M. Tranquada, and D. Reznik.
Effects of charge inhomogeneities on elementary excitations in $La_{2-x}Sr_xCuO_4$.
Phys. Rev. B **84**, 214516 (2011).
23. J. D. Rameau, Z.-H. Pan, H.-B. Yang, G. D. Gu, and P. D. Johnson.
Universal scaling of length, time, and energy for cuprate superconductors based on photoemission measurements of $Bi_2Sr_2CaCu_2O_{8+\delta}$.
Phys. Rev. B **84**, 180511 (2011).
24. J. M. Tranquada. Stripes and superconductivity in cuprates.
Physica B **407**, 1771–1774 (2012).
25. J. S. Wen, Q. Jie, Q. Li, M. Hücker, M. v. Zimmermann, S. J. Han, Z. J. Xu, D. K. Singh, R. M. Konik, L. Y. Zhang, G. D. Gu, and J. M. Tranquada.
Uniaxial linear resistivity of superconducting $La_{1.905}Ba_{0.095}CuO_4$ induced by an external magnetic field.
Phys. Rev. B **85**, 134513 (2012).
26. J. S. Wen, Z. J. Xu, G. Y. Xu, Q. Jie, M. Hücker, A. Zheludev, W. Tian, B. L. Winn, J. L. Zarestky, D. K. Singh, T. Hong, Q. Li, G. D. Gu, and J. M. Tranquada.
Probing the connections between superconductivity, stripe order, and structure in $La_{1.905}Ba_{0.095}Cu_{1-y}Zn_yO_4$.
Phys. Rev. B **85**, 134512 (2012).
27. S. B. Wilkins, M. P. M. Dean, J. Fink, M. Hücker, J. Geck, V. Soltwisch, E. Schierle, E. Weschke, G. Gu, S. Uchida, N. Ichikawa, J. M. Tranquada, and J. P. Hill.
Comparison of stripe modulations in $La_{1.875}Ba_{0.125}CuO_4$ and $La_{1.48}Nd_{0.4}Sr_{0.12}CuO_4$.
Phys. Rev. B **84**, 195101 (2011).
28. I. Zeljkovic, E. J. Main, T. L. Williams, M. C. Boyer, K. Chatterjee, W. D. Wise, Y. Yin, M. Zech, A. Pivonka, T. Kondo, T. Takeuchi, H. Ikuta, J.S. Wen, Z.J. Xu, G. D. Gu, E. W. Hudson, and J. E. Hoffman.
Scanning tunnelling microscopy imaging of symmetry-breaking structural distortion in the bismuth-based cuprate superconductors.
Nat. Mater., advance online publication, May 6, 2012.
29. W. Zhang, J. M. Bok, J. H. Yun, J. He, G. Liu, L. Zhao, H. Liu, J. Meng, X. Jia, Y. Peng, D. Mou, S. Liu, L. Yu, S. He, X. Dong, J. Zhang, J. S. Wen, Z. J. Xu, G. D. Gu, G. Wang, Y. Zhu, X. Wang, Q. Peng, Z. Wang, S. Zhang, F. Yang, C. Chen, Z. Xu, H.-Y. Choi, C. M. Varma, and X. J. Zhou.
Extraction of normal electron self-energy and pairing self-energy in the superconducting state of the $Bi_2Sr_2CaCu_2O_8$ superconductor via laser-based angle-resolved photoemission.
Phys. Rev. B **85**, 064514 (2012).

Crystal Growth and Scattering Studies of Model Cuprate Superconductors

M. Greven (greven@physics.umn.edu)
University of Minnesota

Research Scope

Complex oxides such as the high-T_c cuprate superconductors offer myriad opportunities to discover and investigate novel magnetic, structural, and electronic phenomena and phases. Neutron scattering experiments play an invaluable role in this endeavor, since they provide essential structural and magnetic information about new phases of matter and the transitions between them. Advanced crystal growth and characterization is of enormous importance to this field, and the crystal-size requirements for cutting-edge neutron scattering experiments are particularly demanding.

We have developed the unique capability to grow sizable, high-quality single crystals of arguably the most desirable cuprate superconductor, $HgBa_2CuO_{4+\delta}$ (Hg1201), in order to carry out a comprehensive materials physics effort to address some of the most timely and intellectually challenging problems in the field of correlated-electron materials. It is thought by many that magnetic fluctuations play an important role in bringing about the superconductivity in the cuprates, and part of our research focuses on the investigation of novel magnetism associated with the pseudogap phenomenon through advanced neutron scattering experiments. In parallel, we are investigating charge-ordering phenomena using synchrotron X-ray scattering techniques, and we are pursuing a detailed, quantitative effort to determine the nature of superconducting fluctuations and the planar charge transport properties of this model compound. An important component of this comprehensive effort is our collaborative research with experts using complementary experimental tools, including photoemission, Raman scattering, optical spectroscopy, Kerr effect, NMR, μSR, specific heat, ultrasound, and microwave transport.

Recent Progress

Neutron scattering measurements of new underdoped Hg1201 samples (Y. Li et al., Nature Physics, 2012; M. Chan et al., unpublished work). One of the central issues in the study of the cuprates is to clarify the interplay between magnetism and superconductivity. Intensive efforts have been devoted toward understanding the magnetic resonance and the seemingly universal hourglass-like magnetic dispersion near the antiferromagnetic (AF) wave-vector ($\mathbf{Q}_{AF}$). Building on our earlier work (*Nature 2010*), our recent inelastic neutron scattering experiments (Figure 1; *Nature Physics 2012*) have revealed two novel magnetic excitations in the pseudogap state in optimally-doped (T_c = 95 K) and moderately underdoped (T_c = 65 K) Hg1201. These excitations emanate from the Brillouin zone center ($\mathbf{q}$=0), disperse only weakly, and exist throughout the entire Brillouin zone. In prior work, we observed the well-known magnetic resonance in the superconducting state of Hg1201 (*Nature Physics 2009, Phys. Rev. B 2010*).

Interestingly, our most recent work indicates that the energy of the well-known response at $\mathbf{Q}_{AF}$ coincides with that of the novel pseudogap excitations, thus pointing toward a relationship between the two. We have begun to extend our inelastic neutron scattering study of the rich magnetic fluctuations in Hg1201 to a series of new underdoped samples (Figure 1).

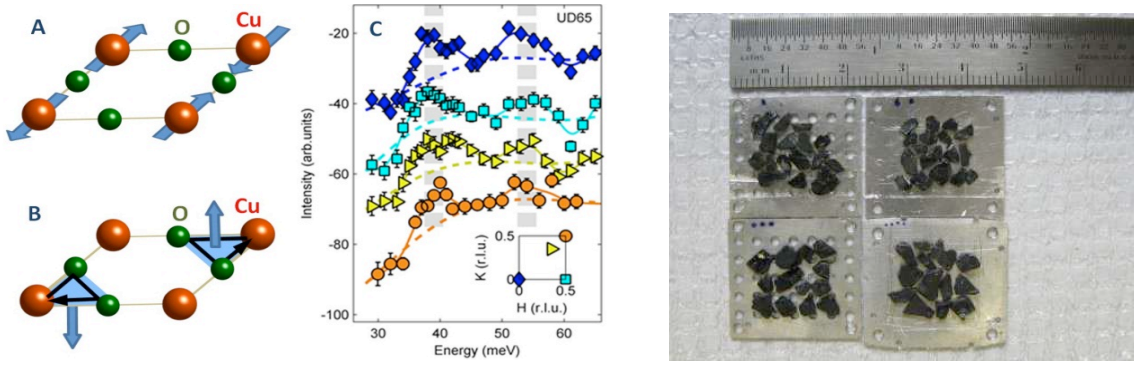

Figure 1: (**A**) The fundamental building block of the copper-oxide superconductors is the Cu-O sheet. The well-studied conventional magnetism is thought to result from localized spin moments on the Cu atoms. (**B**) Proposed novel magnetism due to circulating charge currents. (**C**) Intensity of scattered neutrons at four wave vectors for the model material $HgBa_2CuO_{4+\delta}$. Two magnetic excitations can be discerned, one at about 40 meV and the other at about 55 meV. (**Right**) New underdoped sample (T_c = 57 K, 1.8 gram) for neutron scattering measurements.

Synchrotron X-ray scattering study of oxygen-chain order in Hg1201 (G. Chabot-Couture, manuscript in preparation). At the Advanced Photon Source, we obtained data for more than 10 samples with different doping levels that confirmed our prior discovery of oxygen-chain order in this compound.

Quantitative dc transport measurements of Hg1201 (N. Barišić et al., manuscript in preparation). In the enigmatic cuprates, strong electronic correlations give rise to an insulating parent state from which superconductivity and eventually a Fermi-liquid-like metal emerge upon doping. At intermediate hole concentrations (p), the deviation from a linear-in-temperature planar resistivity ($\rho \propto T$) upon cooling toward the superconducting state is associated with the opening of a gap (the pseudogap) in the 'antinodal' regions of the Fermi surface. Contrary to common belief, we find in the pseudogap phase of structurally simple $HgBa_2CuO_{4+\delta}$ that $\rho \propto T^2$ (Figure 2), as in the putative Fermi-liquid state at very high hole concentrations. By combining these results with prior work for other cuprates, we have been able to obtain the universal resistance per copper-oxygen plaquette in both the linear and quadratic regimes. This work marks a dramatic breakthrough in cuprate physics, since it is demonstrated for the first time that there exists a universal quadratic resistive regime and that the planar resistivity in both regimes can be universally determined for all cuprates. Any theory for the cuprates can now be benchmarked against this simple universal behavior.

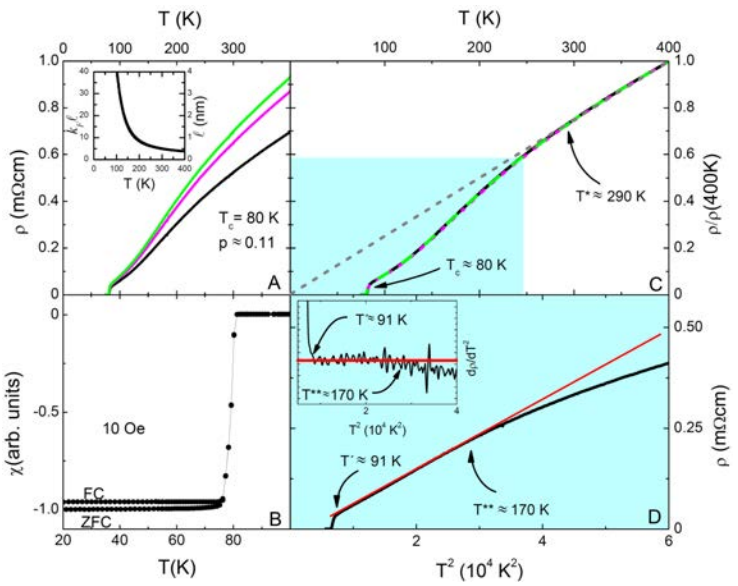

Figure 2: Magnetic susceptibility and *ab*-plane dc-resistivity for underdoped Hg1201 (T_c = 80 K). (**A**) Resistivity as function of temperature for three samples. Inset: estimates of mean free path (l) and $k_F l$. (**B**) Magnetic susceptibility (zero-field-cooled (ZFC) and field-cooled (FC)) for one of the samples after its preparation for resistivity measurements reveals a sharp T_c of 80 K. The FC/ZFC ratio is 97%, indicative of very high sample quality. (**C**) When normalized at 400 K, the data in A) collapse to a single curve, indicating high bulk homogeneity. High-temperature linear behavior, $\rho = \rho_0 + A_1 T$ (gray dashed line), with $\rho_0 \approx 0$. Deviation from linear behavior occurs below the pseudogap temperature $T^* \approx 290$ K. (**D**) The resistivity exhibits a quadratic temperature dependence between $T' \approx 90$ K and $T^{**} \approx 170$ K. This is also seen from the plot of $d\rho/d(T^2)$ (inset). Red lines are guides to the eye. Horizontal and vertical ranges correspond to blue area in C).

Torque magnetization measurements of Hg1201 (G. Yu et al., preprint; D.-D. Xia et al., manuscript in preparation). Superconductivity in the cuprates emerges from a metallic state that is not well understood, with pivotal open questions regarding the universality of observed behaviors and the character of precursor fluctuations above T_c. For the intensively studied single-CuO_2-layer compounds $La_{2-x}Sr_xCuO_4$ (LSCO) and $Bi_2(Sr,La)_2CuO_{6+\delta}$ (Bi2201), some experiments have been interpreted as indicative of very high characteristic temperatures for the onset of SC fluctuations (two to three times T_c^{max}, the T_c value at optimal hole doping), whereas other measurements suggest that SC fluctuations are confined to the vicinity of T_c. We have been using torque magnetometry to resolve this conundrum by studying Hg1201, a more ideal single-layer compound with T_c^{max} = 97 K, a value more than twice those of LSCO and Bi2201. We first demonstrate that the genuine SC fluctuation regime is universally narrow, and that in both Hg1201 and Bi2201 SC diamagnetism at moderately high fields vanishes exponentially with increasing temperature. We furthermore observe that the higher characteristic temperatures reported for LSCO and Bi2201 are close to the SC transition temperature of Hg1201, which suggests a universal temperature scale that in the low-T_c^{max} compounds no longer is associated with genuine SC fluctuations.

Collaborations with experts using complementary techniques (five manuscripts in preparation). We have continued to strengthen and expand our collaborations based on

our unique capability to grow sizable single crystals of Hg1201. We are in the process of writing two NMR papers, one with Prof. W.P. Halperin (Northwestern) and one with Prof. J. Haase (Leipzig, Germany), an optical conductivity paper with Prof. D. van der Marel (Geneva, Switzerland), and a new Raman scattering paper with Prof. Y. Li (Beijing, China), and a resonant ultrasound paper with Drs. A. Migliori and A. Shekther (LANL). At present, we have collaborations based on crystals grown in our lab with about 20 groups, many of which are supported by DOE-BES.

Future Plans

Extension of neutron scattering work to the overdoped and very underdoped sides of the phase diagram. To date, neutron scattering work on overdoped single-layer cuprates has focused solely on LSCO, which features a particularly low T_c. It will be important to contrast this with new results for Hg1201, and to search for the presence of a quantum critical point in Hg1201.
Resonant elastic and inelastic X-ray scattering. Synchrotron X-ray search for novel charge and magnetic order and excitations in Hg1201.
Extension of quantitative transport measurements. Planar dc resistivity measurements of Hg1201 at higher/lower doping and to high magnetic field. Measurement of the Hall effect.
Crystal growth of $HgBa_2CaCu_2O_{6+\delta}$ (Hg1212). Hg1212 is the double-layer cuprate with the highest T_c (~25% larger than, e.g., $YBa_2Cu_3O_{6+\delta}$ (YBCO)), yet there exist very few experimental studies since sizable crystals have not been available. Our initial crystal growth attempts have been successful. We will continue to optimize growth conditions.
Initial characterization work of Hg1212 single crystals. We will begin quantitative transport and torque magnetization work on Hg1212, and assemble the first Hg1212 sample for neutron scattering measurements.
Collaborations. We will continue our successful collaborations with experts using complementary experimental techniques.

Publications (FY12)

1. *Two Ising-like magnetic excitations in a single-layer cuprate superconductor.*
   Yuan Li, G. Yu, M. K. Chan, V. Balédent, Yangmu Li, N. Barišić, X. Zhao, K. Hradil, R. A. Mole, Y. Sidis, P. Steffens, P. Bourges, and M. Greven.
   Nature Physics **8**, 414 (2012).
2. *Feedback effect on high-energy magnetic fluctuations in the model high-temperature superconductor $HgBa_2CuO_{4+\delta}$ observed by electronic Raman scattering.*
   Yuan Li, M. Le Tacon, M. Bakr, D. Terrade, D. Manske, R. Hackl, L. Ji, M. K. Chan, N. Barišić, X. Zhao, M. Greven, and B. Keimer.
   Phys. Rev. Lett. (in press, 2012).
3. *Superconducting fluctuations, pairing, and the phase diagram of the cuprates.*
   G. Yu, D.-D. Xia, N. Barišić, R.-H. He, N. Kaneko, Y. Li, X. Zhao, A. Shekhter, and M. Greven.
   Nature (in review, 2012).

Dmitry Reznik, University of Colorado-Boulder

Neutron and X-ray Scattering Investigation of Electron-Phonon Effects in Cuprate Superconductors and Related Compounds

1. Program scope

The project focuses on using neutron and x-ray scattering and to a lesser extent, angle resolved photoemission (ARPES), to uncover fundamental mechanisms behind high temperature superconductivity in copper oxide and iron-based superconductors, stripe physics, and electrochromism. These phenomena originate from complex electronic correlations and unconventional electron-phonon coupling and there are strong indications that they share some underlying physics. This work builds on recent revolutionary advances in the instrumentation at DOE facilities as well as previous discoveries by the group of the PI.

2. Recent progress

2.1. Direct observation of the dynamic charge stripe spectrum in $La_{1.67}Sr_{0.33}NiO_4$ by inelastic neutron scattering

Electrons in strongly correlated systems sometimes phase-segregate into charge rich and magnetically-ordered charge-poor regions in the form of stripes. [1] Whereas static stripes have been observed in a few compounds, dynamic stripes generate the most interest because of the possibility that they enable high temperature superconductivity. [2,3] There have been numerous reports of experimental signatures of dynamic *magnetic* stripes in the neutron scattering spectra of cuprates. [4,5] However, other interpretations of the same experiments have been proposed. [6] Furthermore, it is generally agreed that the charge channel drives the stripe formation with the magnetic channel playing a secondary role. For example in the prototypical stripe compound, $La_{2-x}Sr_xNiO_4$, charge stripes form at a higher temperature than the spin stripes. Thus charge stripes can exist without magnetic stripes, but magnetic stripes cannot exist without their counterpart in the charge channel. The group of D.R., as well as others, previously reported phonon anomalies possibly associated with dynamic charge stripes in every cuprate superconductor investigated so far including the ones without clear signatures of magnetic stripes. [7, for a recent review, see 8] These observations, however, were indirect and other interpretations of the same data have not been definitively excluded.

One of the main directions of the research program of the group of D.R. is to investigate dynamic *charge* stripes. During the first 8 months of the funded project, D.R. et al. achieved transformational progress in this area: For the first time the temperature-dependent spectrum of dynamic charge stripes has been directly observed and

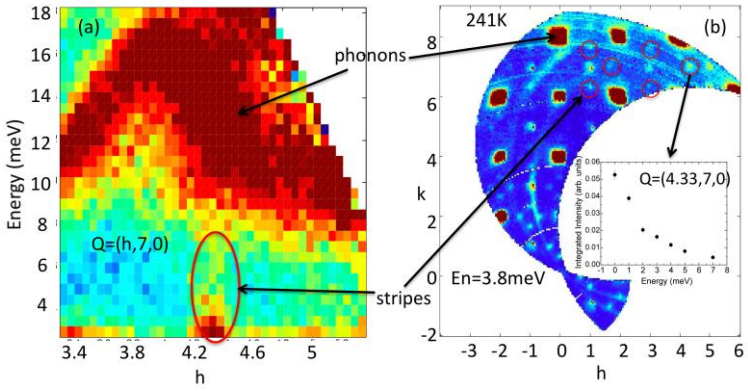

Figure 1: Dynamic charge stripe spectrum measured on the ARCS spectrometer at the SNS. Energy resolution was 3meV FWHM (a) Momentum-energy cut showing steep dispersion of charge stripes (b) Constant-energy cut with red circles indicating dynamic charge stripes. Inset shows the energy-dependence of

investigated by inelastic neutron scattering at HFIR, the SNS, and the Saclay reactor.

These measurements focused on a prototypical stripe system, $La_{1.67}Sr_{0.33}NiO_4$. Dynamic charge stripes appear at nonzero energy transfer as a column of scattering in an energy vs. momentum plot implying a very steep dispersion. (Fig. 1) The following results have been obtained so far: 1. The spectral weight of dynamic charge stripes at low energies is strongest near the charge-ordering temperature. 2. Its temperature-dependence shows that dynamic charge stripes are critical fluctuations, which implies that in materials without static stripe order such as the high T_c cuprates, they can exist only in the quantum critical regime. 3. Dynamic stripes have a 3-dimentional character, i.e. interlayer correlations are much stronger than expected from models based on isolated 2D Ni-O planes.

2.2 Interplay between phonons, electrons, magnetic fluctuations, and superconductivity in an overdoped high-temperature superconductor

High temperature superconductivity in copper oxides may arise from Cooper pairing due to interactions between conduction electrons and bosonic modes, such as (but not necessarily) phonons or magnetic fluctuations. These interactions induce kinks in electronic dispersions observed by angle-resolved photoemission (ARPES). Intense research effort [9-12] focused on determining their origin, since the Bosonic excitation from which the ARPES kinks originate, may provide the pairing glue. Strong correlations may induce new poorly understood phenomena such as enhanced electron-phonon coupling, novel magnetic excitations, the formation of nematic electronic phases, current loops, resonating valence bonds, etc., which may induce the kink and be important for superconductivity. Inelastic neutron and x-ray scattering can directly measure bosonic modes and other excitations associated with exotic electronic correlations, but the strength of their coupling to electrons is difficult to infer. Spin fluctuations and Cu-O bond stretching phonons that have been directly investigated by neutron and x-ray scattering are top contenders in the debate about which bosonic excitation underlies the kink. Spin fluctuations extend in energy up to about 300 meV. [5] Their energy-integrated spectral weight peaks around 40-50meV in many compounds, which is close to the kink energy. Cu-O bond stretching phonons appear close to 70meV and exhibit strong softening and broadening [7], which implies strong electron-phonon coupling. The same phonons exhibit an additional giant anomaly in superconducting compounds or stripe-ordered compounds, which have a static order characterized by charge rich lines alternating with antiferromagnetically-ordered charge-poor regions. [7] Since this anomaly appears near the charge stripe ordering wavevector, it may originate from the interaction of the phonon with dynamic stripes, which may be present even if static stripes do not form. Alternatively, this giant renormalization is a result of an interaction of the phonon with electronic quasiparticles, which are directly observed by ARPES. [16] In the latter scenario the ARPES kink is a reflection of the giant phonon anomaly in the electronic dispersions. Charge fluctuations and loop currents [15] have also recently been suggested as the possible bosonic modes behind the kink.

We cross-correlated our new and previously published ARPES, INS, and IXS results on overdoped $La_{2-x}Sr_xCuO_4$ ($0.2<x<0.3$) and found that the ARPES kink energy does not match the spin fluctuation spectrum, but it does match the Cu-O bond-stretching phonons whose large doping-independent overall broadening in the IXS spectra indicates enhanced electron-phonon coupling. Additional giant softening and broadening of these phonons appears for x=0.2, possibly as a result of electronic stripe fluctuations where charge-rich lines and antiferromagnetic charge-poor regions alternate. However, superconductivity as well as all signatures of stripes disappear by x=0.3

whereas the ARPES kink remains strong. We conclude that stripes may be associated with the mechanism of superconductivity whereas bosonic modes that induce the kink are not. Our data rule out magnetic fluctuations and stripe-related mechanisms as possible origins of the kink leaving enhanced electron-phonon coupling and electron-electron interactions as remaining possibilities.

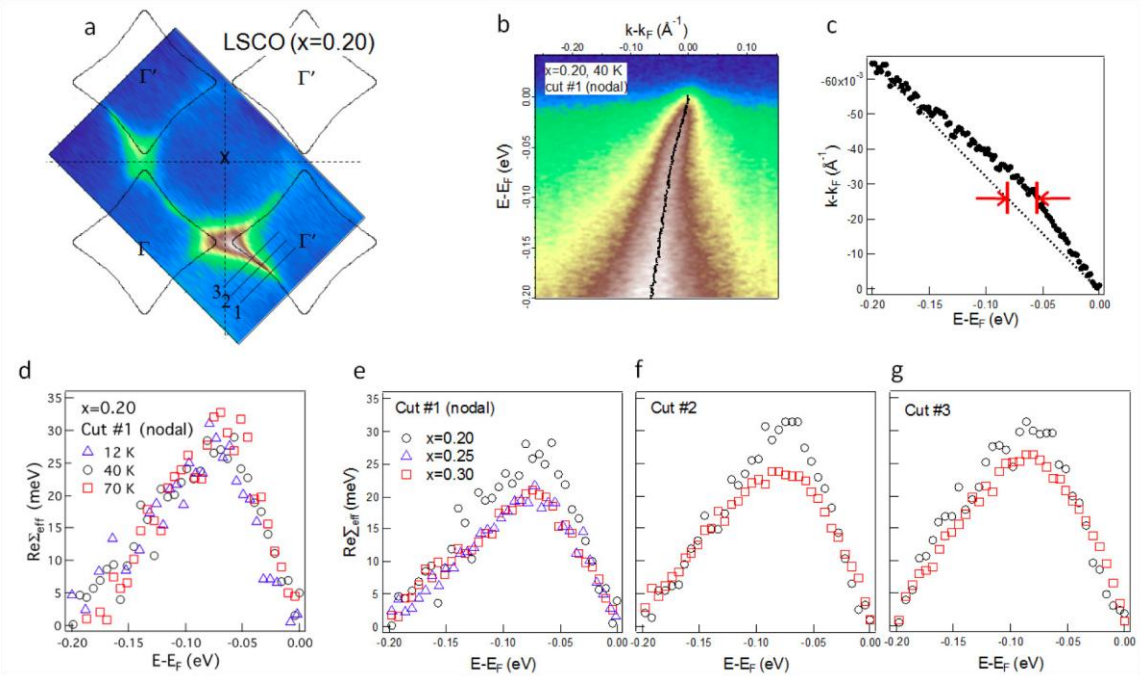

Fig. 2 Doping dependent photoemission kink. (**a**) Photoemission intensity map of $La_{2-x}Sr_xCuO_4$ (x=0.20) at the Fermi energy compared with the tight binding Fermi surfaces. Three straight lines indicate cuts where we show effective real part of the self-energy (Re(Σ_{eff})). This panel shows that the ARPES intensity of LSCO (x=0.20) at the Fermi energy is symmetric, which demonstrates accurate sample alignment. (**b**) Photoemission intensity along nodal direction of $La_{2-x}Sr_xCuO_4$ (x=0.20). Black line represents the experimental band dispersion. (**c**) Momentum distribution curve (MDC) peak positions of ARPES data shown in (b) by fitting with Lorentzian function. The kink is clearly present at about 70 meV. In order to estimate its strength it is necessary to subtract the band dispersion renormalized only by electron-electron interactions. The unrenormalized band should be linear and renormalization due to electron-electron interactions varies very smoothly as a function of energy. Thus the standard procedure followed in the vast majority of the literature is to assume that the band dispersion in the absence of the bosonic modes (bare band) is also linear. An alternative has been to assume a quadratic bare band. Since our conclusions do not depend on the functional form of the bare band, we show only the results based on a linear bare band. Dotted line, connecting peak positions between E_f and 0.2 eV binding energy, represents bare dispersion that we assumed in order to extract Re(Σ_{eff}). Red arrows indicate Re(Σ_{eff}) at about 50 meV. (**d**) Temperature dependent nodal Re(Σ_{eff}) of x=0.20. (**e,f,g**) Doping and momentum dependent Re(Σ_{eff}), whose ARPES data for x=0.20, x=0.25, and x=0.30 are taken at 40 K, 15 K and 40 K, respectively.

3. Future Plans:

We plan to continue our investigation of stripes in high temperature superconductors by investigating the copper oxides, where observing charge stripes is more challenging than in the nickelates. This work will build upon the results described in sec. 2.1. In the field of Fe-based superconductors we plan to investigate an unusual excitation at 18meV that we discovered last year (this work is still unpublished) that seems to defy all possible intrinsic and extrinsic explanations. In particular, we will focus on correlating its spectral weight with other physical

properties such as magnetic resonance peak and magnetic ordering transition temperature. During the next year we also plan to begin investigating electron-phonon coupling in electrochromic compounds by IXS.

4. References:

1. J.M. Tranquada, et al. Nature **375**, 561-563 (1995).
2. V.J. Emery, and S.A. Kivelson, Physica C 209, 507 (1993)
3. S.A. Kivelson Nature Materials **5**, 343 (2006).
4. S.A. Kivelson, et al., Rev. Mod. Phys. **75**, 1201-1241 (2003).
5. J. M. Tranquada, et al. Nature 429, 534-538 (2004).
6. V. Hinkov et al. Nature **430**, 650-654 (2004)
7. D. Reznik et al., Nature **440**, 1170 (2006).
8. D. Reznik, Physica C, in press. (Corrected proof available online at http://www.sciencedirect.com/science/article/pii/S0921453412000469.)
9. A. Lanzara et al., Nature **412**, 510 (2001).
10. P. D. Johnson et al., Phys. Rev. Lett. **87**, 177007 (2001).
11. T. Cuk et al., Phys. Rev. Lett. **93**, 117003 (2004).
12. X. J. Zhou et al., Phys. Rev. Lett. **95**, 117001 (2005).
13. D. Reznik et al., *Nature,* **455**, E6 (2008).
14. S. V. Borisenko et al., Phys. Rev. Lett. **96**, 117004 (2006).
15. C. M. Varma, Phys. Rev. B **73**, 155113 (2006).
16. J. Graf et al., Phys. Rev. Lett. **100**, 227002 (2008).

5. Publications resulting from work supported by the DOE project over the last two years.

Note: DOE support of this project began 8 months ago

1. "Effects of charge inhomogeneities on elementary excitations in $La_{2-x}Sr_xCuO_4$", S. R. Park, A. Hamann, L. Pintschovius, D. Lamago, G. Khaliullin, M. Fujita, K. Yamada, G. D. Gu, J. M. Tranquada, D. Reznik, *Phys. Rev. B,* **84**, 214516 (2011)

2. "Competition between commensurate and incommensurate magnetic ordering in $Fe_{1+y}Te$" D. Parshall, G. Chen, L. Pintschovius, D. Lamago, Th. Wolf, L. Radzihovsky, and D. Reznik, Phys. Rev. B **85**, 140515 (2012) (Rapid Communications).

3. "Phonon anomalies and dynamic stripes", D. Reznik, Invited review article to appear in a special issue of Physica C on stripes. Online publication link: http://dx.doi.org/10.1016/j.physc.2012.01.024

Session II

Correlated Electron Systems (I)

Quantum Correlated Materials and Phenomena

C. Broholm (broholm@jhu.edu)[1,2], N. P. Armitage[1], R J. Cava[4],
T.M. McQueen[1,3], O. Tchernyshyov[1] & Z. Tesanovic[1]
[1] *Department of Physics and Astronomy, Johns Hopkins University, Baltimore, MD 21218*
[2]*NIST Center for Neutron Research, NIST, Gaithersburg, MD 20899*
[3]*Department of Chemistry, Johns Hopkins University, Baltimore, MD 21218*
[4]*Department of Chemistry, Princeton University, Princeton, NJ 08544*

Research Scope

The Institute for Quantum Matter brings together expertise in materials synthesis, theory, and advanced spectroscopy to discover, understand, and control emergent properties of strongly correlated electrons. Materials that expose quantum correlated states of matter are realized and characterized through solid-state synthesis and a full complement of structural and thermo-magnetic measurements. With complementary information on the relevant length and time scales, neutron scattering and optical THz spectroscopy expose emergent properties and their connections to the underlying structure and quantum chemistry. Analytical theories are developed to uncover unifying trends, inform the materials discovery efforts, and contribute towards new ways to analyze neutron, THz, and other experimental data.

Recent Progress

Projects representing the current IQM thrusts of quantum magnetism, correlated superconductivity, and the emerging area of topological materials are summarized here. In keeping with the goal of realizing novel states of matter, a key synthesis objective has been low dimensional magnetic materials with competing quantum degrees of freedom. $LiCuSbO_4$ is such a quasi-one-dimensional frustrated quantum magnet discovered at IQM/Princeton in 2010 [18]. The inelastic data from CNCS at SNS (Fig. 1) shows the magnetic bandwidth is dramatically reduced in comparison to the unfrustrated bond energies. Under these conditions a sequence of nematic phases were predicted and are now being pursued at IQM through single crystal synthesis and high field neutron scattering.

Also discovered in the reporting period is a novel form of frustrated quantum magnetism in $LiZn_2Mo_3O_8$ [10]. Rather than residing on individual atoms, spin-1/2 degrees of freedom arise from one electron each donated by $LiZn_2$ spacing layers to triangular molybdenum clusters (Fig. 2). A reduction by a factor three in the effective moment for T<100 K indicates trimerization and novel correlated physics in this material.

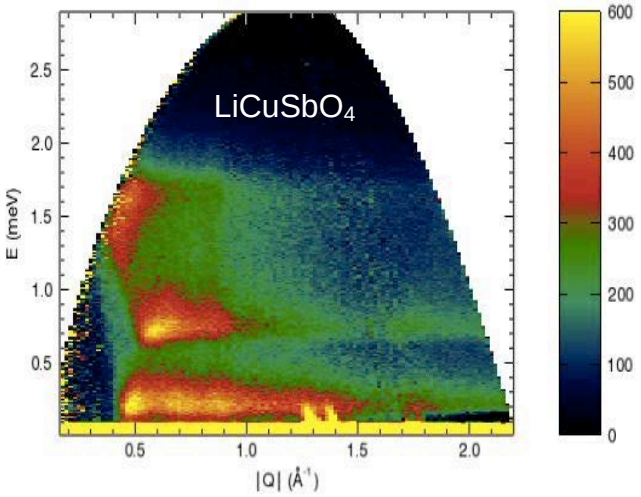

Figure 1. Inelastic neutron scattering from $LiCuSbO_4$ as measured on CNCS at SNS at T=1.8 K. The gap in the excitation spectrum is consistent with the absence of zero-field long-range order.

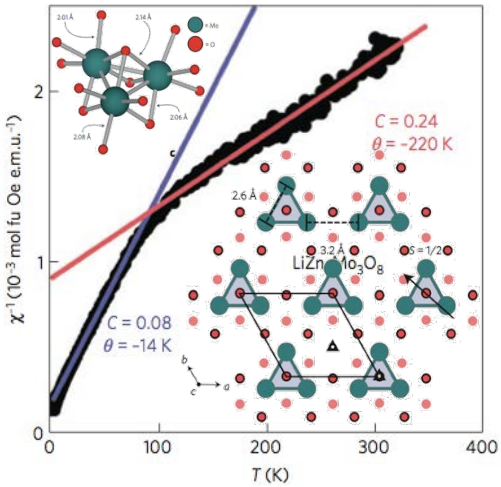

Figure 2. high T inverse susceptibility data for $LiZn_2Mo_3O_8$. The cross over indicates formation of trimers of triangles. The top left corners shows the Mo cluster that carries a spin-1/2 degree of freedom.

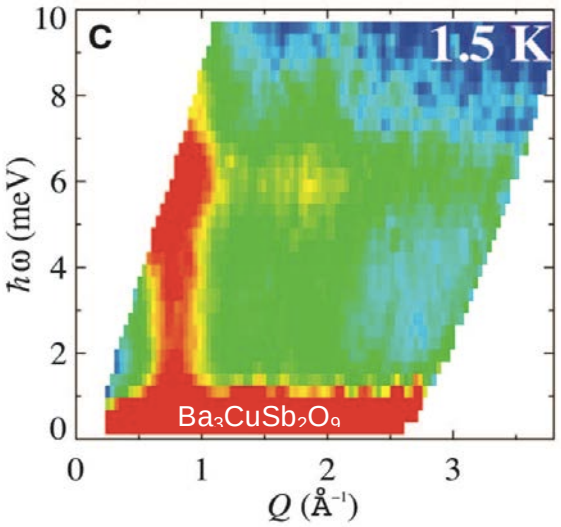

Figure 3. Inelastic neutron scattering from powder sample of $Ba_3CuSb_2O_9$ collected on the MACS spectrometer at NIST.

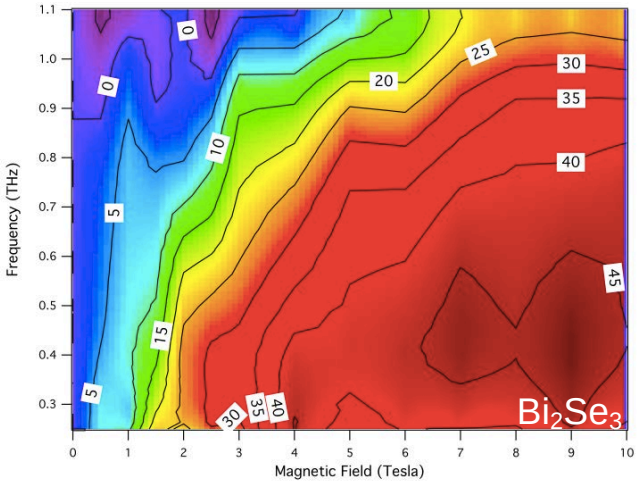

Figure 4. Absolute value of the Kerr rotation as a function of the frequency and magnetic field for a 32 layer thin film of Bi_2Se_3 at 5 K.

The absence of magnetic ordering or spin freezing in the gapless spin system down to 100 mK, leaves open the possibility of a resonating valence bond state; a hypothesis we shall shortly test on CNCS.

The central structural unit of the 6H perovskite $Ba_3CuSb_2O_9$ is the $CuSbO_9$ dumbbells in which 6-fold coordinated Cu^{2+} and Sb^{5+} are in a face-sharing configuration that carries an electric dipole moment. While the previously published structure claimed a uniform orientation of these in planes perpendicular to the 6-fold axis, we found short-range antiparallel correlations that are a consequence – during high temperature synthesis – of frustrated dipolar interactions [15]. The outcome is a nanostructured honeycomb lattice of Cu^{2+} ions that resists a coherent static Jahn-Teller distortion. The resulting two-dimensional random-bond spin-1/2 system on the honeycomb lattice has a broad spectrum of spin-dimer–like excitations (Fig. 3) and low-energy spin degrees of freedom that retain overall hexagonal symmetry.

There is now considerable interest in Ising spins with quantum dynamics on the pyrochlore lattice. Neutron scattering experiments on single crystalline $Pr_2Zr_2O_7$ using ARCS and MACS resulted in the discovery of spin-ice correlations and quantum spin excitations associated with magnetic monopoles. Theoretical work at IQM [6] showed that under a field applied along the crystalline (100) direction, such monopoles are bound by Dirac strings (Fig. 5). It is predicted that these quantum strings with monopoles at their ends manifest themselves as multiple spin-wave branches in the dynamical structure factor. Strong quantum fluctuations make the string tension negative and give rise to deconfinement of monopoles. Inspired by these predictions, large high quality $Pr_2Zr_2O_7$ single crystals are now being grown at IQM for use in high field and high-resolution neutron scattering and THz spectroscopy experiments to test the theory.

Discussions around neutron scattering experiments on quantum magnets also led to two predictions for detection of emergent particles in quantum magnets [11]. Spin-lattice coupling can mix otherwise stealthy excitations with phonons so the phonon spectral function acquires features that can be detected by neutrons scattering, Raman, and Terahertz spectroscopy. Many unconventional quantum phases are expected to host special non-magnetic excitations such as emergent photons and visons. The proposed indirect techniques could be the only or the best way to make contact with them.

In iron-based high temperature superconductivity (HTS), we have recently focused on the relationship between the real and momentum space structures. The multiply connected Fermi surfaces with their separate electron and hole pockets and the ensuing tendency toward formation of various correlated density-wave states, have unusual reflections in real space properties. Notable examples are locally

modulated structures surrounding the spin and charge

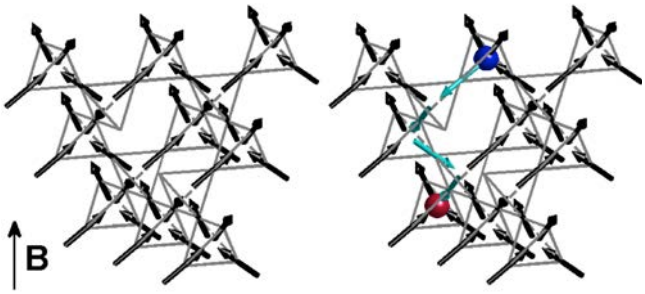

Figure 5. A (100) magnetized spin configuration satisfying the ice rules on the pyrochlore lattice (left). On the right spins were flipped to produce two magnetic monopoles linked by a Dirac string.

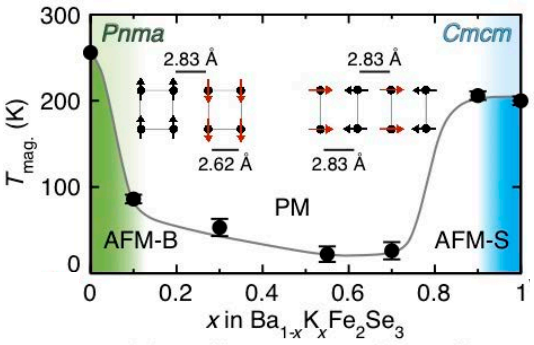

Figure 6. Phase diagram of $Ba_{1-x}K_xFe_2Se_3$, with block antiferromagnetic order (AFM-B) for small *x* and stripe AFM order (AFM-S) for large *x*.

interstitials and impurities. The details of these modulated structures, which can be observed by neutron scattering or STM, encode the inner workings of the Fermi surface correlations, turning such observations into a powerful diagnostic tool for correlated states in iron pnictides and chalcogenides. Two recently completed projects analyze such real space structures, near spinful iron interstitials [20] and near charged cobalt impurities [4].

In detailed diffraction and PDF studies of low dimensional magnetic $Ba_{1-x}K_xFe_2Se_3$ we show 2.80(8)μ_B block antiferromagnetic order of $BaFe_2Se_3$ transforms into 2.1(1)μ_B stripe antiferromagnetic order in KFe_2Se_3 (Fig. 6). The reduction is larger than expected from the change in electron count and occurs with the loss of Fe clustering. Intermediate compositions remain insulating, and magnetic susceptibility measurements show a suppression of magnetic order and probable formation of a spin glass. Reinforced by inelastic experiments on $BaFe_2Se_3$ at ARCS, the results imply an orbital-dependent selection of magnetic versus bonded behavior, driven by relative bandwidths and fillings.

Our program on quantum criticality in correlated superconductors continues apace. Theoretically, a cluster model of superconducting (and other) fluctuations was solved in [19]. Experimentally, we reported the first example of field splitting the superconducting spin resonance. The experiment was conducted on $CeCoIn_5$, where full suppression of superconductivity with a magnetic field is experimentally feasible. We found the previously detected transition into mixed magnetic-superconducting state maybe associated with the Bose-Einstein condensation of the quasi-particles associated with the resonance. THz spectroscopy performed on the related compound $CeCu_2Ge_2$ showed formation of the heavy fermion state is coincident with the occurrence of magnetic order [9], which is at odds with the conventional understanding of competing Kondo and RKKY interactions.

There are intellectual and experimental links between IQM thrusts and the fledgling area of topological insulators. The experimental link was illustrated by THz transmission measurements on thin films of Bi_2Se_3 [1,10]. The THz data are exquisitely sensitive to the topological surface states through a colossal Kerr rotation (Fig. 4), which allows experimental determination of the effective mass of the 2D Dirac electrons.

Plans for the near future

Analysis of single crystal neutron scattering experiments on frustrated magnetic materials such as $MgCr_2O_4$, $SrCr_2O_4$, $SrHo_2O_4$ that were successfully completed will be a significant focus in the coming year. Planned single crystal experiments on frustrated materials include $Pr_2Zr_2O_7$ and $Pr_2Ir_2O_7$. In addition, single crystal synthesis of frustrated quantum magnets such as $Y_2Ru_2O_7$, $LiCuSbO_4$ and

$Ba_3CuSb_2O_9$ for neutron, Raman, and THz spectroscopy is being attempted. Further work in developing the phenomenonology of the reduced dimensionality 'spin-ladder' iron chalcogenides is also in progress.

A preliminary theoretical analysis of magnetic susceptibility of $LiZn_2Mo_3O_8$ has resulted in a tentative Hamiltonian for this compound, which contains two well-separated energy scales (J = 200 K and J' = 20 K). We plan to work out a low-energy theory of this model and compare its predictions with results of thermodynamic measurements. A plausible Hamiltonian for $SrCr_2O_4$ has been deduced on the basis of spin-wave dispersions obtained through neutron scattering. Further theoretical analysis will be performed to elucidate the origin of as-yet unidentified modes in this compound, which may be hybrids of phonons and magnons.

Our theoretical program on correlated superconductors and related materials remain two-pronged: (1) We aim to elucidate new conceptual directions in investigations of emergent behavior in strongly interacting systems and, (2) utilize these new concepts to craft a useful phenomenology of new materials that can support and guide experimental efforts, at IQM and elsewhere. A theoretical description of correlated superconductors and its numerical explorations are currently being analyzed and organized for publication [4], while keeping a close eye on Armitage's ongoing THz experiments on underdoped cuprates.

In topological insulators, recent work is focusing on In doping Bi_2Se_3 through the topological transition into a conventional insulating state as well as schemes for gating these compounds. We are also revisiting the subject of high-resolution THz polarimetry applied to Bi_2Se_3.

Publications (2010-June 2012)

Submitted for Publication

1. "Aging and reduced bulk conductance in thin films of the topological insulator Bi_2Se_3", R. Valdés Aguilar, L. Wu, A. V. Stier, L. S. Bilbro, M. Brahlek, N. Bansal, S. Oh, N. P. Armitage, submitted to Phys. Rev. B (2012).
2. "Quantum Magnetic Coulomb Phase in $Pr_2Zr_2O_7$" K. Kimura, S. Nakatsuji, J.-J. Wen, C. Broholm, M. B. Stone, E. Nishibori, H. Sawa, Y. Karaki, Y. Shimura, T. Sakakibara, submitted to Science (2012).
3. "Fractionalized excitations in the spin liquid state of a kagome lattice antiferromagnet", T. H. Han, J. S. Helton, S. Chu, D. G. Nocera, J. A. Rodriguez-Rivera, C. Broholm, and Y. S. Lee, submitted to Nature (2012)
4. "Dimer impurity scattering, "reconstructed" nesting, and density-wave diagnostics in iron-pnictides," J. Kang and Z. Tesanovic, arXiv:1205.5280, Phys. Rev. B. (accepted for publication).
5. "Magnetic field splitting of the spin-resonance in $CeCoIn_5$", C. Stock, C. Broholm, Y. Zhao, F. Demmel, H. J. Kang, K. C. Rule, and C. Petrovic, arXiv:1203.2189, submitted to Phys. Rev. Lett. (2012).
6. "Quantum strings in quantum spin ice," Y. Wan and O. Tchernyshyov, arXiv:1201.5314, Phys. Rev. Lett. (accepted for publication).
7. "Magnetic charge and ordering in kagome spin ice," G.-W. Chern and O. Tchernyshyov, arXiv:1109.0275, Phil. Trans. Roy. Soc. A (accepted for publication).
8. "Correlated topological insulators of Cooper pairs induced by proximity effect," P. Nikolic and T. Duric, arXiv:1109.0017.

2012

9. "Low energy electrodynamics of the Kondo-lattice antiferromagnet $CeCu_2Ge_2$", G. Bossé, L. S. Bilbro, R. Valdés Aguilar, LiDong Pan, Wei Liu, A. V. Stier, Y. Li, L. H. Greene, J. Eckstein, and N. P. Armitage, Phys. Rev. B **85**, 155105 (2012).
10. "Terahertz Response and Colossal Kerr Rotation from the Surface States of the Topological Insulator Bi_2Se_3", R. Valdes Aguilar, A. V. Stier, W. Liu, L. S. Bilbro, D. K. George, N. Bansal, L. Wu, J.Cerne, A.G.Markelz, S.Oh, and N.P.Armitage, Phys. Rev. Lett. **108**, 087403 (2012)
11. "Detecting non-magnetic excitations in quantum magnets," Z. H. Hao, arXiv:1110.5241; Phys. Rev. B **85**, 174432 (2012).

12. "Bonding, ion mobility, and rate-limiting steps in deintercalation reactions with $ThCr_2Si_2$-type KNi_2Se_2," J.R. Neilson and T.M. McQueen, J. Am. Chem. Soc. **134**, 7750 (2012).
13. "Possible valence-bond condensation in the frustrated cluster magnet $LiZn_2Mo_3O_8$," J.P. Sheckelton, J.R. Neilson, D.G. Soltan and T.M. McQueen, Nat. Mat. **11**, 493 (2012).
14. "Orbital Selective Magnetism in the Spin-Ladder Iron Selenides $Ba_{1-x}K_xFe_2Se_3$," J.M. Caron, J.R. Neilson, D.C. Miller, K. Arpino, A. Llobet, and T.M. McQueen, Phys. Rev. B **85**, 180405(R) (2012); arXiv:1202.3676
15. "Spin-orbital short-range order on a honeycomb-based lattice," S. Nakatsuji, K. Kuga, K. Kimura, R. Satake, N. Katayama, E. Nishibori, H. Sawa, R. Ishii, M. Hagiwara, F. Bridges, T. U. Ito, W. Higemoto, Y. Karaki, M. Halim, A. A. Nugroho, J. A. Rodriguez-Rivera, M. A. Green, and C. Broholm, Science **336**, 559 (2012).
16. "Dynamical structure factor of quasi-2D antiferromagnet in high fields", W. T. Fuhrman, M. Mourigal, M. E. Zhitomirsky, and A. L. Chernyshev, arXiv:1203.1621, Phys. Rev. B **85**, 184405 (2012).
17. "Dominant ferromagnetism in the spin-1/2 half-twist ladder 334 compounds $Ba_3Cu_3In_4O_{12}$ and $Ba_3Cu_3Sc_4O_{12}$", S. E. Dutton, M. Kumar, Z. G. Soos, C. L. Broholm, and R. J. Cava, arXiv:1203.0322, J. Phys. Cond. Matter **24**, 166001 (2012).
18. "Quantum spin liquid in frustrated one dimensional $LiCuSbO_4$", S. E. Dutton, M. Kumar, M. Mourigal, Z. G. Soos, J.-J. Wen, C. L. Broholm, N. H. Andersen, Q. Huang, M. Zibri, R. Toft-Petersen, and R. J. Cava, arXiv:1109.4061, Phys. Rev. Lett., **108**, 187206 (2012).
19. "Quantum criticality for extended nodes on a Bethe lattice in the large connectivity limit," J. Murray, A. Del Maestro, and Z. Tesanovic, arXiv:1111.2011, (Editors Highlight) Phys. Rev. B **85**, 115117 (2012).
20. "Friedel-like Oscillations from Interstitial Iron in Superconducting Fe1+yTe0.62Se0.38", V. Thampy, J. Kang, J. A. Rodriguez-Rivera, W. Bao, A. T. Savici, J. Hu, T. J. Liu, B. Qian, D. Fobes, Z. Q. Mao, C. B. Fu, W. C. Chen, Q. Ye, R. W. Erwin, T. R. Gentile, Z. Tesanovic, and C. Broholm, Phys. Rev. Lett. **108**, 107002 (2012), arXiv:1109.5196.

2011

21. "On the possibility of fast vortices in the cuprates: A vortex plasma model analysis of THz conductivity and diamagnetism in $La_{2-x}Sr_xCuO_4$," L. S. Bilbro, R. Valdés Aguilar, G. Logvenov, I. Bozovic, and N. P. Armitage, Phys. Rev. B **84**, 100511(R) (2011).
22. "Magnetic properties of hole-doped SCGO, $SrCr_8Ga_{4-x}M_xO_{19}$ (M=Zn, Mg, Cu)," S. E. Dutton, E. D. Hanson, C. L. Broholm, J. S. Slusky, and R. J. Cava, J. Phys.: Condens. Matter **23**, 386001 (2011).
23. "Iron displacements and magnetoelastic coupling in the antiferromagnetic spin-ladder compound $BaFe_2Se_3$," J.M. Caron, J.R. Neilson, D.C. Miller, A. Llobet, and T.M. McQueen, Phys. Rev. B **84**, 180409 (2011), arXiv:1108.2928.
24. "Isolated vortex and vortex lattice in a holographic p-wave superconductor," J. M. Murray and Z. Tesanovic, Phys. Rev. D **83**, 126011 (2011); arXiv:1103.3232.
25. "Destruction of valence-bond order in a S=1/2 sawtooth chain with a Dzyaloshinskii-Moriya term," Z. H. Hao, Y. Wan, I. Rousochatzakis, J. Wildeboer, A. Seidel, F. Mila, and O. Tchernyshyov, Phys. Rev. B **84**, 094452 (2011); arXiv:1107.2896.
26. "^{4}He Luttinger liquid in nanopores", A. del Maestro, M. Boninsegni, and I. Affleck, Phys. Rev. Lett. **106**, 105303 (2011); arXiv:1101.2206.
27. "A wide angle neutron spin filter system using polarized 3He", C.B. Fu, T. R. Gentile, G. L. Jones, W. C. Chen, R. Erwin, S. Watson, C. Broholm, J. A. Rodriguez-Rivera, J. Scherschligt, Physica B **406**, 2419-2423 (2011).
28. "Two-stage ordering of spins in a dipolar spin ice on the kagome lattice", G.-W. Chern, P. Mellado, and O. Tchernyshyov, Phys. Rev. Lett. **106**, 207202 (2011); arXiv:0906.4781.
29. "Successive phase transitions and phase diagrams for the quasi-two-dimensional easy-axis triangular antiferromagnet $Rb_4Mn(MoO_4)_3$", R. Ishii, S. Tanaka, K. Onuma, Y. Nambu, M. Tokunaga, T. Sakakibara,

N. Kawashima, Y. Maeno, C. Broholm, D. P. Gautreaux, J. Y. Chan, and S. Nakatsuji, EPL **94**, 17001 (2011).

30. "Cooper pair insulators and theory of correlated superconductors", P. Nikolic and Z. Tesanovic, arXiv:1008.4369, (Editors Choice) Phys. Rev. B **83**, 064501 (2011).
31. "Copper-oxide superconductivity: the mystery and the mystique", Z. Tesanovic, Nature News & Views, Nature Physics **7**, 283 (2011).
32. "Sensitivity of the magnetic properties of $ZnCr_2O_4$ and $MgCr_2O_4$ to nonstoichiometry", S. E. Dutton, Q. Huang, O. Tchernyshyov, C. L. Broholm, and R. J. Cava, Phys. Rev. B **83**, 064407 (2011); arXiv:1101.0753.
33. "Helical magnetism and structural anomalies in triangular lattice alpha-$SrCr_2O_4$", S. E. Dutton, E. Climent-Pascual, P. W. Stephens, J. P. Hodges, A. Huq, C. L. Broholm, and R. J. Cava, arXiv:1102.3125, J. Phys. Condens. Matter **23**, 246005 (2011).
34. "Theory of valley-density wave and hidden order in iron-pnictides", J. Kang and Z. Tesanovic, Phys. Rev. B **83**, 020505(R) (2011); arXiv:1011.2499.
35. "Robust accidental nodes and zeroes and critical quasiparticle scaling in iron-based multiband supersonductors", V. Stanev, B. S. Alexandrov, P. Nikolic, and Z. Tesanovic, Phys. Rev. B **84**, 014505 (2011); arXiv:1006.0447.

2010

36. "Incommensurate Magnetism in FeAs Strips: Neutron Scattering from $CaFe_4As_3$", Yusuke Nambu, Liang L. Zhao, Emilia Morosan, Kyoo Kim, Gabriel Kotliar, Pawel Zajdel, Mark Green, William Ratcliff, Jose A. Rodriguez, and Collin Broholm, Phys. Rev. Lett., **106**, 037201 (2010).
37. "Temporal correlations of superconductivity above the transition temperature in $La_{2-x}Sr_xCuO_4$ probed by THz spectroscopy", L.S. Bilbro, R. Valdes-Aguilar, G. Logvenov, O. Pelleg, I. Bozovic, and N. P. Armitage, Nature Physics **7**, 298 (2011).
38. "Pair-breaking effects and coherence peak in the THz conductivity of superconducting $BaCo_{2x}Fe_{2-2x}As_2$ thin films", R. Valdes-Aguilar, L.S. Bilbro, S. Lee, C.-B. Eom, and N. P. Armitage, arXiv:1007.3677, Phys. Rev. B **82**, 180514(R) (2010).
39. "Large D-2 theory of superconducting fluctuations in magnetic field and its application to iron-pnictides", J. M. Murray and Z. Tesanovic, arXiv:1004.5277, Phys. Rev. Lett. **105**, 037006 (2010).
40. "Anisotropic and quasipropagating spin excitations in superconducting $Ba(Fe_{0.926}Co_{0.074})_2As_2$", H. F. Li, C. Broholm, D. Vaknin, R. M. Fernandes, D. L. Abernathy, M. B. Stone, D. K. Pratt, W. Tian, Y. Qiu, N. Ni, S. O. Diallo, J. L. Zarestky, S. L. Bud'ko, P. C. Canfield, and R. J. McQueeney, Phys. Rev. B **82**, 140503 (2010).
41. "Incommensurate itinerant antiferromagnetic excitations and spin resonance in the $FeTe_{0.6}Se_{0.4}$ superconductor", D. N. Argyriou, A. Hiess, A. Akbari I. Eremin, M. M. Korshunov, J. Hu, B. Qian, Z. Q. Mao, Y. M. Qiu, C. Broholm, and W. Bao, Phys. Rev. B **81**, 220503 (2010).
42. "From (pi,0) Magnetic Order to Superconductivity with (pi,pi) Magnetic Resonance in $Fe_{1.02}(Te_{1-x}Se_x)$", T.J. Liu, J. Hu, B. Qian, D. Fobes, Z.Q. Mao, W. Bao, M. Reehuis, S.A.J. Kimber, K. Prokes, S. Matas, D.N. Argyriou, A. Hiess, A. Rotaru, H. Pham, L. Spinu, Y. Qiu, V. Thampy, A.T. Savici, J. A. Rodriguez, and C. Broholm, Nature Materials **9**, 716 (2010).
43. "Divergent effects of static disorder and hole doping in geometrically frustrated beta-$CaCr_2O_4$", S. E. Dutton, R. J. Cava, and C. Broholm, J. Solid State Chem. **183**, 1798 (2010); arXiv:1004.1390.
44. "Structure factor of low-energy spin excitations in a S=1/2 kagome antiferromagnet", Z. H. Hao and O. Tchernyshyov, arXiv:1004.2293, Phys. Rev. B **81**, 214445 (2010).
45. "Paramagnetic spin correlations in $CaFe_2As_2$ single crystals", S. O. Diallo, D. K. Pratt, R. M. Fernandes, W. Tian, J. L. Zarestky, M. Lumsden, T. G. Perring, C. L. Broholm, N. Ni, S. L. Bud'ko, P. C. Canfield, H.-F. Li, D. Vaknin, A. Kreyssig, A. I. Goldman, and R. J. McQueeney, Phys. Rev. B **81**, 214407 (2010).

46. "Control of Tetrahedral Coordination and Superconductivity in $FeSe_{0.5}Te_{0.5}$ Thin Films", S. X. Huang, C. L. Chien, V. Thampy, and C. Broholm, Phys. Rev. Lett. **104**, 217002 (2010).
47. “Three-band superconductivity and time-reversal breaking order parameter”, V. Stanev and Z. Tesanovic, arXiv:0912.5214, Phys. Rev. B **81**, 134522 (2010).
48. "Quantum 120° model on pyrochlore lattice: Orbital ordering in MnV_2O_4," G.-W. Chern, N. Perkins, and Z.H. Hao, Phys. Rev. B **81**, 125127 (2010).
49. "Magnetic monopoles: No longer on thin ice," News & Views, O. Tchernyshyov, Nature Physics **6**, 323 (2010).
50. "Progress and perspectives in the electron-doped cuprates", N. P. Armitage, P. Fournier, and R. L. Greene, Rev. Mod. Phys. **82**, 2421 (2010).

Correlations and Competition Between the Lattice, Electrons, and Magnetism

R. J. McQueeney (mcqueeney@ameslab.gov), V. P. Antropov, A. I. Goldman, B. N. Harmon, A. Kreyssig, D. Vaknin, J. L. Zarestky

Ames Laboratory and Dept. of Physics and Astronomy, Iowa State University, Ames, IA 50011

Program Scope

The properties of modern novel materials, such as high-temperature superconductors, charge/orbital ordering systems, and multiferroics, are all sensitively controlled by correlations and competition among the lattice, electronic, and magnetic degrees-of-freedom. A complete understanding of the interrelations between these different subsystems and the necessary conditions for enhancing or tailoring desirable physical properties has been identified as a Grand Challenge to the scientific community. Neutron and x-ray scattering are powerful probes that directly investigate the structural, electronic, and magnetic aspects of complex ground states, phase transitions, and corresponding excitations. Any one of the many different scattering techniques alone can reveal detailed information about the underlying physics. Within this FWP, the varied expertise of the PIs in different scattering methods is employed in a synergistic approach and systems are studied using a wide range of neutron and x-ray techniques. The experimental program is supported by a closely coupled effort in *ab initio* band structure calculations, theoretical modeling, and scattering simulations. The emphasis of close coupling between different scattering techniques and theory is the unique approach of this FWP.

Recent Progress

The FWP is currently investigating several important systems, such as; the AFe$_2$As$_2$ (A = Ca, Sr, Ba) and RFeAsO (R = rare-earth) families of high-temperature superconductors, LiMPO$_4$ (M = Fe,Co,Ni) magnetoelectric compounds, and RFeO$_3$ and RBaFe$_2$O$_5$ (R = rare earth) based charge ordered systems. Over the last few years, the study of Fe-based superconductors have been the focal point of this FWP. At the previous PI meeting, we reported several new discoveries in the iron-based superconductors. We were among the first groups to report the strong coupling between magnetism and structure, as illustrated by the observation of a simultaneous transition from a paramagnetic, tetragonal (T) phase to an antiferromagnetic (AFM) ordered, orthorhombic (O) phase.[1] Chemical doping reduces both the AFM ordering and structural transition temperatures and the superconducting (SC) state appears. While reduction of the AFM and T-O transition temperatures is necessary for SC to occur, our previous studies have shown that the transitions need not be completely suppressed, and SC and long-range AFM order can coexist in "underdoped" (UD) compositions. We have observed that both the static AFM order [2] and O-lattice distortion [P14] are significantly suppressed below T_C. The suppression of the static AFM order in the SC state can be understood from the competition between the energy gaps formed from spin-density wave antiferromagnetism and SC for electrons on the Fermi surface.[P8] Thus, even beyond their intrinsic interest as a new class of high temperature SC, the iron-based superconductors continue to provide a nearly ideal family of compounds to explore the fundamental relationships between lattice, electronic and magnetic degrees of freedom.

Over the last two years, we have continued to investigate the iron-based superconductors and our major emphasis has turned to the study of the systematic evolution of materials properties with chemical doping. Perhaps the most well studied system by our group is the Ba(Fe$_{1-x}$Co$_x$)$_2$As$_2$ system. With fine control of the Co composition, we discovered that the well-known

commensurate stripe AFM order gives way to incommensurate AFM ordering over a narrow range of composition ($0.56 < x < 0.6$).[P38] A susceptibility towards incommensurate order in the iron-based superconductors had long been predicted based on density-functional theory. Similar to the suppression of AFM order itself, we show that the development of incommensurate AFM order with doping can also be understood qualitatively in a simple rigid band model.

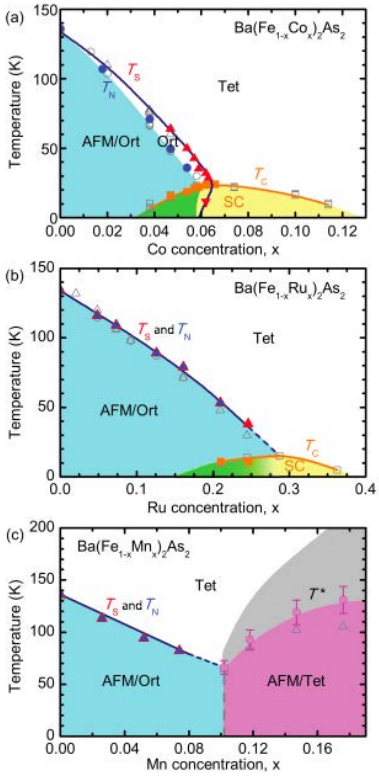

FIG. Phase diagrams transition metal substituted $BaFe_2As_2$. (a) Co (electron-doped), (b) Ru (isovalent), and (c) Mn (hole-doped).[P36]

The surprisingly successful rigid band model applies to Co-doped $BaFe_2As_2$ by simply assuming that each Co donates an electron to the conduction band, thereby changing the sizes of electron and hole Fermi pockets which in turn modifies the nesting condition. It is worthwhile to investigate whether such a simple picture applies to other metal dopants in $Ba(Fe_{1-x}M_x)_2As_2$. To complement our detailed understanding of the behavior of Co-doped $BaFe_2As_2$, we have systematically investigated different chemical dopants with an eye towards unraveling the different roles of charge carrier doping, disorder, and magnetic impurities. Phase diagrams for some of these systems as determined by neutron and x-ray scattering are shown in the figure. We found that Rh doping (in the same column of the Periodic Table as Co) behaves identically to Co-doping, including the suppression of AFM ordering below T_C in underdoped samples, further supporting the rigid band model.[P9] Very recent investigations have examined the role that electron doping and impurity scattering play in both the suppression of T_N and the appearance of incommensurate AFM order with M = Co, Ni, Cu.[P64] We find that Co and Ni follow the rigid band picture while Cu, with the strongest impurity scattering, does not. The strength of the Cu impurity scattering may also explain why SC is absent in this compound.

On the other hand, Ru substitutions are nominally isovalent to Fe and while much more Ru substitution (~20%) is required to induce superconductivity, the behavior of the magnetism, including the suppression of AFM ordering below T_C, is quite similar to Co doping.[P36] Such behavior in the Ru system highlights the potential importance of disorder and magnetic dilution as another method for inducing superconductivity via the suppression of AFM order.

Finally, we have investigated the nominally hole-doped series $Ba(Fe_{1-x}Mn_x)_2As_2$. Despite the appearance of SC in hole-doped $Ba_{1-x}K_xFe_2As_2$, Mn doping rather induces a competing magnetic state for $x > 10\%$.[P23] This new magnetic state is peculiar in that the magnetic propagation vector is identical to the stripe AFM state [$\mathbf{Q}_{AFM} = (1/2,1/2,1)$], however the attendant T-O transition is absent, suggesting that the new magnetic state possesses four-fold symmetry. A possible candidate for the new magnetic state is a non-collinear $2\mathbf{Q}_{AFM}$ structure. Recent preliminary inelastic neutron scattering data for $x = 7\%$ show that Mn-doping gives rise to spin fluctuations from a competing checkerboard AFM state at wavevector $\mathbf{Q}_{CB} = (1,0,1)$.[P65]

This fascinating behavior of the Mn-doped system has inspired investigations of the magnetic excitations in the parent $BaMn_2As_2$ compound, which is found to be local moment insulator with checkerboard AFM order.[3] We find that the excitations are quasi-2D and consistent with the

J_1-J_2 Heisenberg model commonly used to discuss the magnetic dynamics in the iron arsenide compounds, although the nearest-neighbor exchange (J_1) is dominant in $BaMn_2As_2$. Due to its similarity to the AFM insulating copper oxide superconductors, carrier doping of $BaMn_2As_2$ may reveal yet another class of unconventional superconductors. We have found that K substitutions do induce metallic behavior in $BaMn_2As_2$, however strong AFM ordering (T_N > 500 K) remains, suggesting that charge conductivity and AFM order are independent of one another.[P60]

Future Plans

Our studies of the systematic dependence of the magnetic, structural, and superconducting properties of the iron-based superconductors with transition metal substitution has identified several new research directions. One direction is to perform inelastic studies of the spin fluctuations for different transition metal substitutions and compositions. Our earlier work discovered a strong anisotropy of spin fluctuations in the Fe layer in the paramagnetic state of $CaFe_2As_2$ [P7] and $Ba(Fe_{0.926}Co_{0.074})_2As_2$ [P25], including the development of novel diffuse magnetic modes propagating at very high energies along the ferromagnetic direction (perpendicular to $\mathbf{Q}_{AFM}$). A central goal is to determine the nature of the excitations in underdoped compositions, i.e. whether they are predominantly spin-wave like or of a different nature, such as Stoner excitations or longitudinal excitations predicted by our *ab initio* calculations of the dynamical susceptibility. Such a distinction, if possible, presents stringent limitations on theories of spin fluctuation-induced SC that can appear in a system with long-range AFM order. The tunability of the electron-doped systems will also allow us to study how the spin resonance evolves from underdoped compositions with strong AFM order and weak SC ($T_N/T_C >> 1$) to the optimally doped compounds with an absence of AFM order. This includes the study of nematic fluctuations, where the spin-space anisotropy is broken without long-range AFM order. Finally, we will extend these inquiries to address spin fluctuations in the LaFeAsO system, where we have obtained a single-crystal sample large enough for inelastic studies.

Our current research has opened up new directions with the intent to test the applicability of the rigid band model and the role that disorder and impurity scattering plays in the development of AFM order and superconductivity. Different kinds of transition metal substitutions are currently being examined to ascertain differences in the magnetic and structural behavior, such as incommensurability. This will be extended to include $Ca(Fe_{1-x}Co_x)_2As_2$, where strong magnetoelastic coupling leads to a competing non-magnetic collapsed tetragonal phase.

Lastly, we will extend our inelastic studies of $Ba(Fe_{1-x}Mn_x)_2As_2$ to include those compositions where the new magnetic structure is observed (x > 10%). This should help us to understand how strong magnetic Mn impurities can coalesce to form the new magnetic state. On the Mn-rich side, inelastic studies of $Ba_{1-x}K_xMn_2As_2$ will address how robust local moment AFM order and metallic conduction can coexist in this nominal copper oxide prototype.

References (citations starting with "P" are from Publications list)

1. A. I. Goldman, *et al*., Phys. Rev. B **78**, 100506 (2008).
2. D. K. Pratt, *et al.*, Phys. Rev. Lett. **103**, 087001 (2009).
3. Y. Singh, *et al.*, Phys. Rev. B **80**, 100403 (2009).
4. A. Kreyssig, *et al.*, Phys. Rev. B **78**, 184517 (2008).

Publications (FY2010-2012, 65 total)

1. *Intrinsic Pinning on Structural Domains in Underdoped Single Crystals of $Ba(Fe_{1-x}Co_x)_2As_2$*
   R. Prozorov, M.A. Tanatar, N. Ni, A. Kreyssig, S. Nandi, S.L. Bud'ko, A.I. Goldman, P.C. Canfield
   Phys. Rev. B, **80**, 174517 (2009).
2. *Single-crystal Neutron Diffraction Study of Short-range Magnetic Correlations in Tb_5Ge_4*
   W. Tian, A. Kreyssig, J.L. Zarestky, L. Tan, S. Nandi, A.I. Goldman, T.A. Lograsso, D.L. Schlagel, K.A. Gschneidner, V.K. Pecharsky, R.J. McQueeney
   Phys. Rev. B, **80**, 134422 (2009).
3. *Flux Growth at Ambient Pressure of Millimeter-sized Single Crystals of LaFeAsO*
   $LaFeAsO_{1-x}F_x$, and $LaFe_{1-x}Co_xAsO$"
   J.Q. Yan, S. Nandi, J.L. Zarestky, W. Tian, A. Kreyssig, B. Jensen, A. Kracher, K.W. Dennis, R.J. McQueeney, A.I. Goldman, R.W. McCallum, T.A. Lograsso
   Appl. Phys. Lett., **95**, 222504 (2009).
4. *Anisotropy of Antiferromagnetic 180° Domains in Magnetoelectric $LiMPO_4$ (M = Fe, Co, Ni)*
   A.S. Zimmermann, B.B. Van Aken, H. Schmid, J.P. Rivera, J. Li, D. Vaknin, M. Fiebig
   Euro. Phys. J. B, **71**, 355 (2009).
5. *Enhanced Ordering Temperatures in Antiferromagnetic Manganite Superlattices*
   S.J. May, P.J. Ryan, J.L. Robertson, J.W. Kim, T.S. Santos, E. Karapetrova, J.L. Zarestky, X. Zhai, S.G.E. te Velthuis, J.N. Eckstein, S.D. Bader, A. Bhattacharya
   Nat. Mater., **8**, 892 (2009).
6. *Solution Growth of a Binary Icosahedral Quasicrystal of $Sc_{12}Zn_{88}$*
   P.C. Canfield, M.L. Caudle, C.S. Ho, A. Kreyssig, S. Nandi, M.G. Kim, X. Lin, A. Kracher, K.W. Dennis, R.W. McCallum, A.I. Goldman
   Phys. Rev. B, **81**, 020201 (2010).
7. *Paramagnetic Spin Correlations in $CaFe_2As_2$ Single Crystals*
   S.O. Diallo, D.K. Pratt, R.M. Fernandes, W. Tian, J.L. Zarestky, M. Lumsden, T.G. Perring, C.L. Broholm, N. Ni, S.L. Bud'ko, P.C. Canfield, H.F. Li, D. Vaknin, A. Kreyssig, A.I. Goldman, R.J. McQueeney
   Phys. Rev. B, **81**, 214407 (2010).
8. *Unconventional Pairing in the Iron Arsenide Superconductors*
   R.M. Fernandes, D.K. Pratt, W. Tian, J. Zarestky, A. Kreyssig, S. Nandi, M.G. Kim, A. Thaler, N. Ni, P.C. Canfield, R.J. McQueeney, J. Schmalian, A.I. Goldman
   Phys. Rev. B, **81**, 140501 (2010).
9. *Suppression of Antiferromagnetic Order and Orthorhombic Distortion in Superconducting $Ba(Fe_{0.961}Rh_{0.039})_2As_2$*
   A. Kreyssig, M.G. Kim, S. Nandi, D.K. Pratt, W. Tian, J.L. Zarestky, N. Ni, A. Thaler, S.L. Bud'ko, P.C. Canfield, R.J. McQueeney, A.I. Goldman
   Phys. Rev. B, **81**, 134512 (2010).
10. *Magnetic Form Factor of Iron in $SrFe_2As_2$*
    Y. Lee, D. Vaknin, H.F. Li, W. Tian, J.L. Zarestky, N. Ni, S.L. Bud'ko, P.C. Canfield, R.J. McQueeney, B.N. Harmon
    Phys. Rev. B, **81**, 060406 (2010)
11. *Soft X-ray Resonant Scattering Study of Single-crystal $LaSr_2Mn_2O_7$*
    H.F. Li, Y. Su, T. Chatterji, A. Nefedov, J. Persson, P. Meuffels, Y. Xiao, D. Vaknin, T. Bruckel
    Euro. Phys. J. B, **74**, 457 (2010).
12. *Phase Transitions and Iron-ordered Moment Form Factor in LaFeAsO*
    H.F. Li, W. Tian, J.Q. Yan, J.L. Zarestky, R.W. McCallum, T.A. Lograsso, D. Vaknin
    Phys. Rev. B, **82**, 064409 (2010).
13. *Experimental and Computer Simulation Determination of the Structural Changes Occurring Through the Liquid-glass Transition in Cu-Zr Alloys*
    M.I. Mendelev, M.J. Kramer, R.T. Ott, D.J. Sordelet, M.F. Besser, A. Kreyssig, A.I. Goldman, V. Wessels, K.K. Sahu, K.F. Kelton, R.W. Hyers, S. Canepari, J.R. Rogers
    Phil. Mag., **90**, 3795 (2010).
14. *Anomalous Suppression of the Orthorhombic Lattice Distortion in Superconducting $Ba(Fe_{1-x}Co_x)_2As_2$ Single Crystals*
    S. Nandi, M.G. Kim, A. Kreyssig, R.M. Fernandes, D.K. Pratt, A. Thaler, N. Ni, S.L. Bud'ko, P.C. Canfield, J. Schmalian, R.J. McQueeney, A.I. Goldman
    Phys. Rev. Lett., **104**, 057006 (2010).

15. *Synthesis, Structure, and Properties of Tetragonal $Sr_2M_3As_2O_2$ (M_3=Mn_3, Mn_2Cu, and $MnZn_2$) Compounds Containing Alternating CuO_2-type and FeAs-type Layers*
    R. Nath, V.O. Garlea, A.I. Goldman, D.C. Johnston
    Phys. Rev. B, **81**, 224513 (2010).
16. *Dispersion of the Superconducting Spin Resonance in Underdoped and Antiferromagnetic $BaFe_2As_2$*
    D.K. Pratt, A. Kreyssig, S. Nandi, N. Ni, A. Thaler, M.D. Lumsden, W. Tian, J.L. Zarestky, S.L. Bud'ko, P.C. Canfield, A.I. Goldman, R.J. McQueeney
    Phys. Rev. B, **81**, 140510 (2010).
17. *Evidence from Neutron Diffraction for Superconductivity in the Stabilized Tetragonal Phase of $CaFe_2As_2$ Under Uniaxial Pressure*
    K. Prokes, A. Kreyssig, B. Ouladdiaf, D.K. Pratt, N. Ni, S.L. Bud'ko, P.C. Canfield, R.J. McQueeney, D.N. Argyriou, A.I. Goldman
    Phys. Rev. B, **81**, 180506 (2010).
18. *Magnetism and Exchange Coupling in Iron Pnictides*
    J.J. Pulikkotil, L. Ke, M. van Schilfgaarde, T. Kotani, V.P. Antropov
    Supercond. Sci. & Technology, **23**, 054012 (2010).
19. *Zero Field Magnetic Phase Transitions and Anomalous Low Temperature Upturn in Resistivity of Single Crystalline α-$TmAlB_4$*
    N.H. Sung, A. Kreyssig, H. Kim, M.A. Tanatar, J.S. Rhyee, B.Y. Kang, M.G. Kim, J.Y. Kim, P.C. Canfield, R. Prozorov, A.I. Goldman, B.K. Cho
    J. Appl. Phys., **107**, 09e148 (2010).
20. *Uniaxial-strain Mechanical Detwinning of $CaFe_2As_2$ and $BaFe_2As_2$ Crystals: Optical and Transport Study*
    M.A. Tanatar, E.C. Blomberg, A. Kreyssig, M.G. Kim, N. Ni, A. Thaler, S.L. Bud'ko, P.C. Canfield, A.I. Goldman, I.I. Mazin, R. Prozorov
    Phys. Rev. B, **81**, 184508 (2010).
21. *Magnetic Order in $TbCo_2Zn_{20}$ and $TbFe_2Zn_{20}$*
    W. Tian, A.D. Christianson, J.L. Zarestky, S. Jia, S.L. Bud'ko, P.C. Canfield, P.M.B. Piccoli, A.J. Schultz
    Phys. Rev. B, **81**, 144409 (2010).
22. *Neutron Diffraction Investigation of the Crystal and Magnetic Structures in $KCrF_3$ Perovskite*
    Y. Xiao, Y. Su, H.F. Li, C.M.N. Kumar, R. Mittal, J. Persson, A. Senyshyn, K. Gross, T. Brueckel
    Phys. Rev. B, **82**, 094437 (2010).
23. *Antiferromagnetic Ordering in the Absence of Structural Distortion in $Ba(Fe_{1-x}Mn_x)_2As_2$*
    M.G. Kim, A. Kreyssig, A. Thaler, D.K. Pratt, W. Tian, J.L. Zarestky, M.A. Green, S.L. Bud'ko, P.C. Canfield, R.J. McQueeney A.I. Goldman
    Phys. Rev. B, **82**, 220503 (2010).
24. *Commensurate antiferromagnetic ordering in $Ba(Fe_{1-x}Co_x)_2As_2$ determined by x-ray resonant magnetic scattering at the Fe K-edge*
    M.G. Kim, A. Kreyssig, Y.B. Lee, J.W. Kim, D.K. Pratt, A. Thaler, S.L. Bud'ko, P.C. Canfield, B.N. Harmon, R.J. McQueeney A.I. Goldman
    Phys Rev. B, **82**, 180412(R) (2010).
25. *Anisotropic and Quasipropagating Spin Excitations in Superconducting $Ba(Fe_{0.926}Co_{0.074})_2As_2$*
    H.F. Li, C. Broholm, D. Vaknin, R.M. Fernandes, D.L. Abernathy, M.B. Stone, D.K. Pratt, W. Tian, Y. Qiu, N. Ni, S.O. Diallo, J.L. Zarestky, S.L. Bud'ko, P.C. Canfield R.J. McQueeney
    Phys. Rev. B, **82**, 140503 (2010).
26. *Potassium tantalate substrates for neutron experiments on antiferromagnetic perovskite films*
    H.M Christen, G.J. MacDougall, H-S Kim, D.H. Kim, L.A. Boatner, C.J. Callender, J.L. Zarestky, S.E. Nagler
    J. Physics: Conf. Series, **251** 021021 (2010).
27. *Magnetic structure of epitaxial multiferroic $BiFeO_3$ films with engineered ferroelectric domains*
    X. Ke, P.P. Zhang, S.H. Baek, J. Zarestky, W. Tian, C.B. Eom
    Phys. Rev. B, **82**, 134448 (2010).
28. *Relation between superconductivity and tetragonal phase stabilized by uniaxial pressure in $CaFe_2As_2$*
    K. Prokeš , A. Kreyssig , B. Ouladdiaf, D.K. Pratt , N. Ni , S.L. Bud'ko , P.C. Canfield , R.J. McQueeney, A.I. Goldman, D.N. Argyriou
    J. Phys. **273**, 012102 (2011).
29. *Character of the structural and magnetic phase transitions in the parent and electron-doped $BaFe_2As_2$ compounds*

M.G. Kim, R.M. Fernandes, A. Kreyssig, J.W. Kim, A. Thaler, S.L. Bud'ko, P.C. Canfield, R.J. McQueeney, J. Schmalian, A.I. Goldman
Phys. Rev. B, **83**, 134522 (2011).

30. *Rapid chemical and topological ordering in supercooled liquid $Cu_{46}Zr_{54}$*
V. Wessels, A.K. Gangopadhyay, K.K. Sahu, R.W. Hyers, S.M. Canepari, J.R. Rogers, M.J. Kramer, A.I. Goldman, D. Robinson, J.W. Lee, J.R. Morris, K.F. Kelton
Phys. Rev. B, **83**, 134522 (2011).
31. *Neutron Scattering Studies of $LiCoPO_4$ and $LiMnPO_4$*
W. Tian, J.Y. Li, H.F. Li, J.W. Lynn, J.L. Zarestky, D. Vaknin
J. Physics: Conf. Series, **251** 012005 (2010).
32. *Temperature Dependence of Low-Energy Phonons in Magnetic Nonsuperconducting $TbNi_2B_2C$*
S. Anissimova, A. Kreyssig, O. Stockert, M. Loewenhaupt, D. Reznik
Phys. Rev. B, **84**, 104509 (2011).
33. *In-Plane Anisotropy of Electrical Resistivity in Strain-Detwinned $SrFe_2As_2$*
E.C. Blomberg, M.A. Tanatar, A. Kreyssig, N. Ni, A. Thaler, R.W. Hu, S.L. Bud'ko, P.C. Canfield, A.I. Goldman, R. Prozorov
Phys. Rev. B, **83**, 134505 (2011).
34. *High-Energy X-Ray Diffraction Studies of i-$Sc_{12}Zn_{88}$*
A.I. Goldman, A. Kreyssig, S. Nandi, M.G. Kim, M.L. Caudle, P.C. Canfield
Phil. Mag., **91**, 2427 (2011).
35. *Low-Energy Coherent Stoner-Like Excitations in $CaFe_2As_2$*
L.Q. Ke, M. van Schilfgaarde, J.J. Pulikkotil, T.K. Kotani,V. Antropov
Phys. Rev. B, **83**, 060404 (2011).
36. *Magnetic Ordering and Structural Distortion in Ru-Doped $BaFe_2As_2$ Single Crystals Studied by Neutron and X-Ray Diffraction*
M.G. Kim, D.K. Pratt, G.E. Rustan, W. Tian, J.L. Zarestky, A. Thaler, S.L. Bud'ko, P.C. Canfield, R.J. McQueeney, A. Kreyssig, A.I. Goldman
Phys. Rev. B, **83**, 054514 (2011).
37. *Competing Magnetic Ground States in Nonsuperconducting $Ba(Fe_{1-x}Cr_x)_2As_2$ as Seen Via Neutron Diffraction*
K. Marty, A.D. Christianson, C.H. Wang, M. Matsuda, H. Cao, L.H. VanBebber, J.L. Zarestky, D.J. Singh, A.S. Sefat, M.D. Lumsden
Phys. Rev. B, **83**, 060509 (2011).
38. *Incommensurate Spin-Density Wave Order in Electron-Doped $BaFe_2As_2$ Superconductors*
D.K. Pratt, M.G. Kim, A. Kreyssig, Y.B. Lee, G.S. Tucker, A. Thaler, W. Tian, J.L. Zarestky, S.L. Bud'ko, P.C. Canfield, B.N. Harmon, A.I. Goldman, R.J. McQueeney
Phys. Rev. Lett., **106**, 257001 (2011).
39. *Magnetization Distribution in the Tetragonal $Ba(Fe_{1-x}Co_x)_2As_2$, x=0.066 Probed by Polarized Neutron Diffraction*
K. Prokes, A. Gukasov, D.N. Argyriou, S.L. Bud'ko, P.C. Canfield, A. Kreyssig, A.I. Goldman
Euro. Phys. Lett., **93**, 32001 (2011).
40. *Stabilization of an Ambient-Pressure Collapsed Tetragonal Phase in $CaFe_2As_2$ and Tuning of the Orthorhombic-Antiferromagnetic Transition Temperature by over 70 K Via Control of Nanoscale Precipitates*
S. Ran, S.L. Bud'ko, D.K. Pratt, A. Kreyssig, M.G. Kim, M.J. Kramer, D.H. Ryan, W.N. Rowan-Weetaluktuk, Y. Furukawa, B. Roy, A.I. Goldman, P.C. Canfield
Phys. Rev. B, **83**, 144517 (2011).
41. *High-Field Magnetic Phase Transitions and Spin Excitations in Magnetoelectric $LiNiPO_4$*
R. Toft-Petersen, J. Jensen, T.B.S. Jensen, N.H. Andersen, N.B. Christensen, C. Niedermayer, M. Kenzelmann, M. Skoulatos, M.D. Le, K. Lefmann, S.R. Hansen, J.Y. Li, J.L. Zarestky, D. Vaknin
Phys. Rev. B, **84**, 054408 (2011).
42. *Consistent Model of Magnetism in Ferropnictides*
A.L. Wysocki, K.D. Belashchenko. V.P. Antropov
Nat. Phys., **7**, 485 (2011).
43. *Magnetic order in GdBiPt studied by x-ray resonant magnetic scattering*
A. Kreyssig, M.G. Kim, J.W. Kim, S.M. Sauerbrei, S.D. March, G.R. Tesdall, S.L. Bud'ko, P.C. Canfield, R.J. McQueeney, A.I. Goldman
Phys. Rev. B, **84**, 220408(R) (2011).

44. *Role of Magnetic Exchange Energy on Charge Ordering in $R_{1-x}Sr_xFeO_3$ (R=La, Pr, and Nd)*
J. Ma, J.-Q. Yan, S.O. Diallo, R. Stevens, A. Llobet, F. Trouw, D.L. Abernathy, M.B. Stone, R.J. McQueeney
Phys. Rev. B, **84**, 224115 (2011).
45. *Spin-state transitions in $PrCoO_3$ studied with neutron powder diffraction*
Y. Ren, J.-Q. Yan, J.-S. Zhou, J.B. Goodenough, J.D. Jorgensen, S. Short, H.-J. Kim, Th. Proffen, S. Chang, R.J. McQueeney
Phys. Rev. B, **84**, 214409 (2011).
46. *Spin and orbital ordering in $Y_{1-x}La_xVO_3$*
J.-Q. Yan, J.-S. Zhou, J.G. Cheng, J.B. Goodenough, Y. Ren, A. Llobet, R.J. McQueeney,
Phys. Rev. B, **84**, 214405 (2011).
47. *Magnetic Exchange Interactions in $BaMn_2As_2$: A Case Study of the J_1-J_2-J_c Heisenberg Model*
D.C. Johnston, R. J. McQueeney, B. Lake, A. Honecker, M.E. Zhitomirsky, R. Nath, Y. Furukawa, V.P. Antropov, Yogesh Singh
Phys. Rev. B, **84**, 094445 (2011).
48. *Anisotropic magnetoelastic coupling in single-crystalline CeFeAsO as seen via high-resolution x-ray diffraction*
H.F. Li, J.Q. Yan, J.W. Kim, R.W. McCallum, T.A. Lograsso, D. Vaknin,
Phys. Rev. B, **85**, 220501 (2011).
49. *Delta Doping of Ferromagnetism in Antiferromagnetic Manganite Superlattices*
T.S. Santos, B.J. Kirby, S. Kumar, S.J. May, J.A. Borchers, B.B. Maranville, J.L. Zarestky, S.G.E Te Velthuis, J. van den Brink, A. Bhattacharya,
Phys. Rev. Lett., **107**, 167202 (2011).
50. *Kinetically inhibited order in a diamond-lattice antiferromagnet*
G.J. MacDougall, D. Gout, J.L. Zarestky, G. Ehlers, A. Podlesnyak, M.A. McGuire, D. Mandrus, S.E. Nagler
PNAS **108**, 15693 (2011).
51. *Antiferromagnetic order and superlattice structure in nonsuperconducting and superconducting $Rb_yFe_{1.6+x}Se_2$*
M. Wang, M. Wang G.N. Li, Q. Huang C.H. Li, G.T. Tan, C.L. Zhang, H. Cao, W. Tian, Y. Zhao, Y.C. Chen, X.Y. Lu, B. Sheng, H.Q. Luo, S.L. Li, M.H. Fang, J.L. Zarestky, W. Ratcliff, M.D. Lumsden, J.W. Lynn, P. Dai
Phys. Rev. B, **84**, 094504 (2011).
52. *Spin waves and magnetic exchange interactions in insulating $Rb_{0.89}Fe_{1.58}Se_2$*
M, Wang, C. Fang, D-X Yao, G-T Tan, L.W. Harriger, Y. Song, T. Netherton, C. Zhang, M. Wang, M.B. Stone, W. Tian, J. Hu, P. Dai
Nat. Commun., **2**, 580 (2011).
53. *Phonons of the anomalous element cerium*
M. Krisch, D.L. Farber, R. Xu, D. Antonangeli, C.M. Aracne, A. Beraud, T-C Chiang, J.L. Zarestky, D-Y Kim, E.I. Isaev, R. Ahuja, B. Johansson
PNAS, **108**, 9342 (2011).
54. *Zn-Doping Dependence of Stripe Order in $La_{1.905}Ba_{0.095}CuO_4$*
M. Hucker, M. von Zimmermann, Z.J. Xu, J.S. Wen, G.D. Gu, W. Tian, J.L. Zarestky, J.M. Tranquada
J. Supercond. and Novel Magnet., **24**, 1229 (2011).
55. *Emergent electronic and magnetic state in $Ca_3Ru_2O_7$ induced by Ti doping*
X. Ke, J. Peng, D.J. Singh, T. Hong, W. Tian, C.R. Dela Cruz, Z. Q. Mao
Phys. Rev. B, **84**, 201102(R) (2011)
56. *Effect of molybdenum 4d hole substitution in $BaFe_2As_2$*
A.S. Sefat, K. Marty, A.D. Christianson, B. Saparov, M.A. McGuire, M.D. Lumsden, W. Tian, B.C. Sales
Phys. Rev. B, **85**, 024503 (2012).
57. *Antiferromagnetic transitions in tetragonal-like $BiFeO_3$*
G.J. MacDougall, H.M. Christen, W. Siemons,M.D. Biegalski, J.L. Zarestky, S. Liang, E. Dagotto, S.E. Nagler
Phys. Rev. B, **85**, 100406 (2012).
58. *Neutron scattering study of underdoped $Ba_{1-x}K_xFe_2As_2$ ($_x$=0.09 and 0.17) self-flux-grown single crystals and the universality of the tricritical point*
C.R. Rotundu, W. Tian, K.C. Rule, T.R. Forrest, J. Zhao, J.L. Zarestky, R.J. Birgeneau
Phys. Rev. B, **85**, 144506 (2012).
59. *Probing the connections between superconductivity, stripe order, and structure in $La_{1.905}Ba_{0.095}Cu_{1-y}Zn_yO_4$*
J.S. Wen, Z.J. Xu, G.Y. Xu, Q. Jie, M. Hucker, A. Zheludev, W. Tian, B.L. Winn, J.L. Zarestky, D.K. Singh, T. Hong, Q. Li, G.D. Gu, J.M. Tranquada
Phys. Rev. B, **85**, 134512 (2012).

60. *$Ba_{1-x}K_xMn_2As_2$: An Antiferromagnetic Local-Moment Metal*
Abhishek Pandey, R.S. Dhaka, J. Lamsal, Y. Lee, V.K. Anand, A. Kreyssig, T.W. Heitmann, R.J. McQueeney, A.I. Goldman, B.N. Harmon, A. Kaminski, D.C. Johnston
Phys. Rev. Lett., **108**, 087005 (2012).
61. *Effect of tensile stress on the in-plane resistivity anisotropy in $BaFe_2As_2$*
E.C. Blomberg, A. Kreyssig, M.A. Tanatar, R.M. Fernandes, M.G. Kim, A. Thaler, J. Schmalian, S.L. Bud'ko, P.C. Canfield, A.I. Goldman, R. Prozorov
Phys. Rev. B, **85**, 144509 (2012).
62. *Antiferromagnetic order in the quasicrystal approximant Cd_6Tb studied by x-ray resonant magnetic scattering*
M.G. Kim, G. Beutier, A. Kreyssig, T. Hiroto, T. Yamada, J.W. Kim, M. de Boissieu, R. Tamura, A.I. Goldman
Phys. Rev. B, **85**, 134442 (2012).
63. *Magnetically polarized Ir dopant atoms in superconducting $Ba(Fe_{1-x}Ir_x)_2As_2$*
M.P.M. Dean, M.G. Kim, A. Kreyssig, J.W. Kim, X. Liu, P.J. Ryan, A. Thaler, S.L. Bud'ko, W. Strassheim, P.C. Canfield, J.P. Hill, A.I. Goldman
Phys. Rev. B, **85**, 140514 (2012).
64. *Transition metal substitutions, incommensurability and spin fluctuations in $BaFe_2As_2$:What's different about Cu?*
M.G. Kim, J. Lamsal, T.W. Heitmann, G.S. Tucker, D.K. Pratt, S.N. Khan, Y.B. Lee, A. Alam, A. Thaler, N. Ni, S. Ran, S.L. Bud'ko, K.J. Marty, M.D. Lumsden, P.C. Canfield, B.N. Harmon, D.D. Johnson, A. Kreyssig, R.J. McQueeney, A.I. Goldman
arXiv:1204.1538 (2012).
65. *Competition between stripe and checkerboard magnetic instabilities in Mn-doped $BaFe_2As_2$*
G.S. Tucker, D.K. Pratt, M.G. Kim, S. Ran, A. Thaler, G. E. Granroth, K. Marty, W. Tian, J.L. Zarestky, M.D. Lumsden, S.L. Bud'ko, P.C. Canfield, A. Kreyssig, A.I. Goldman, R. J. McQueeney
manuscript available upon request (2012).

Progress Report (2010-2012): DE-FG-02-05ER46202

USING NEUTRON AS A PROBE TO STUDY MAGNETIC EXCITATIONS IN STRONGLY CORRELATED ELECTRON MATERIALS

Professor Pengcheng Dai
Department of Physics and Astronomy
The University of Tennessee
Knoxville, Tennessee 37996-1200
http://pdai.phys.utk.edu
Phone: 865-607-8067, E-mail: pdai@utk.edu

DOE/Office of Science Program Office: Neutron Scattering
DOE/Office of Science Program Manager Contact: P. Thiyagarajan
Phone: (301) 903-9706, e-mail: p.thiyagarajan@science.doe.gov
DOE Grant Number: DE-FG02-05ER46202
Report covering period: 6/01/2010 till 6/01/2012
Date of Report: 06/20/2012

Research Scope:

Understanding the interplay between magnetism and superconductivity continues to be a "hot" topic in modern condensed matter physics. The discovery of high-temperature superconductivity in iron-based materials in 2008 provided an unique opportunity to compare and contrast these materials with traditional high-T_c copper oxide superconductors. Neutron scattering plays an important role in determining the dynamical spin properties in these materials. This proposal is a continuation of previous DOE support proposal. This report summarizes the progress we have made over the past 24 months from June 2010 till March 2012. Overall, we continue to carry out extensive neutron scattering experiments on Fe-based materials, focusing on understanding magnetic properties. In addition, we have established a materials laboratory at UT that has allowed us to grow these superconductors. Because neutron scattering typically demands a large amount of samples, by growing these materials in our own laboratory, we can now pursuit neutron scattering experiments over the entire electronic phase diagram, focusing on regions of interests. The material synthesis laboratory at UT was established entirely with the support of DOE funding. Our papers are cited on average about 900 times per year. Over the past two years, we have made significant contribution in our understanding of the magnetic properties in Fe-based superconductors.

RESEARCH PROGRESS:

Spin waves in the (π,0) magnetically ordered iron chalcogenide $Fe_{1.05}Te$:

We use neutron scattering to show that spin waves in the iron chalcogenide $Fe_{1.05}Te$ display novel dispersion clearly different from both the first principles density functional calculations and recent observations in the related iron pnictide $CaFe_2As_2$. By fitting to a Heisenberg Hamiltonian, we find that although the nearest-neighbor exchange couplings in the two systems are quite different, their next nearest-neighbor (NNN) couplings are similar. This suggests that superconductivity in the pnictides and chalcogenides share a common magnetic origin that is intimately associated with the NNN magnetic coupling between the irons. [Summary paper: *PRL* **106**, 057004 (2011).]

Electron-spin excitation coupling in an electron-doped copper oxide superconductor.

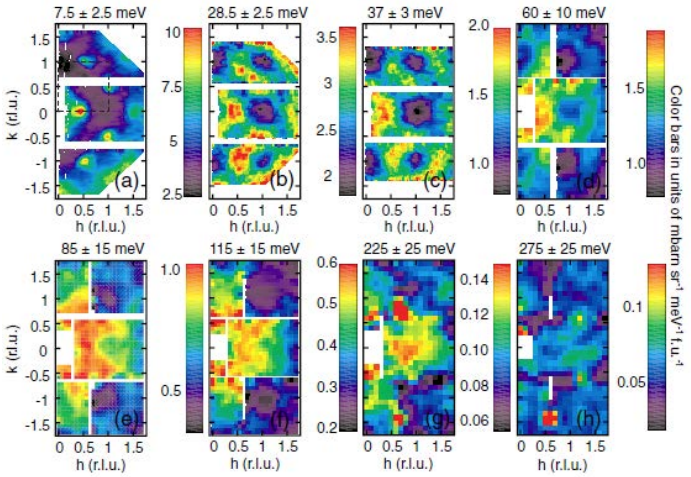

Fig. 1 Spin waves of FeTe at different energies as seen on ARCS chopper spectrometer at SNS, Oak Ridge National Laboratory. From PRL 106, 057004 (2011).

High-temperature (high-*T*c) superconductivity in the copper oxides arises from electron or hole-doping of their antiferromagnetic (AF) insulating parent compounds. The evolution of the AF phase with doping and its spatial coexistence with superconductivity are governed by the nature of charge and spin correlations, which provides clues to the mechanism of high-*T*c superconductivity. Here we use neutron scattering and scanning tunnelling spectroscopy (STS) to study the evolution of the bosonic excitations in electron-doped superconductor Pr0:88LaCe0:12CuO4 (PLCCO) with different transition temperatures (*T*c) obtained through the oxygen annealing process. We find that spin excitations detected by neutron scattering have two distinct modes that evolve with *T*c in a remarkably similar fashion to the low-energy electron tunnelling modes detected by STS. These results demonstrate that antiferromagnetism and superconductivity compete locally and coexist spatially on nanometre length scales, and the dominant electron–boson coupling at low energies originates from the electron-spin excitations.

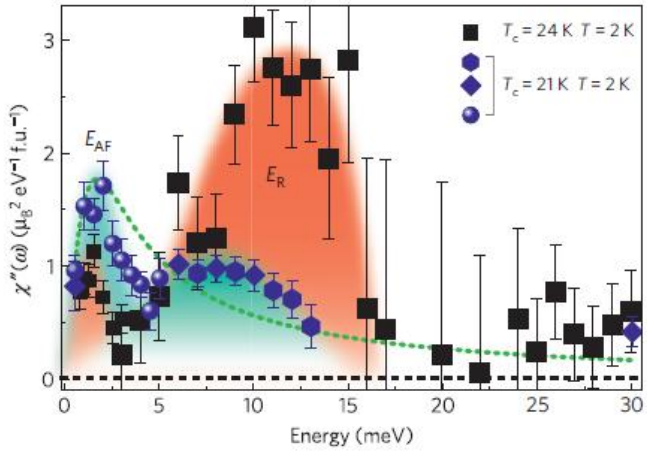

Fig. 2 Doping dependence of the neutron spin resonance in PLCCO.

[Summary paper: *Nature Physics* **7**, 720 (2011).]

Nematic spin fluid in the tetragonal phase of $BaFe_2As_2$

We use inelastic neutron scattering to study spin waves below and above T_N in iron-arsenide BaFe2As2. In the low-temperature orthorhombic phase, we find highly anisotropic spin waves with a large damping along the antiferromagnetic *a*-axis direction. On warming the system to the paramagnetic tetragonal phase, the low-energy spin waves

evolve into quasi-elastic excitations, while the anisotropic spin excitations near the zone boundary persist. These results strongly suggest the presence of a spin nematic fluid in the tetragonal phase of $BaFe_2As_2$, which may cause the electronic and orbital anisotropy observed in these materials. [Summary papers: *Phys. Rev. B* **84**, 054544 (2011).]

Neutron Scattering studies of spin excitations in hole-doped $Ba_{0.67}K_{0.33}Fe_2As_2$ superconductor

We report inelastic neutron scattering experiments on single crystals of superconducting Ba0.67K0.33Fe2As2 (Tc =38 K). In addition to confirming the resonance previously found in powder samples, we find that spin excitations in the normal state form longitudinally elongated ellipses along the Q_{AFM} direction in momentum space, consistent with density functional theory predictions. On cooling below Tc, while the resonance preserves its momentum anisotropy as expected, spin excitations at energies below the resonance become essentially isotropic in the in-plane momentum space and dramatically increase their correlation length. These results suggest that the superconducting gap structures in Ba0.67Ka0.33Fe2As2 are more complicated than those suggested from angle resolved photoemission experiments. [Summary paper: *Scientific Reports* **1**, 115 (2011).]

Spin waves and magnetic exchange interactions in insulating $Rb_{0.89}Fe_{1.58}Se_2$.

The parent compounds of iron pnictide superconductors are bad metals with a collinear antiferromagnetic structure and N é el temperatures below 220 K. Although alkaline iron selenide *A y* Fe 1.6 + *x* Se 2 (*A* = K, Rb, Cs) superconductors are isostructural with iron pnictides, in the vicinity of the undoped limit they are insulators, forming a block antiferromagnetic order and having N é el temperatures of roughly 500 K. Here we show that the spin waves of the insulating antiferromagnet $Rb_{0.89}Fe_{1.58}Se_2$ can be accurately described by a local moment Heisenberg Hamiltonian. A fitting analysis of the spin wave spectra reveals that the next-nearest neighbor couplings in $Rb_{0.89}Fe_{1.58}Se_2$, (Ba,Ca,Sr)Fe_2As_2 , and $Fe_{1.05}Te$ are of similar magnitude. Our results suggest a common origin for the magnetism of all the Fe-based superconductors, despite having different ground states and antiferromagnetic orderings. [Summary paper: *Nature Communications* **2**, 580 (2011).]

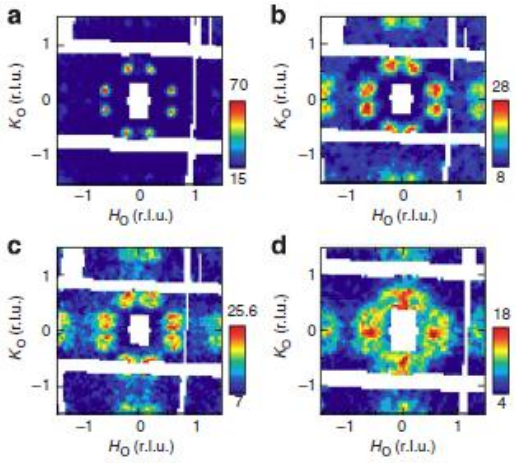

Fig. 2 Spin waves of $Rb_{0.89}Fe_{1.58}Se_2$ obtained from ARCS spectrometer at SNS, ORNL.

Future Plans

In the upcoming funding period, we will continue to focus on magnetic excitations in FeAs-based materials and will start to work on Na(Fe,Co)As family of materials. From intensive efforts of the past year, we can now grow large quantity of very high quality single crystals of Na(Fe,Co)As. We will gradually map out spin waves and spin excitations in this family of materials.

Journal publications from May 2010 till June 2012:

1. “Evidence of a Spin Resonance Mode in the Iron-Based Superconductor Ba0.6K0.4Fe2As2 from Scanning Tunneling Spectroscopy”, Lei Shan, Jing Gong, Yong-Lei Wang, Bing Shen, Xingyuan Hou, Cong Ren, Chunhong Li, Huan Yang, Hai-Hu Wen, Shiliang Li, and Pengcheng Dai, *Phys. Rev. Lett.* ***108****, 227002 (2012).*
2. “Magnetic field dependence of spin-lattice relaxation in the s+- state of Ba0.67K0.33F2As2”, Sangwon Oh, A. M. Mounce, W. P. Halperin, C. L. Zhang, Pengcheng Dai, A. P. Reyes, and P. L. Kuhns, *Phys. Rev. B* ***85****,174508 (2012).*
3. “Temperature dependence of the resonance and low-energy spin excitations in superconducting FeTe0.6Se0.4”. Leland W. Harriger, O. J. Lipscombe, Chenglin Zhang, Huiqian Luo, Meng Wang, K. Marty, M. D. Lumsden, Pengcheng Dai, *Phys. Rev. B* **85**, 054511 (2012).
4. “Evolution of normal and superconducting properties of single crystals of NaFeAs upon interaction with environment”, M. A. Tanatar, N. Spyrison, K. Cho, E. C. Blomberg. T. Tan, Pengcheng Dai, Chenglin Zhang, and R. Prozorov, *Phys. Rev. B* **85**, 014510 (2012).
5. “Common origin of the two types of magnetic fluctuations in iron chalcogenides”, Songxue Chi, J. A. Rodriguez-Rivera, J. W. Lynn, Chenglin Zhang, D. Phelan, D. K. Singh, R. Paul, and Pengcheng Dai, *Phys. Rev. B* **84**, 214407 (2011).
6. “Superconductivity and spin fluctuations”, Shiliang Li and Pengcheng Dai, Front. Physics **6**, 429-439 (2011).
7. “Spin waves and magnetic exchange interactions in insulating Rb0.89Fe1.58Se2”, Miaoyin Wang, Chen Fang, Dao-Xin Yao, GuoTai Tan, Leland W. Harriger, Yu Song, Tucker Netherton, Chenglin Zhang, Meng Wang, Matthew B. Stone, Wei Tian, Jiangping Hu, Pengcheng Dai, *Nature Communications* **2**, 580 (2011).
8. “Neutron Scattering Studies of spin excitations in hole-doped Ba0.67K0.33Fe2As2 superconductor”, Chenglin Zhang, Meng Wang, Huiqian Luo, Miaoyin Wang, Mengshu Liu, Jun Zhao, D. L. Abernathy, T. A. Maier, Karol Marty, M. D. Lumsden, Songxue Chi, Sung Chang, J. A. Rodriguez-Rivera, J. W. Lynn, Tao Xiang, J. P. Hu, and Pengcheng Dai, *Scientific Reports* **1**, 115 (2011).
9. “Nemantic spin fluid in the tetragonal phase of BaFe2As2”, Leland W. Harriger, Huiqian Luo, Mengshu Liu, T. G. Perring, C. Frost, Jiangping Hu, M. R. Norman, Pengcheng Dai, *Phys. Rev. B* **84**, 054544 (2011).
10. “Antiferromagnetic order and superlattice structure in nonsuperconducting and superconducting RbyFe1.6+xSe2” Meng Wang, Miaoyin Wang, G. N. Li, Q. Huang, C. H. Li, G. T. Tan, C. L. Zhang, Huibo Cao, Wei Tian, Yang Zhao, Y. C. Chen, X. Y. Lu, Bin Sheng, H. Q. Luo, S. L. Li, M. H. Fang, J. L. Zarestky, W. Ratcliff, M. D. Lumsden, J. W. Lynn, and Pengcheng Dai, *Phys. Rev. B* **84**, 094504 (2011).
11. “Effect of the in-plane magnetic field on the neutron spin resonance in optimally doped FeSe0.4Te0.6 and BaFe1.9Ni0.1As2 superconductors” Shiliang Li, Xingye Lu, Meng Wang, Hui-qian Luo, Miaoyin Wang, Chenglin Zhang, Enrico

Faulhaber, Louis-Pierre Regnault, Deepak Singh, and Pengcheng Dai, *Phys. Rev. B* **84**, 024518 (2011).
12. "Antiferromagnetic spin excitations in single crystals of nonsuperconducting Li1-xFeAs " Meng Wang, X. C. Wang, D. L. Abernathy, L. W. Harriger, H. Q. Luo, Yang Zhao, J. W. Lynn, Q. Q. Liu, C. Q. Jin, Chen Fang, Jiangping Hu, and Pengcheng Dai, *Phys. Rev. B* **83**, 220515(R) (2011).
13. "Electron-spin excitation coupling in an electron-doped copper oxide superconductor" J. Zhao, F. C. Niestemski, S. Kunwar, S. Li, P. Steffens, A. Hiess, H. J. Kang, S. D. Wilson, Z. Wang, Pengcheng Dai, and V. Madhavan, *Nature Physics* **7**, 719 (2011).
14. "Three-dimensionality of band structure and a large residual quasiparticle population in Ba0.67K0.33Fe2As2 as revealed by c-axis polarized optical measurements" B. Cheng, Z. G. Chen, C. L. Zhang, R. H. Ruan, T. Dong, B. F. Hu, W. T. Guo, S. S. Miao, P. Zheng, J. L. Luo, G. Xu, Pengcheng Dai, and N. L. Wang, *Phys. Rev. B* **83**, 144522 (2011).
15. "Spin waves in the $(\pi,0)$ magnetically ordered iron chalcogenide $Fe_{1.05}Te$", O. J. Lipscombe, G. F. Chen, Chen Fang, T. G. Perring, D. L. Abernathy, A. D. Christianson, T. Egami, Nanlin Wang, Jaingping Hu, Pengcheng Dai, *Phys. Rev. Lett.* **106**, 057004 (2011).
16. "Observation of a ubiquitous three-dimensional superconducting gap function in optimally doped $Ba_{0.6}K_{0.4}Fe_2As_2$" Y-M. Xu, Y-B. Huang, X-Y. Cui, E. Razzoli, M. Radovic, M. Shi, G-F. Chen, P. Zheng, N-L.Wang, C-L. Zhang, P-C. Dai, J-P. Hu, Z.Wang, and H. Ding, Nature Physics **7**, 198 (2011).
17. "Anisotropic structure of the order parameter in FeSe0.45Te0.55 revealed by angle-resolved specific heat". B. Zeng, G. Mu, H.Q. Luo, T. Xiang, I.I. Mazin, H. Yang, L. Shan, C. Ren, P.C. Dai & H.-H. Wen, *Nature Communications* **1**, 112 (2011).
18. "Normal state hourglass dispersion of the spin excitations in $FeSe_xTe_{1-x}$" Shiliang Li, Chenglin Zhang, Meng Wang, Hui-qian Luo, Xingye Lu, E. Faulhaber, A. Schneidewind, P. Link, Jiangping Hu, Tao Xiang, and Pengcheng Dai, *Phys. Rev. Lett*. **105**, 157002 (2010).
19. "Anisotropic neutron spin resonance in superconducting $BaFe_{1.9}Ni_{0.1}As_2$", O. J. Lipscombe, L. W. Harriger, P. G. Freeman, M. Enderle, Chenglin Zhang, Miaoyin Wang, T. Eagami, Jiangping Hu, T. Xiang, M. R. Norman, and Pengcheng Dai, *Phys. Rev. B* **82**, 064515 (2010).
20. "Electron-doping evolution of the low-energy spin excitations in the iron arsenide superconductor $BaFe_{2-x}Ni_xAs_2$", Miaoyin Wang, Huiqian Luo, Jun Zhao, Chenglin Zhang, Meng Wang, Karol Marty, Songxue Chi, Jeffrey W. Lynn, Astrid Schneidewind, Shiliang Li, and Pengcheng Dai, *Phys. Rev. B **81**, 174524 (2010).*
21. "Magnetic form factor of SrFe2As2: Neutron diffraction measurements", W. Ratcliff, II, P. A. Kienzle, Jeffrey W. Lynn, Shiliang Li, Pengcheng Dai, G. F. Chen, and N. L. Wang, *Phys. Rev. B **81**, 140502(R) (2010).*

Phase Competition in Bulk Materials: Superconductivity *vs* Spin and Charge Density Waves

R. Osborn (rosborn@anl.gov), S. Rosenkranz, O. Chmaissem*, S. Avci, J.-P. Castellan, F. Weber
Materials Science Division, Argonne National Laboratory, Argonne, IL 60439
**Department of Physics, Northern Illinois University, DeKalb, IL 60115*

Research Scope

Harnessing phase competition to produce specific material properties is a long-term goal that requires a coordinated strategy integrating synthesis, theory, and advanced characterization. In such materials, there is a subtle balance between competing interactions involving charge, spin, orbital and strain degrees of freedom, and the materials respond to this complexity either by selecting novel ground states or by producing short-range order on the nano- or mesoscale. We have been investigating the competition between spin density waves (SDW) and superconductivity and the analogous competition between charge density waves (CDW) and superconductivity. Both CDW and SDW order require the relevant (electronic or magnetic) susceptibility to diverge at a specific wavevector, *e.g.*, from Fermi surface nesting, but if this divergence is suppressed by disorder or other interactions, superconductivity often results. We have been performing systematic investigations of the phase diagrams of iron arsenide compounds and doped transition metal chalcogenides, using both diffraction and inelastic scattering with neutrons and x-rays. The work on iron arsenides has uncovered unusual scaling resulting from strong magnetoelastic coupling and highlighted the role of Fermi surface nesting in generating the unconventional superconductivity. The work on the dichalcogenides has provided detailed insights into the nature of the CDW phase transitions themselves, showing that the role of electronic instabilities and electron-phonon coupling is quite different in two canonical compounds, $TiSe_2$ and $NbSe_2$.

Recent Progress

Magnetic and Orbital Fluctuations in Novel Superconductors

We have completed a systematic investigation of the phase diagram of the hole–doped $Ba_{1-x}K_xFe_2As_2$ [1], using high resolution neutron and x-ray powder diffraction on samples prepared by the MSD group led by Mercouri Kanatzidis. Improvements in the control of the volatile precursors during synthesis have resulted in much better homogeneity than in previous studies, producing sharper superconducting transitions and allowing a much more accurate determination of the phase boundaries. We find that the orthorhombic (O) and antiferromagnetic (AF) transition temperatures are coincident and first-order over the range $0 \leq x \leq 0.25$, with strong magnetoelastic coupling [7]. Fig. 1 shows that the two order parameters show identical scaling over the entire dopant range, indicating a possible quantum phase transition at $x = 0.252$. Superconductivity starts at $x = 0.13$ and T_c increases linearly with x, until crossing the AF/O phase boundary. Between $0.13 \leq x \leq 0.25$, our results show that there is microscopic phase coexistence of superconductivity and AF/O order, not phase separation as previously reported.

We have also studied in detail the evolution of the resonant magnetic excitation with hole doping from $0.3 \leq x \leq 0.9$ using inelastic neutron scattering [4]. In the hole doped systems, the superconducting phase extends over a much broader range of dopant concentration than with electron-doping; ARPES data shows that the hole pockets approximately double in radius and the electron pockets shrink to zero close to $x = 1$. This allows a detailed investigation of the role of Fermi surface nesting. The mismatch in the sizes of the hole and electron pockets produces a

split of the magnetic scattering into two incommensurate peaks just when T_c starts to fall. This split can be fitted well to a tight-binding model with $s^{\pm}$-symmetry pairing. We also observe that the scaling of the resonance energy to the superconducting gap is strongly dependent on the degree of Fermi surface nesting and is not a universal property of unconventional superconductors as has been suggested by others. There is a decrease in the resonant spectral weight that is linear in the resonance binding energy, as predicted by itinerant RPA models of the superconductivity. This is the first time that the complete collapse of the resonant spectral weight has been observed in the iron arsenides.

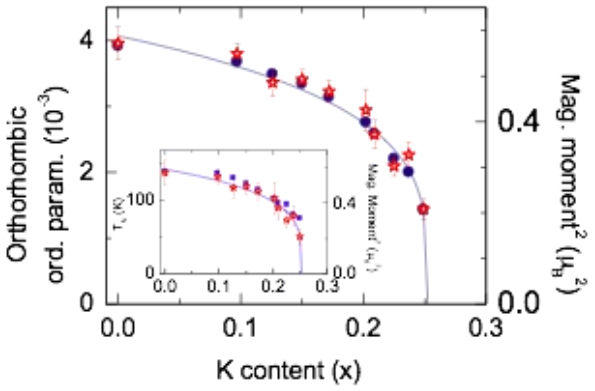

Fig. 1: Dependence of the square of the magnetic moment, μ^2 (red stars), and the orthorhombic order parameter, $\delta = (a-b)/(a+b)$ (blue circles), at 1.7 K on the potassium concentration, x. The inset shows a comparison of T_N and μ^2 *vs* x, showing that $T_N \propto \mu^2$. Solid lines in the main panel and the inset are a fit to $(1 - x/x_c)^{2\beta}$ with $\beta = 0.125$ (Ref. 1).

Charge Density Wave Instabilities in Layered Chalcogenides

We have been investigating the origin of charge density wave (CDW) formation in transition metal dichalcogenides and its destruction upon introducing disorder. Using inelastic synchrotron x-ray scattering, we have measured the momentum and temperature dependence of the soft phonon modes associated with the CDW formation. While for $TiSe_2$, we find a cusp-like softening of the phonon at the CDW wavevector as expected in standard models of CDW transitions [2], for $NbSe_2$ we observe that phonons soften to zero frequency and become over-damped over an extended region around the CDW wavevector [5]. These results, combined with *ab initio* DFT calculations, provide direct evidence that the CDW wavevector in $NbSe_2$ is determined by the wavevector dependence of the electron-phonon coupling matrix elements and not by a nesting-induced electronic instability as was commonly assumed. This work resolves a long-standing controversy regarding the nature of the CDW and the behavior of the electronic

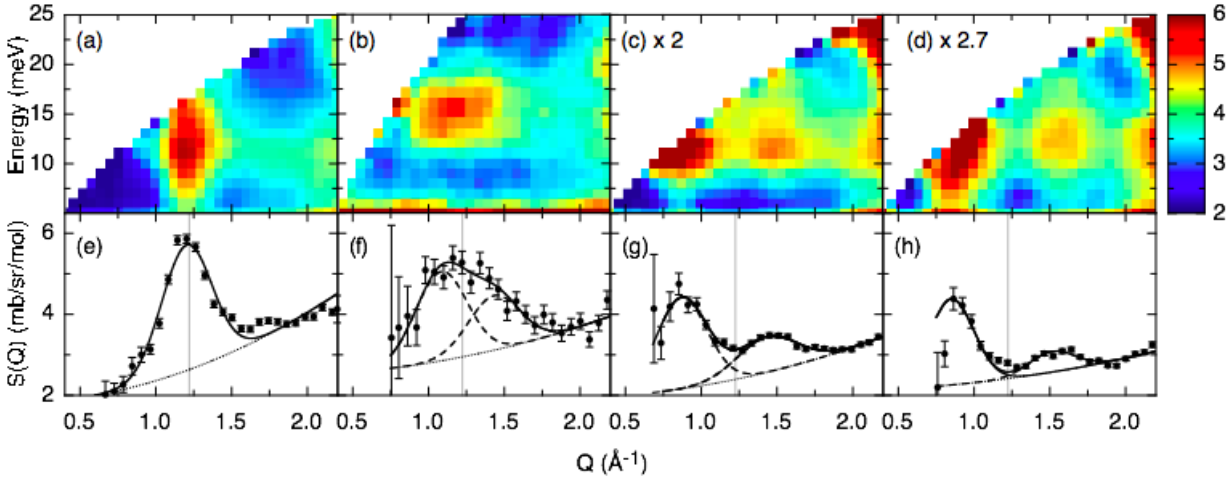

Fig. 2: Inelastic neutron scattering from $Ba_{1-x}K_xFe_2As_2$ measured in the superconducting phase at a temperature of 5K at (a,e) $x = 0.3$, (b,f) $x = 0.5$, (c,g) $x = 0.7$, and (d,h) $x = 0.9$ (Ref. 4).

properties in $NbSe_2$. We also found unusual behavior of an acoustic phonon branch in a bilayer manganite at the onset of charge order [3], indicating that a strong link between electron-phonon coupling and charge order is relevant to manganites and possibly other strongly correlated oxides as well and may be an important ingredient in determining their unusual physical properties.

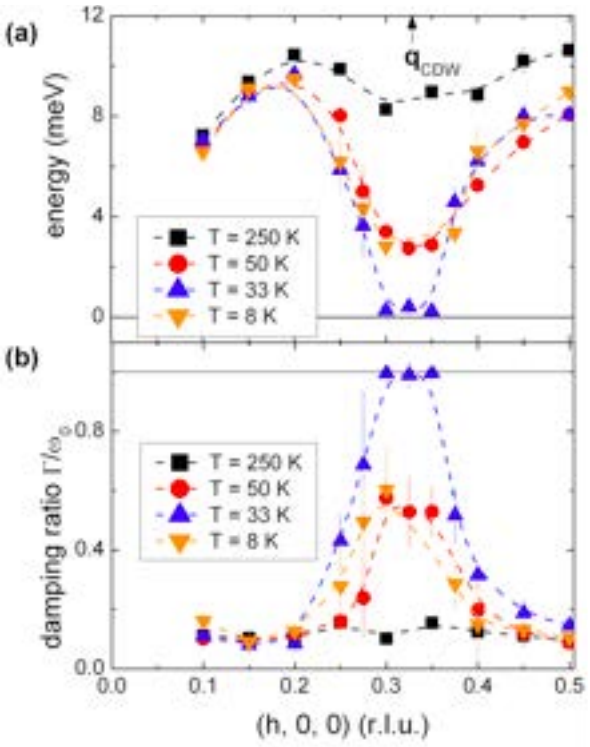

Fig. 3: (a) Dispersion (ω_0 *vs* Q) and (b) damping ratio (Γ/ω_0 *vs* Q) of the soft-phonon branch in 2*H*-$NbSe_2$ measured above and below T_c = 33K (Ref. 5).

Future Plans

Magnetic and Orbital Fluctuations in Novel Superconductors

We have already started an investigation of both the $Ba_{1-x}Na_xFe_2As_2$ and $BaFe_2As_{2-x}P_x$ phase diagrams. The former series is similar to the K-doped materials that we have already studied and a comparison could help to separate the role of structure and Fermi surface nesting in optimizing superconductivity. Phosphor substitution was expected to be isovalent, although there are ARPES results suggesting that it is equivalent to hole-doping, a discrepancy that the doping dependence of the resonance will help to explain. Furthermore, the phosphor doped samples show clear evidence of quantum criticality so inelastic neutron scattering measurements of the magnetic fluctuations will be particularly important.

Charge Density Wave Instabilities in Layered Chalcogenides

We have started a detailed investigation of how unusual the electronic properties of the doped dichalcogenides are connected to short-range charge density wave correlations by combining synchrotron x-ray scattering, angle resolved photoemission (ARPES), and scanning tunneling microscopy measurements. We believe that these observations will be of relevance in explaining the pseudogap behavior observed in other systems, such superconducting cuprates and manganites. We will also use inelastic x-ray scattering to extend our measurements of soft modes to $TiSe_2$ and $NbSe_2$ as a function of transition metal intercalation, providing detailed information on the evolution of the electronic susceptibility and the electron-phonon coupling as the CDW is suppressed and superconductivity is established.

Publications

1. S. Avci, O. Chmaissem, D. Y. Chung, S. Rosenkranz, E. A. Goremychkin, J.-P. Castellan, I. S. Todorov, J. A. Schlueter, H. Claus, A. Daoud-Aladine, D. D. Khalyavin, M. G. Kanatzidis, and R. Osborn
   "Phase diagram of $Ba_{1-x}K_xFe_2As_2$"
   Phys. Rev. B **85**, 184507 (2012).
2. F. Weber, S. Rosenkranz, J.-P. Castellan, R. Osborn, G. Karapetrov, R. Hott, R. Heid, K.-P. Bohnen, and A. Alatas
   "Electron-Phonon Coupling and the Soft Phonon Mode in $TiSe_2$"
   Phys. Rev. Lett. **107**, 266401 (2011).

3. F. Weber, S. Rosenkranz, J.-P. Castellan, R. Osborn, H. Zheng, J. Mitchell, Y. Chen, S. Chi, J. Lynn, and D. Reznik
"Response of Acoustic Phonons to Charge and Orbital Order in the 50% Doped Bilayer Manganite $LaSr_2Mn_2O_7$"
Phys. Rev. Lett. **107**, 207202 (2011).
4. J.-P. Castellan, S. Rosenkranz, E. Goremychkin, D. Chung, I. Todorov, M. Kanatzidis, I. Eremin, J. Knolle, A. Chubukov, S. Maiti, M. Norman, F. Weber, H. Claus, T. Guidi, R. Bewley, and R. Osborn
"Effect of Fermi Surface Nesting on Resonant Spin Excitations in $Ba_{1-x}K_xFe_2As_2$"
Phys. Rev. Lett. **107**, 177003 (2011).
5. F. Weber, S. Rosenkranz, J.-P. Castellan, R. Osborn, R. Hott, R. Heid, K.-P. Bohnen, T. Egami, A. Said, and D. Reznik
"Extended Phonon Collapse and the Origin of the Charge-Density Wave in 2*H*-$NbSe_2$"
Phys. Rev. Lett. **107**, 107403 (2011).
6. U. Chatterjee, D. Ai, J. Zhao, S. Rosenkranz, A. Kaminski, H. Raffy, Z.Z. Li, K. Kadowaki, M. Randeria, M.R. Norman, J.C. Campuzano
"Electronic phase diagram of high temperature copper oxide superconductors"
Proc. Natl. Acad. Sci. **108**, 9346 (2011)
7. E. Goremychkin, R. Osborn, C. Wang, M. Lumsden, M. Mcguire, A. Sefat, B. Sales, D. Mandrus, H. Rønnow, Y. Su, and A. Christianson
"Spatial inhomogeneity in $RFeAsO_{1-x}F_x$ (R = Pr, Nd) determined from rare-earth crystal-field excitations"
Phys. Rev. B **83**, 212505 (2011).
8. S. Avci, O. Chmaissem, E. Goremychkin, S. Rosenkranz, J.-P. Castellan, D. Chung, I. Todorov, J. Schlueter, H. Claus, M. Kanatzidis, A. Daoud-Aladine, D. Khalyavin, and R. Osborn
"Magnetoelastic coupling in the phase diagram of $Ba_{1-x}K_xFe_2As_2$ as seen via neutron diffraction"
Phys. Rev. B **83**, 172503 (2011).
9. M. R. Norman, A. Kaminski, S. Rosenkranz, J.C. Campuzano
Comment on "Circular dichroism in the angle-resolved photoemission spectrum of the high-temperature $Bi_2Sr_2CaCu_2O_{8+\delta}$ superconductor: Can these measurements be interpreted as evidence for time-reversal symmetry breaking?"
Phys. Rev. Lett. **105**, 189701 (2010).
10. F. Weber, S. Rosenkranz, J.-P. Castellan, R. Osborn, J. F. Mitchell, H. Zheng, D. Casa, J. H. Kim, and T. Gog
"*d-d* excitations in bilayer manganites probed by resonant inelastic x-ray scattering"
Phys. Rev. B **82**, 085105 (2010).
11. P. Manuel, L. C. Chapon, I. S. Todorov, D. Y. Chung, J.-P. Castellan, S. Rosenkranz, R. Osborn, P. Toledano, and M. G. Kanatzidis
"Incommensurate spin-density wave and magnetic lock-in transition in $CaFe_4As_3$"
Phys. Rev. B **81**, 184402 (2010).
12. F. Weber, J.-P. Castellan, S. Rosenkranz, R. Osborn, D. Rosenmann, and M. Iavarone
"Extended X-ray Absorption Fine Structure spectroscopy in $Co_{0.013}NbSe_2$"
J. Phys.: Conf. Series **200**, 012224 (2010).
13. F. Weber and L. Pintschovius
"Superconductivity-induced distortions of phonon lineshapes in niobium"
Phys. Rev. B **82**, 024509 (2010)
14. E. A. Goremychkin, R. Osborn, I. L. Sashin, P. Riseborough, B. D. Rainford, D. T. Adroja, and J. M. Lawrence
"Transition from Heavy-Fermion to Mixed-Valence Behavior in $Ce_{1-x}Y_xAl_3$: A Quantitative Comparison with the Anderson Impurity Model"
Phys. Rev. Lett. **104**, 176402 (2010).

Session III

Correlated Electron Systems (II)

Complex Electronic Materials

J. D. Thompson (jdt@lanl.gov), E. D. Bauer, M. Janoschek, R. Movshovich, F. Ronning and H. Yasuoka*

Los Alamos National Laboratory, Los Alamos, NM 87545

**Visiting scientist, Japan Atomic Energy Agency, Tokai, Japan*

Program Scope

Complex electronic behaviors are most pronounced near the magnetic/non-magnetic and metal/insulator boundaries in correlated materials and become particularly poorly understood as these boundaries are tuned to absolute zero temperature, i.e., to a quantum-critical point. With typically small characteristic energy scales, states of strongly correlated intermetallic compounds based principally on Ce, Yb, U and Pu can be tuned to these interesting boundaries with rather modest changes in a control parameter. This project focuses on developing an understanding of complex electronic materials and phenomena by discovering new examples of these and related materials that reveal both new states of electronic matter and the essential physics underlying their complex and collective states. Knowledge gained from studying correlated f-electron materials in parallel with technologically important d-electron materials provides a broad and unifying perspective necessary to guide the development of a microscopic theory of complex electronic materials. Success in this project of discovering new physics through new materials requires integration of materials preparation, in single crystal form where possible, with a necessarily broad suite of materials characterization techniques that probe static and dynamic degrees-of-freedom and their interactions on multiple length and time scales. Our approach is two-fold: one of initial exploratory research on new materials and phenomena and a second of in-depth investigations leading to microscopic understanding of those materials and phenomena. At the exploratory stage, simple structure, transport, magnetic and thermodynamic measurements, often at very low temperatures, high pressures and high magnetic fields, are sufficient to identify new states that deserve more detailed study by various spin and charge spectroscopies, particularly neutron scattering, nuclear quadrupole/magnetic resonance and photoemission. DOE neutron and photon facilities, the Los Alamos NHMFL Pulsed Field Facility and Center for Integrated Nanotechnologies as well as an extensive network of experimental and theoretical collaborators substantially leverage in-house capabilities and are important to the success of this project. An associated subtask, led by J. Joyce and T. Durakiewicz, on photoemission spectroscopy of transuranic materials complements objectives of our project. Its progress and future plans are not discussed in this abstract.

Recent Progress

The highly tunable family of heavy-fermion compounds $CeMIn_5$ (M=Co, Rh Ir), discovered in this project, has proven especially fertile for discovering new states and new physics, but the Pu-analogs also are proving quite interesting. We highlight three examples that have come from studies of these materials.

$CeCoIn_5$ is a d-wave superconductor on the verge of a zero-temperature magnetic instability. In the course of exploring the response of $CeCoIn_5$ to the addition of small amounts of non-magnetic dopants, we found that the electronic coefficient of specific heat γ_0 in the zero-temperature limit, deep in the superconducting state, increases significantly, irrespective of whether the dopant is substituted on the Ce or In sites. The ratio of γ_0 to the normal-state

Sommerfeld coefficient γ_N, determined by applying a magnetic field just sufficient to completely suppress superconductivity, increases linearly with the concentration of non-magnetic impurities but with an impurity-dependent slope. On the other hand, all data collapse onto a single linear relationship, as shown in Fig. 1, when this ratio γ_0/γ_N is plotted as a function of the reduction of the superconducting condensation energy $R_U=[U_{SC}(x)/T_c^2(x)]/[U_{SC}(0)/T_c^2(0)]$, where the condensation energy $U_{SC}=\int_0^{Tc}(S_N-S_{SC})dT$, x is the impurity concentration and S is the entropy of normal (N) and superconducting (SC) states. This linear correlation in Fig. 1 implies that the doping-induced normal state fraction comes precisely at the expense of the superconducting state fraction. In effect, the non-magnetic dopants 'eat a hole' in the superconducting condensate, producing an electronically heterogeneous state analogous to Swiss cheese—an idea introduced first in the context of the anomalous suppression of the superfluid density in Zn-doped cuprate superconductors.[1] As we showed, the linear relation between γ_0/γ_N and $1\text{-}R_U$ is not limited to the dopants in Fig. 1 or to $CeCoIn_5$ but appears to be a general response of a superconducting Kondo lattice to dopants.[2]

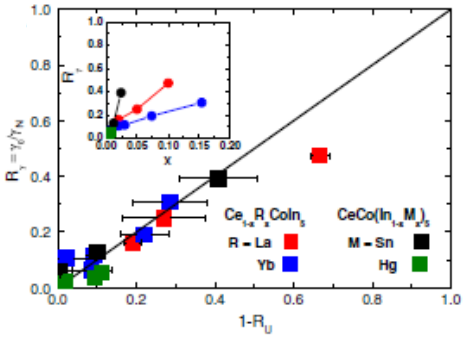

Fig. 1 Ratio γ_0/γ_N as a function of $1\text{-}R_U$ for various 'impurity' substitutions on the Ce and In sites of $CeCoIn_5$. Note that the solid line, with unity slope, passes through the origin. The inset is a plot of raw data.

But, electronic Swiss cheese is not the only form of heterogeneity in correlated electron systems. Our study of $CeRhIn_5$ as a function of applied pressure has revealed evidence for 'superconducting texture', a difference between resistive and bulk superconducting transitions, that is a consequence of coexisting antiferromagnetic order and d-wave superconductivity. From measurements of the specific heat and electrical resistivity, we found that the resistivity drops to zero, or at least to an immeasurably small value, at a temperature well above the thermodynamically determined superconducting T_c (Fig. 2) and, further, that the resistively determined transition temperature appears to break four-fold rotational symmetry of the underlying tetragonal crystal structure. Once sufficient pressure is applied to suppress evidence for long range antiferromagnetic order and to leave only a d-wave superconducting state, the resistive and bulk superconducting transitions coincide to within 10 mK. The superconducting texture found when antiferromagnetic order and superconductivity coexist in $CeRhIn_5$ is reminiscent of behaviors in underdoped cuprates when spin/charge stripe order coexists with superconductivity. Stripes also are symmetry breaking and, in the case of 1/8-hole doped La_2CuO_4, result in a pronounced difference between resistive and bulk transitions.[3] In this example, even the temperature dependence of the resistive transition is similar to that observed in $CeRhIn_5$, as shown in Figs. 3a and b. Evidence for textured superconductivity is not unique to $CeRhIn_5$, which has large-moment incommensurate magnetic order, but is found as well when superconductivity coexists with commensurate

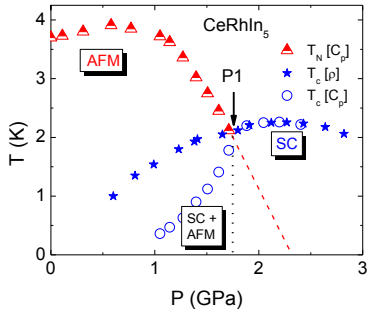

Fig. 2 Temperature versus pressure phase diagram of $CeRhIn_5$. Up triangles and open circles denote the Néel (T_N) and bulk superconducting ($T_c[C_p]$) transition temperatures, respectively. Stars denote the resistively determined mid-point superconducting transition. Above P1, there is no evidence for antiferromagnetic (AFM) order.

antiferromagnetic order (Cd-doped $CeCoIn_5$), a pseudo-gap-like state ($CeIrIn_5$), or a weak incommensurate spin-density wave (A/S-$CeCu_2Si_2$), suggesting that real-spaced texture is a generic response to a coexisting broken symmetry.[4]

With their more extended 5f-wavefunctions, correlated Pu-based compounds can have both d-and 4f-electron characters. $PuRhIn_5$ is one of the more interesting of several new materials discovered recently in our project.[5] What makes it of particular interest is the clear evidence for its d-wave superconductivity (from NQR measurements) developing out of a non-Fermi liquid normal state that is quite similar to what we have found in several 4f-heavy-electron materials. As shown in Figs. 4a and b, the large specific heat of $PuRhIn_5$ decreases with increasing temperature approximately as γ-A$\sqrt{T}$ and its resistivity is T-linear over a substantial temperature range above T_c=1.2K. This discovery, along with $PuCoIn_5$ (T_c=2.2K) and the previously known isostructural Ga-analogs ($PuCoGa_5$ and $PuRhGa_5$) that have nearly 25% smaller unit cell volumes, opens a remarkably rich phase space for exploring the relationship among quantum-criticality, magnetism, valence fluctuations and unconventional superconductivity.

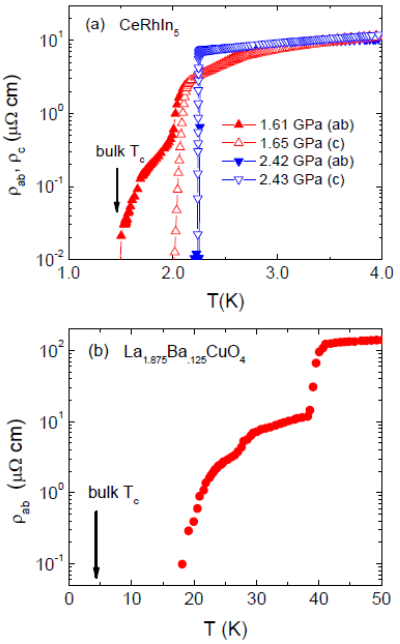

Fig. 3 (a).Resistive transitions in $CeRhIn_5$ with current in the ab-plane or along the c-axis when pressure is below (up triangles) or above (down triangles) P1. (b) In-plane resistive transition in 1/8-doped La_2CuO_4. After ref. 3.

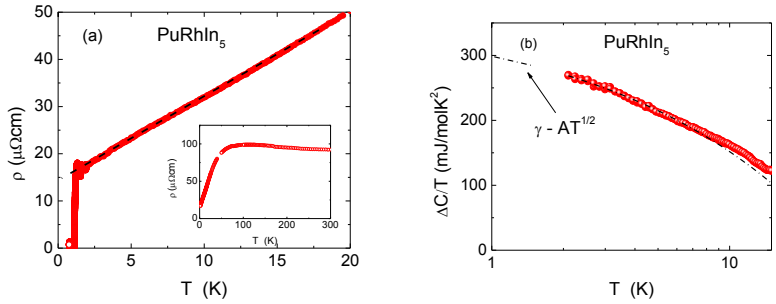

Fig. 4 (a) Resistivity and (b) magnetic contribution to the specific heat divided by temperature ΔC/T versus temperature.

Future Plans

Preliminary inelastic neutron scattering studies of $PuCoGa_5$ suggest the presence of a spin resonance in its superconducting state at an energy expected of its 18.5-K T_c. Confirming this possible resonance and its momentum dependence will provide yet another similarity between correlated d- and f-electron superconductors. Our discovery of the ^{239}Pu NMR resonance in PuO_2 opens the opportunity to apply this new technique as one of very few probes that directly reveals the nature of fluctuations (magnetic or valence) responsible for Cooper pairing and non-Fermi-liquid behaviors in the growing family of Pu-based 115 superconductors. The competition between Kondo and RKKY interactions in heavy-fermion systems is, in general, a form of frustration, but some of these systems crystallize in structures that also frustrate the RKKY interaction. Geometric frustration alone can produce physical properties that mimic those due to competing Kondo and RKKY interactions, but the possible role of geometric frustration in heavy-fermion materials has been explored little. We will begin to explore ways to identify how these special crystal structures may affect the heavy-fermion state. We continue to

develop new experimental probes, for example scanning magnetic force and point-contact spectroscopy, and will apply them to discovering and understanding complex electronic states.

References

[1] B. Nachumi et al., Phys. Rev. Lett.**77**, 5421 (1996).
[2] E. D. Bauer et al., Proc. Nat. Acad. Sci. USA **108**, 6857 (2011).
[3] Q. Li et al., Phys. Rev. Lett. **99**, 067001 (2007).
[4] T. Park et al., Phys. Rev. Lett. **108**, 077003 (2012).
[5] E. D. Bauer et al., unpublished.

Publications from this subtask (FY11-FY12) Only more significant publications are listed from among approximately 108 since the beginning of FY11.

H. Yasuoka, G. Koutrolakis, H. Chudo, S. Richmond, D. K. Veirs, A. I. Smith, E. D. Bauer, J. D. Thompson, G. D. Jarvinen and D. L. Clark, "Observation of ^{239}Pu nuclear magnetic resonance," *Science* **336**, 901 (2012).

P. Aynajian, E. H. da Silva Neto, A. Gyenis, R. E. Baumbach, J. D. Thompson, Z. Fisk, E. D. Bauer and A. Yazdani, "Visualizing the emergence of heavy fermions in a Kondo lattice," *Nature* (in press).

J. D. Thompson, "Heavy electron seeks same," *Nature Phys.* **7**, 838 (2011).

Q. Wang, Z. Sun, E. Rotenberg, F. Ronning, E. D. Bauer, H. Lin, R. S. Markiewicz,
M. Lindroos, B. Barbiellini, A. Bansil and D.S. Dessau, "Uniaxial "nematic-like" electronic structure and Fermi surface of untwinned $CaFe_2As_2$**,**" *Proc. Natl. Acad. Sci. USA* (submitted).

E.D. Bauer, Y.-F. Yang, C. Capan, R.R. Urbano, C.F. Miclea, H. Sakai, F. Ronning, M.J. Graf, A.V. Balatsky, R. Movshovich, A.D. Bianchi, A.P. Reyes, P.L. Kuhns, J.D. Thompson, and Z. Fisk, "Electronic inhomogeneity in a Kondo lattice," *Proc. Nat. Acad. Sci. USA* **108**, 6857 (2011).

J. D. Thompson, "Holes in a Kondo lattice," *Proc. Natl. Acad. Sci. USA* **108**, 18191 (2011).

X. Lu, H.-O. Lee, T. Park, F. Ronning, E. D. Bauer and J. D. Thompson, "Heat-capacity measurements of energy-gap nodes of the heavy-fermion superconductor $CeIrIn_5$ deep inside the pressure-dependent superconducting dome structure of its superconducting phase diagram," *Phys. Rev. Lett.* **108**, 027001 (2012).

M.M. Altarawneh, N. Harrison, G. Li, L. Balicas, P. H. Tobash, F. Ronning and E. D. Bauer, "Superconducting pairs with extreme uniaxial anisotropy in URu_2Si_2," *Phys. Rev. Lett.* **108,** 066407 (2012).

T. Park, H. O. Lee, I. Martin, X. Lu, V. A. Sidorov, K. Gofryk, F. Ronning, E. D. Bauer and J. D. Thompson, "Textured superconducting phase in the heavy fermion $CeRhIn_5$," *Phys. Rev. Lett.* **108**, 077003 (2012).

C. Stock, D. Sokolov, P. Bourges, P. H. Tobash, K. Gofryk, F. Ronning, E. D. Bauer, K.C. Rule, and A.D. Huxley, "Anisotropic critical magnetic fluctuations in the ferromagnetic superconductor UCoGe," *Phys. Rev. Lett.* **107**, 187202 (2011).

H. Sakai, S. E. Brown, S.-H. Baek, F. Ronning, E. D. Bauer and J. D. Thompson, "Magnetic-field-induced enhancement of nuclear spin-relaxation rates in the heavy-fermion superconductor $CeCoIn_5$ using ^{59}Co nuclear magnetic resonance," *Phys. Rev. Lett.* **107**, 137001 (2011).

K. Gofryk, F. Ronning, M. N. Ou, P. H. Tobash, S. S. Stoyko, X. Lu, A. Mar, T. Park, E. D. Bauer, J. D. Thompson and Z. Fisk, "Electronic tuning and uniform superconductivity in $CeCoIn_5$," Phys. Rev. Lett. (submitted).

Neutron Scattering Studies of Fe-based Superconductors

G. Y. Xu (gxu@bnl.gov), I. A. Zaliznyak, G.D. Gu, and J. M. Tranquada
Condensed Matter Physics & Materials Science Department
Brookhaven National Laboratory, Upton, NY 11973-5000

Program Scope

The discovery of high-temperature superconductivity in iron pnictides and chalcogenides has demonstrated that there are opportunities beyond cuprates. Neutron scattering measurements by many groups have established a close connection between antiferromagnetic correlations and superconductivity in these materials. In particular, the low-energy spin fluctuations tend to develop a gap and resonance peak when the material is cooled below the superconducting transition temperature, T_c. The magnetic energy scale is large, with excitation dispersing to above 100 or 200 meV. While the big question involves understanding how the magnetism may be involved in the electron pairing mechanism, an underlying problem concerns the nature of the magnetism itself.

In our program, we apply neutron scattering to investigate the character of the magnetism, focusing primarily on the $Fe_{1+y}Te_{1-x}(Se,S)_x$ systems. In particular, we address the possible role of magnetic moments from localized electrons (meaning electrons at energies much greater than kT from the Fermi energy) and their interaction with conduction electrons. We consider the role of competing magnetic interactions and frustration, as well as the role of degenerate Fe 3*d* orbitals and possible orbital ordering.

Recent Progress

Recent studies by our group and others have established that iron interstitials strongly influence the superconductivity, so that $Fe_{1+y}Te_{1-x}Se_x$ samples with same Se doping can be either superconducting or non-superconducting, depending on y. Thus, it is important to understand the effect of Fe interstitials on electronic, magnetic and structural properties of these materials. One place to do that is in the antiferromagnetic end member $Fe_{1+y}Te$. We have developed a procedure for preparing single-phase samples of $Fe_{1+y}Te$ with well quantified off-stoichiometry, y, and have investigated its magnetic and structural phase diagram using powder and single crystal neutron diffraction, susceptibility, and heat capacity measurements. We have established that, with the increasing y, a first-order magnetostructural transition transforms into a sequence of continuous structural and magnetic transitions, which occur at different temperatures. We find that these instabilities are weak compared to the strength of the underlying interactions, and that the impact of the Fe interstitials on the transitions can be understood with random-field models. Further evidence for this conclusion is provided by measurements on $Fe_{1+y-z}Cu_zTe$. Analysis of inelastic and quasielastic scattering indicates that each Fe interstitial tends to cause the plaquette of four nearest-neighbor Fe sites to align ferromagnetically, with antiferromagnetic correlations between neighboring plaquettes.

We have performed inelastic scattering measurements on a series of $Fe_{1+y}Te_{1-x}(Se,S)_x$ single crystals. An example, obtained by triple-axis measurements at HFIR, is shown in Fig. 1. The diffuse nature of the scattering suggests short-range correlations and frustrated interactions. Zaliznyak has developed a model for analyzing the excitation spectra (including the diffuse character), and is applying it to the data in collaboration with the group of S.-H. Lee (U. Virginia).

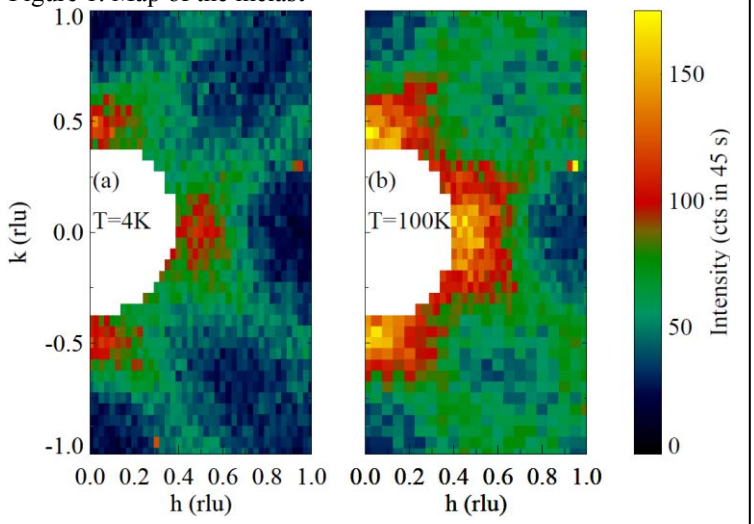

Figure 1. Map of the inelastic magnetic scattering in $Fe_{1+y}Te_{0.87}S_{0.13}$ sample at E = 6 meV at T = 4 K and 100 K.

Xu has been pursuing studies of magnetic excitations in $Fe_{1+y}Te_{1-x}Se_x$ with partial substitution of Ni or Cu for Fe. The substitutions drive T_c towards zero fairly rapidly; however, they also reveal interesting characteristics of the magnetic excitations. In superconducting samples, the magnetic excitations disperse in the transverse direction about a characteristic wave vector Q_{AF}. For $T < 3T_c$, the dispersion forms a "U" shape, with the bottom at Q_{AF}, while at higher temperatures the bottom of the "U" opens up, forming columns at incommensurate wave vectors. This dramatic change in the spectrum indicates unusual electronic changes with temperature.

Future Plans

In our experiments on $Fe_{1.1}Te$ we have discovered an unusual excitation mode, which exists at low wave vectors and disperses down to E = 0 towards q=0. This mode has temperature dependence similar to the rest of magnetic scattering. Its strong intensity at small q is untypical for a phonon, while it is also unusual for an antiferromagnet, where intensity at q = 0 is small, or absent. Hence, this excitation could be either a hybrid magneto-structural mode, or a mode associated with orbital fluctuation. In either case this is a unique observation and requires further studies. We plan such investigations in this and other chalcogenide samples using the unique capability for small-angle inelastic neutron scattering provided by the HYSPEC spectrometer at the SNS.

There are still many unsolved problems remaining for the 1:1 system, one of them being the true nature of the low-energy diffuse scattering. In our previous studies, in addition to the dispersive magnetic scattering near Q_{AF}, a broad diffuse type of scattering is always observed for $\hbar\omega < 8$ meV in a much larger area of reciprocal space. This diffuse scattering is also gapped in the superconducting phase, suggesting its possible magnetic nature. However, detailed studies on this diffuse component, examining the variation of its spectral weight with temperature and/or doping, have not yet been done. Note that the energy scale of this diffuse component is comparable to that of the spin resonance, implying a possible connection to superconductivity in the system. With the commissioning of the HYSPEC spectrometer at SNS, which provides the

perfect matching energy and momentum space for this type of measurements, we plan to extend our study on this diffuse component of (possibly) magnetic scattering in the 1:1 system.

We also plan to carry out more studies on the temperature-dependent transformation of magnetic excitations. Due to the strongly correlated nature of these materials, it is expected that other electronic/magnetic/structural properties could also be affected at the transformation near 3Tc. We have some preliminary data showing an abnormal change in the in-plane lattice expansion in the 4% Ni-doped sample at about the sample temperature range. Measurements on samples with different doping levels and superconducting properties are planned.

Publications (past two years)

1. C. C. Homes, A. Akrap, J. S. Wen, Z. J. Xu, Z. W. Lin, Q. Li, and G. D. Gu.
   Electronic correlations and unusual superconducting response in the optical properties of the iron chalcogenide $FeTe_{0.55}Se_{0.45}$.
   Phys. Rev. B **81**, 180508 (2010).
2. S.-H. Lee, G. Y. Xu, W. Ku, J. S. Wen, C. C. Lee, N. Katayama, Z. J. Xu, S. Ji, Z. W. Lin, G. D. Gu, H.-B. Yang, P. D. Johnson, Z.-H. Pan, T. Valla, M. Fujita, T. J. Sato, S. Chang, K. Yamada, and J. M. Tranquada.
   Coupling of spin and orbital excitations in the iron-based superconductor $FeSe_{0.5}Te_{0.5}$.
   Phys. Rev. B **81**, 220502(R) (2010).
3. Z. J. Xu, J. S. Wen, G. Y. Xu, Q. Jie, Z. W. Lin, Q. Li, S. X. Chi, D. K. Singh, G. D. Gu, and J. M. Tranquada.
   Disappearance of static magnetic order and evolution of spin fluctuations in $Fe_{1+\delta}Se_xTe_{1-x}$.
   Phys. Rev. B **82**, 104525 (2010).
4. H. Gretarsson, A. Lupascu, Jungho Kim, D. Casa, T. Gog, W. Wu, S. R. Julian, Z. J. Xu, J. S. Wen, G. D. Gu, R. H. Yuan, Z. G. Chen, N.-L. Wang, S. Khim, K. H. Kim, M. Ishikado, I. Jarrige, S. Shamoto, J.-H. Chu, I. R. Fisher, and Y.-J. Kim.
   Revealing the dual nature of magnetism in iron pnictides and iron chalcogenides using x-ray emission spectroscopy.
   Phys. Rev. B **84**, 100509 (2011).
5. C. C. Homes, A. Akrap, J. S. Wen, Z. J. Xu, Z. W. Lin, Q. Li, and G. D. Gu.
   Optical properties of the iron-chalcogenide superconductor $FeTe_{0.55}Se_{0.45}$.
   J. Phys. Chem. Solids **72**, 505–510 (2011).
6. N. Katayama, S. Ji, D. Louca, S.-H. Lee, M. Fujita, T. J. Sato, J. S. Wen, Z. J. Xu, G. D. Gu, G. Y. Xu, Z. W. Lin, M. Enoki, S. Chang, K. Yamada, and J. M. Tranquada.
   Investigation of the Spin-Glass Regime between the Antiferromagnetic and Superconducting Phases in $Fe_{1+y}Se_xTe_{1-x}$.
   J. Phys. Soc. Jpn. **79**, 113702 (2010).
7. X. Liu, C.-C. Lee, Z. J. Xu, J. S. Wen, G. Gu, W. Ku, J. M. Tranquada, and J. P. Hill.
   X-ray diffuse scattering study of local distortions in $Fe_{1+x}Te$ induced by excess Fe.
   Phys. Rev. B **83**, 184523 (2011).
8. S. J. Moon, C. C. Homes, A. Akrap, Z. J. Xu, J. S. Wen, Z. W. Lin, Q. Li, G. D. Gu, and D. N. Basov.
   Incoherent c-Axis Interplane Response of the Iron Chalcogenide $FeTe_{0.55}Se_{0.45}$

Superconductor from Infrared Spectroscopy.
Phys. Rev. Lett. **106**, 217001 (2011).
9. J. S. Wen, G. Y. Xu, G. D. Gu, J. M. Tranquada, and R. J. Birgeneau.
Interplay between magnetism and superconductivity in iron-chalcogenide superconductors: crystal growth and characterizations.
Rep. Prog. Phys. **74**, 124503 (2011).
10. Z. J. Xu, J. S. Wen, G. Y. Xu, S. X. Chi, W. Ku, G. D. Gu, and J. M. Tranquada.
Local-moment magnetism in superconducting $FeTe_{0.35}Se_{0.65}$ as seen via inelastic neutron scattering.
Phys. Rev. B **84**, 052506 (2011).
11. I. A. Zaliznyak, A. T. Savici, V. O. Garlea, R. W. Hu, and C. Petrovic.
Absence of localized-spin magnetism in the narrow-gap semiconductor $FeSb_2$.
Phys. Rev. B **83**, 184414 (2011).
12. H. Miao, P. Richard, Y. Tanaka, K. Nakayama, T. Qian, K. Umezawa, T. Sato, Y.-M. Xu, Y. B. Shi, N. Xu, X.-P. Wang, P. Zhang, H.-B. Yang, Z.-J. Xu, J. S. Wen, G.-D. Gu, X. Dai, J.-P. Hu, T. Takahashi, and H. Ding.
Isotropic superconducting gaps with enhanced pairing on electron Fermi surfaces in $FeTe_{0.55}Se_{0.45}$.
Phys. Rev. B **85**, 094506 (2012).
13. I. A. Zaliznyak, Z. J. Xu, J. M. Tranquada, G. D. Gu, A. M. Tsvelik, and M. B. Stone.
Unconventional Temperature Enhanced Magnetism in $Fe_{1.1}Te$.
Phys. Rev. Lett. **107**, 216403 (2011).
14. I. A. Zaliznyak, Z. J. Xu, J. S. Wen, J. M. Tranquada, G. D. Gu, V. Solovyov, V. N. Glazkov, A. I. Zheludev, V. O. Garlea, and M. B. Stone.
Continuous magnetic and structural phase transitions in $Fe_{1+y}Te$.
Phys. Rev. B **85**, 085105 (2012).

Vibrational Thermodynamics of Materials

B. Fultz (btf@caltech.edu) *Dept. of Applied Physics and Materials Science, California Institute of Technology, Pasadena, CA 91125*

Research Scope

The objective is to understand the origins of the vibrational entropy of materials, and how it affects phase stability and phase transformations. Today our understanding of the vibrational entropy of materials at low and moderate temperatures is emerging nicely. Our present research addresses phenomena that are less well understood, especially at high temperatures. At elevated temperatures, atom vibrations are the primary source of entropy of materials, and vibrational entropy can be assessed with accurate phonon densities of states (DOS). Most of our work uses inelastic neutron scattering measurements with direct geometry chopper spectrometers like ARCS at the SNS.

At high temperatures our understanding of vibrational entropy must include phonon interactions with other phonons or with electronic excitations. These topics are intellectually rich, and of practical importance because most methods for synthesizing metals and oxides involve high temperatures, and thermodynamics is especially relevant to materials processing at high temperatures. A challenge is to separate and quantify the different sources of non-harmonic entropy, for which we combine measurements at elevated temperature and pressure with computational work. Our experimental plans must be compatible with these methods, but there is no lack of good cases where non-harmonic effects are likely to be large, measurable by inelastic scattering methods, and interpretable by computational materials science. The main focus of our work is on thermodynamics, which determines the structure of materials. Nevertheless, the work is also relevant to properties such as thermal conductivity and thermal expansion.

Recent Progress

Anharmonic Phonons in fcc Metals and Oxides: At high temperatures there is a hierarchy of non-harmonic effects, and we have developed methods for separating them into quasiharmonic entropy, and anharmonic entropy from cubic and quartic behavior of different orders. In the quasiharmonic approximation, at elevated temperature the phonons are assumed to be harmonic, but shifted a bit in energy. In reality, however, the phonons rarely behave as independent normal modes. Short phonon lifetimes are caused by coupling the energy of one phonon to other phonons through cubic anharmonic parts of the interatomic potentials. We used a new real-space DFT computational method to calculate the cubic anharmonicity tensor for the fcc structure, and we developed a code to sort through phonon dispersion information to extract all three-phonon processes that conserve energy and momentum. This allowed calculations of phonon lifetimes. Some results for Al are shown in Fig. 1. We published similar results for Cu, Ag, Au, and we are completing work on Pd and Pt.

In work with Raman spectrometry, we identified and classified the different anharmonic modes in HfO_2 and ZrO_2. In recent work on rutile TiO_2, we calculated the kinematically-allowed three- and four-phonon processes that are responsible for phonon linewidths and

shifts, and used these functions to fit the Raman spectra at elevated temperature. (Pressure-dependent results were used to account for the quasiharmonic contributions.)

An emerging trend for phonon lifetimes is that the cubic anharmonicity arises primarily from first-nearest neighbor interactions, and does not vary strongly with direction. Instead, the kinematically-allowed up-scattering and down-scattering phonon processes dominate the phonon lifetime broadening. We are testing whether we can obtain the phonon lifetimes needed for understanding thermal conductivity from only phonon dispersion curves and their kinematically-allowed phonon-phonon interactions. The cubic anharmonicity tensor may be possible to approximate with a simple form, and we are exploring practical ways to estimate it from a few experimental measurements.

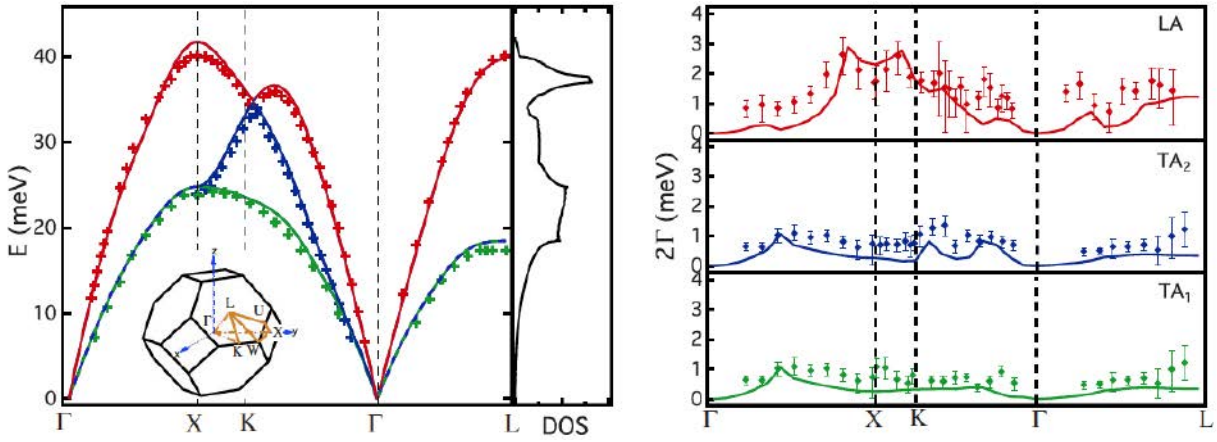

Fig. 1. Left: Calculated phonon dispersion of fcc Al at 0 K (with DOS appended at right). Right: Corresponding linewidths at 300 K (solid lines). Symbols are 3-axis neutron spectrometry measurements from the literature.

Electron-Phonon Interactions in Metals and Alloys: Electron-phonon interactions were once considered low-temperature phenomena, but they have also proved important in the high-temperature thermodynamics of some metallic alloys. Their high temperature systematics are little explored, but we can get help from calculations of the electronic structure near Fermi surfaces. We measured the phonon DOS of Fe-50%V as this alloy underwent an ordering phase transformation. In all cases measured to date, ordering causes a stiffening of phonon modes and a reduction of vibrational entropy. For B2 ordering in FeV, however, the phonons softened by a significant amount, increasing the vibrational entropy by 0.22 k_B/atom. The origin of this effect was a change in the electron-phonon interaction. Electronic structure calculations showed the development of a high density of states at the Fermi level when ordering occurred. An anomalous feature was observed in the temperature-dependence of the phonon DOS of the superconductor $Mg^{11}B_2$, which could be attributable to electron-phonon interactions.

Negative Thermal Expansion and Quartic Phonons: Cubic scandium trifluoride (ScF_3) has a large negative thermal expansion over a wide range of temperatures (Fig. 2a). Inelastic neutron scattering was used to measure the temperature dependence of the lattice dynamics of ScF_3 from 7 to 750 K. The measured phonon DOS curves (Fig. 2b) show a large anharmonic

contribution with a thermal stiffening of modes around 25 meV. Frozen phonon calculations showed that some of these modes with F atom motions transverse to their bond direction were quantum quartic oscillators (Fig. 2c). The quartic potential originates from how phonon coordinates in the DO_9 structure project onto the harmonic forces between atoms. The quartic phonon potential accounts for phonon stiffening with temperature and a significant part of the negative thermal expansion.

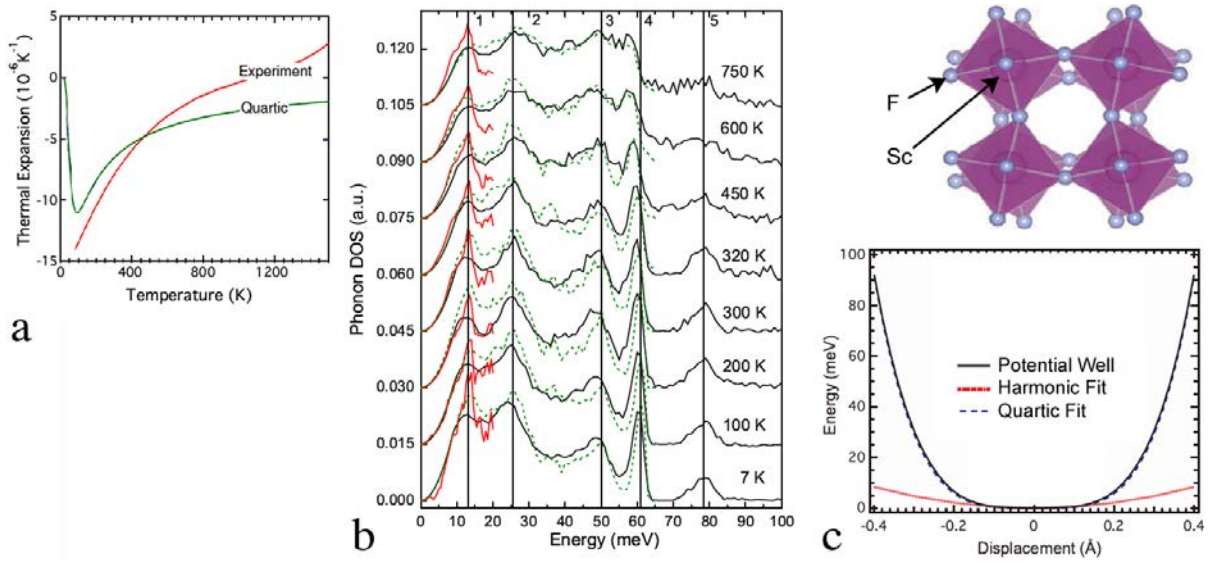

Fig. 2. (a) Thermal expansion of ScF_3. (b) Phonon DOS of ScF_3 from inelastic neutron scattering at different temperatures and with different incident energies. (c) A quartic mode at the R-point from frozen phonon calculations.

Future Plans

We plan to study materials with large phonon-phonon anharmonicity or electron-phonon interactions that should alter phase stability and phase transformations at elevated temperatures. For phonon anharmonicity, both crystal structure and thermal expansion anomalies are guiding our selection of experiments. We will study crystals where some atoms do not have inversion symmetry. (With inversion symmetry the cubic anharmonicity vanishes to first order, but without inversion symmetry the cubic anharmonicity can have first-order effects that are probably large.) The mineral structure fayalite (Fe_2SiO_4), $FeGe_2$, and also cementite (Fe_3C) seem promising for study. After accounting for the quasiharmonic contributions, we can interpret their anharmonicities with approaches based on the perturbation theory of Maradudin and Fein. For strongly anharmonic materials we are in unexplored territory, however, and interpretations may be challenging for upcoming work on Ag_2O and Cu_2O.

For electron-phonon interactions, we are studying carbon structures of different dimensionality, and gold-iron alloys, which have predominantly free electron character with localized *d*-states at iron atoms. For both we are developing interpretations based on their generalized electronic susceptibilities, which account for how periodic perturbations generate kinematically-allowed coupling of electron states across the Fermi surface.

To improve experimental methodology, we will continue to develop furnaces for inelastic neutron scattering with chopper spectrometers. The ARCS instrument is acquiring radial collimators that should further suppress backgrounds from the sample environment and allow higher quality data and higher sample temperatures. Combining nuclear resonant inelastic x-ray scattering data (from sectors 3 or 16 at the APS) with inelastic neutron scattering data has proved a powerful combination for iron alloys, allowing us to obtain both an accurate total DOS and both partial DOS curves for binary alloys.

Refereed Publications (2009-2011)

C.W. Li, M.M. McKerns, and B. Fultz, "Raman spectrometry study of phonon anharmonicity of hafnia at elevated temperatures," Phys. Rev. B **80**, 054304 (2009).

M.S. Lucas, O. Delaire, M.L. Winterrose, T. Swan-Wood, M. Kresch, I. Halevy, B. Fultz, J. Hu, M. Lerche, M.Y. Hu, M. Somayazulu, "Effects of Vacancies on Phonon Entropy of B2 FeAl," Phys. Rev. B **80**, 214303 (2009).

B. Fultz, "Vibrational Thermodynamics of Materials," Progress in Materials Science **55**, 247-352 (2010).

M. S. Lucas, J. A. Muñoz, L. Mauger, C.W. Li, A. Sheets, Z. Turgut, J. Horwath, D.L. Abernathy, M.B. Stone, O. Delaire, Yuming Xiao, and B. Fultz, "Effects of chemical composition and B2 order on phonons in bcc Fe-Co alloys," J. Appl. Phys. **108**, 023519 (2010).

X. Tang, C.W. Li, and B. Fultz, "Anharmonicity-induced phonon broadening in aluminum at high temperatures," Phys. Rev. B **82**, 184301 (2010).

M.S. Lucas, J.A. Muñoz, O. Delaire, N. Markovskiy M.B. Stone, D. L. Abernathy, I. Halevy, L. Mauger, J.B. Keith, M.L. Winterrose, Yuming Xiao, M. Lerche, and B. Fultz, "Effects of composition, temperature, and magnetism on phonons in bcc Fe-V alloys," Phys. Rev. B **82**, 144306 (2010).

J. A. Munoz, M. S. Lucas, O. Delaire, M. L. Winterrose, L. Mauger, C.W. Li, A. O. Sheets, M. B. Stone, D. L. Abernathy, Yuming Xiao, Paul Chow, and B. Fultz, "Positive vibrational entropy of chemical ordering in FeV," Phys. Rev. Lett. **107**, 115501 (2011).

C.W. Li, M.M. McKerns, and B. Fultz, "Raman spectrometry study of phonon anharmonicity of zirconia at elevated temperatures," J. Amer. Ceramic Soc. **94**, 125-130 (2011).

X. Tang and B. Fultz, "A first-principles study of phonon linewidths in noble metals," Phys. Rev. B **84**, 054303 (2011).

N. D. Markovskiy, J. A. Munoz, M. S. Lucas, C.W. Li, O. Delaire, M. B. Stone, D. L. Abernathy and B. Fultz, "Non-harmonic phonons in MgB_2 at elevated temperatures," Phys. Rev. B **83**, 174301 (2011).

C.W. Li, X. Tang, J.A.Muñoz, J.B. Keith, S.J. Tracy, D.L. Abernathy, and B. Fultz, "The structural relationship between negative thermal expansion and anharmonicity of cubic ScF_3," Phys. Rev. Lett. **107**, 195504 (2011). Also see: J. Paul Attfield, "Condensed-matter physics: A fresh twist on shrinking materials," Nature **480**, 465466 (22 December 2011). Also see: Focus article in Physics **4**, 90 (2011).

Neutron Scattering Study of Strongly Correlated Systems

T. Egami (egami@utk.edu)
Joint Institute for Neutron Sciences, University of Tennessee, Knoxville, TN 37996
Oak Ridge National Laboratory, Oak Ridge, TN 37831

Program Scope

Neutron scattering study is an important component in two research projects supported by DOE-BES, *Atomistic and mesoscopic study of metallic glasses* (FWP-ERKCM40) and *Neutron Scattering Research Network for EPSCoR States* (DE-FG02-08ER46528). In the metallic glass FWP neutron scattering is used in the study of the atomic structure and dynamics of metallic glasses and liquids in order to determine the mechanism of mechanical failure, viscosity, atomic transport and glass transition in metallic glasses. In the EPSCoR project it is used in the study of spin and lattice dynamics in Fe-based superconductors. In both cases strong correlations, among atoms in the case of liquids and glass, and among electrons in the case of Fe superconductors, pose a major challenge in scientific efforts to understand these systems. We use a real-space approach to analyze the results of neutron scattering in order to determine these correlations directly. Neutron scattering research is closely coupled with the effort on simulation and theory, particularly in the case of research on metallic glasses.

Recent Progress

1. Atomic Dynamics in Metallic Glasses and Liquids

Most thermal properties of crystalline materials can be understood and calculated through statistical mechanics with phonons as the elementary excitations whose dispersion can be readily determined by diagonalizing the dynamical matrix [1]. However, the same does not apply to liquids and glasses, because phonons are strongly scattered and have a short life-time. In particular in liquids the dynamical matrix itself is time-dependent, thus diagonalization of the dynamical matrix does not lead to elementary excitations. Consequently the total energy of a liquid is not proportional to temperature, but follows a $T^{3/5}$ law [2]. We proposed a solution to this conundrum by showing that the dynamics of atomic level stresses [3] follow the equipartition theorem [4-6]. The atomic level stresses are mainly determined by the nearest neighbor atoms, thus their dynamics describes the dynamics of the nearest neighbor shell [7]. In order to prove this concept we calculated the dynamic pair-density function (DPDF) for a liquid iron by molecular dynamics. DPDF, $\rho(r,\omega)$, is obtained as the Fourier-transform of $S(Q,\omega)$, and describes the local dynamics [8]. The result shown in Fig. 1 clearly demonstrates super-localization of atomic vibration to the nearest neighbor above 10 meV (Debye frequency is 40 meV). We measured the DPDF for liquid Sn using the ARCS of the SNS. The preliminary result shown in Fig. 2 is promising and indicates strong dynamic localization, but termination errors are too intense to draw a definite conclusion. We are working on improving the background subtraction and normalization to reduce the termination errors. We also measured $S(Q,\omega)$ using ARCS for a metallic glass, $Zr_{50}Cu_{40}Al_{10}$, under a compressive stress of 1.51 GPa which is 80% of the yield stress. Marked increase in the density of excitations, thus softening, was observed at low energies (10 – 20 % at 5 – 10 meV). This energy range coincides with that for the boson peak. This softening is consistent with the idea that applied shear stress can induce the glass transition and viscous flow even at low temperatures [P3, P21].

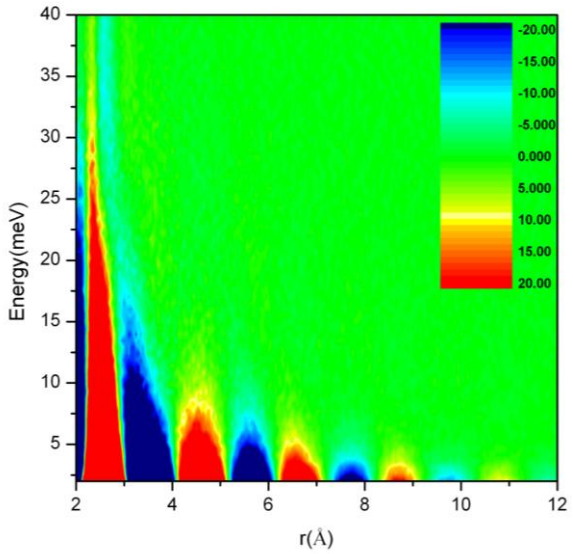

Fig. 1 Dynamic PDF of liquid iron calculated by MD for $T = 3000$K. Above 10 meV vibrational amplitude is seen only for the nearest neighbor at 2.6 Å, confirming super-localization.

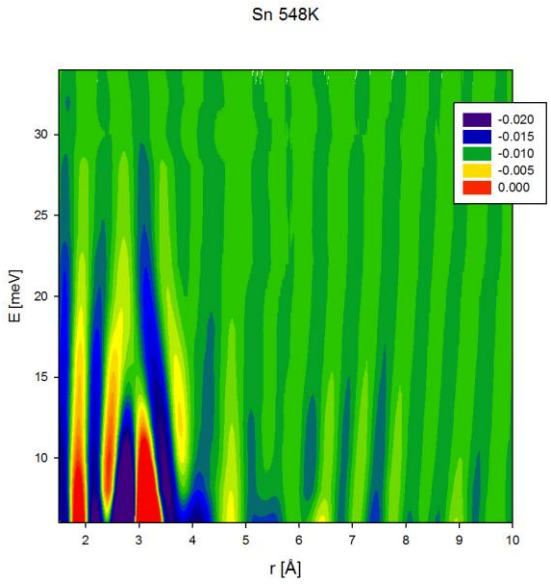

Fig. 2 DPDF for liquid Sn at 548K measured with ARCS. Termination errors are too large to draw a definite conclusion.

2. Spin Dynamics in Fe Based Superconductors

In spite of intense research effort after the discovery of high-temperature superconductivity in Fe onictides a few years ago the mechanism of high-temperature superconductivity remains a mystery. In our effort to understand the basic spin interactions [P18] we found that the high-energy spin excitations (Fig. 3) are very similar among all of the iron pnictides and tellurides, in spite of significant differences in the spin order. This is because the common and strongest magnetic interaction is the second neighbor Fe-Fe exchange, J_2, and it determines the overall spin dynamics. The nearest neighbor interaction, J_1, determines the static magnetic structure, but is less important for dynamics, and possibly for superconductivity.

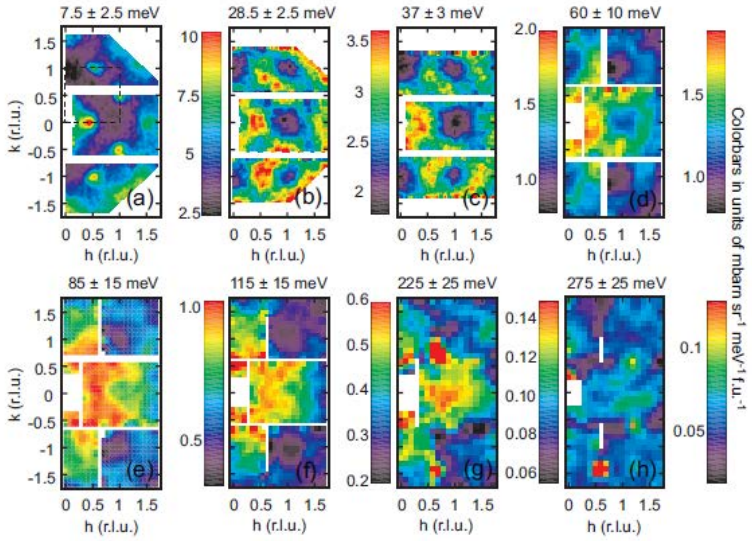

Fig. 3 Spin excitations in $Fe_{1.05}Te$ single crystal measured with ARCS [P18].

Future Plans

We are currently building an electro-static liquid levitator in collaboration with K. Kelton of Washington University. We plan to carry out a study of the structure and dynamics of metallic liquid without contact with a container, thus enabling deep supercooling, using this method. We

will use this system with NOMAD (SNS) to study the structure, and with ARCS to study the dynamics. The levitator will give us clean scattering data with less background, which will be helpful in obtaining the DPDF with less noise. We hope to confirm the predicted superlocalization in the liquid using this levitator. With Fe superconductors we focus on obtaining direct evidence of spin-phonon coupling predicted earlier [P8, P12], by observing the spin signal from phonons. Even though the conventional electron-phonon (*e-p*) coupling via the charge channel is weak in Fe pnictides, this spin-channel *e-p* coupling may be much stronger.

References

1. M. Born and K. Huang, "Dynamical theory of crystal lattices" (Clarendon Press, Oxford, 1954).
2. Y. Rosenfeld and F. Tarazona, "Density functional theory and the asymptotic high density expansion of the free energy of classical solids and fluids," *Molecular Physics* **95,** 141 (1998).
3. T. Egami, K. Maeda, and V. Vitek, "Structural Defects in Amorphous Solids: A Computer Simulation Study", *Phil. Mag. A* **41**, 883 (1980).
4. T. Egami and D. Srolovitz, "Local Structural Fluctuations in Amorphous and Liquid Metals: A Simple Theory of Glass Transition", *J. Phys. F* **12**, 2141 (1982).
5. S.-P. Chen, T. Egami and V. Vitek, "Local Fluctuations and Ordering in Liquid and Amorphous Metals", *Phys. Rev. B* **37**, 2440 (1988).
6. V. A. Levashov, R. S. Aga, J. R. Morris and T. Egami, "Equipartition Theorem and the Dynamics of Liquids", *Phys. Rev. B,* **78,** 064205 (2008).
7. T. Egami, "Atomic Level Stresses", *Progr. Mater. Sci.* **56,** 637 (2011).
8. W. Dmowski, S. B. Vakhrushev, I.-K. Jeong, M. P. Hehlen, F. Trouw and T. Egami, "Local Lattice Dynamics and the Origin of the Relaxor Ferroelectric Behavior", *Phys. Rev. Lett.*, **100,** 137602 (2008).

Publications (FY10-12)

P1. *Structural Rejuvenation in a Bulk Metallic Glass Induced by Severe Plastic Deformation*, W. Dmowski, Y. Yokoyama, A. Chuang, Y. Ren, M. Umemoto, K. Tuchiya, A. Inoue, and T. Egami, *Acta Materialia*, **58,** 429 (2010).

P2. *Understanding the Properties and Structure of Metallic Glasses at the Atomic Level*, T. Egami, *Journal of Metals*, **62,** 2, 70 (2010).

P3. *On the Stress-Temperature Scaling for Steady-State Flow in Metallic Glasses*, P. Guan, M.-W. Chen and T. Egami, *Phys. Rev. Lett.,* **104,** 205701 (2010).

P4. *Elastic Heterogeneity in Metallic Glasses*, W. Dmowski, T. Iwashita, C.-P. Chuang, J. Almer and T. Egami, *Phys. Rev. Lett.* **105,** 205502 (2010).

P5. *Statistical Mechanics of Metallic Glasses and Liquids*, T. Egami, V. A. Levashov, J. R. Morris and O. Haruyama, *Mater. Trans. A*, **41,** 1628 (2010).

P6. *A quantitative comparison of simulated crystal nucleation for the Lennard-Jones system with classical nucleation theory*, L. J. Peng, J. R. Morris and R.S. Aga, *J. Chem. Phys* **133**, 084505 (2010).

P7. *Specimen Size Effects on Zr-based Bulk Metallic Glasses Investigated by Uniaxial Compression and Spherical Nanoindentation*, H. Bei, Z. P. Lu, S. Shim, G. Chen, and E. P. George, *Metall. Mater. Trans*. **41** A 1735-1742 (2010).

P8. *Spin-Lattice Coupling and Superconductivity in Fe Pnictides*,
T. Egami, B. Fine, D. Parshall, A. Subedi and D. J. Singh, *Adv. Cond. Mat. Phys*., **2010,** 164916 (2010).

P9. *Neutron scattering patterns show Superconductivity in $FeTe_{0.5}Se_{0.5}$ likely results from itinerant electron fluctuations*,
H. A. Mook, M. D. Lumsden, A. D. Christianson, B. C. Sales, R. Jin, M. A. McGuire, A. S. Sefat, D. G. Mandrus, S. E. Nagler, T. Egami, and Clarina de la Cruz, *Phys. Rev. Lett.*, **104,** 187002 (2010)

P10. *2D Order in Ni^{1+}/Ni^{2+} (d^9/d^8) Nickelate, $La_4Ni_3O_8$, Isoelectronic with Superconducting Cuprates*,
V. V. Poltavets, K. A. Lokshin, A. H. Nevidomskyy , M. Croft, T. A. Tyson, J. Hadermann, G. Van Tendeloo, T. Egami, G. Kotliar, Martha Greenblatt, *Phys. Rev. Lett.*, **104,** 206403 (2010).

P11. *Anisotropic Neutron Spin Resonance in Superconducting $BaFe_{1.9}Ni_{0.1}As_2$*,
O. J. Lipscombe, L. W. Harriger, P. G. Freeman, M. Enderle, C. Zhang, M. Wang, T. Egami, J. Hu, T. Xiang, M. R. Norman, and P. Dai, *Phys. Rev. B,* **82,** 064515 (2010)

P12. *Spin-Lattice Coupling in Iron Pnictide Superconductors*,
T. Egami, B. Fine, D. J. Singh, D. Parshall, C. de la Cruz and P. Dai, *Physica C,* **470,** S294 (2010).

P13. *Viscosity and Atomic Level Stress Correlation in a Supercooled Liquid*,
V. A. Levashov, J. R. Morris and T. Egami, *Phys. Rev. Lett.* **106,** 115703 (2011).

P14. *Linear Response Theory for Hard and Soft Glassy Materials*,
E. Bouchbinder and J. S. Langer, *Phys. Rev. Lett.* **106,** 148301 (2011).

P15. *Atomic Level Stresses*,
T. Egami, *Progr. Mater. Sci.* **56,** 637 (2011).

P16. *Mechanical Failure and Glass Transition in Metallic Glasses*,
T. Egami, *J. Alloys and Compounds*, **509S,** S82 (2011).

P17. *Crystalline and Amorphous Models of Highly Damaged Fe*,
M. Ojha, D. M. Nicholson, B. Radhakrishnan, R. E. Stoller and T. Egami, *MRS Symp. Proc.* **1363,** 05-32 (2011).

P18. *Spin Waves in the (π, 0) Magnetically Ordered Iron Chalcogenide $Fe_{1.05}Te$*,
O. J. Lipscombe, G. F. Chen, Chen Fang, T. G. Perring, D. L. Abennathy, A. D. Christianson, Takeshi Egami, Nanlin Wang, Jiangpin Hu and Pengcheng Dai, *Phys. Rev. Lett*. **106,** 057004 (2011).

P19. *Phonon Softening Near Structural Transition in $BaFe_2As_2$ Observed by Inelastic X-ray Scattering*,
Jennifer Niedziela, D. Parshall, K. Lokshin, A. S. Sefat, A. Alatas and T. Egami, *Phys. Rev. B*, **84,** 224305 (2011).

P20. *Glass Formability and Al-Au System*,
T. Egami, M. Ojha, D. M. Nicholson, D. Louzguine-Luzgin, N. Chen and A. Inoue, *Phil. Mag. A*, **92,** 655 (2012).

P21. *Atomic Mechanism of Flow in Simple Liquids under Shear*,
T. Iwashita and T. Egami, *Phys. Rev. Lett.*, **108,** 196001 (2012).

Session IV

Energy Materials

From Fundamental Understanding to Predicting New Nanomaterials for High-Capacity Hydrogen/Methane Storage and Carbon Capture

Taner Yildirim [1,2]
[1]Department of Materials Science and Eng., University of Pennsylvania, Philadelphia, PA 19104
[2]National Institute of Standards and Technology, NCNR, Gaithersburg, MD 20899
Phone: (301) 975-6228, Email: taner@seas.upenn.edu

Research Scope

On-board hydrogen/methane storage in fuel cell-powered vehicles is a major component of the national need to achieve energy independence and protect the environment. Fundamental breakthrough discoveries in materials science will be required to achieve light-weight, low-volume, safe, economical and recyclable storage technology. The main obstacles in hydrogen storage are slow kinetics, poor reversibility and high dehydrogenation temperatures for the chemical hydrides; and very low desorption temperatures/energies for the physisorption materials (MOF's, porous carbons). Carbon capture suffers from similar problems where the current technology is based on absorption in amine-based solvents which has limited reversibility and high regeneration cost. The solid-absorbers such as MOFs are either not stable against real flue-gas conditions and/or do not have large enough CO_2 capture (i.e. working) capacity to be practical and cost effective.

The main scope of our research is to use neutron scattering methods along with first-principles computation to achieve fundamental understanding of the chemical and structural interactions governing the storage and release of hydrogen/methane and carbon capture in a wide spectrum of candidate materials. The main goals are to study the effect of scaffolding, nanosizing, doping of the candidate materials on their storage and dynamics properties and to provide timely feedback and guidance from theory to de novo materials design and targeted syntheses throughout the DOE programs.

Recent Progress

We are currently working on many research avenues along the lines discussed in our original proposal. Below we briefly discuss some selected recent results.

1. Direct Observation of Activated Hydrogen Binding to a Supported Organometallic Compound at Room Temperature

The optimum conditions for viable room temperature hydrogen storage require materials that possess isosteric heats of adsorption in between that of standard physisorbers and chemisorbers, typically in the ~20-30 kJ/mol regime. Theoretical works have shown that the incorporation of transition metal atoms onto a porous support can provide such binding energies with multiple hydrogen molecules adsorbed. However, despite the very large number of theoretical works, there is no direct experimental proof of these predictions yet. Herein, we present direct experimental evidence for dihydrogen-Ti binding on a silica-supported Ti(III) organometallic complex (Fig. 1a) using detailed sorption and inelastic neutron scattering (INS) measurements. Our experimental findings are further supported by extensive first principles DFT and reaction path calculations.

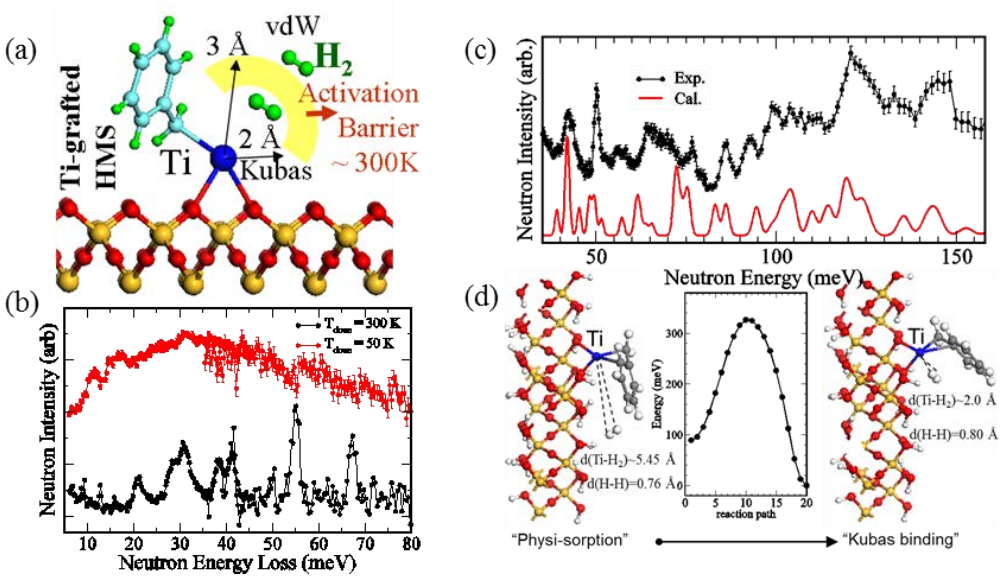

Fig. 1 (a) A schematic view of Ti-HMS, exhibiting activated hydrogen bonding at room temperature. (b) Comparison of the INS spectra at 4 K, showing the low energy modes from H_2 adsorbed at low temperature (50 K, red) and at room temperature (300 K, black). Room temperature sorption of hydrogen leads to a dramatically different spectra as compared to the spectrum from the hydrogen that was adsorbed at low temperature. The signatures of molecularly adsorbed hydrogen, namely the low energy (~ 12 meV to 17 meV) rotational peaks and recoil background, are entirely absent. Instead, there are several vibrational bands in the 20 meV to 100 meV range which are attributed to Kubas-like hydrogen binding. (c) Comparison of the INS spectra of the activated Ti-HMS and a simple DFT model where Ti-benzyl is attached to hydrogen-passivated HMS surface. (d) The calculated reaction path from physisorption to Kubas like hydrogen binding with an activation barrier, consistent with our measurements.

Surprisingly, from INS measurements (Fig. 1b) we discover that the H_2—Ti binding is a thermally activated process; exposing the supported organometallic to hydrogen below 150 K results in only physisorption while near room temperature it forms H_2—Ti moieties that are stable for extended periods of time. This surprising finding is very important and it suggests that in the search for new hydrogen storage materials, one should not limit the measurements at 77 K (which is a standard procedure) but also check absorption isotherms at room or higher temperatures for a possible activated binding. Having experimentally established the efficacy of these supported dihydrogen complexes, future work can be focused on optimizing the surface and volume density of the binding sites through choice of ligands and supports.

2. Structure and Rotational Tunneling of Methane in Metal-Organic Frameworks

Metal-organic framework (MOF) compounds are nanoporous materials that show promise for storage of gases such as H_2 and CH_4. In order to optimize these materials for practical adsorption--based applications, it is of great importance to understand the fundamental physics of the MOF-gas molecule interaction. Methane molecule is classical in terms of center of mass motion but it acts like a spherical quantum rotor for the rotational motion, yielding tunnel splitting. Its hindered rotational spectrum provides rich information about the strength and symmetry of local potentials. Therefore, studying methane dynamics in MOFs can yield very accurate and invaluable information about the

guest-host interactions. Here, we first directly determined the CH_4 adsorption sites in MOF5 using the difference-Fourier analysis of neutron powder diffraction data. Remarkably, the orientation of CH_4 molecule was clearly revealed, implying strong molecule-host lattice interaction and relatively large energy barriers to rotation. Using INS, we have studied the quantum rotational dynamics of CH_4 molecules by measuring rotational tunnel splitting. A calculation using rotational potential barriers of 41 and 22 meV around the 3- and 3'-fold axes respectively is in good agreement with the measurements and in reasonable agreement with the results of total energy calculations using density functional theory.

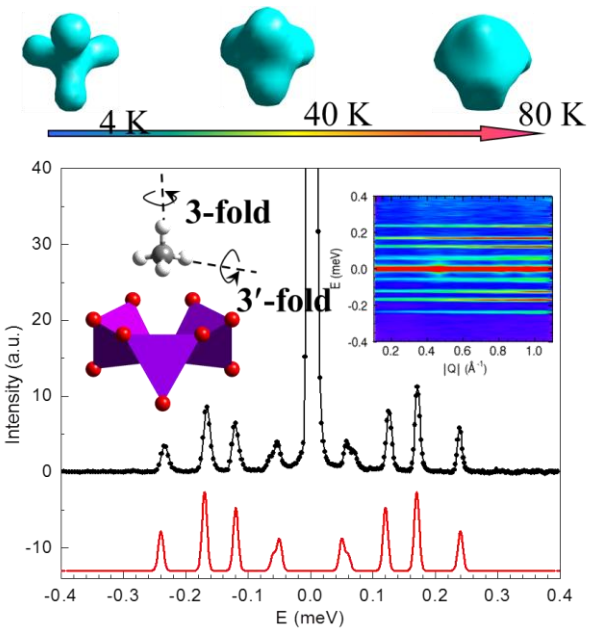

3. *Efficient Carbon Capture in Metal-Organics Frameworks (MOFs)*

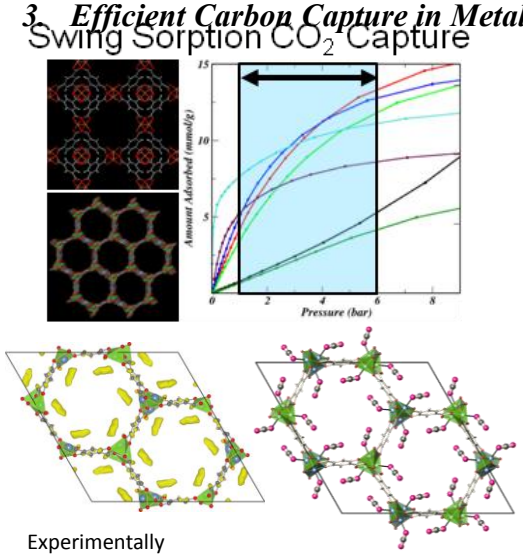

Investigations of the application of MOFs to adsorptive carbon capture have focused on their appreciable storage capacities but fail to address the more pertinent issue of how MOFs perform under common industrial separation processes that are at the heart of carbon capture. Typical processes rely on swing adsorption and are limited to relatively low CO_2 partial pressures such that the total pore volume and the surface area are under-utilized. Here, we investigate the performance of a number of metal–organic frameworks with particular focus on their behavior at the low pressures commonly used in swing adsorption. This comparison clearly shows that it is the process that determines which MOF is optimal rather than there being one best MOF, though MOFs that possess enhanced binding at open metal sites generally perform better than those with high surface area. In particular, using neutron scattering we unrevealed the mechanism of carbon capture and found that MOFs that possess coordinatively unsaturated metal centers offer as much as 9 mmol g-1 swing capacity under certain conditions. This work will be an important guideline for deciding the best pair of carbon capture process and MOF material for optimum carbon capture.

Future Directions

We will continue investigating H_2/CH_4 and CO_2 absorption mechanism/kinetics of a large number of candidate materials using tightly coupled neutron scattering and first-principles computation. We will perform more work on nanoporous carbon materials

derived from Graphene oxide and MOFs, functionalize them such as B and N doping to tune their hydrogen storage and carbon capture properties.

Recent Publications acknowledging the DOE BES grant (2010-2012)

1. *Direct Observation of Activated Hydrogen Binding to a Supported Organometallic Compound at Room Temperature*, J. M. Simmons, T. Yildirim, A. Hamaed, D. M. Antonelli, M. I. Webb, and C. J. Walsby, Chem. Eur. J. **18**, 4170 (2012).
2. *Metal hydrazinoborane $LiN_2H_3BH_3$ and $LiN_2H_3BH_3 \bullet 2N_2H_3BH_3$: Crystal structures and high-extent dehydrogenation*, H. Wu, W. Zhou, F. Pinkerton, T. Udovic, T. Yildirim and J. Rush , Energy Environ. Sci., DOI: 10.1039/C2EE21508J, Communication (2012)
3. *Graphene oxide derived carbons (GODCs): synthesis and gas adsorption properties*, G. Srinivas, J. Burress and T. Yildirim, Energy Environ. Sci. 5, 6453-6459 (2012, commun.)
4. *Carbon capture in metal–organic frameworks—a comparative study*, J. M. Simmons, H. Wu, W. Zhou and T. Yildirim, Energy Environ. Sci. **4**, 2177-2185 (2011).
5. *Porous graphene oxide frameworks: Synthesis and gas sorption properties*, G. Srinivas, J. W. Burress, J. Ford and T. Yildirim, J. Mater. Chem. **21**, 11323-11329 (2011).
6. *Sodium magnesium amidoborane: the first mixed-metal amidoborane*, H. Wu, W. Zhou, F. E. Pinkerton, M. S. Meyer, Q. Yao, S. Gadipelli, T. J. Udovic, T. Yildirim and J. J. Rush, Chem. Commun. **47**, 4102-4104 (2011).
7. "*A highly practical route for large-area, single layer graphene from liquid carbon sources such as benzene and methanol*", G. Srinivas, I. Calizo, J. Ford, G. Cheng, A. H. Walker, and Taner Yildirim, J. Mater. Chem. **21**, 16057-16065 (2011).
8. *Zn-MOF assisted dehydrogenation of ammonia borane: Enhanced kinetics and clean hydrogen generation*, G. Srinivas, J. Ford, Wei Zhou, and Taner Yildirim, Int. Journal of Hydrogen Energy, doi:10.1016/j.ijhydene.2011.04.008 (2011).
9. *Nanoconfinement and catalytic dehydrogenation of ammonia borane by magnesium-metal-organic-framework-74*, G. Srinivas, J. Ford, W. Zhou, H. Wu, T. J. Udovic, and Taner Yildirim, Chem. Eur. J. 17, doi:10.1002/chem.201100090 (2011)
10. *Graphene-Oxide-Framework (GOF) Materials; Theoretical Predictions and Experimental Results*, J. Burress, G. Srinivas, J. M. Simmons, J. Ford, W. Zhou, Taner Yildirim, Angew. Chem. Int. Ed.**, 49**, 8902-8904 (2010).
11. *Structural stability and elastic properties of prototypical covalent organic frameworks*, W. Zhou, H. Wu, Taner Yildirim, Chem. Phys. Lett. **499**, 103-107 (2010).
12. *A new family of metal borohydride ammonia borane complexes: Synthesis, structures, and hydrogen storage properties*, H. Wu, W. Zhou, F. E. Pinkerton, M. S. Meyer, G. Srinivas, Taner Yildirim, T. J. Udovic, J. Mat. Chem. **20**, 6550 (2010).
13. *Adsorption Sites and Binding Nature of CO_2 in Prototypical Metal-Organic Frameworks: A Combined Neutron Diffraction and First-Principles Study,* H. Wu, J. M. Simmons, G. Srinivas, W. Zhou, and Taner Yildirim J. Phys. Chem. Lett. **1**, 1946 (2010).
14. *Metal-Organic Frameworks with Exceptionally High Methane Uptake: Where and How is Methane Stored?*, H. Wu, J. M. Simmons, Y. Liu, C. M. Brown, X.-S. Wang, S. Ma, V. K. Peterson, P. D. Southon, C. J. Kepert, H.-C. Zhou, T. Yildirim, and W. Zhou, *Chem. Eur. J.*, 16, 5205–5214 (2010).
15. *Alkali and alkaline-earth metal dodecahydro-closo-dodecaborates: Probing structural variations via neutron vibrational spectroscopy*, N. Verdal, W. Zhou, V. Stavila, J.-H. Her, M. Yousufuddin, T. Yildirim, and T. J. Udovic, J. Alloys Comp. (2010).
16. *Metal Amidoboranes", Hui Wu, Wei Zhou, and Taner Yildirim, in "Boron Hydrides, High Potential Hydrogen Storage Materials*, edited by Umit B. Demirci and Philippe Miele, Nova Publishers (2010).

In-situ Neutron Scattering Determination of 3D Phase-Morphology Correlations in Fullerene Block Copolymer Systems

Alamgir Karim, Department of Polymer Engineering, University of Akron, Akron, OH
David Bucknall, School of Materials Science and Engineering,
Georgia Institute of Technology, Atlanta, GA
Dharmaraj Raghavan, Department of Chemistry, Howard University, Washington D.C.
Scott Sides, Tech-X Corporation, Boulder, CO

Research Scope

The efficiencies of OPV materials and devices must be enhanced several fold to make these next generation solar cells competitive with current inorganic or hybrid photovoltaics systems. To this end, the majority of current research in OPVs is largely focused on creating or developing new materials, processes and constructs for more efficient devices, which for the most part ignores a fundamental understanding of morphology effects. In order to achieve profound advances in OPVs, a fundamental understanding of a correlation between morphology and efficiency is however essential. The research objectives of this project has focused on investigating model disordered bulk heterojunction (BHJ) systems consisting of mixtures of fullerenes and conjugated homopolymer (P3HT), as well as model ordered BHJ's that would involve block copolymers (BCPs), acting either as nanostructured templates for ordered BHJ fabrication, or as conjugated BCPs with electron accepting nanoparticles.

The tunability of the morphology and structure of these model systems through synthesis of new materials, novel processing strategies and characterization of which a large component is neutron and X-ray scattering allow us to test fundamental issues that are currently poorly understood, and will ultimately offer vast potential for dramatic improvements in OPVs. Fundamental questions that we aim to address include a) how does the phase domain architecture, i.e. morphology of BHJ blend (phase domain evolution and crystallinity of both conjugated polymer and nanoparticle) correlate with OPV efficiency? b) how does the electronic levels of fullerene derivatives in BHJ blends impact the evolving morphology and efficiency? c) can we control the Z-segregated profile in BHJ blends using soft surface energy confinement d) can fullerene percolation in selective BCP domains be attained? *e*) how can simulations help understand these issues at a fundamental level?

We have developed important 3-way correlations that establish relationships between the complex temporally evolving hierarchical fullerene-BCP architecture with both the corresponding photoelectronic properties, representative of potential device efficiency, as well as the corresponding complex molecular fullerene-BCP interactions for a host of synthesized and commercial electron accepting nanoparticles, as well as with a recently synthesized conjugated P3HT-PS block copolymer. Advanced neutron scattering and imaging techniques are exploited to determine the detailed hierarchical structural information of model fullerene-BCP systems to address the critical questions (a-e) listed above.

Recent Progress

We summarize our recent progress in areas organized under **A) New organic photovoltaic materials synthesis B) Directed Assembly and Scattering Characterization for BHJs and C) Model device characterization d) Theory and Simulations.** Advances in each of these areas are discussed in more detail below.

A) New OPV Nanomaterials Synthesis and Characterization

i) Synthesis and characterization of electron acceptor nanoparticles: Following electron accepting nanoparticles (N-methyl fulleropyrrolidine derivatives) were synthesized and characterized as Tabulated below and fluorescence emission spectra are compared in Figure. 1.

Figure 1. Steady state Fluorescence spectra of fulleropyrrolidine derivatives in benzonitrile upon excitation at of 398 nm.

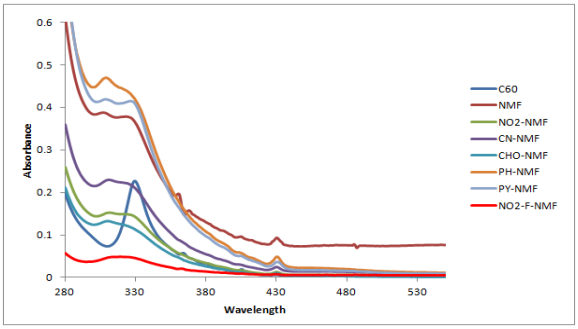

Table 3. Reduction potential of synthesized fulleropyrrolidine derivatives

	Reduction Potential (mV) / Ag/Ag^+			
Compounds	**E1/2(1)**	**E1/2(2)**	**E1/2(3)**	**LUMO (eV)**
C60 (Ref.)	-827	-1329	-1915	
C60 (Exp.)	-841	-1337	-1909	-4.04
PCBM	-940	-1435	-2029	-3.91
NMF	-971	-1463	-2064	-3.86
NO2-NMF	-951	-1432	-2119	-3.89
CN-NMF	-948	-1425	-2069	-3.90
CHO-NMF	-945	-1429	-2057	-3.90
PH-NMF	-968	-1468	-2096	-3.88
PY-NMF	-967	-1464	-2097	-3.88
NO2-F-NMF	-933	-1423	-2044	-3.91

Table I: Listed are the various fullerene acceptor nanoparticles derivatives with electronic properties listed and whose chemical yield was in the range of (35-55) %.

The LUMO energy level of these compounds was estimated from E_{red}^{on} value according to the following equation: LUMO = -e (E_{red}^{on} + 4.71) eV where the potential unit is V vs Ag/Ag^+. The important observation is that the LUMO levels of these nanoparticles are in the range of PCBM, so that their incorporation with P3HT model BHJ's should provide systematic trend on the correlational effect of molecular structure and electronic properties on device morphology and device output.

ii) Synthesis of PS-b-P3HT block copolymer

A block copolymer, PS-b-P3HT with one conjugated block (P3HT) was synthesized and characterized via the chemistry steps illustrated below. The PS block is short relative to P3HT, as the key idea is for it to sequester the electron accepting nanoparticles in close contact with the P3HT block to form well-ordered BHJ's with block copolymer solar cells. The concept of directed assembly of a conjugated block copolymer with 40% nanoparticles is novel, but requires much optimization and testing of processing parameters as the next challenge on this task.

Schematic 1: 5 Step Reaction Scheme used for Synthesis of PS-b-P3HT block copolymers

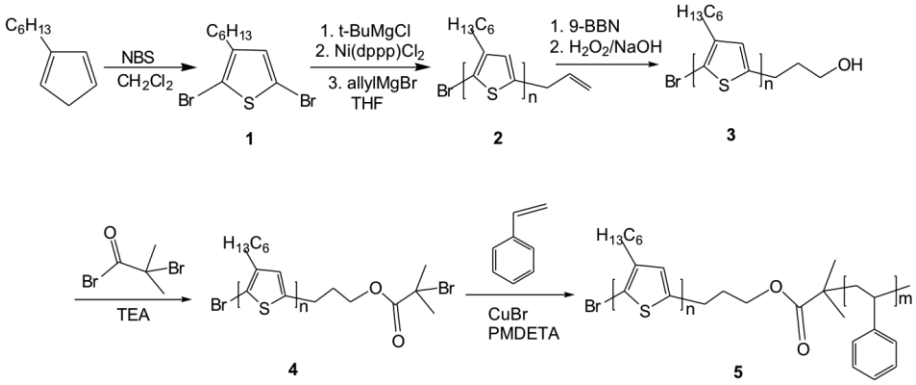

B) Directed Assembly and Scattering Characterization for BHJs:

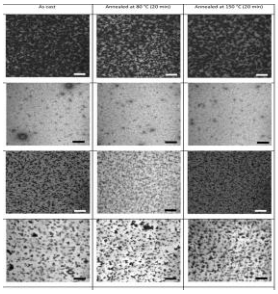

Thin Film Deposition and Characterization: Thin films of annealed poly(3-hexylthiophene) (P3HT) with different functionalized fulleropyrrolidines.

Figure 2 P3HT:Nanoparticle (60:40 w/w) blend dispersion morphology showed a non-monotonic trend in nanoparticle dispersion with a phase inversion in structure due to varying P3HT-Nanoparticle interaction. (Scale bar = 50 μm)

To understand polymer-fullerene interactions and explore the effect of ligands on the fullerene in the phase behavior with polymers and ultimately how this affects device performance, we have studied two homologous polymer systems – amorphous polyvinyls (polystyrene (PS), poly(vinyl naphthalene) (P2VN), and poly(vinyl phenanthrene (P9VP)), and semicrystalline polythiophenes (poly(3-butyl thiophene) (P3BT), poly(3-hexyl thiophene) (P3HT) and poly(3-octyl thiophene) (P3OT)). The fullerenes we have been exploring to date are the commercially available C_{60}, PCBM and bis-PCBM. Evaluation of their miscibility and morphology in thin films has been made and compared in the case of the polythiophene-fullerene systems to organic photovoltaic (OPV) devices. The miscibility of C_{60} in the vinyl polymers has been shown to increase non-linearly from 1 wt% to 12.5 wt% with increasing aromaticity of the side group (see Table II). This behavior has been explained due to the T-junction π-interactions between the phenyl side-group of the polymer and the symmetric C_{60} cage.[1] In comparison, using DSC analysis of the PCBM melt peak, we have determined the miscibility limit in these vinyl polymers to increase from 16.5 wt% to 74.9 wt % (Table II), reasons for this dramatic increase in solubility due to the presence of the phenyl-butyl methacrylate ligand under investigation via DFT studies.

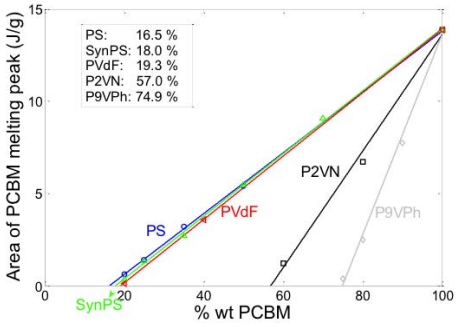

Figure 3: Results of DSC analysis of PCBM melt peak area as a function of composition for a range of polymers.

Table II: Miscibility limit (wt%) of C60 and PCBM in polyvinyls

Fullerene	PS	P2VN	P9VPh
C_{60}	1	2	12.5
PCBM	16.5	57.0	74.9

Next generation candidates for *ordered bulk heterojunctions* (O-BHJs) are conjugated block copolymers with molecularly spaced and oriented donor-acceptor block copolymer domains. While these molecules were being synthesized at Howard U. and ORNL-we have applied our unique in-house developed method of sharp cold zone annealing (CZA-S) to obtain an unprecedented 1 micron thick film with vertically oriented cylinders relevant for O-BHJ's using PS-PMMA and characterized them with Rotational SANS and GI-SAXS.

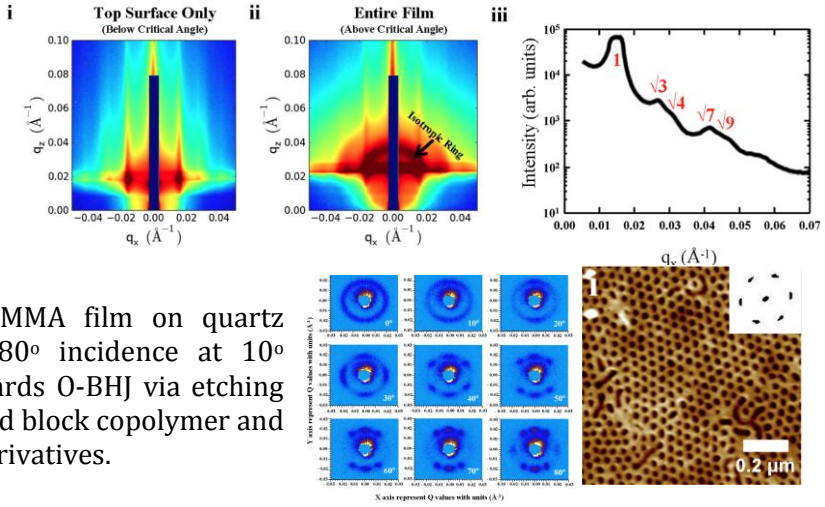

Figure 4. (Top) GISAXS measurements at BNL and CHESS, Cornell U. of CZA-S block copolymers to characterize vertical orientation and long range order (Bottom) (left) Rotational Small Angle Neutron Scattering (R-SANS) data of a CZA-S annealed 250 nm *d*PS-PMMA film on quartz substrate collected from 0° - 80° incidence at 10° increments. (right) Strategy towards O-BHJ via etching CZA-S processed vertically ordered block copolymer and backfilling with PCBM and C60 derivatives.

C) Model Device Characterization (with Prof. Xiong Gong): P*olythiophene-Fullerene System* The morphology of three polythiophenes and three fullerenes in thin film device geometry using NR show that for all the systems the BHJ is composed of three distinct components. Al interface has an excess of fullerene while a fullerene is depleted at the PEDOT:PSS interface. Comparing these to device performance, implies that there is little effect of the fullerene enrichment at the Al surface, but the depletion at the PEDOT:PSS interface is a dominant factor in the device performance.

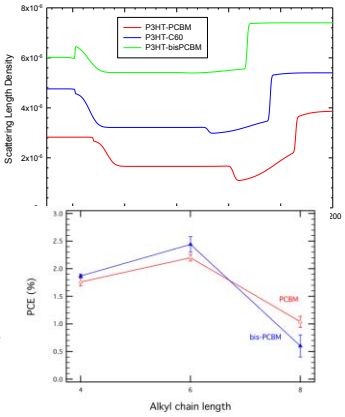

Figure 5 (right): NR profiles and PCE (%) versus polythiophene alkyl chain length for BHJ films with PCBM (red) and bis-PCBM (blue).

D) Modeling Nanoparticle Filled Ordered BCP - BHJs

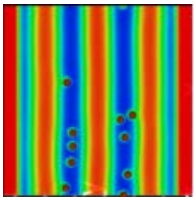

Figure 6 (left) shows snapshot from a hybrid SCFT simulation in PolySwift++ for a nanoparticles -- BCP film subject to broad zone annealing initialized with a random placement of nanoparticles. The Flory χ parameter on the trailing side of the zone is above the ODT and this particular system orders into lamellar layers. The nanoparticles segregate into one type of lamellar layer via preferential wetting. Details for the hybrid-- ‐ SCFT algorithm can be found in Phys. Rev. Lett. 96, 250601 (2006).

Publications (FY10-FY12)

1. "Facile Route to Fabricating Vertically Aligned High-Aspect Ratio Block Copolymer Films via Sharp Dynamic Zone Annealing", Gurpreet Singh, Kevin G. Yager, Detlef-M. Smilgies, Manish M. Kulkarni, David G. Bucknall and Alamgir Karim, ***Macromolecules, Submitted****.*

2. "Fullerene Nanoparticles as Molecular Surfactant for Dewetting of Phase-Separating Polymer Blend Films" Diya Bandyopadhyay, Jack F. Douglas, and Alamgir Karim, ***Macromolecules, In Press.***

3. Influence of C_{60} Nanoparticles on the Stability and Morphology of Miscible Polymer Blend Films, Diya Bandyopadhyay, Jack F. Douglas, and Alamgir Karim, ***Macromolecules,*** *pp 8136–8142 Publication Date (Web): September 28, 2011 (Article) DOI: 10.1021/ma201201v*

4. "Combinatorial Block Copolymer Ordering on Tunable Rough Substrates" Manish M. Kulkarni, Kevin G. Yager, Ashutosh Sharma and Alamgir Karim, ***Macromolecules****, (1 May 2012), doi:10.1021/ma300169a.*

5. "*Phase-Morphology and Molecular Structure Correlations in Model Fullerene-Polymer Nanocomposites*." Bucknall, D. G.; Bernardo, G.; Shofner, M. L.; Deb, N.; Raghavan, D.; Sumpter, B. G.; Sides, S. W.; Huq, A.; Karim, A., *Materials Science Forum,* **2012,** 714, 63-66

6. "*Phase Morphology in Poly(thiophene)-Fullerene Thin Film Devices*." Bucknall, D. G.; Deb, N.; Skoda, M.; Sumpter, B.; Karim, A., *MRS Proceedings,* ***MRSF11-1390-H13-57.R1***.

7. "*Directed Assembly of Model Block Copolymer-PCBM Blend System for Photovoltaic Applications*" G. Singh, M. M. Kulkarni, D. Smilgies, S. Sides, B. Berry, D. Raghavan, D.G. Bucknall, B Sumpter and A. Karim MRS Proceedings (2012) 1390 : **mrsf11-1390-h13-54**

Future Plans

a) Fabricate BHJ thin film devices utilizing disordered BHJs (blends), and ordered BHJs via both sacrificial block copolymer templates and conjugated BCPs with Raghavan's NPs.
b) Extensive characterization of devices in a) by neutron and X-ray scattering and correlation of Z-directed BHJ morphology with soft surface energy control and suppressed crystallinity.
c) Complete DFT and SCF calculations of key systems above (i.e. a), to capture trends on how morphology correlates with interaction strength for disordered and ordered BHJs.

Inelastic Neutron Scattering Studies of Phonons in Thermoelectrics

O. Delaire[1] (delaireoa@ornl.gov), J. Ma[2], A. May[1], B. Sales[1]
[1]*Materials Science and Technology Division, Oak Ridge National Laboratory, Oak Ridge, TN 37831*
[2]*Quantum Condensed Matter Division, Oak Ridge National Laboratory, Oak Ridge, TN 37831*

Research Scope

The current intensive interest in thermoelectric materials has re-emphasized the importance of understanding of microscopic mechanisms affecting the transport of energy. Strategies for developing efficient thermoelectrics seek materials that are poor thermal conductors, but good electron conductors. This is achieved by engineering thermal and electrical transport at the mesoscale (phonon and electron mean free paths range from nano- to micrometers) by tuning the dynamics and microstructure. The electron-phonon interaction, phonon-phonon interaction (resulting from anharmonicity), and the scattering by lattice defects and strains are responsible for finite electrical and thermal conductivities at the macroscopic scale. Understanding and controlling these mechanisms is key to achieving high thermoelectric efficiencies. In this context, phonon dispersions and linewidths provide critical insights into phonon mean-free-paths, and hence the microscopic origins of thermal conductivity, which directly affects the thermoelectric figure-of-merit *zT*. The electron-phonon interaction is also directly responsible for the thermoelectric "phonon drag" effect, controls electrical resistivity, and renormalizes the electronic structure at high temperature. The impact of these scattering mechanisms on phonon dispersions and linewidths of thermoelectric materials is currently insufficiently characterized, however.

Studies of phonon scattering mechanisms with neutron scattering have so far been limited by traditional measurements, in which reciprocal-space was sampled sparsely (typically along high-symmetry directions only). Our measurements leverage the new time-of-flight instruments at the Spallation Neutron Source, which enable the efficient sampling of the full four-dimensional scattering function, S(**Q**,E). With this approach, we identified a strong phonon anharmonicity in PbTe, associated with the nearness to the ferroelectric coupling. We also showed that most phonon modes in FeSi are affected by the metallization of the narrow gap with increasing thermal disorder.

Recent Progress

Ferroelectric Lattice Instability and Phonon Anharmonicity in PbTe: PbTe has one of the highest thermoelectric figure-of-merit [1, 2], favored by an unusually low thermal conductivity for a simple rocksalt structure (low thermal conductivities in semiconductors are typically associated with disordered alloys or complex unit cells). It is long known that PbTe is an incipient ferroelectric, but

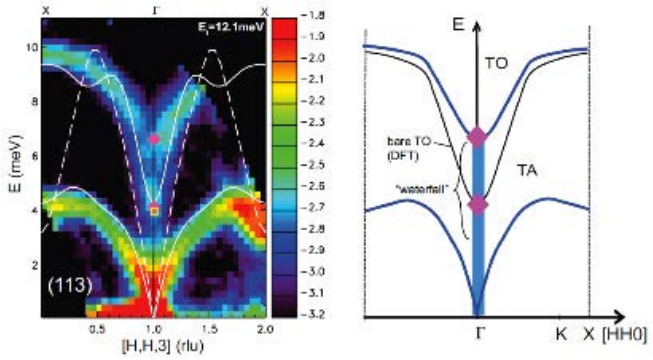

Fig. 1 Inelastic neutron scattering data (left) showing the presence of a waterfall effect arising from strong non-harmonic mixing of optical and acoustic lattice vibrations (right) in PbTe [4].

the origin of the low thermal conductivity in the paraelectric high-symmetry phase has remained unexplained. It was theoretically suggested following first-principles calculations of the transverse-optic (TO) mode vibration potential that a coupling between longitudinal acoustic and TO modes could scatter the LA modes, lowering the lattice thermal conductivity [3]. We performed detailed inelastic neutron scattering measurement on single-crystalline PbTe, and observed signatures of this strongly anharmonic behavior [4]. In particular, a "waterfall" effect is seen in the TO branch at the zone center, with a very broad phonon spectrum. The TO mode at the zone center tends to split into two modes with increasing temperature, as observed in reflectivity measurements [5], and as also reported in a following study [6]. The extreme broadening of the TO near the zone center and the LA-TO scattering are consequences of strong anharmonicity, as was shown with first-principles anharmonic lattice dynamics calculations [7].

Electron-Phonon Coupling in FeSi: FeSi is a promising thermoelectric material for refrigeration applications, with a Seebeck coefficient over 500μV/K at 40K [8]. FeSi is a narrow band-gap semiconductor at low temperature (B20 structure), and undergoes a metal-insulator transition around room temperature. Using inelastic neutron scattering, phonons were measured on both single crystals and powders as a function of composition and temperature. We observed a strong coupling between the phonons and the semiconductor-to-metal transition, upon increasing temperature and carrier concentration [9]. Using first-principles electronic structure calculations and ab-initio molecular dynamics, we showed that the band gap and the sharp features around the band edges are strongly affected by the thermal disordering induced by phonon excitations. This adiabatic electron-phonon coupling mechanism is general, and was previously shown to account for the anomalous temperature dependence of phonons in superconducting vanadium alloys and compounds [10, 11].

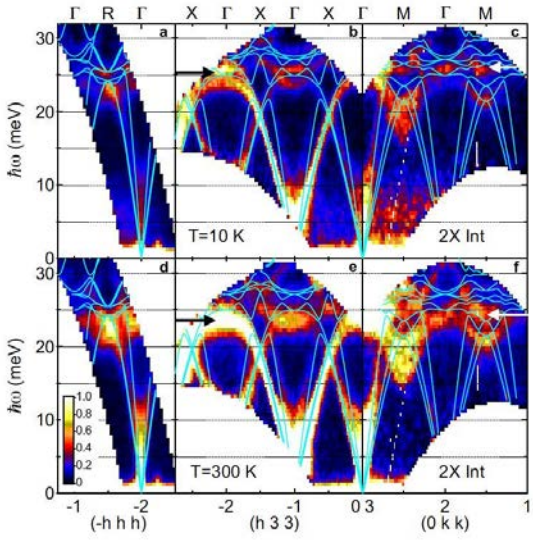

Fig. 2: Single crystal phonon dispersions of FeSi measured using time-of-flight inelastic neutron scattering. Comparison of these data with first-principles calculations (light blue lines) provides clear evidence of the unusual softening of the atom motions with increasing temperature [9].

Future Plans:

Anharmonicity in rocksalt tellurides: We propose to systematically investigate the connection between anharmonicity and lattice instabilities in ferroelectric/thermoelectric materials with rocksalt telluride structure. The occurrence of the waterfall effect at the zone center in rocksalt tellurides is a clear difference from the case of perovskite ferroelectrics (where the waterfall occurs at finite $\boldsymbol{q}$), and it is not obvious whether the underlying physics are related. We have synthesized large single-crystals of Ge-doped PbTe, SnTe, and $AgSbTe_2$ and performed transport characterizations as well as preliminary neutron scattering measurements.

Electron-phonon interaction and transport in thermoelectrics: We propose to investigate the electron-phonon coupling in skutterudites $Ni_xCo_{1-x}Sb_3$ and $Mo_3(Sb,Te)_7$. It was shown that small

amounts of Ni alloying in $CoSb_3$ lead to a strong suppression of the lattice thermal conductivity, indicative of strong electron-phonon coupling [12]. Similarly, Te-alloying in Mo_3Sb_7 leads to an surprising increase in thermal conductivity, owing to the suppression of electron-phonon coupling by decreasing the carrier concentration [13]. Both compounds thus exhibit a similar effect as FeSi [8]. Phonons will be investigated as a function of temperature in these compounds to investigate anomalous temperature behaviors.

References:

[1] Y. Pei, X. Shi, A. LaLonde, H. Wang, L. Chen, and G.J. Snyder, "Convergence of electronic bands for high performance bulk thermoelectrics", Nature **473**, 69 (2011).

[2] K. Biswas, J. He, Q. Zhang, G. Wang, C. Uher, V. Dravid, and M.G. Kanatzidis, "Strained endotaxial nanostructures with high thermoelectric figure of merit", Nature Chemistry **3**, 160 (2011).

[3] J. An, A. Subedi, and D.J. Singh, "Ab initio phonon dispersions for PbTe", Solid State Commun. 148, 417_419 (2008).

[4] O. Delaire, J. Ma, K. Marty, A.F. May, M.A. McGuire, M.H. Du, D.J. Singh, A. Podlesnyak, G. Ehlers, M.D. Lumsden, and B.C. Sales, "Giant anharmonic phonon scattering in PbTe," Nature Materials **10**, 614-619 (2011).

[5] H. Burkhard, G. Bauer, and A. Lopez-Otero, "Submillimeter spectroscopy of TO-phonon mode softening in PbTe", J. Opt. Soc. Am. 67, 943_946 (1977).

[6] K. M. Ø. Jensen, E. S. Božin, C. D. Malliakas, M. B. Stone, M. D. Lumsden, M. G. Kanatzidis, S. M. Shapiro, and S. J. L. Billinge, "Lattice dynamics reveals a local symmetry breaking in the emergent dipole phase of PbTe", arXiv:1203.5943v2

[7] T. Shiga, J. Shiomi, J. Ma, O. Delaire, T. Radzynski, A. Lusakowski, K. Esfarjani, and G. Chen, "Microscopic mechanism of low thermal conductivity in lead telluride", Phys. Rev. B **85**, 155203 (2012)

[8] B. C. Sales, O. Delaire, M. A. McGuire, and A. F. May, "Thermoelectric properties of FeSi and Related Alloys: Evidence for Strong Electron-Phonon Coupling", Phys. Rev. B **83**, 125209 (2011).

[9] O. Delaire, K. Marty, M. B. Stone, P. R. C. Kent, M. S. Lucas, D. L. Abernathy, D. Mandrus, and B. C. Sales, "Phonon softening and metallization of a narrow-gap semiconductor by thermal disorder", Proc. Nat. Acad. Sci. USA **108**, 4725 (2011).

[10] O. Delaire, M. Lucas, J. Muñoz, M. Kresch and B. Fultz, "Adiabatic Electron-Phonon Interaction and High-Temperature Thermodynamics of A15 Compounds", Phys. Rev. Letters **101**, 105504 (2008).

[11] O. Delaire, M. Kresch, M. Lucas, J. Muñoz, J.Y.Y. Lin and B. Fultz, "Electron-Phonon Interaction and High-Temperature Thermodynamics in Vanadium Alloys", Phys. Rev. B **77**, 214112 (2008)

[12] J. Yang, D. T. Morelli, G. P. Meisner, W. Chen, J. S. Dyck, and C. Uher, "Influence of electron-phonon interaction on the lattice thermal conductivity of $Co_{1-x}Ni_xSb_3$", Phys. Rev. B **65**, 094115 (2002).

[13] X. Shi, Y. Pei, G. J. Snyder, and L. Chen, "Optimized thermoelectric properties of Mo3Sb7_xTex with significant phonon scattering by electrons", Energy Environ. Sci. **4**, 4086 (2011).

Publications (FY10-FY12):

T. Shiga, J. Shiomi, J. Ma, O. Delaire, T. Radzynski, A. Lusakowski, K. Esfarjani, and G. Chen, "Microscopic mechanism of low thermal conductivity in lead telluride", Phys. Rev. B **85**, 155203 (2012).

A.F. May, M. A. McGuire, J. Ma. O. Delaire, A. Huq, R. Custelcean, "Properties of single crystalline AZn_2Sb_2 (A=Ca,Eu,Yb)", J. Appl. Phys. **111**, 033708 (2012).

A.F. May, M. A. McGuire, J. Ma. O. Delaire, A. Huq, D. J. Singh, W. Cai, H. Wang, "Thermoelectric transport properties of $CaMg_2Bi_2$, $EuMg_2Bi_2$, and $YbMg_2Bi_2$", Phys. Rev. B **85**, 035202 (2012).

O. Delaire, J. Ma, K. Marty, A. F. May, M. A. McGuire, M.-H. Du, D. J. Singh, A. Podlesnyak, G. Ehlers, M.Lumsden, B. C. Sales, "Giant Anharmonic Phonon Scattering in PbTe", Nature Materials **10**, 614 (2011).

O. Delaire, K. Marty , M. B. Stone, P. R. C. Kent, M. S. Lucas, D. L. Abernathy, D. Mandrus, B. C. Sales, "Phonon softening and metallization of a narrow-gap semiconductor by thermal disorder", Proc. Natl. Acad. Sci. USA **108**, 4725 (2011).

B. C. Sales, O. Delaire, M. A. McGuire, and A. F. May, "Thermoelectric properties of FeSi and Related Alloys: Evidence for Strong Electron-Phonon Coupling", Phys. Rev. B **83**, 125209 (2011).

O. Delaire, A. F. May, M. A. McGuire, W. D. Porter, M. S. Lucas, M. B. Stone, D. L. Abernathy, and G. J. Snyder, "Phonon Density of States and Heat Capacity of $La_{3-x}Te_4$", Phys. Rev. B **80**, 184302 (2009).

Session V

Organic Photovoltaics and Soft Matter

Polymer Based Materials for Harvesting Solar Energy: Design, Synthesis and Controlled Assemblies.

Dhandapani Venkataraman

DOE PhaSE Energy Frontier Research Center

University of Massachsuetts Amherst, MA 01003

Using polymer-based materials to harvest solar energy mandates that all aspects of the processes used in the fabrication of organic photovoltaic (OPV) devices be addressed. This requires synthesis of new materials, along with fundamental, quantitative characterization of the physical properties of the materials in the truly — not simple and qualitative —analytical sense. It also requires characterization of the photophysical properties of the subunits or "mers" of the corresponding polymers. Finally, it requires characterization of the polymers in a device setting, i.e., in the condensed state and in the presence of other electronic components. It is crucial to understand the ordering of these materials in the solid state and the morphologies that are produced under a range of different processing conditions, in considerable, nanoscopic detail. It is essential that the orientation and ordering of these polymers in thin films be understood, as well as procedures to generate reproducible morphologies that effectively capture light throughout the solar spectrum and produce hole-electron pairs (excitons). The electro-active materials must allow transport of excitons within the medium, provide an interface where their dissociation to individual charges can effectively occur, and support transport of the electrons and holes to their respective electrodes to generate an electric current.

Accomplishing all of this requires understanding the morphology of the active layer in a device setting and of transport mechanisms of the exciton-generated electrons and holes across organic/organic and organic/inorganic interfaces. Making morphologies on length scales (~10 nm) commensurate with exciton lifetime in organic polymers necessitates kinetic trapping of morphologies in a reproducible, robust manner, and in a state very far removed from equilibrium. Thus, understanding and developing novel processing strategies is essential for advancing the OPV field. My talk will focus on the recent progress and future directions of the DOE EFRC PhaSE at the University of Massachusetts Amherst.

Recent Progress: Researchers in Energy Research Group 1 at PhaSE are synthesizing new monomers, polymers and nanocomposite materials with well-defined structures and architectures, designed to harvest light, produce electron-hole pairs from excited states, and generate photocurrent. A large portion of the effort in ERG 1 is aimed at developing new conjugated systems that favor charge separation upon photoexcition, and/or absorb in the 550-1200 nm region that is not well utilized by conventional OPVs designs. Electronic structure "tuning" of monomers/oligomers and polymers focus on conduction band (LUMO) and valence band (HOMO) energies that match classic redox energetics. For example, EFRC Researchers Coughlin and Lahti are developing hole transporting, low bandgap polymers based on thienothiophene (Figure 1). Similarly Venkataraman is developing electron-transporters low bandgap aryl-vinylene polymers. These polymers have electron moblities similar to PCBM, the archetypical electron transporter in OPVs.

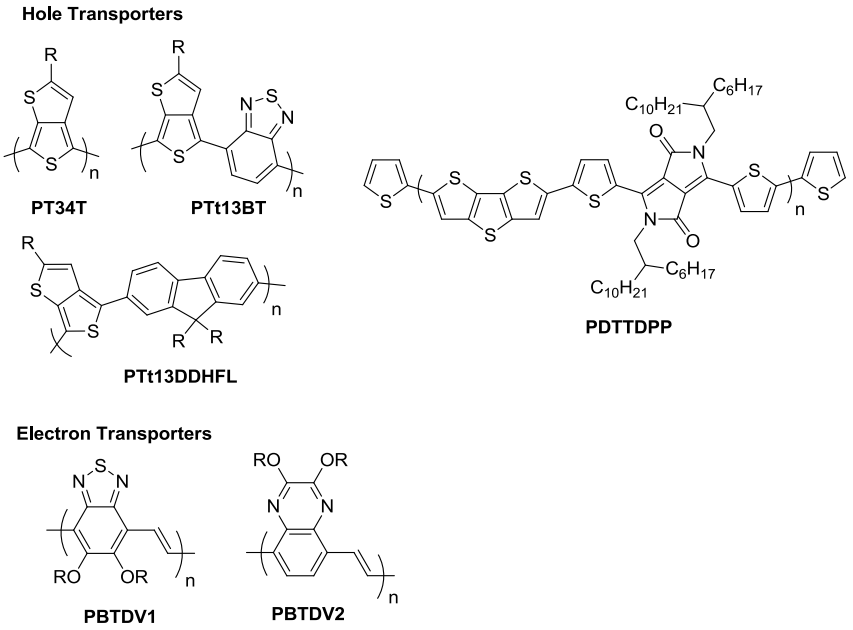

Figure 1: Chemical Structures of New Hole and Electron-Conducting Polymers Developed by EFRC PhaSE researchers.

A novel low bandgap conjugated polymer PDTTDPP (Figure 1) has been developed by Jae Woong Jong (Seoul National University) working at the Center with Emrick and Russell. PDTDPP has a low bandgap E_g = 1.39 eV, and onset absorption at 1020 nm due to intrachain charge transfer thiophene and keto-containing units. It has a moderately low–lying highest occupied molecular orbital (HOMO) level of 5.19 eV. PDTTDPP exhibits strong intermolecular π–π stacking with edge–on chain orientation in thin films, which contributes to a high hole mobility of 0.68 $cm^2 \cdot V^{-1} \cdot s^{-1}$ in OFETs without post treatment. The high hole mobility and broad light absorption of PDTTDPP gives a PCE of 6.05% with J_{SC}=13.9 mA/cm^2, V_{OC}=0.66 V, and FF=65.7%.

The researchers in the Energy Research Group 2 evaluate and develop strategies to control the morphology and overall solid-state structure of polymer-based and polymer/inorganic-based materials used in hybrid photovoltaic devices – as well as packing in related molecular solids – in order to optimize their efficiencies. The design and fabrication of high efficiency photovoltaic devices requires precise control over nanoscale morphology, molecular ordering and interfacial properties of all the components comprising the device. Analysis of morphology under device fabrication conditions is especially targeted. In order to control the morphology of the active layers, it is important to understand the evolution of bulk heterojunction morphology at the molecular level. From the work at the Center[1-4] and from the literature, we know that thin films of P3HT—PCBM, upon annealing, develop interconnected crystalline domains of P3HT, interconnected crystalline domains of PCBM and an interface between the domains. The PCBM domains are concentrated in areas where P3HT is amorphous. It is now well understood that there are three factors that concurrently facilitate the formation of a BHJ in the P3HT—PCBM system. These are (1) the propensity of P3HT to rapidly crystallize in the presence of PCBM, (2) the large diffusion coefficient of PCBM in amorphous P3HT and (3) the slow kinetics of crystallization of PCBM in the presence of P3HT. Based on this understanding, researchers in PhaSE are developing methods to direct the assembly of hole-and electron transporters.

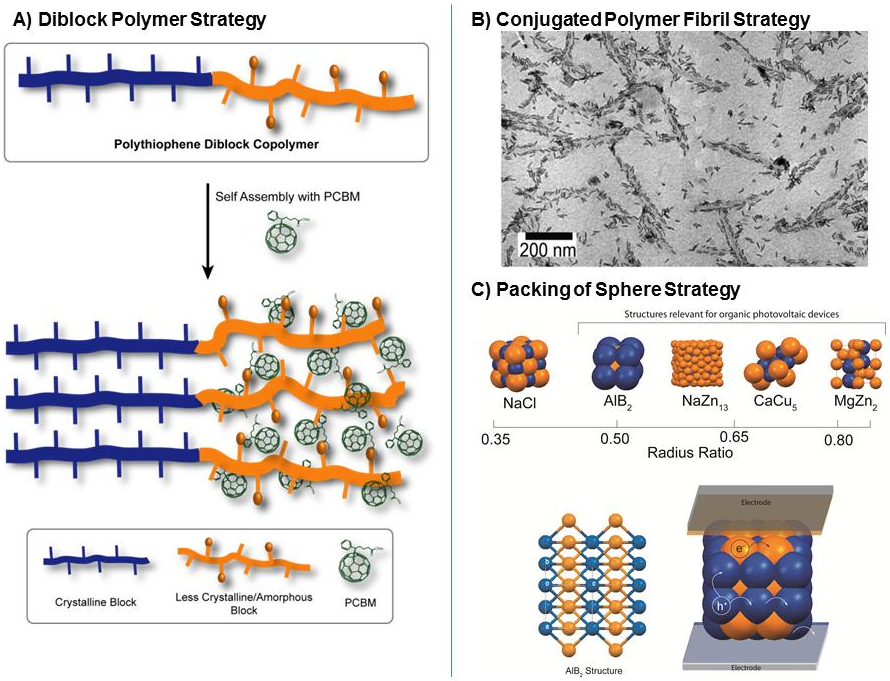

Figure 2: Illustration of the (a) diblock polymer of using crystalline and amorphous blocks (b) conjugated polymer fibril and (c) packing of spheres strategies to direct the active layer morphology.

For example, reseachers at EFRC PhaSE are developing conjugated diblock copolymers based on polythiophene to direct the active layer morphology (Figure 2a). One system consists of a highly crystalline first block covalently linked to a second, amorphous block; for the other system, the second block is just *less* crystalline. Conjugated diblock copolymers with different block ratios (P3HT-b-PrT) were synthesized via GRIM polymerization. The PrT block is amorphous due to the changing of the hexyl group of P3HT to an alkyl silane group, which drives microphase separation of the polythiophenes based block copolymer and variation in crystallinity between the two blocks. Thermal and solvent annealing were used to control the self-assembly of the BCPs and the orientation of the P3HT crystals, while the domain size was controlled by the block molecular weights. The BCPs were blended with ntype semiconductors, like phenyl-C61-butyric acid methyl ester (PCBM), which segregated to the amorphous domains by solvent and heat treatment. In the second block copolymer system both blocks are designed to absorb light in the solar spectrum. The first block of diblock system consists of rrP3HT. The second block is random polymer of 3-hexylthiophene and a thiophene with bulky triisopropylsiloxane (TIPS) side chains. The rrP3HT block provides higher crystallinity and charge carrier mobility while the second block provides a photoactive matrix to keep the e-acceptor fullerene in the vicinity of the e-donor polymer on the nanoscale.

Emrick and Hayward are investigating the co-organization of the p-type polymer poly(3-hexylthiophene) (P3HT) into robust fibrils using cross linked block copolymer architecture, and then incorporating ntype cadmium selenide (CdSe) nanorods that bear P3HT ligands. Self-assembly of P3HT into crystalline fibers via π-π stacking of the thiophene rings can be induced by careful management of solvent, and CdSe nanorods with P3HT ligands can be co-crystallized with free P3HT, with overall assembly yielding composite p/n type nanowires (Figure 2b). These hybrid materials are promising as nano-scale building blocks in photovoltaic devices, since they are simultaneously crystalline and well-organized on the scale of ~20 nm. Recently, the

investigators have been able to obtained ordered assemblies over large areas. A third approach that is being pursued at the center organizes the electron-rich and electron-poor moieties into separate spherical nanoparticles and exploits their attractive interactions to organize semiconductors into segregated nanostructures.[5] Akin to the formation of binary ionic crystals, two types of nanoparticles can also self-assemble into ordered "superlattices" at a much larger scale. The packing of the nanoparticles also depends on the ratio of the radii of the particles ($\gamma = R_{small}/R_{large}$), but the self-assembly of nanoparticle mixtures occur even if the nanoparticles do not have electrostatic attraction.

Researchers in the Energy Research Group 3 elucidate photophysical details of charge transport and energy transfer within nanostructured materials. Single-molecule spectroscopy and time-resolved optical spectroscopy provide mechanistic insight and feedback for synthetic design and assembly (ERG 1 and ERG 2), especially the role of molecular architecture, crystal packing and nanoparticle assembly, and confinement geometry on energy transfer and charge transport in photovoltaic systems. Recent work has unraveled the intricate packing patterns of P3HT in fibrils and in the nanoparticles and the impact of the packing patters on the photophysics.

Future Work: The researchers in the PhaSE center will be focusing on (a) Building novel polymeric and nanocomposite platforms for OPV, including solution assembled fibrils composed of low band gap polymers (i.e., PCBTBT and related structures), benzothiadiazole vinylene homopolymers / copolymers and related systems as novel electron transporting structures, and zwitterionic conjugated polymers that enhance charge injection when used in device constructs. (b) Optimizing developed platforms (exemplified by, but not restricted to P3HT and P3HT-nanorod platforms) to understand the relationship between the photophysics and morphology and to elucidate key elements of charge transport and interfacial behavior. (c) Elucidate structural and morphological characteristics of active layers made with low-band gap polymers synthesized in ERG1; (d) Direct and control assembly of pre-formed, polymeric nanoscale aggregates into BHJ super-structures that improve charge transport; (e) Direct and control the assembly of pre-formed nanoscale aggregates of polymers and inorganic nanostructures; (f) Develop strategies to direct the self-assembly of block copolymers into nanoscale architectures relevant to OPV devices; and (g) Develop and optimize strategies to control and stabilize kinetically trapped morphologies.

Acknowledgement. We thank PHaSE Energy Frontier Research Center supported by the US Department of Energy, Office of Basic Energy Sciences, through grant DE-SC0001087 for financial support of this work

References

(1) Venkataraman, D.; Yurt, S.; Venkatraman, B. H.; Gavvalapalli, N. *Journal of Physical Chemistry Letters* **2010**, *1*, 947.
(2) Chen, D.; Liu, F.; Wang, C.; Nakahara, A.; Russell, T. P. *Nano Lett.* **2011**, *11*, 2071.
(3) Chen, D. A.; Nakahara, A.; Wei, D. G.; Nordlund, D.; Russell, T. P. *Nano Lett.* **2011**, *11*, 561.
(4) Gu, Y.; Wang, C.; Russell, T. P. *Adv. Energy Mater.* **2012**, In Press.
(5) Labastide, J. A.; Baghgar, M.; Dujovne, I.; Yang, Y. P.; Dinsmore, A. D.; Sumpter, B. G.; Venkataraman, D.; Barnes, M. D. *Journal of Physical Chemistry Letters* **2011**, *2*, 3085.

Structure and Properties of Conjugated Polymer Networks for Organic Photovoltaics

Danilo C. Pozzo (dpozoz@uw.edu), Gregory M. Newbloom, Jeffery J. Richards, Katie M. Weigandt and Pablo de la Iglesia

Dept. of Chemical Engineering, University of Washington Seattle WA 98195

I. Research Scope

There is an increasing need for the production of clean and renewable energy on a global scale. Though many technologies will inevitably contribute to the final solution, photovoltaic power production will undoubtedly play a central role. This is because the earth receives more than 120,000 TW/year of solar energy, making it our most abundant renewable energy resource.[1] Several new technologies are being developed to effectively harvest this resource.

Photovoltaic devices based on organic materials (OPVs) hold cost-saving advantages over traditional inorganic solar cells. They are made with inexpensive and abundant materials, can be processed using low-temperature solution-based methods and can be mass produced using available roll-to-roll printing technology.[2] Nevertheless, the physics of charge generation, separation and transport in semi-conducting organic materials shows that specific photoactive layer morphologies are needed to maximize device efficiency: 1) There must be a bicontinuous, interpenetrating network of p-type and n-type materials that bridges the electrodes to separate and transport charges, 2) The domain size of each material (p-type or n-type) must be smaller than approximately 20 nm to minimize exciton recombination losses and 3) Material properties (e.g. crystallinity) must maximize charge transport to the electrodes.[3][4] It is necessary to consider these morphological constraints so that efficiency of OPV devices can be improved. Unfortunately, steps taken to meet these constraints often compromise other important aspects such as processability and stability, both of which are also essential for OPVs to remain competitive with inorganic photovoltaics.

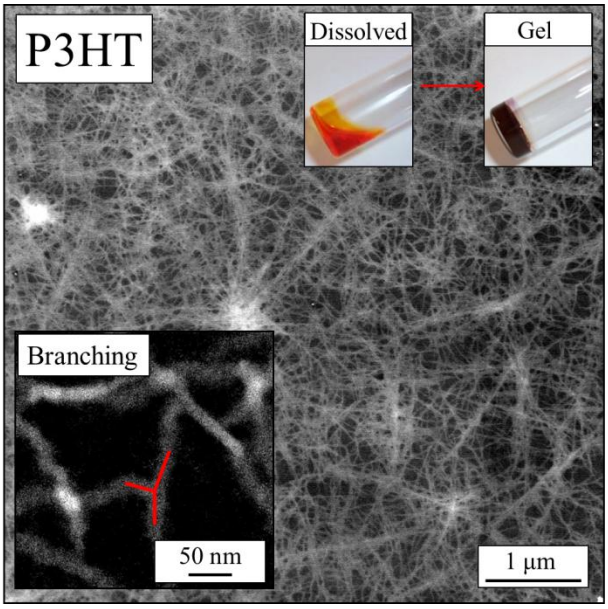

Figure 1. TEM image of a dried P3HT organogels. Insets: Pictures of vials containing P3HT in solution before and after gelation (Top). TEM image highlighting individual fibers (Bottom).

Our research seeks to develop gelation as a versatile platform to engineer photoactive layer structures that maximize charge generation, separation and transport. For this, we utilize and manipulate the natural tendency of conjugated polymers to self-assemble in organic solvents.

Gelation is a common phenomenon amongst semi-conducting polymers due to their highly conjugated and rigid polymer backbone. When solubility is reduced, often by changes to temperature or solvent quality, π-orbitals between multiple polymer chains overlap and stack resulting in the formation of semi-crystalline fiber network structures (Figure 1).[4-6] Gelation and fiber formation of conjugated polymers, such as poly(3-hexylthiophene) (P3HT), results in significant increases in charge transport properties, are by definition interconnected over long distances and have nanoscale and porous structures. Unfortunately, the elastic nature of all gels makes them difficult to process into thin films while preserving their desired structures. We have recently addressed this issue via the creation of aqueous-phase microgel dispersions that maintain the network structures while enabling solution processing.[6] Herein, we describe our progress towards the development of a flexible gel-based platform that allows for engineering of stable conjugated polymer network functional devices.

II. Recent Progress:

Structure – Property Relationships

Using *in-situ* small angle neutron scattering (SANS), rheology and impedance spectroscopy, we have fully characterized the self-assembly and gelation of two different types of conjugated polymers: poly(3-hexylthiophene) (P3HT) and poly(9,9-dioctylfluorene) (PFO). Both P3HT and PFO self-assemble into nanowire/fiber structures, with domains smaller than 20 nm (mean exciton diffusion length is ~20 nm) when the solvent quality and/or temperature are reduced. Importantly, we also have demonstrated that the fiber and network structures are tunable by adjusting self-assembly conditions. This opens the door to the optimization of network properties with externally controllable parameters.

P3HT dissolved in aromatic solvents (e.g. p-xylene, toluene and benzene) forms elastic organogels at concentrations exceeding ~5 mg/mL.[4] At lower concentrations, the polymers form branched nanowire networks that are tens of micrometers in size but still fail to percolate and the samples thus remain fluid. Figure 1 also shows that, at high temperatures (>80 °C), P3HT is fully dissolved with a characteristic orange color. Upon cooling (< ~35 °C) or after adding a non-solvent, polymer chains stack and grow into nanowires and interconnected networks that form an elastic network with a characteristic purple color. Organogels formed under variable conditions also show that the kinetics of gelation can be altered to manipulate the network structure and the conductive and elastic properties. Despite this, SANS experiments show that gels formed in different solvents, at different concentrations and different temperatures all form rectangular fiber structures with similar dimensions (width 5-6 nm and length 20-25 nm). This suggests that the nanofiber cross-section is primarily determined by molecular architecture of the individual chains. By tracking the kinetics of self-assembly and carefully analyzing SANS, SAXS and USANS data, we accurately determine and track the different stages of structure and property development (Figure 2).[7] In all cases, increases to the network fractal dimension result in increases to the bulk ac conductivity of the gel, with order of magnitude increases right after gelation. We also show that PFO and several other conjugated polymers also self-assemble into branching fiber organogels with nanoscale structural features and that their structure is also

tunable with changing processing conditions. Systematic results obtained for P3HT and PFO provide a firm foundation to demonstrate that it is possible to use gelation as a platform to design active layers in OPV devices.

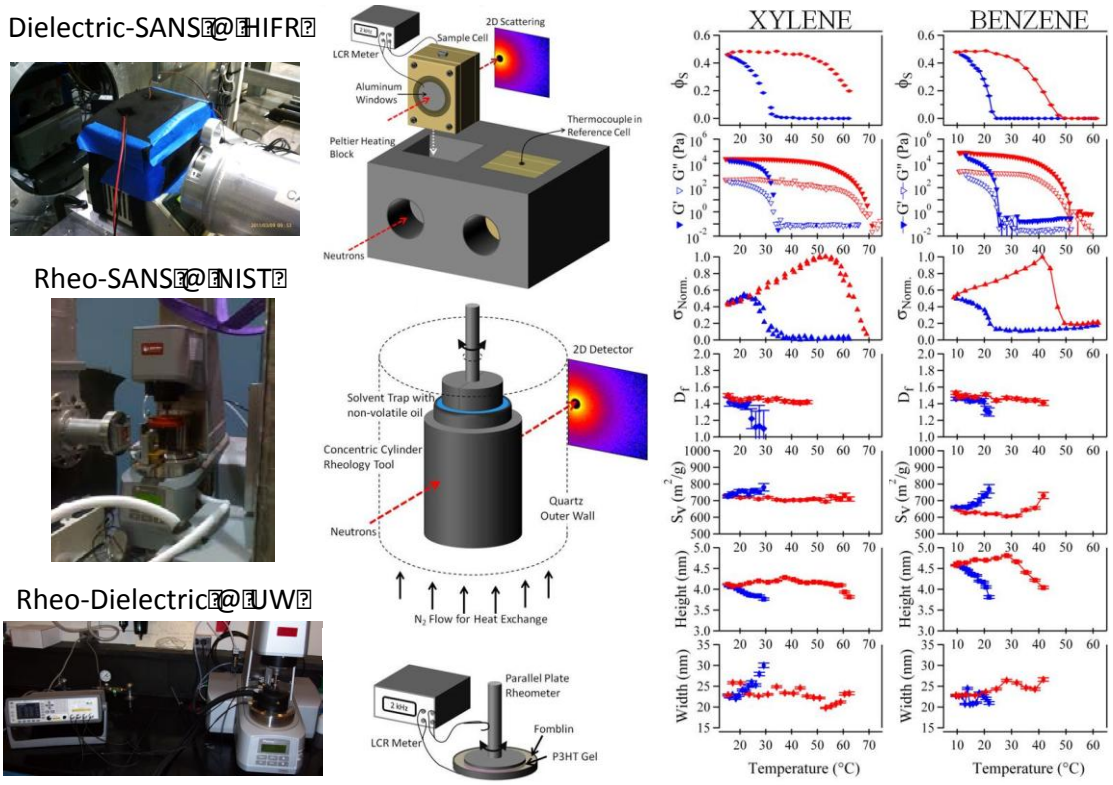

Figure 2: (Left and Center) Pictures and schematics of setups for the three types of combined experiments. (Right) Parameters extracted as a function of temperature during gel formation (cooling cycle = blue) and during gel dissolution (heating cycle = red) for 30 mg/mL P3HT in p-xylene and benzene. Parameters include the fiber volume fraction (ϕ), the elastic gel modulus (G'), the viscous modulus (G"), the conductivity (σ), the gel fractal dimension (D_f), the specific surface area (S_v) and the fiber cross-sectional dimensions (height and width).

Processing of Organogels for Use in OPVs

One of the great challenges of engineering self-assembled materials is to translate the desired structure for use in the target application. For fabricating OPVs, we have recently developed a processing platform in which the desired porous and interconnected structure of bulk organogels is preserved by dispersing it within an aqueous fluid medium as shown in Figure 3. SANS studies confirm that the interconnected fiber network of the bulk organogel is largely maintained within these "microgels" and that this is also preserved after coating via spin-coating or spray-coating methods. We have also demonstrated that the properties of the particles are tunable via changes to the microgel preparation method and that, after incorporation of fullerenes, functional OPVs are generated. SANS, GISAXS, electron microscopy, fluorescence and device

performance evaluation have been systematically utilized to identify all of the parameters that affect structure and properties in working devices.

Enhanced Stability for OPVs

Although substantial progress has been made towards enhancing the efficiency of OPV devices, very little has been advanced towards stabilizing their long-term operation under normal conditions. Many OPV devices degrade within days or hours after they are made due to oxidative, mechanical or morphological failure. A major degradation pathway is due to the kinetic instability of the n-type fullerene phase that is composed primarily of phenyl-C_{61}-butyric acid methyl ester (PCBM). It has been shown that PCBM tends to form large crystalline aggregates over time that limit the p-type/n-type interfacial area and lead to degradation.

Recently, we have demonstrated that the addition of C_{60}, a similar fullerene derivative, to PCBM helps to inhibit the formation of larger aggregates within thin films. C_{60} acts as a nucleating agent for PCBM and allows for the rapid formation of small aggregates (r <1 μm) compared to pure PCBM systems that form much larger aggregates (r > 10 μm). We have found that the addition of C_{60} slightly decreases the performance of OPVs due to a lower hole mobility in the fullerene phase. However, PCBM devices degrade faster than C_{60}-PCBM and eventually have lower performance values. With further optimization, C_{60}-PCBM blends may provide the stability and efficiency that is needed for sustained performance of all (i.e. gel-based and traditional) OPV devices.

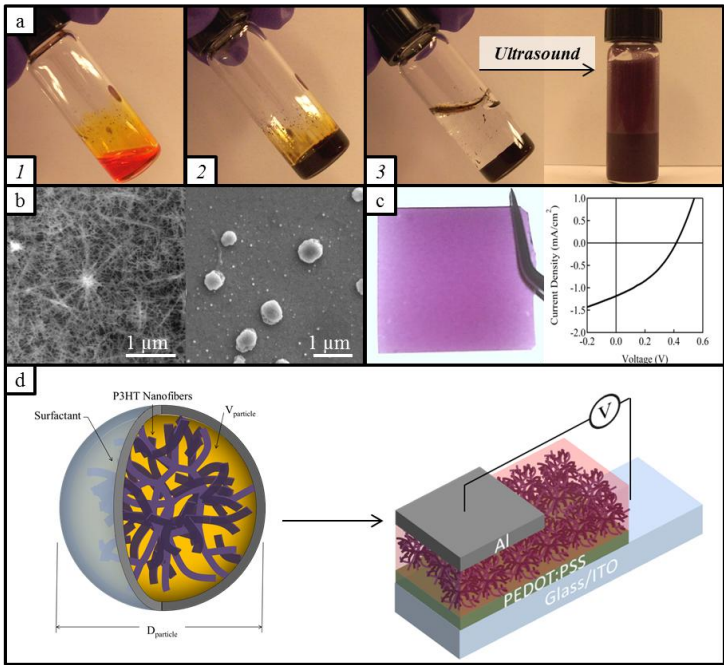

Figure 3: (a) Emulsification method used to generate conjugated polymer microgel dispersions. (b) Electron microscope images of bulk gel and microgel particles. (c) Spray-coated microgel film and IV curve for solar cell prototype. (d) Schematic of solar cell devices.

III. Future Plans

Though good power conversion efficiencies (~5%) have been shown for polythiophene-based devices (i.e. P3HT), these values are still below the ~10% efficiency that is needed to compete economically with current inorganic devices.[9] Recently, devices incorporating new polymer materials such as thiazolothiazole-based polymers and low band-gap donor-acceptor copolymers have reached much higer efficiency values.[10] For the first time, we have also recently demonstrated that self-assembly and gelation can also be induced in these novel conjugated

copolymers. We will continue running systematic experiments to demonstrate that gel formation will also enhance electronic properties in these novel and promising systems in similar ways to what we have observed and quantified with P3HT. Furthermore, we will adapt these high-efficiency polymers to generate microgel dispersions that can also be used to enhance device efficiency while maintaining the processing advantage of organic materials.

Finally, we have recently demonstrated that the microgel platform can also be utilized to generate coatings and functional devices via layer-by-layer (LBL) electrostatic particle deposition methods. This novel and flexible processing approach will allow us to develop functional devices by simple dipping of substrates into different baths containing microgels or other dispersed components necessary for the fabrication of functional devices (e.g. PEDOT:PSS, ITO and ZnO). LBL coating will directly address the issue of controlling the layer thickness. Furthermore, the use of multiple microgel dispersion containing different conjugated polymers could provide a platform to generate tandem solar cell devices that absorb a larger fraction of the solar spectrum and thus have much larger efficiencies. Tandem solar cells currently hold the record efficiency for OPV devices but are increasingly difficult to manufacture at large scales.

IV. References

[1] - Department of Energy, Basic Research Needs for Solar Energy Utilization, **2005**.

[2] - Krebs, F.C. *Sol. Ener. Mater. Sol. Cell* **2009**, *93*, 394.

[3] - Newbloom, G. M.; Kim, F. S.; Jenekhe, S. A.; Pozzo, D. C. *Macromolecules* **2011**, *44*, 3801-3809.

[4] - Newbloom, G. M.; Weigandt, K. M.; Pozzo, D. C. *Macromolecules* **2012**, *45*, 3452-3462.

[5] - Malik, S.; Jana, T.; Nandi, A. K. *Macromolecules* **2001**, *34*, 275-282

[6] - Richards, J. J.; Weigandt, K. M.; Pozzo, D. C. *J. Colloid Interface Sci.* **2011**, 364, *341*-350.

[7] - Newbloom, G. M.; Weigandt, K. M.; Pozzo, D. C. *Soft Matt.* **2012** (Submitted).

[8] - Ma, W.; Yang, C.; Gong, X.; Lee, K.; Heeger, A. J. *Adv. Func. Mater.* **2005**, *15*, 1617-1622.

[9] - Subramaniyan, S.; Xin, H.; Kim, F. S.; Shoaee, S.; Durrant, J. R.; Jenekhe, S. A. *Adv. Energ. Mater.* **2011**, *1*, 854-860.

V. Publications (FY11-FY12)

Impact of Mesoscale Morphology on Charge Transport of Colloidal Networks of P3HT
G.M. Newbloom, F.S. Kim, S.A. Jenekhe and D.C. Pozzo, Macromolecules, 44, 3801 (2011)

Aqueous Dispersions of Colloidal Poly(3-hexylthiophene) Gel Particles
J. Richards, K. Weigandt and D.C. Pozzo, J. Colloid and Interface Science, 364: 341 (2011)

Electrical, Mechanical and Structural Characterization of Self-Assembly in P3HT Organogels
G. Newbloom, K. Weigandt and D.C. Pozzo, Macromolecules, 45(8), 3452 (2012)

Investigating Multiphasic Soft Colloids Using Neutron Scattering, Simulations and Specific Tailored Synthesis

W.-R. Chen (chenw@ornl.gov)
Biology and Soft Matter Division, Oak Ridge National Laboratory, Oak Ridge, TN 37831
B. Sumpter and K. Hong
Center for Nanophase Materials Sciences, Oak Ridge National Laboratory, Oak Ridge, TN 37831

Research Scope

Multiphasic soft colloids are synthetic globular macromolecules that possess at least two different types of functional groups located at the particle periphery. This novel class of materials represents a unique microscopic building block for designing bulk materials that perform multiple functions simultaneously. Their structural heterogeneity establishes interactions between colloidal particles that are directional in nature due to multiphasic characteristics, introducing new functionality. However, their complex nature must be understood in order to control the spatial arrangement of these particles on the microscopic length scale to produce optimized macroscopic morphologies for functional devices. Thus, the overarching goal of this research program is to develop a fundamental understanding of the chemical and physical processes occurring on the nanometer length scale that are critical for the molecular-level design of multiphasic soft colloidal systems with desirable macroscopic properties.

The fundamental knowledge gained from this research will provide the scientific foundation required for development of exquisitely designed, heteromulti-functional soft colloidal materials that will ultimately lead to new materials with properties and functions that address DOE challenges such as the need for light-harvesting nanostructures, organic light emitting diodes, photonic bandgap devices, recoverable biofuel catalysts, and supercapacitors for sustainable energy applications, and for energy conversion applications.

To address the overarching goal, two specific aims form the basis of the proposed research: The first seeks to understand the microscopic interaction mechanisms, at the molecular level, giving rise to spatial organization on the length scale from that of an individual colloid to collective phase behavior. The second aim focuses on elucidating the relationship between dynamics and structure on both local and collective length scales that give rise to rich equilibrium and non-equilibrium phase behavior. Underpinned by specific tailored synthesis of targeted systems, these two specific aims provide the critical link between the bulk material properties and the microscopic features of their precursor solution state. Throughout the project, emphasis will be placed on understanding and controlling the anisotropic inter-particle interactions which determine structural organization in the solution and ultimately in their solid functional forms. A combination of the core research capabilities of Oak Ridge National Laboratory will be employed to study the structure and dynamics of these materials: neutron scattering utilizing the Spallation Neutron Source, specifically-tailored macromolecular synthesis and characterization utilizing the Center for Nanophase Materials Sciences, and computational studies using the National Center for Computational Sciences. Isotopically labeled materials will be used to highlight the structural and dynamical signatures of neutron scattering, and computer simulations will be performed to provide a unified basis for interpreting the neutron scattering measurements and to give deeper insight into the microscopic behavior of these soft colloids. This coordinated approach will be utilized to generate timely feedback to help guide and design our experimental strategies.

Thermodynamics of Self-Assembly in Globular Protein-Polymer Conjugates

Bradley D. Olsen
Department of Chemical Engineering, Massachusetts Institute of Technology
DOE-BES Award ER46824

Program Scope

Engineering enzymes and optically active proteins into bioelectronic devices for the production of H_2,[1,2] the reduction of CO_2,[3,4] the conversion of sunlight into electricity,[5] or the production of biofuels[6,7] allows the evolutionarily optimized performance of the protein to be exploited to produce high-performance biomolecular variants of catalysts and optoelectronics. Engineering bioelectronic or biocatalytic materials requires achieving a high protein activity and active site density, controlling electron/hole or substrate/product transport through the material, maintaining protein stability, and developing low-cost processes for material fabrication. Analogous to synthetic catalysts[8,9] or organic electronics,[10,11] this requires the arrangement and orientation of the protein at an interface between two phases that provide for the transport of each reagent or charge carrier.

The self-assembly of block copolymers containing an enzyme or optically active protein block could provide a bottom-up method to produce nanostructures that simultaneously achieve control over transport through two phases and yield a high density of oriented protein at an interface. This project investigates the fundamental structure and thermodynamics of block copolymer systems containing a globular protein block, enabling the production of functional nanomaterials (Figure 1). Both the folded protein chain shape and the specific interactions between globular proteins differ significantly from the Gaussian coil block copolymers, adding significant complexity to the phase behavior of these systems. Despite this complexity, we hypothesize that universal rules of self-assembly may be elucidated for these protein-polymer hybrjds, and we aim to answer three fundamental scientific questions:

(1) What is the effect of protein shape (steric interactions) on self-assembly?
(2) What is the effect of protein-protein interactions on self-assembly?
(3) How do the processing conditions used to induce self-assembly affect the folded structure and function of the globular protein block in a block copolymer?

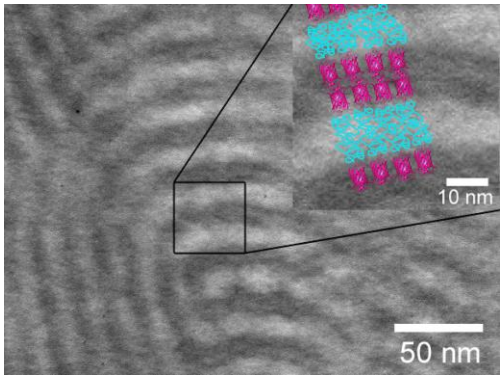

Figure 1. Transmission electron micrograph of mCherry-poly(N-isopropylacrylamide) block copolymer self-assembled into lamellar structures. Protein nanodomains appear dark due to staining.

Recent Accomplishments

In order to maintain the functional secondary and tertiary structure of globular proteins, self-assembly must be induced by the evaporation of water from aqueous conjugate solutions to form solid-state self-assembled materials or globular protein block copolymer gels (Figure 2).[12] Aqueous processing of globular protein-polymer diblock copolymers into solid-state materials and subsequent solvent annealing

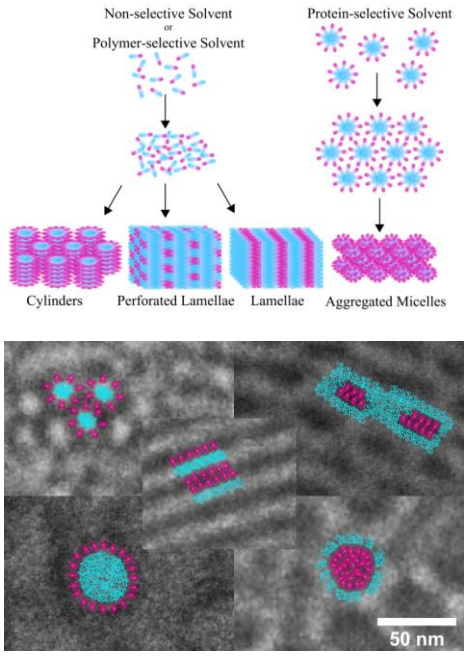

Figure 2. Processing pathways through good and poor solvents for the polymer block enable kinetic control over self-assembly (top). Formation of hexagonal cylinders, perforated lamellae, lamellae, and micellar phases (bottom).

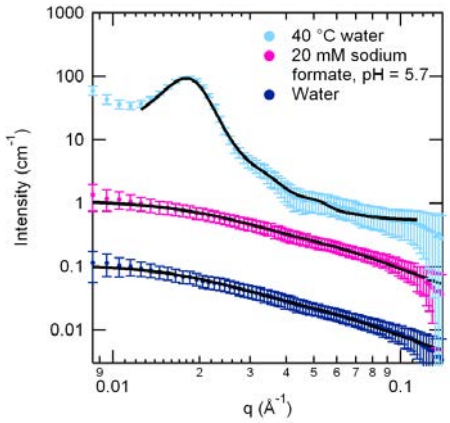

Figure 3. Small-angle neutron scattering patterns of a 3 wt.% solution of mCherry-PNIPAM29 (f_{PNIPAM} = 0.51). Solid lines show fits to the data. Non-selective (room temperature water) and polymer-selective (room temperature pH 5.7) solvents contain conjugates in the monomeric state, while samples in a protein-selective solvent (40 °C water) result in aggregation. The 20 mM sodium formate pH = 5.7 and 40 °C water traces have been vertically offset by 10 and 100 cm^{-1}, respectively, for clarity.

enables kinetic and thermodynamic control of nanostructure formation to produce block copolymer morphologies that maintain a high degree of protein fold and function. Using model diblock copolymers composed of mCherry-b-poly(N-isopropylacrylamide), orthogonal control over solubility of the protein block through changes in pH and the polymer block through changes in temperature is demonstrated during casting and solvent annealing. Small-angle neutron scattering demonstrates that for these materials the solubility of the polymer block dominates the solution behavior of the conjugate, with good solvents for the polymer block resulting in homogeneous solution and poor solvents for the polymer block leading to aggregation and eventual macrophase separation (Figure 3). When solution processing pathways with different solvent quality are used to induce self-assembly, hexagonal cylinders, perforated lamellae, lamellae, or hexagonal and disordered micellar phases are observed depending upon the coil fraction of the block copolymer and the kinetic pathway used for self-assembly. Good solvents for the polymer block produce ordered structures reminiscent of coil-coil diblock copolymers, while an unfavorable solvent results in kinetically trapped micellar structures. Decreasing solvent quality for the protein improves long-range ordering, suggesting that the strength of protein interactions influences nanostructure formation. Subsequent solvent annealing results in evolution of the nanostructures, with the best ordering and the highest protein function observed when annealing in a good solvent for both blocks. While protein secondary structure was found to be almost entirely preserved for all processing pathways, UV-vis spectroscopy of solid-state films indicates that using a good solvent for the protein block enables up to 70% of the protein to be retained in its functional form.

In order to understand which interactions are governing self-assembly, the phase behavior of conjugates in concentrated aqueous solutions (20-50% w/w) is measured. Phase diagrams generated using SAXS and SANS (Figure 4) show that the order-disorder transition concentration first decreases then increases with increasing coil fraction, consistent with

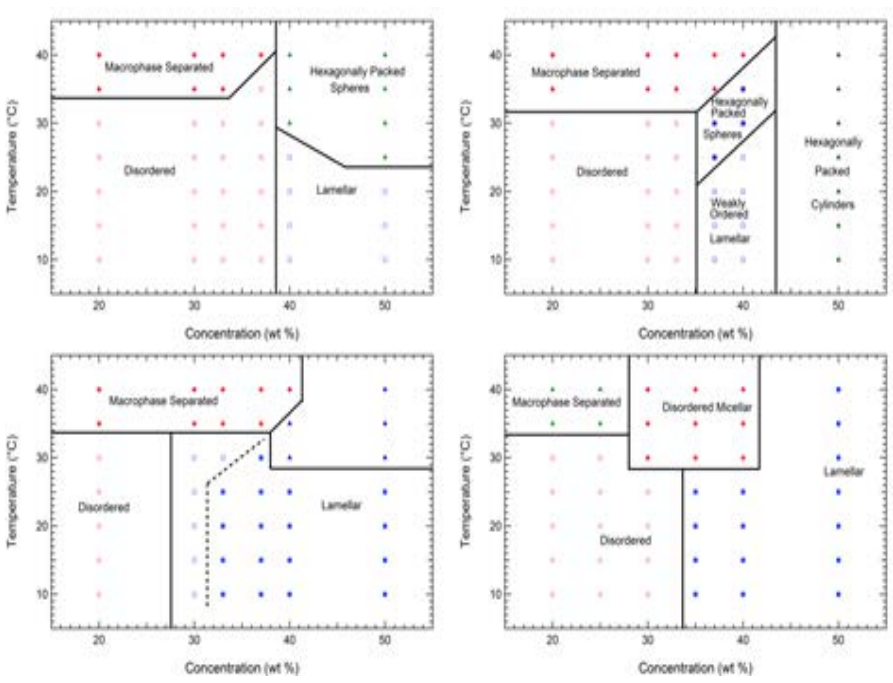

Figure 4. Phase diagram of (a) mCherryS131C-*b*-PNIPAM8k (b) mCherryS131C-*b*-PNIPAM17k (c) mCherryS131C-*b*-PNIPAM30k (d) mCherryS131C-*b*-PNIPAM57k in aqueous solutions.

the behavior of traditional polymer systems where effective repulsive interactions between the two blocks govern self-assembly. This suggests that solvent-mediated protein-polymer repulsion may drive self-assembly in globular protein polymer conjugates. Measurements of second virial coefficients and cross-virial coefficients are currently underway using small-angle light scattering to quantify these observations.

Protein-protein interactions in self-assembly consist of both steric interactions (protein shape effects) and surface interactions between different proteins. These two contributions to the total interaction may be isolated through comparison of phylogenetically related proteins, in particular pairs of proteins with a highly similar folded structure but significantly different amino acid sequence. Enhanced green fluorescent protein (EGFP) and mCherry represent such a pair of proteins; we have prepared bioconjugate block copolymers from both of these proteins with identical coil block molecular weights and similar conjugation sites on the protein surface to specifically test the effect of protein surface interactions on self-assembly. Comparison of the phase behavior of these two materials shows that for symmetric block copolymers the order-disorder transition concentration increases by approximately 7% w/w, but the type of self-assembled nanodomains formed in different regions of the phase diagram or solid-state materials do not change.

Beyond control over processing of block copolymers, activity and stability of the protein block may be further improved through the introduction of hydrogen bonding additives. Using trehalose or glycerol as plasticizers in solid nanostructures can improve retention of function up to 100% and may improve chemostability by approximately a factor of four.

Future Plans

Building upon results from the first nine months of this project, future work will focus on detailed explorations of interaction potentials, steric effects, and protein configuration in self-assembled nanostructures. Characterization of conjugate solutions will be expanded to a wider variety of coil fractions to produce the first comprehensive phase diagram for globular protein-

polymer diblock copolymers. Using this phase diagram as a guide, the effects of protein interactions will be explored in targeted areas of the phase diagram by preparing mCherry mutants that maintain protein fold but have markedly different electrostatic interactions. Protein-polymer interactions will also be tuned through exploration of several alternative polymer chemistries with different hydrogen bonding and ionic content. Small-angle neutron scattering will be applied to measure the effect of changing polymer chemistry on the configuration of bioconjugates and to measure the folded structure of proteins in the self-assembled state using contrast matching experiments. Finally, catalytically active proteins such as carbonic anhydrase will be incorporated into conjugates to explore the ability to produce catalytically active self-assembled materials.

References

(1) Hambourger, M.; Gervaldo, M.; Svedruzic, D.; King, P. W.; Gust, D.; Ghirardi, M.; Moore, A. L.; Moore, T. A. *Journal of the American Chemical Society* **2008**, *130*, 2015.
(2) Krassen, H.; Schwarze, A.; Friedrich, B.; Ataka, K.; Lenz, O.; Heberle, J. *Acs Nano* **2009**, *3*, 4055.
(3) Reda, T.; Plugge, C. M.; Abram, N. J.; Hirst, J. *Proceedings of the National Academy of Sciences of the United States of America* **2008**, *105*, 10654.
(4) Parkinson, B. A.; Weaver, P. F. *Nature* **1984**, *309*, 148.
(5) Das, R.; Kiley, P. J.; Segal, M.; Norville, J.; Yu, A. A.; Wang, L. Y.; Trammell, S. A.; Reddick, L. E.; Kumar, R.; Stellacci, F.; Lebedev, N.; Schnur, J.; Bruce, B. D.; Zhang, S. G.; Baldo, M. *Nano Letters* **2004**, *4*, 1079.
(6) Iso, M.; Chen, B. X.; Eguchi, M.; Kudo, T.; Shrestha, S. *Journal of Molecular Catalysis B-Enzymatic* **2001**, *16*, 53.
(7) Velonia, K.; Rowan, A. E.; Nolte, R. J. M. *Journal of the American Chemical Society* **2002**, *124*, 4224.
(8) Benson, E. E.; Kubiak, C. P.; Sathrum, A. J.; Smieja, J. M. *Chemical Society Reviews* **2009**, *38*, 89.
(9) Mikkelsen, M.; Jorgensen, M.; Krebs, F. C. *Energy & Environmental Science*, *3*, 43.
(10) Yang, X.; Loos, J. *Macromolecules* **2007**, *40*, 1353.
(11) Boudouris, B. W.; Frisbie, C. D.; Hillmyer, M. A. *Macromolecules* **2008**, *41*, 67.
(12) Thomas, C. S.; Glassman, M. J.; Olsen, B. D. *Acs Nano* **2011**, *5*, 5697.

Publications Resulting from Work Supported by DOE-BES Neutron Program

1. "Kinetically Controlled Nanostructure Formation in Self-Assembled Globular Protein-Polymer Diblock Copolymers." C.S. Thomas, L. Xu, and B.D. Olsen. *Submitted.*
2. "Self-Assembled Nanomaterials from Globular Protein-Polymer Diblock Copolymers." B.D. Olsen, C.S. Thomas, C.N. Lam, and L. Xu. POLY Preprints, March 2012.
3. "Kinetic Processes for Nanostructure Self-Assembly in Globular Protein-Polymer Block Copolymers." B.D. Olsen, C.S. Thomas, C.N. Lam, and L. Xu. PMSE Preprints, August 2012.
4. "Protein-Based Conjugates and Self-Assembled Nanostructures." International Patent Application PCT/US2001/057941.

Session VI

Advanced Capabilities (I)

Data and analysis: maximizing the impact of neutron scattering at ORNL

R.L. McGreevy (mcgreevyrl@ornl.gov)

Neutron Sciences Directorate, Oak Ridge National Laboratory, Oak Ridge, TN37831

It is increasingly recognized that the full capabilities of new (and old) multidisciplinary facilities, whether neutron or photon sources, will only be properly exploited through a concomitant investment in all aspects of data – acquisition, management, analysis, visualization, modeling and simulation. The scale and complexity of the problem means that the bulk of the development required, and the ongoing support that will be needed for the infrastructure developed, has to be handled by the facilities and can no longer be delegated to the users. While some aspects are specific to particular facilities and scientific fields, other aspects are common and overlap strongly with developments in, for example, high performance computing and high energy physics. Consequently there is significant scope for collaboration.

The primary focus of the Neutron Sciences Directorate in the period during 2007-11 has been to develop and implement the core data reduction software for the rapidly increasing number of SNS beam lines. Since 2010 most data reduction software for SNS scattering instruments, and for some HFIR instruments, has been developed within a single software framework known as MANTID. This is a framework based upon C++ algorithms, which incorporate thread parallelism using OpenMP, with a Python layer and a Qt GUI. The MANTID software was already being developed by the ISIS facility as a reduction platform for data from its own neutron scattering beam lines. This framework has many advantages for the architecture that is desired for SNS data reduction, principally the ability to reuse algorithms in different contexts and the inherent thread parallelism. Therefore, rather than re-inventing the basic software structure, a formal collaboration between SNS and ISIS was agreed to develop MANTID as a package covering both facilities.

One of the main innovations introduced at ORNL has been the “event-workspace” and the algorithms for manipulating such workspaces. Data from SNS neutron beam lines is acquired as a data stream of events and is stored in an ‘event-NeXus’ file. NeXus is a neutron and x-ray scattering specific version of an HDF5 file, which is a format widely used for the storage of large scientific and computational datasets. Other relevant information, for example the sample temperature, are also stored in the NeXus files as time logs; algorithms have been developed to filter the neutron data using this metadata. In general the event-workspaces are smaller in size and more quickly processed than equivalent histogram workspaces. This has been used to advantage in developing new code for visualizing large 3 and 4 dimensional data sets, such as single crystal S(Q) and S(Q,E) data collected on ARCS, CNCS, SEQUOIA and in future on TOPAZ, MANDI and CORELLI. Visualization software within the MANTID framework, which is based on the ParaView package for visualizing supercomputer simulation results, is ~10x to 20x faster than earlier software such as MSLICE and HORACE.

The framework nature of MANTID has also allowed the development of “automated reduction” capabilities for a number of the SNS beam lines where this is appropriate. The C++ algorithms do not need to be called from the Qt GUI, instead they can be called from Python scripts, which can be included in the data translation and cataloguing chain. Currently, once an experimental run is finished, the data acquisition system takes the experimental data and creates a NeXus file via a process known as “translation” and then catalogues the meta-data associated with the file. As part of this process the Python script is executed that effectively runs MANTID in background mode to produce a reduced data file for the user. This is very useful on high throughput beam lines such

as POWGEN where the data reduction procedure can be easily defined from the meta-data associated with the run.

For instruments with the highest data rates, such as NOMAD, there is still a bottleneck because the (very large) data files are only created, and moved to processing, at the end of a run. A new system is being developed to create the NeXus data files effectively "instantly" at the end of a run, and to perform data reduction during the run, while the data is being acquired. The ADARA project (Accelerating Data Acquisition, Reduction and Analysis) is a collaboration between the Data Analysis and Visualisation Division, the Data Acquisition Support team in the SNS Accelerator Division and the Technology Integration group in the National Center for Computational Science (NCCS). This project is developing (i) the software to stream data from SNS beam lines over a high speed network (Stream Management Service – SMS), (ii) the software that can subscribe to this data stream and create the event-NeXus files on-the-fly (Streaming Translation Service – STS) and (iii) the software within MANTID so that it can subscribe to the data stream and perform the reduction of the data live (Streaming Reduction Service – SRS). In Figure 1 a schematic layout for the ADARA hardware is shown. Data can be streamed both to the local data analysis workstation on the beam line and to computational resources co-located with ORNL's high performance computing resources in NCCS.

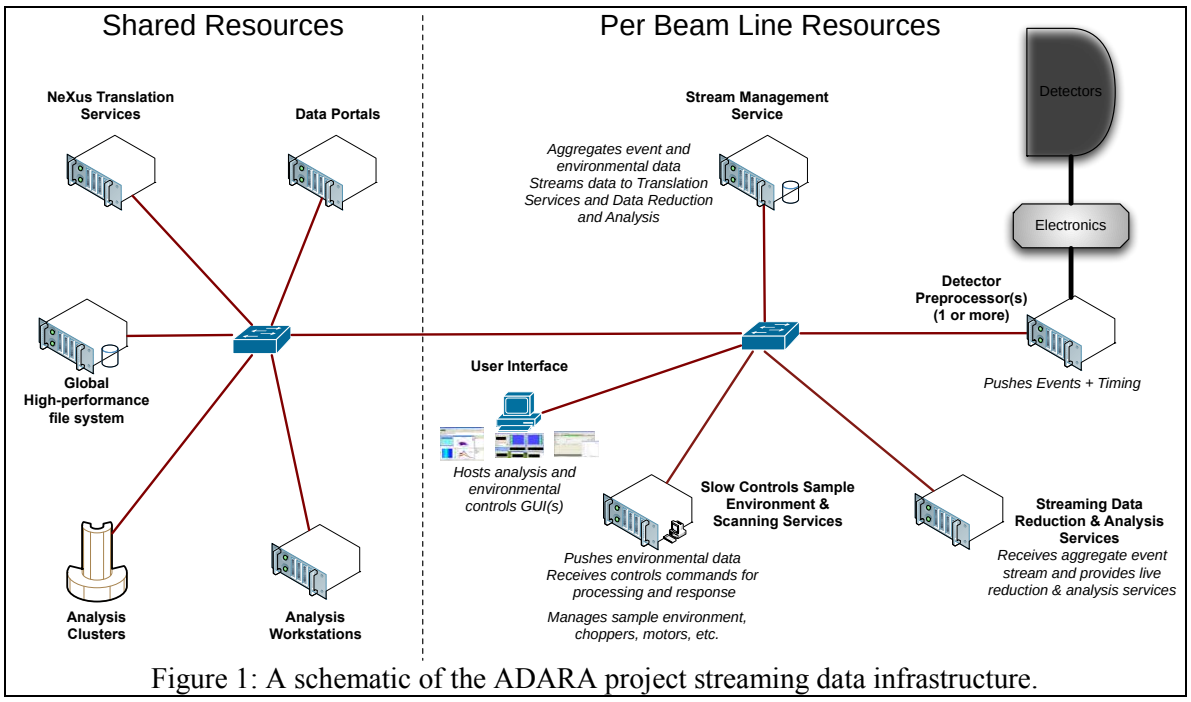

Figure 1: A schematic of the ADARA project streaming data infrastructure.

The computational resources in NCCS are based around a high performance parallel file system. Although the data file size from some SNS beam lines (e.g. BASIS and HYSPEC) is only a few ~100's of Mbytes, those from other beam lines (e.g. NOMAD) are 10's of Gbytes up to 1 – 2 Tbytes. Thus, in order to perform fast post-acquisition processing of the large data files, it is necessary to be able to read the data in parallel and process it in parallel using a computing cluster. MANTID is therefore being developed to exploit the computing clusters. Again this is made possible because of the framework nature of MANTID, which allows algorithms to be run from Python scripts that can be run in parallel on individual nodes of the cluster.

The next step will be to integrate higher level analysis, modeling and simulation codes, e.g. molecular dynamics or density functional theory. Software must be developed to automatically calculate/predict neutron scattering data from such simulations, corresponding to specific instruments (e.g. including instrumental resolution effects). To provide such capabilities for general users will require a significant level of infrastructure and support.

As well as providing improved resources to 'process' the raw data that is being produced, much more effective use must be made of the resulting 'analysed' data. This is the core idea behind the 'Materials Genome' initiative. SNS data are currently being automatically archived and cataloged, along with relevant metadata. This needs to be extended to general archives of analysed data, similar to the databases of e.g. crystallographic data that are widely used, but more generalized and publicly accessible. Such developments will require both a change of policy and of culture, but can be shared and mutually exploited across a wide range of user facilities.

Neutron scattering at LANSCE; Capabilities and scientific hilights

M.A.M. Bourke (bourke@lanl.gov)

Lujan Neutron scattering center, Los Alamos National Laboratory, Los Alamos, NM 87545

The Lujan center which is a 20Hz, ISIS caliber, spallation source at Los Alamos National Laboratory hosts 8 instruments (out of a total of 16 flight paths) in an Office of Science sponsored user program. This talk will describe recent scientific highlights that illustrate their breadth of capability. It will draw attention to the sample environments and personnel that offer unique opportunities. In addition to the 8 instruments in the user program several more operate in a "friendly user" mode. These pose opportunities for complementary collaborations which include testing novel concepts and speculative research. The extent to which Lujan complements LANL strategic initiatives relating to mesoscale, theory modeling and computing as well as MaRIE (which is LANL's decadal vision for the LANSCE mesa) will also be described.

The National Institute of Standards and Technology (NIST) Center for Neutron Research: Current and future capabilities

Dan Neumann, National Institute of Standards and Technology, Gaithersburg, MD

The NIST Center for Neutron Research (NCNR) is currently being expanded, nearly doubling the size of the cold-neutron guide hall and installing five new guides to transport neutrons into this space. Here we will discuss the scope this expansion and the current state of instrumentation at the NCNR describing both new and upgraded instruments that are coming on line over the next years. These include a reflectometer for off-specular scattering, a very small angle scattering instrument, and a white-beam reflectometer. In addition to entire instruments, we will discuss new measurement capabilities that have recently become available at the NCNR including a new rheometer, new shear cell geometries, humidity cells that allow *in-situ* contrast variation, and improved polarization analysis. The use of recently developed instrumentation will be demonstrated through scientific results.

Optics for advanced neutron imaging and scattering

B. Khaykovich[1,a], M. V. Gubarev[2,b], D. Liu[1], B. D. Ramsey[2], and D. E. Moncton[1,c]

[1]Nuclear Reactor Laboratory, Massachusetts Institute of Technology, 138 Albany St., Cambridge, MA 02139, USA
[2]Marshall Space Flight Center, NASA, VP62, Huntsville, AL 35812, USA
[3]Department of Physics, Massachusetts Institute of Technology, 77 Massachusetts Ave., Cambridge, MA 02139, USA

I. Program scope

Collecting as many neutrons on a sample as possible is not the only motivation for developing neutron focusing optics, albeit the most obvious. Modern optical instruments for visible and synchrotron light use a variety of focusing devices, such as lenses, Fresnel zone plates or mirrors. These devices are used to increase the signal rate, resolution, or both. Thermal neutron beams can also be focused by such devices. Even though refractive indices for x-rays and neutrons are similar, direct application of x-ray optics for neutrons is often difficult or impossible because of the difference in size and divergence of the sources. However, the relative weakness of neutron sources and slow incremental improvements of their strength provide the motivation for developing novel neutron optics. The efficient use of existing sources can be as important a path toward more powerful instruments as the development of brighter sources. Although existing neutron optical components, such as guides, are constantly improving, new techniques for manipulating neutron beams might bring significant, even transformative, improvements of neutron instrumentation, and enable new science.

We have initiated a program to develop such a new tool: grazing-incidence mirrors based on full figures of revolution, often referred to as Wolter mirrors [1]. Axisymmetric mirrors can now be made of Ni by a replication technique, which is a mature technology developed for x-ray astronomy. This technology permits nesting coaxial mirrors and coating mirrors with neutron supermirror multilayers, as done for neutron guides with large critical grazing angle. Both nesting and coating lead to significant improvements in collection efficiency of the mirrors. Most importantly, axisymmetric mirrors allow collecting the beam from a large source and large angular divergences.

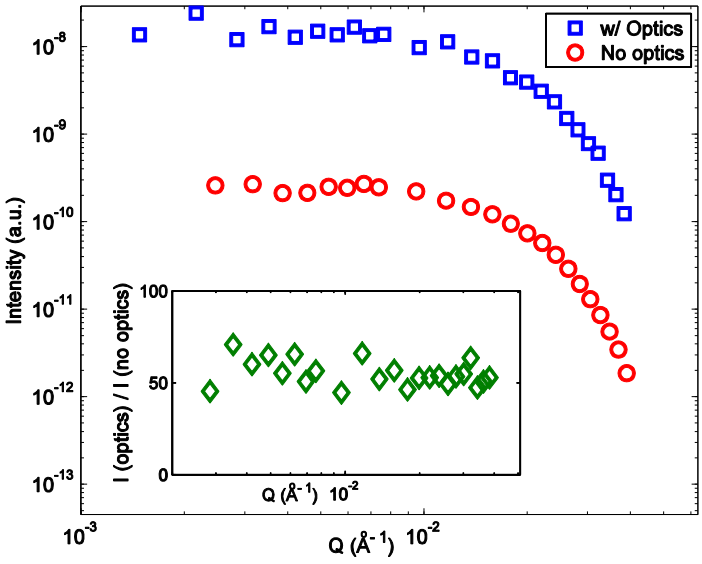

Figure 1. Simulation results of SANS spectra with and without focusing mirrors. The test sample has the radius of gyration of 100 Å and transmission of 0.9. Blue squares and red circles are SANS spectra simulated with and without the optics; the source and sample apertures are of 5 mm radius. The neutron wavelength λ = 13 Å. **Inset**: The ratio of intensities of the two spectra.

[a] bkh@mit.edu
[b] Mikhail.V.Gubarev@nasa.gov
[c] dem@mit.edu

II. Recent progress

SANS diffractometers serve a large multidisciplinary community of users. Therefore, improvements in their performance would have major impact. Most existing SANS instruments use a collimation system that consists of two small apertures (often referred to as sample and source pinholes), which together limit the divergence of the beam. The beam is well collimated to achieve high resolution, even though the two small apertures severely constrain the neutron flux on the sample and thus the signal rate. Significant improvements in both the signal rate and resolution of SANS instruments are possible by using focusing optics, while axisymmetric mirrors present major advantages such as the absence of chromatic aberrations [2]. Results of ray-tracing simulations of a SANS instrument equipped with such optics are shown in Fig. 1. The signal is predicted to increase by a factor of fifty or more, and the minimum wave vector transfer Q to decrease by a factor of two, for a SANS instrument equipped with a 0.4 m-long Ni ellipsoidal mirror as shown on Fig. 2 (Parameters of the new Extended-Q SANS instrument at Spallation Neutron Source were used. SANS spectra were calculated using a standard test sample). The schematic of a traditional SANS instrument with two collimating apertures is shown in Fig. 2 (top). The optics-based instrument is shown in Fig. 2 (bottom), where only one ellipsoid mirror is shown for simplicity. When optics is used, the source and the detector are at the foci of the optics, while the sample is between the optics and the detector. The improvements stem from the ability of the optics to collect neutrons from a much larger solid angle than is possible with traditional designs. Our optics can be easily optimized for SANS instruments at both pulsed and reactor sources, leading to major enhancements in their performance.

In traditional SANS instruments, long vacuum tanks contain movable detectors in order to adjust the sample-to-detector distance (SDD) to change the Q coverage. To reach the smallest required Q_{min}, long SDD's are used, thus requiring evacuated detector tanks of 10 to 20 m in length. These huge vacuum tanks are expensive and cumbersome. By utilizing the mirrors, SANS instruments would reach the smallest Q_{min} with shorter SDD, which is equal to the focal length of the optics, and the resolution is limited by the detector's pixel size. Modern multi-channel-plate detectors have pixel sizes of less than 40 μm, which is much smaller than that of traditional SANS detectors. The combination of novel optics and detectors could lead to revolutionary changes in SANS instruments, including extended Q-range, very fast (seconds) SANS measurements of standard samples and *in situ* studies of kinetic processes. Short mirror-based instruments could be especially useful for compact accelerator-based sources at

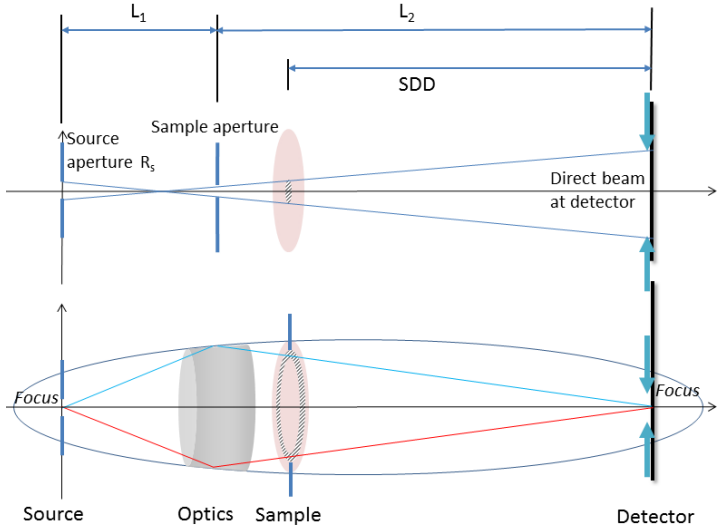

Figure 2. Schematics of SANS instruments without (top) and with focusing optics (bottom). R_s is the source aperture radius. SDD is the sample-to-detector distance. L_1 is the source-to-optics distance (SOD). L_2 is the optics-to-detector distance (ODD). Magnification is defined by $M = L_2/L_1$. The two arrows indicate the direct beam spot at the detector. In the presence of focusing optics, the radius of the direct beam at the detector is $R = R_sM$. The neutron beam illuminates the shaded area of the sample.

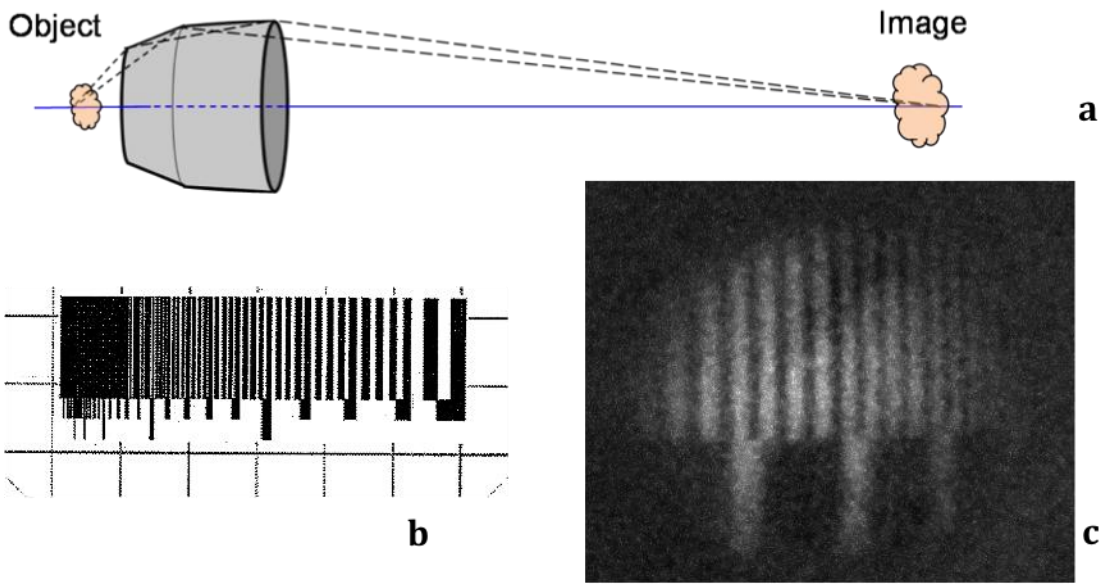

Figure 3. (a) Schematic illustration of a single pair of Wolter mirrors acting as an image-forming lens. In the microscope-like configuration shown here, the neutron beam travels from left to right. The object is in the upstream focal plane of the optics. The magnified image is formed at the downstream focal plane. The source of the neutron beam is located upstream from the object. Only one axisymmetric mirror is shown for clarity, but several co-axial mirrors could be used to increase the neutron flux reaching the detector. (b) Neutron absorbing test mask (made of Gd) and the image of its fragment. The bottom line pattern was used for the neutron imaging experiment. (c) The image is of line groups with periods of 0.83, 0.71, 0.59 and 0.5 mm (from left to right). The image is magnified by the factor of 4, the magnification of the mirrors.

universities (LENS at Indiana University) or industrial facilities.

Neutron imaging is one of the fastest-developing neutron methods. The two key challenges for this technique are weak source brilliance and poor detector spatial resolution. These challenges can be addressed by using focusing optics, as in optical microscopes. The mirrors could play the role of image-forming lenses, as shown on Fig. 3a. We have demonstrated this approach both experimentally and with ray-tracing simulations [3,4]. The experiment was done at HFIR (cold beamline CG1-D) at Oak Ridge National Laboratory (ORNL). A Gd test object was placed after a source in the focal plane of the optics (Fig. 3b). The mirrors were placed such that the magnified image of a portion of the grid can be recorded (Fig. 3c). The analysis of the images has shown that the resolution is limited by the pixel size of the detector, rather than by the mirrors. Similar to SANS, traditional neutron imaging instruments resemble a pinhole camera, which requires the use of a small aperture as the source to achieve good resolution. Application of mirrors would allow the use of much larger sources, thus significantly improving the signal rate at the detector [3,4]. Mirrors of magnification one would increase the signal rate, while magnification of ten would increase the spatial resolution**.**

Coating of reflecting surfaces by supermirror multilayers will significantly increase the collection efficiency of the optics relative to Ni due to the increase in the critical angle. We are developing the technology for multilayer coating of axisymmetric mirrors since commercial neutron supermirrors are prepared on flat substrates. A mandrel is coated with a separation layer and the supermirror multilayer, followed by the Ni mirror. The mirror and the multilayer are then separated from the mandrel to form the replicated neutron mirror. We demonstrated and tested flat NiC/Ti neutron supermirrors with m = 1.9 (m is the ratio between the critical angles of the

supermirror and Ni) [3], as well as coating and releasing flat replicas. Neutron reflectivity showed that the quality of our supermirrors is similar to that of modern commercial neutron guides. Such supermirror-coated mirrors should be useful for a range of applications, including SANS and imaging.

III. Future plans

A major theme will be the experimental realization of SANS and imaging applications of Wolter mirrors, combined with ray-tracing simulations. Surprisingly, the test beamline at the MIT Nuclear Reactor can be configured for SANS when using our mirrors. We are currently testing SANS capabilities at MIT and experiments at HFIR (ORNL) are planned. An experimental demonstration of SANS will be combined with ray-tracing simulations to assess effects of mirrors imperfections. As for neutron imaging, further experiments are planned at NIST, for imaging fuel cells and batteries with improved resolution due to magnification.

We are finishing ray-tracing simulations of high-efficiency neutron collection mirrors, based on the idea that increasing the number of reflections and the number of nested mirrors is beneficial for the collection efficiency. Such optical designs could be used to replace neutron guides by mirrors with long focal lengths. This work is scheduled for presentation at the SPIE Conference in August 2012 and will be submitted for publication soon. Next, we will work on the design of an imaging instrument for SNS equipped with only mirrors without neutron guides.

The supermirror-coated axisymmetric mirrors should be demonstrated in the near future, as all preliminary developments on flat replicated substrates have been successfully finished.

Research supported by the U.S. Department of Energy, Office of Basic Energy Sciences, under Awards # DE-FG02-09ER46556 and DE-FG02-09ER46557.

IV. Publication resulting from work supported by the DOE project over the last two years

[1] B. Khaykovich, M. V. Gubarev, Y. Bagdasarova, B. D. Ramsey, and D. E. Moncton, “From x-ray telescopes to neutron scattering: Using axisymmetric mirrors to focus a neutron beam.” Nucl. Instrum. Methods Phys. Res. Sect. A: Accel. Spectrom. Det. Ass. Equip. 631 (2011), 98.

[2] D. Liu, M. V. Gubarev, G. Resta, B. D. Ramsey, D. E. Moncton, and B. Khaykovich, “Axisymmetric Grazing-Incidence Focusing Optics for Small-Angle Neutron Scattering”, Nucl. Instrum. Methods Phys. Res. Sect. A: Accel. Spectrom. Det. Ass. Equip. To be published (2012); doi:10.1016/j.nima.2012.05.056; arxiv:1205.0524v1

[3] M. V. Gubarev, B. Khaykovich, B. D. Ramsey*, et al*, “From x-ray telescopes to neutron focusing”, Proc. SPIE 8147 (2011), 81470B-1.

[4] B. Khaykovich, M. V. Gubarev, V. E. Zavlin, *et al*, “Novel neutron focusing mirrors for compact neutron sources”, Physics Procedia 26 (2012), 299.

Session VII

Heterostructures

Neutron Scattering Studies of Cobaltite Crystals and Heterostructures

Chris Leighton

Materials Science, University of Minnesota, Minneapolis, MN 55455

leighton@umn.edu, www.cems.umn.edu/about/people/faculty.php?id=20233

Program Scope: Complex oxides such as perovskites display extraordinarily diverse physical phenomena in addition to a rich interplay between structure and properties. These properties provide some of the most significant challenges to our understanding of correlated electrons in solids (*e.g.* high temperature superconductivity, colossal magnetoresistance, and electronic inhomogeneity), at the same time providing great potential for applications. The applications are varied and include solid oxide fuel cells, Ferroelectric RAM, oxygen separation membranes, oxide spintronics, and indeed oxide electronics in general. One of the most important recent advances in this field is the realization that well-controlled growth of epitaxial thin films and heterostructures is possible. This opens up a plethora of opportunities for basic science (such as stabilization of new ground states and strain-stabilization of non-equilibrium structures), in addition to fundamental studies of novel device concepts in films and heterostructures.

This research program (Fig. 1) is aimed at two of the biggest challenges that emerge from the above: The need for an understanding of electronic and magnetic behavior in complex oxides, and the need for a full appreciation of what can be achieved with complex oxide interfaces and hetero-structures. We are tackling these questions using the doped cobaltites due to some unique attributes that make them model systems for the phenomena studied here. These include nanoscopic magnetoelectronic phase separation (MEPS), spin-state transitions, and the influence of interfaces, defects, and strain on magnetism and transport. The cobaltites employed here include low bandwidth perovskites, layered perovskites, and model epitaxial structures. In addition to synthesis, characterization, and a battery of property measurements, the work relies heavily on neutron scattering methods. These include small-angle neutron scattering (SANS) as a probe of magnetic inhomogeneity and short-range order, neutron diffraction (ND) as a probe of crystal/magnetic structures, and polarized neutron reflectometry (PNR) as a probe of interface magnetism.

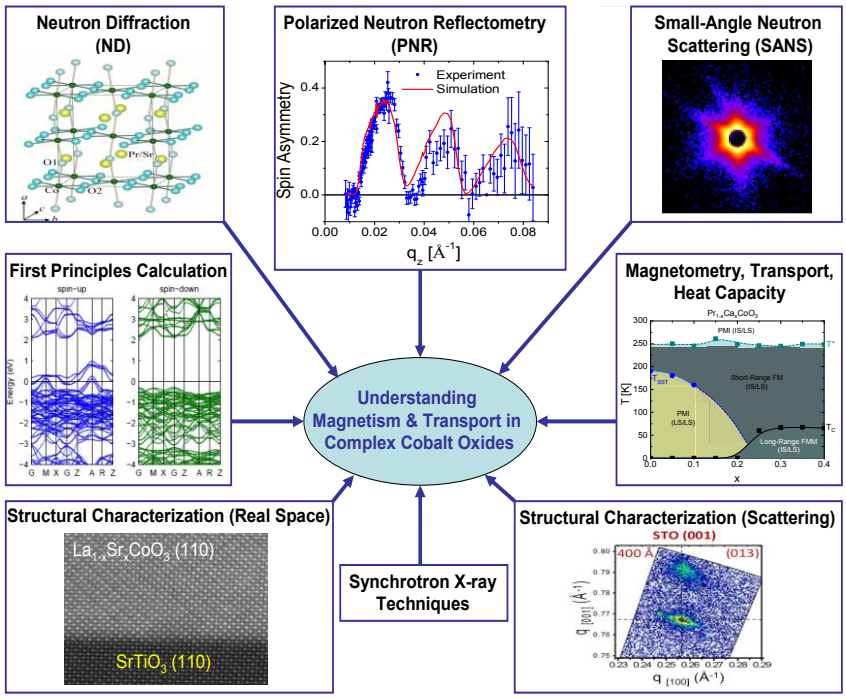

Fig. 1. Illustration of the complementary experimental and theoretical techniques employed in this project, emphasizing neutron scattering.

Recent Progress: **Spin-State Transitions and Short-Range Magnetic Ordering in $La_{1-x}Sr_xCoO_3$:** Our extensive studies of the magneto-electronic phase separation (MEPS) in this model system has established the detailed phenomenology (Fig. 2), a complete understanding of the influence of MEPS on the physical properties, and the first quantitative model capable of explaining all aspects of the available data. Our most recent work is aimed at understanding the least understood aspect to the behavior of these materials - the interplay between spin-state physics and MEPS in lightly hole- and electron-doped $LaCoO_3$. In this region (see Fig. 2) an evolution from magnetic polarons to phase-separated clusters must somehow occur, although the details remain unclear. Due to its general nature, and its relevance to such a wide variety of inhomogeneous magnetic materials, this is a particularly important problem. Our magnetometry, transport, heat capacity, and SANS data reveal a fascinating coexistence of spin excitons, spin-state polarons, and ferromagnetic clusters in this region, and we are in the process of tracking their complex evolution with doping. With the potential to cast much light on the spin-state transition problem in $LaCoO_3$ we have also recently advanced the electric field gradient at the Co nucleus, via the NMR electric quadrupole splitting, as a simple and direct probe of the Co ion spin-state. Collaborative work is underway to test this prediction.

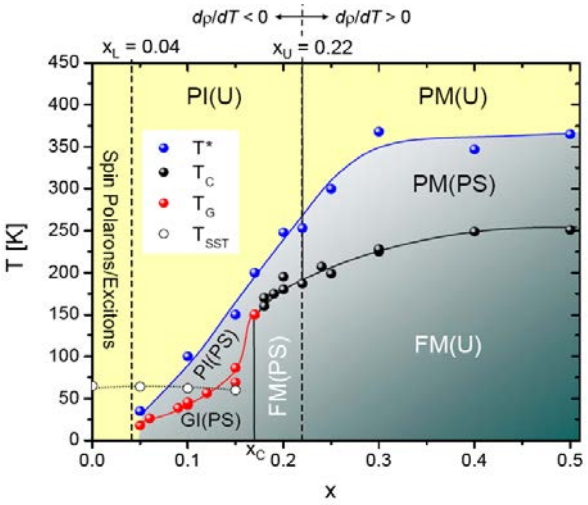

Fig. 2. Revised LSCO phase diagram. PI = paramagnetic insulator, PM = paramagnetic metal, GI = glassy insulator, FM = ferromagnetic metal, T_{SST} = spin-state transition onset temp. U and PS indicate uniform and phase-separated regions.

Spin-State Physics and Magnetic Phase Separation in Narrow Bandwidth Cobaltites: Continuing with the theme of understanding the interplay between spin-state transitions and MEPS, we are also exploring narrow bandwidth perovskite cobaltites, where the competition between competing electronic and magnetic phases is particularly acute due to the stabilization of the low spin-state. This effort has yielded a plethora of new insights into this interesting problem, including; (i) a full appreciation of the interplay between spin-state transitions and short-range magnetic ordering in $Pr_{1-x}Ca_xCoO_3$, (ii) a rare opportunity to study the *interactions* between coexisting phases in MEPS systems, (iii) continued study of the unique *first-order* spin-state transitions in $Pr_{1-x}Ca_xCoO_3$ and $(Pr_{1-y}Y_y)_{1-x}Ca_xCoO_3$, (iv) the discovery of oxygen vacancy ordering in a bulk perovskite cobaltite and its intriguing relation to enhanced magnetocrystalline anisotropy, and (v) the elucidation of the anomalous ferrimagnetism in $Nd_{1-x}Ca_xCoO_3$.

Cobaltite Interfaces and Heterostructures: As discussed above, thin films, interfaces, and heterostructures represent a new frontier in the study of complex oxides. Following initial work refining the epitaxial growth and characterization of $La_{1-x}Sr_xCoO_3$ films our first work in this area was aimed at perhaps the oldest problem in complex oxide thin film magnetism – the rapid deterioration in electronic and magnetic properties at interfaces with dissimilar oxides. Although this problem is widespread, and could present a significant roadblock to the development of heterostructured devices, there is no consensus as to its origin. In our work, using $SrTiO_3(001)/La_{1-x}Sr_xCoO_3$ as a model system, we combined epitaxial growth via high pressure oxygen sputtering with high resolution x-ray diffraction, atomic resolution electron microscopy

and spectroscopy, and magnetic, transport, SANS and PNR measurements to determine the fundamental origin of the deterioration in interfacial transport and magnetism. The effect was found to be due to nanoscopic MEPS in the near-interface region driven by a significant depletion in interfacial hole doping due to accumulation of O vacancies (Fig. 3). This occurs due to a novel mechanism for accommodation of lattice mismatch with the substrate based on formation and long-range ordering of O vacancies, thus providing a fundamental link between strain state and O vacancy density. Further impacts of the O vacancy ordering and interfacial MEPS, such as formation of a spin-state superlattice and an extraordinary coercivity enhancement, were also investigated in recent publications.

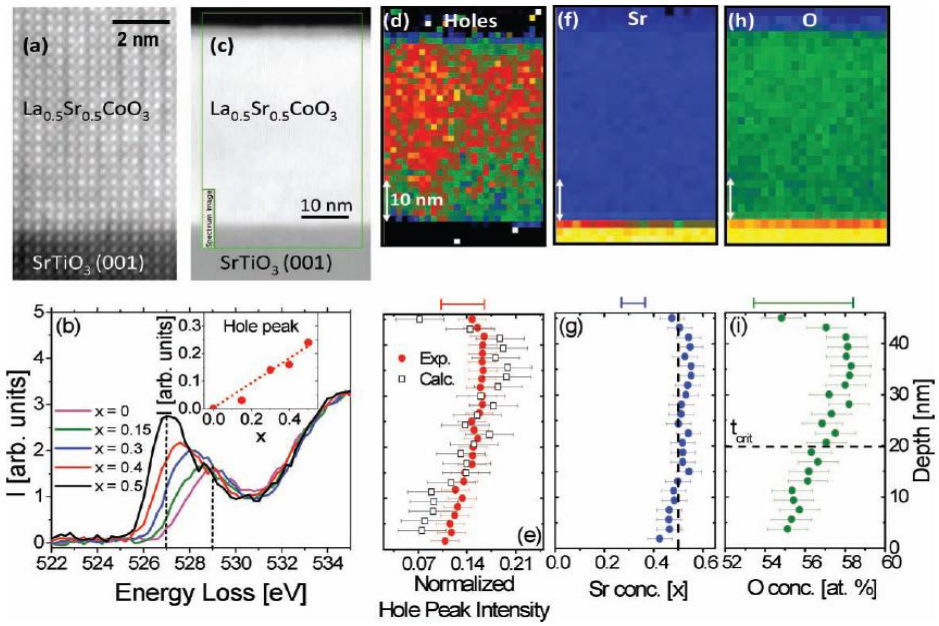

Fig. 3. STEM imaging (a,c) and EELS mapping of hole density (d), Sr (f) and O (h). (e,g,i) show depth-wise variations (laterally averaged) from (d,f,h). The large error bars at the top indicate absolute error. (b) shows how the hole peak near the O *K* edge at 527 eV is calibrated from *bulk* specimens.

Application to Other Materials Systems: A final area of research in this project deals with applying the tools discussed above to other materials systems where short-range order and magnetic inhomogeneity play a role. Off-stoichiometric Heusler alloys such as $Ni_{50-x}Co_xMn_{25+y}Sn_{25-y}$ provide an excellent example. These materials, which are derived from the base Heusler Ni_2MnSn, provide compositional tuning of the exchange interactions, the magnetic and martensitic phase transformation temperatures, and the temperature hysteresis at the martensitic phase transformation. This has recently enabled development of an alloy, $Ni_{44}Co_6Mn_{40}Sn_{10}$, with an antiferromagnetic ferroelastic martensitic phase, transforming at just above room temperature to a soft ferromagnetic austenite phase with high magnetization. The giant magnetization change and low hysteresis at this transition have stimulated intense discussion of potential applications in energy conversion, actuation, sensing, *etc*. Using SANS (Fig. 4), and more recently ND, we have studied this system in considerable detail, improving our understanding of the nature of the magnetic orderings, the various phase transitions, and the origin of the unusual magnetism.

Future Plans: Neutron scattering and physical property studies of lightly hole- and electron-doped $LaCoO_3$ will be continued in order to fully elucidate the evolution from a polaronic to clustered state. When the complementary work on narrow bandwidth systems such as $(Pr_{1-y}Y_y)_{1-x}Ca_xCoO_3$ and $Nd_{1-x}Ca_xCoO_3$ is completed this will provide a global picture of the interplay between spin-state transitions and MEPS, a significant advance. Most importantly, our work on $La_{1-x}Sr_xCoO_3$ films clearly opens up a broad spectrum of additional opportunities. Primary among these is the possibility of manipulating the strain state via control of the crystallographic

orientation, in order to engineer oxygen vacancy ordering and thus interface magnetism and transport. Success with this approach would be relevant beyond magnetism, potentially being important for a number of O transport based technologies.

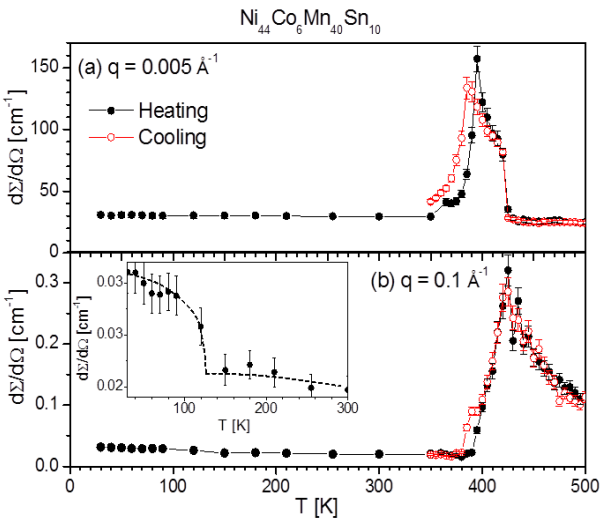

Fig. 4. Temperature dependence of the SANS cross section from $Ni_{44}Co_6Mn_{40}Sn_{10}$ at a scattering wavevector of (a) 0.005 $Å^{-1}$ and (b) 0.1 $Å^{-1}$. Data taken on heating (black solid points) and cooling (red open points) are shown (with error bars). The inset to (b) shows an enlarged view of the 0.1 $Å^{-1}$ data at low T.

Publications (2010 - 2012)

1. "*Spontaneous formation of an exchange-spring composite via magnetic phase separation in* $Pr_{1-x}Ca_xCoO_3$", S. El-Khatib, S. Bose, C. He, J. Kuplic, M. Laver, J.A. Borchers, Q. Huang, J.W. Lynn, J.F. Mitchell and C. Leighton, Phys. Rev. B. Rapid Comm. **82**, 100411 (2010).

2. "*Cobalt spin states and hyperfine interactions in* $LaCoO_3$ *investigated by LDA+U calculations*", H. Hsu, P. Blaha, R.M. Wentzcovitch and C. Leighton, Phys. Rev. B. Rapid. Comm. **82**, 100406 (2010).

3. "*Application of aberration corrected scanning transmission electron microscopy and electron energy loss spectroscopy to thin oxide films and interfaces*", M. Varela, J. Gazquez, A.R. Lupini, J.T. Luck, M.A. Torija, M. Sharma, C. Leighton, M.G. Biegalski, H.M. Christen, M. Murfitt, N. Dellby, O. Krivanek and S.J. Pennycook, Int. J. Mat. Res. (Proc. of 7th Int. Workshop on Interfaces) **101,** 21 (2010).

4. "*Chemically-driven nanoscopic magnetic phase separation at the* $SrTiO_3(001)/La_{1-x}Sr_xCoO_3$ *interface*", M.A. Torija, M. Sharma, J. Gazquez, M. Varela, C. He, J. Schmitt, J.A. Borchers, M. Laver, S. El-Khatib and C. Leighton, Adv. Mater. **23** 2711 (2011).

5. "*Atomic resolution imaging of spin-state superlattices in nanopockets within cobaltite thin films*", J. Gazquez, W. Luo, M.P. Oxley, M. Prange, M.A. Torija, M. Sharma, C. Leighton, S.T. Pantiledes, S.J. Pennycook and M. Varela, Nano. Lett. **11** 973 (2011).

6. "*Coercivity enhancement driven by interfacial magnetic phase separation in* $SrTiO_3(001)/Nd_{0.5}Sr_{0.5}CoO_3$", M. Sharma, J. Gazquez, M. Varela, J. Schmitt and C. Leighton, Phys. Rev. B., **84** 024417 (2011).

7. "*Growth temperature control of the epitaxy, magnetism, and transport in* $SrTiO_3(001)/La_{1-x}Sr_xCoO_3$ *thin films*", M. Sharma, J. Gazquez, M. Varela, J. Schmitt and C. Leighton, J. Vac. Sci. Technol. **29** 051511 (2011).

8. "*Transverse susceptibility as a probe of the magnetocrystalline anisotropy-driven phase transition in* $Pr_{0.5}Sr_{0.5}CoO_3$", N.A. Frey-Huls, N.S. Bingham, M.H. Phan, H. Srikanth, D.D. Stauffer and C. Leighton, Phys. Rev. B. **83** 024406 (2011).

9. "*Small-angle neutron scattering study of magnetic ordering and inhomogeneity across the martensitic phase transformation in* $Ni_{50-x}Co_xMn_{40}Sn_{10}$ *alloys*", K.P. Bhatti, S. El-Khatib, V. Srivastava, R.D. James and C. Leighton, Phys. Rev. B. **85** 134450 (2012).

10. "$RbFe^{2+}Fe^{3+}F_6$*: Synthesis, structure, and characterization of a new charge-ordered magnetically frustrated pyrochlore-related mixed-metal fluoride*", S.W. Kim, S-H. Kim, P.S. Halasyamani, M. Green, K.P. Bhatti, C. Leighton, H. Das and C. Fennie, Chem. Sci. **3,** 741 (2012).

11. "*Magnetocaloric effect and critical behavior in* $Pr_{0.5}Sr_{0.5}MnO_3$*: An analysis on the validity of the Maxwell relation and the nature of phase transitions*", R. Caballero-Flores, N.S. Bingham, M.H. Phan, M.A. Torija, C. Leighton, V. Franco, A. Conde and H. Srikanth, submitted, Phys. Rev. B. (2012).

12. "*Syntheses, crystal structures, and characterizations of two new Tl-*Cu^{2+}*-*Te^{6+} *oxides:* Tl_4CuTeO_6 *and* $Tl_6CuTe_2O_{10}$", J. Yeon, S.-H. Kim, M.A. Green, K.P. Bhatti, C. Leighton and S. Halasyamani, submitted, J. Sol. Stat. Chem. (2012).

13. "*Ferrimagnetism in* $PrCoO_3$ *epitaxial films*", V.V. Mehta, S. Bose, J.M. Iwata, E. Arenholz, C. Leighton and Y. Suzuki, submitted, Phys. Rev. B. Rapid Comm. (2012).

Neutron and X-Ray Studies of Spin and Charge Manipulation in Magnetic Nanostructures

Eric E. Fullerton[1] and Sunil Sinha[2]
[1] Departments of Electrical and Computer Engineering and NanoEngineering
University of California, San Diego
efullerton@ucsd.edu

[2] Department of Physics
University of California, San Diego
ssinha@physics.ucsd.edu

Program scope: The interrogation and manipulation of electron charge, spin, and magnetization in thin films and magnetic nanostructures is currently one of the frontier areas of research in Condensed Matter Physics and Materials Science [1, 2]. These include issues that are directly related to scaling down the dimensions such that finite size, interfacial and collective effects dominate the behavior. Examples include magnetization reversal of single domain and dense arrays of nano-magnets, influence of surfaces on magnetic behavior, and the broad field of spintronics which relies on manipulating the spin rather than the charge of the electron via spin injection, manipulation and detection [2]. Magnetic materials and devices have also played a major role in science and technology for information storage [3] and more recently in magnetic memories [4]. Combined with advances in semiconductor science and technology, that have until recently ignored the spin of the electron, has spurred the field of spintronics, ushering in a range of new magnetic sensors, memories [4, 5] and provides a spin-based vision for the electronics of the future. A thorough understanding of the underlying materials and electronic properties and their response at the nano-scale spatial dimensions and sub-nanosecond temporal scale are needed.

Our research provides a close coupling between state-of-the-art thin film growth and patterning techniques with cutting-edge characterization techniques. The increasing role of interfacial structure and the modification of the physical and magnetic structure at interfaces highlight the importance of structural and magnetic measurements at the atomic scale. The application of synchrotron [6] and neutron techniques [7] to attack this problem provides opportunities for detailed structural and magnetic description of nano-scale magnetic systems and are crucial ingredients in the understanding of the physical properties.

Recent Progress:

Patterned magnetic nanostructures: Interest in patterned magnetic structures is driven by interesting physics of dense-packed arrays of nano-magnetic systems and the potential for new applications such as high density magnetic data storage, magnetic logic and biomagnetic functionality. For instance, bit-patterned media is a leading candidate to increase magnetic recording densities beyond those achievable by currently used perpendicular magnetic recording. We have recently performed neutron scattering experiments on densely packed, patterned magnetic heterostructures. The starting films are [Co (0.25 nm)/Pd (0.7 nm)]$_5$/Fe (2 nm)/[Co (0.25 nm)/Pd (0.7 nm)]$_5$ heterostructures that combine perpendicular anisotropy Co/Pd multilayers with relatively magnetically soft Fe layers. The films are patterned in nano-dot arrays using self-assembling di-block co-polymer [polystyrene–poly(methyl methacrylate) (PS–PMMA)] annealed in 200 ºC. The polymers phase segregate and the PMMA dots are selectively removed by oxygen plasma etching and the resulting holes were filled with spin-on-glass that act as an etch mask. The underlying magnetic film was patterned by Ar ion milling through the

spin-on-glass mask. This allows patterning large surface areas with patterns as small as 25-nm islands on a 35-nm pitch (see Fig. 1). The patterned islands are covered by a C layer for protection.

The neutron scattering experiment will be carried out on MAGICS reflectometer at Beamline 4A at the Spallation Neutron Source. Since the samples have perpendicular anisotropy and the polarized neutron reflectometer only tracks the in plane moment, performed we performed several measurements with the neutron polarization and applied magnetic field perpendicular to the scattering vector to gain access to the in-plane component of the magnetization. The non-spin-flip (R^{++} and R^{--}) scattering tracks the chemical depth profile of the

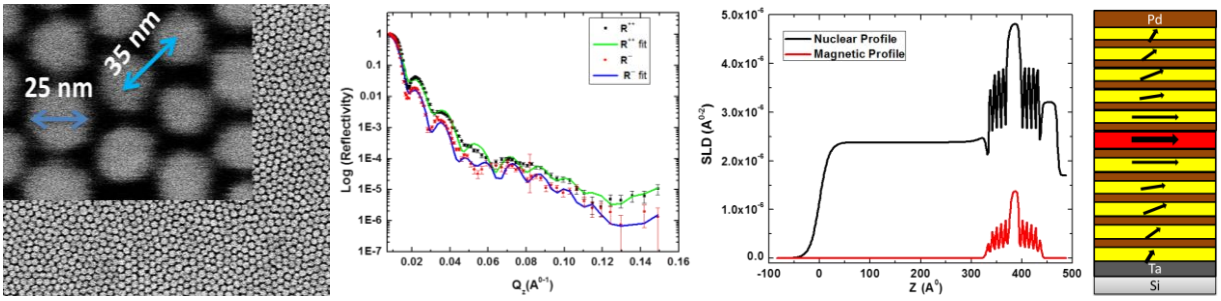

***Figure 1**: Pulsed neutron reflectometry results for a patterned multilayer structure: Ta(3 nm)/Pd(2 nm)/[Co (0.25 nm) /Pd (0.7 nm)]$_5$/Fe (2 nm) /[Co (0.25 nm) Pd (0.7 nm)]$_5$ patterned to form 25-nm dots on a 35-nm pitch. The left panel shows an SEM image of the patterned structures. The middle-left panel shows the non-spin-flip (R^{++} and R^{--}) scattering that tracks the chemical depth profile of the film and the parallel component of the magnetization along with least-squared fit (solid lines) of the data. The middle-right panel shows the resulting fit of the nuclear and magnetic profiles. The magnetic profile shows a non-uniform magnetic structure along the depth of the structure shown schematically in the right panel.*

film and the eventual parallel component of the magnetization. Shown in Figure 1 is the scattering result for an intermediate magnetic field along with the least squares fits. The nuclear profile was determined from fitting of the x-ray reflectivity. There is a clear non-uniform magnetic structure resulting from the large Fe moment and modulated exchange across the Pd layers. We have further tracked the magnetization as a function of applied field and have compared the results to micro-magnetic modeling.

Slow Domain Wall fluctuations in a Dysprosium Film: We have used coherent X-rays tuned to the Dy M-edge at Beam line 12.0.2 at the Advanced Light source to study magnetic speckle around the magnetic satellite peak in the spiral antiferromagnetic phase of Dy metal. Dy is ferromagnetic at low temperatures , then at a Curie Temperature of 75.7 K it enters a spiral antiferromagnetic spiral phase where the spins are aligned in ferromagnetic sheets in the a-b planes which rotate by a given (temperature-dependent) angle from sheet to sheet along the c-axis, and finally loses magnetic order at a Néel temperature of 179.3 K. We find that the speckle (which is presumably from domain walls and other defects in the spin structure) is static until very close to the Neel temperature, where it develops fluctuations which relax

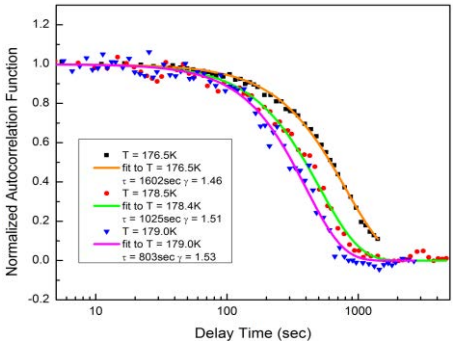

***Figure 2**: Time autocorrelation function $g_2(t)$ obtained from the XPCS results on magnetic speckle from Dy film at temperatures near the transition temperature.*

via a compressed exponential with an exponent of ~ 1.0. (Fig. 2) This seems to be in accordance with several studies of so-called jammed or frustrated systems such as domain walls in the antiferromagnet Cr, and nanoparticles entangled in gel frameworks which all show a similar exponent. This will lead to a better understanding of the universal aspects of domain wall motion in magnetic systems. It is domain wall fluctuations in magnetic films which leads to noise in magnetic devices.

Time-resolved x-ray scattering of FeRh films: We use time-resolved x-ray diffraction and magnetic optical Kerr effect to study the laser induced AFM to FM phase transition in FeRh. The structural response is given by the nucleation of independent ferromagnetic domains (τ_1 ~ 30ps). This is significantly faster than the average magnetic response (τ_2 ~ 100ps) which is given by the subsequent domain realignment X-ray diffraction shows that the two phases co-exist on short time-scales (Fig. 3) as expected for a first order phase transition, and fits a simple nucleation model which describes both structural and magnetic dynamics well is presented. This study reveals that the structural and magnetic domains nucleate simultaneously. The phase transition contributes to the observed strain wave and is ultimately limited by the speed of sound.

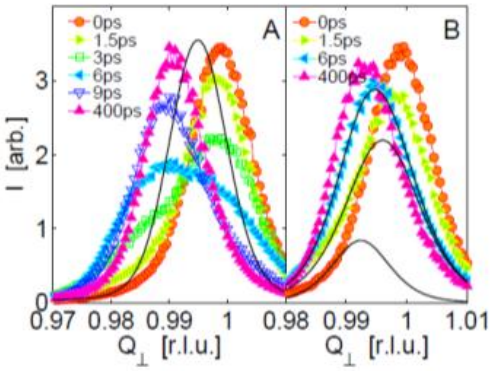

***Figure 3**: Bragg reflections obtained at different time delays for a pump fluence of (A) 5.2mJ/cm^2 and (B) 2.7mJ/cm^2. The solid line in (A) is the simulated Bragg reflection at t=9ps under the sole influence of thermal strain.*

Permalloy/CoO bilayers: Permalloy (Py)/CoO bilayer is a widely studied exchange bias system because the ordering temperature of CoO (T_N ~ 290K) is close to room temperature and because of the magnetic softness of Py. Recent studies by some of us reported that there is a thin interfacial layer in the polycrystalline Py/CoO system which has net Co moments above T_N. The Co moments are pinned antiparallel to the cooling field in the biased state.

We have extended our previous study and, using the polarized neutron reflectometer at beamline 4A of the Spallation Neutron source at ORNL, measured the polarized neutron reflectivity in both polycrystalline and (111)-epitaxial Py/CoO bilayers. The nuclear and magnetic parts were uncoupled in the fitting program. The nuclear part was constrained by the Cu K_α x-ray reflectivity fitted parameters. Only the magnetic depth profile was fitted to the polarized neutron data. Polarized neutron reflectivity data were taken in the exchange-biased state for both positive and negative saturation fields after cooling to 5K in a 1.15T cooling field. By fitting the magnetic depth profile to both, the pinned and unpinned components of the magnetization profile could be obtained.

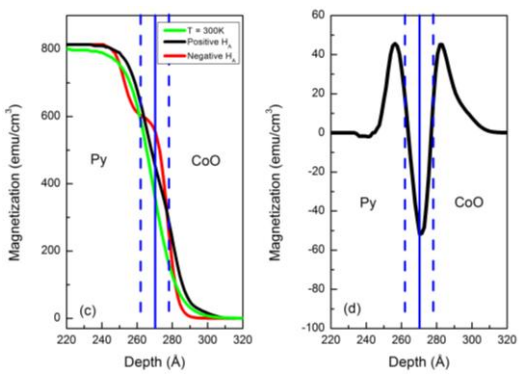

***Figure 4**: Magnetization profile of Py/ polycrystalline CoO film at 300K (green) and in the exchange biased state for positive and negative applied fields; right hand figure shows pinned moment profile.*

A detailed analysis of the neutron reflectivity results has now been completed, and the depth profile of the pinned and unpinned components have been obtained and compared. The results show some surprising features and differences. The

pinned component of the polycrystalline sample is shown in figure 4. At the chemical interfacial region, the pinned moments are anti-parallel to the cooling field, while in the vicinity of the chemical interface, both the Py and CoO region show pinned moments parallel to the cooling field. This shows that the spins near the interface are antiferromagnetically coupled, which agrees with the resonant soft x-ray result. Pinned spins extend into both the Py and CoO region about 1.5 nm each side. The ratio between the pinned spins to the total spins at the interfacial region is about 10%.

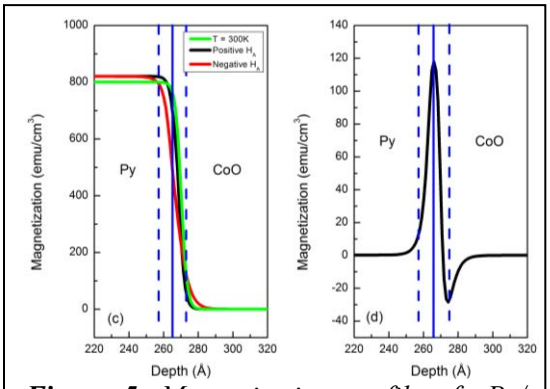

Figure 5*: Magnetization profile of Py/ (111) CoO film at 300K (green) and in the exchange biased state for positive and negative applied fields; right hand figure shows pinned moment profile.*

The same analysis procedure was applied to the (111) epitaxial film. The fitted magnetization profile at 5K is shown in Fig. 5. The magnetization profile shows that unlike the polycrystalline sample, the variation is confined in the chemical interfacial region. The pinned moments are localized in the interfacial region, parallel to the cooling field near the Py side and antiparallel at the CoO side. The net pinned moments per unit area is about +7.6 X 10^{-6} emu/cm^2. The result shows that although the exchange bias is much weaker in an (111) epitaxial film compare to the polycrystalline bilayer, the amount of the pinned moments is greater. Instead the distribution of pinned spins is very different. In the polycrystalline film, the pinned moments extends into both Py and CoO region as well as the chemical interface. In the (111) epitaxial film, the pinned moments are located at the structural interface and no significant moments are found in Py and CoO region. The result also shows that the origin of the pinned and unpinned moments is highly related to the magnetic structure at the unbiased state. In the (111) epitaxial film, we found there are interfacial spins above the Néel temperature within the structural roughness at the interface, and the pinned spins are located at the same region. These results show that the details of the exchange bias in this system depend on a magnetization structure at the interface that is complex and dependent on the crystalline structure of the interface.

1. Bader, S.D., *Colloquium: Opportunities in nanomagnetism.* Reviews of Modern Physics, **78**, 1-15, (2006).
2. Chappert, C., A. Fert, and F.N.V. Dau, *The emergence of spin electronics in data storage.* Nat. Mat., **6**, 813, (2007).
3. Moser, A., K. Takano, D.T. Margulies, M. Albrecht, Y. Sonobe, Y. Ikeda, S.H. Sun, and E.E. Fullerton, *Magnetic recording: advancing into the future.* Journal of Physics D-Applied Physics, **35**, R157-R167, (2002).
4. Gallagher, W.J. and S.S.P. Parkin, *Development of the magnetic tunnel junction MRAM at IBM: From first junctions to a 16-Mb MRAM demonstrator chip.* IBM J. Res. and Dev, **50**, 5, (2006).
5. Engel, B.N., J. Akerman, B. Butcher, R.W. Dave, M. DeHerrera, M. Durlam, G. Grynkewich, J. Janesky, S.V. Pietambaram, N.D. Rizzo, J.M. Slaughter, K. Smith, J.J. Sun, and S. Tehrani, *A 4-Mb toggle MRAM based on a novel bit and switching method.* IEEE Trans. Mag., **41**, 132, (2005).
6. Srajer, G., L.H. Lewis, S.D. Bader, A.J. Epstein, C.S. Fadley, E.E. Fullerton, A. Hoffmann, J.B. Kortright, K.M. Krishnan, S.A. Majetich, T.S. Rahman, C.A. Ross, M.B. Salamon, I.K. Schuller, T.C. Schulthess, and J.Z. Sun, *Advances in nanomagnetism via X-ray techniques.* Journal of Magnetism and Magnetic Materials, **307**, 1-31, (2006).
7. Fitzsimmons, M.R., S.D. Bader, J.A. Borchers, G.P. Felcher, J.K. Furdyna, A. Hoffmann, J.B. Kortright, I.K. Schuller, T.C. Schulthess, S.K. Sinha, M.F. Toney, D. Weller, and S. Wolf, *Neutron scattering studies of nanomagnetism and artificially structured materials.* Journal of Magnetism and Magnetic Materials, **271**, 103-146, (2004).

Phase Competition in Interfacial Materials: Magnetic Heterostructures

S.G.E. te Velthuis (tevelthuis@anl.gov), Yaohua Liu,
Materials Science Division, Argonne National Laboratory, Argonne, IL 60439

Cristina Visani, Norbert Nemes, Jacobo Santamaria
Facultad de Fisica, Universidad Complutense, 28040, Madrid, Spain

Research Scope

The artificial layering of thin films is a pathway for creating new materials with modified macroscopic properties compared to those of the individual constituents. The properties of the created heterostructures can be profoundly modified due to strain, surface and finite size effects, chemical intermixing, and, most interestingly, interactions or phase competition between competing ground states (e.g. ferromagnetism, antiferromagnetism, superconductivity, ferroelectricity) in adjacent layers. These modifications can be of great interest as new phenomena can occur as a result. In all cases, understanding the macroscopic phenomena and relating them to the physical properties requires detailed knowledge of the magnetic, electronic, and chemical structure within the layers and especially close to these interfaces. We use polarized neutron reflectometry and scattering at grazing incidence, complemented with neutron diffraction, x-ray magnetic circular dichroism techniques, and MOKE Kerr Microscopy, to probe the magnetic structure within each layer of the film, at interfaces, and within individual magnetic domains, and thereby obtain insight into the underlying phase competition.

Recent Progress

Interactions at Ferromagnetic/Superconducting Interfaces

The study of phase competition between ferromagnetism(FM) and superconductivity(S), especially in trilayers[1-4], remains a very vital field of research as many open questions remain. For example, there has been an ongoing debate regarding the origin of the *inverse* superconducting spin switch behavior, as has been observed in superconducting cuprate / ferromagnetic manganite spin valves [5]. While theory predicts that the superconducting transition temperature T_C should be lower for parallel alignment of the magnetization of the two ferromagnetic layers of the spin valve than for anti-parallel alignment [2, 3], the opposite behavior is observed in $La_{0.7}Ca_{0.3}MnO_3$(LCMO)/$YBa_2Cu_3O_{7-\delta}$ (YBCO)/$La_{0.7}Ca_{0.3}MnO_3$ trilayers. In the past we have characterized the magnetic properties of the LCMO layers and determined differences in magnetization and anisotropy of the two nominally identical layers, and have attributed these differences to differences in strain. With X-ray Magnetic Circular Dichoism (XMCD) experiments we have confirmed the presence of an interfacial Cu spin polarization for our samples, as previously reported by J. Chakhalian *et al.* [6, 7] and concluded to be the result of electronic reconstruction at the interface. This net interfacial Cu spin polarization has been shown to accompany an extended exchange field beyond the interface in YBCO layer [8]. Most recently we have proven that, contrary to several accepted theoretical scenarios, the relative orientation between the two LCMO's magnetizations is not sufficient to determine the magnetoresistance. Our Polarized Neutron Reflectometry (PNR) measurements tracked the direction of the magnetization of the two LCMO layers as a moderate magnetic field was rotated

in-plane at the superconducting transition temperature. Comparison of the determined magnetic configurations to the resistance showed that the direction of the magnetization of the bottom LCMO layer correlated with the resistance. Therefore, the field dependence of the magnetoresistance is explained by the interplay between the applied magnetic field and the (exponential tail of the) induced exchange field in YBCO.

Complex Oxide Magnetic Tunnel Junctions

Due to the high degree of spin polarization of the conduction band of manganites, it is expected that magnetic tunnel junctions (MTJs) based on manganites will yield large tunneling magnetoresistance (TMR), which is advantageous for spintronic and magnetic recording applications. To explore this possibility, we are studying $La_{0.7}Ca_{0.3}MnO_3$ /$PrBa_2Cu_3O_7$(PBCO)/$La_{0.7}Ca_{0.3}MnO_3$ magnetic tunnel junctions grown on $SrTiO_3$. We have obtained a better understanding of the temperature dependent TMR behavior observed in this system [9] by mapping out the magnetic behavior of the ferromagnetic LCMO layers by combined studies of PNR, x-ray absorption with polarization analysis, SQUID magentometry and magneto-transport. By studying the magnetization reversal we have discovered differences in the anisotropy direction and strength of the two LCMO layers, which also change with temperature. Similarly to what was observed for the YBCO/LCMO system, with XMCD we have found a non-zero net magnetic moment on the Cu of PBCO that varies with temperature in the same way as the adjacent LCMO magnetization. Hysteresis loops measured at the Cu L-edge show a two-step behavior of this moment that is correlated to the two separate coercive fields of the top and bottom LCMO layers, indicating the interfacial origin and the direct link to the adjacent LCMO. Effectively the induced moment in the PBCO creates a double spin filter [10], and thereby modifies the TMR.

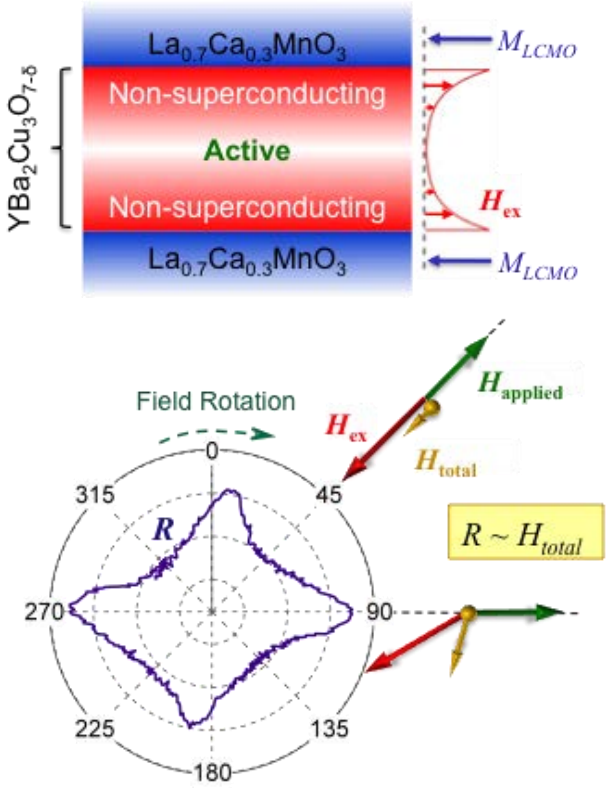

Figure 1. Top) Schematic of the sample. On the right the direction of the magnetization in the LCMO layers (M_{LCMO}) and interface-induced exchange field (H_{ex}) within the superconductor is indicated. Bottom) The resistance measured for a rotating field of 150 Oe at 26K after having applied a saturating field. The arrows schematically indicate how the total field (H_{total}) acting on the superconducting layer is a combination of the applied field ($H_{applied}$) and H_{ex}, taken to be anti-parallel to the magnetization of the bottom LCMO layer. The two extreme conditions are represented to show the correlation of the resistance with H_{total}.

Engineered Interfaces

We have studied $La_{0.67}Sr_{0.33}MnO_3$/$SrTiO_3$(STO) superlattices with PNR to explore the idea that by using engineered interfaces, the magnetic properties can be improved provided an electronic reconstruction at the interface can be tuned by slightly modifying the electronic doping at the interface via compositional changes. Electronic reconstruction at the interface between insulating non-magnetic oxides has been shown to give rise to a highly conductive interface, as well as magnetism and is driven by the potential build-up at the interface, i.e. a polar discontinuity,

which occurs when there are different valence states on either side of the interface. This work is in collaboration with Gertjan Koster (University of Twente, The Netherlands). Magnetometry data indicates that a higher overall magnetization can be obtained by inserting a monolayer of $La_{0.33}Sr_{0.67}MnO_3$ which has an intermediate net charge and should suppress the potential build-up. Conductivity is also improved. If the increased magnetization occurs within this interfacial layer, it would imply that electronic reconstruction at the interface can be controlled by engineering the interface appropriately. Instead, our PNR data indicate there is a change in the interfacial roughness, which can explain the change in observed magnetization.

Future Plans

The majority of our program will focus on studies of magnetic complex oxide superlattices. The broad range of properties that these oxides can have, (e.g., ferromagnetism, antiferromagnetism, superconductivity, ferroelectricity), some of which can be varied by doping, enable us to study the competition between many different ordering parameters within epitaxial superlattices.

Ferromagnetic vs Charge-Orbital Ordering

In perovskite manganites the competition between the ferromagnetism and the charge-orbital (CO) ordering causes phase separation that can be controlled by magnetic fields. By using artificial multilayers rather than bulk materials it is possible to precisely and systematically control the real-space boundaries between the FM-metallic phase and CO-insulating phase, which has not been possible in bulk compounds. In collaboration with Dr. M. Nakamura and Dr. D. Okuyama (Y. Tokura group, Advanced Science Institute, RIKEN, Japan) we will study $Pr_{0.5}Ca_{0.5}MnO_3$ (PCMO)/$La_{0.5}Sr_{0.5}MnO_3$ (LSMO) superlattices fabricated on (011)-oriented LSAT ($(LaAlO_3)_{0.3}(SrAl_{0.5}Ta_{0.5}O_3)_{0.7}$) substrates. Nakamura *et al.*[11] have shown temperature and magnetic field dependences of the total magnetization in this system that indeed indicate changing fractions of the FM and CO phases, presumably centered on the LSMO and PCMO layers, respectively. PNR will allow us to directly determine the location and thickness of FM ordered phase regions. The correlation between the size of the FM regions and CMR is an outstanding issue in bulk materials. Besides the fundamental interest, these superlattices can be used to form magnetic tunnel junctions with a magnetic-field sensitive barrier, resulting in a tunable TMR.

Multiferroic Complex Oxides

We have started to investigate the interfacial magnetism in a range of multiferroic perovskite-oxide heterostructures, including ferromagnetic-ferroelectric $La_{0.7}Sr_{0.3}MnO_3/BaTiO_3$. From XMCD studies we find that there is an induced spin polarizations on the Ti ions. Therefore, the modification of the spin structure may be ubiquitous at the interfaces between transition metal oxides. Building on these results we will further investigate this systems. Beside the novelty of observing a moment on Ti in $BaTiO_3$, we have indications that this moment plays a role in the transport characteristics of magnetic tunnel junctions based on this system. Peak features in differential conductance curves measured on junctions suggest there is resonant transport through barrier states. Because the peak features depend on the magnetic configuration (parallel or antiparallel alignment of the $La_{0.7}Sr_{0.3}MnO_3$ layers) it is possible that these resonant states are related to the magnetic moment on Ti and the exchange coupling with $La_{0.7}Sr_{0.3}MnO_3$. Full understanding of this behavior warrants further study of the magnetic properties, as can be obtained with XMCD and PNR.

References

[1] A. Buzdin, Rev. Mod. Phys. **77**, 935 (2005).
[2] L. Tagirov, Phys. Rev. Lett. **83**, 2058 (1999).
[3] A. Buzdin, *et al*., Europhys. Lett. **48**, 686 (1999).
[4] F. Bergeret *et al*., Rev. Mod. Phys. **77**, 1321 (2005).
[5] V. Peña *et al*., Phys. Rev. Lett. **94**, 057002 (2005).
[6] J. Chakhalian *et al*., Nature Physics **2**, 244 (2006).
[7] J. Chakhalian *et al*., Science **318**, 1114 (2007).
[8] J. Salafranca and S. Okamoto, Phys. Rev. Lett. **105**, 256804 (2010).
[9] Z. Sefrioui *et al*., Appl. Phys. Lett. **88**, 022512 (2006).
[10] G-X Miao *et al.*, Phys. Rev. Lett. **102**, 076601 (2009).
[11] M. Nakamura *et al.*, Adv. Mater. **22**, 500 (2010).

Publications (July 2010-2012)

1. *Magnetic memory based on $La_{0.7}Ca_{0.3}MnO_3/YBa_2Cu_3O_7/La_{0.7}Ca_{0.3}MnO_3$ ferromagnet/ superconductor hybrid structures*
   N. M. Nemes, C. Visani, C. Leon, M. Garcia-Hernandez, F. Simon, T. Fehér, S. G. E. te Velthuis, A. Hoffmann, J. Santamaria
   Appl. Phys. Lett. **97**, 032501 (2010).
2. *Application of Polarized Neutron Reflectometry and X-Ray Resonant Magnetic Reflectometry for Determining the Inhomogeneous Magnetic Structure in Fe/Gd Multilayers*
   E. A. Kravtsov, D. Haskel, S. G. E. te Velthuis, J. S. Jiang, and B. J. Kirby
   Izvestiya Rossiiskoi Akademii Nauk. Seriya Fizicheskaya **74**, 1531 (2010).
   Bulletin of the Russian Academy of Sciences: Physics **74**, 1471 (2010).
3. *Magnetic Structure in Fe/Sm-Co Exchange Spring Bilayers with Intermixed Interfaces*
   Yaohua Liu, S.G.E. te Velthuis, J.S. Jiang, Y. Choi, S.D. Bader, A.A. Parizzi, H. Ambaye, and V. Lauter
   Phys. Rev. B **83**, 174418 (2011).
4. *Symmetric interfacial reconstruction and magnetism in $La_{0.7}Ca_{0.3}MnO_3/YBa_2Cu_3O_7/La_{0.7}Ca_{0.3}MnO_3$ heterostructures*
   C. Visani, J. Tornos, N. M. Nemes, M. Rocci, C. Leon, J. Santamaria, S. G. E. te Velthuis, Yaohua Liu, A. Hoffmann, J. W. Freeland, M. Garcia-Hernandez, M.R. Fitzsimmons, B.J. Kirby, M. Varela, S. J. Pennycook
   Phys. Rev. B **84**, 060405(R) (2011).
5. *Delta Doping of Ferromagnetism in Antiferromagnetic Manganite Superlattices*
   T.S. Santos, B.J. Kirby, S. Kumar, S.J. May, J.A. Borchers, B.B. Maranville, J. Zarestky, S. G. E. te Velthuis, J. van den Brink, and A. Bhattacharya
   Phys. Rev. Lett. **107**, 167202 (2011).
6. *Effect of Interface-Induced Exchange Fields on Cuprate-Manganite Spin Switches*
   Yaohua Liu, C. Visani, N. M. Nemes, M. R. Fitzsimmons, L. Y. Zhu, J. Tornos, M. Garcia-Hernandez, M. Zhernenkov, A. Hoffmann, C. Leon, J. Santamaria, and S. G. E. te Velthuis
   Phys. Rev. Lett. **108**, 207205 (2012).

Neutron and Ellipsometry Studies of Multiferroics: Magnetic Structure, Excitations, and Hybrid Modes.

S-W. Cheong (sangc@physics.rutgers.edu), V. Kiryukhin
Rutgers Center for Emergent Materials and Department of Physics and Astronomy, Rutgers University, Piscataway, NJ 08854

A. Sirenko, T. Zhou
Department of Physics, New Jersey Institute of Technology, Newark, NJ 07102

Research Scope

Multiferroics are materials that possess both ferroelectric and (anti-)ferromagnetic orderings. Until recently, only a small number of single-phase multiferroics were known, and the observed magnetoelectric effects were mostly linear and small. Recent discoveries of novel oxide multiferroics (*e.g*. Tb(Dy)MnO_3 and Tb(Dy)Mn_2O_5) with highly-non-linear and large magnetoelectric effects have resulted in a spectacular progress in this field. Giant magnetoelectric effects, such as the flipping of electric polarization, huge change of dielectric constant with applied magnetic fields, or large magnetization change induced by applying electric fields, have been reported. These effects open up entirely new ways of phase control with potential for device applications in many areas, such as transducers, field sensors, data recording, *etc*. Giant magnetoelectric effects are closely associated with the collective nature of simultaneous magnetic and ferroelectric phase transitions. This Project aims to reveal the features of the magnetic structure and the corresponding magnetic and lattice excitations underlying the giant effects associated with these transitions. For this goal, a complementary combination of neutron scattering and far IR ellipsometry, together with closely coordinated crystal growth activities, are used.

Among the topics of this Project are studies of the magnetoelectric properties of $BiFeO_3$ (BFO), which is the only known room-temperature multiferroic with recognized potential for applications. Another compound family under investigation is hexagonal $R MnO_3$ (R=Eb-Lu) that exhibit strong signature of the magnetoelectric coupling in their excitation spectra.

Recent Progress

Spin Waves in $BiFeO_3$. BFO is, arguably, the most important multiferroic material because it is the only known room-temperature ferroelectric (FE) with strong coupling between the magnetic and FE orders. It is, so far, the only candidate multiferroic single-phase system for potential applications, such as information storage, photovoltaics, and spintronic devices. While this compound is known since the 1950's, the magnetic interactions between the Fe magnetic moments have not been so far determined in a direct experiment. We have, for the first time, investigated spin waves in single-crystalline BFO over the full Brillouin zone using inelastic neutron scattering (Figure 1), and determined the microscopic magnetic interactions, including the nearest- and next-nearest-neighbor exchange, and the Dzyaloshinskii-Moriya term.[1] The experiments were made possible by the breakthrough in the synthesis of large single crystals. This work provides a fundamental ingredient needed for understanding any of the magnetic properties of BFO.

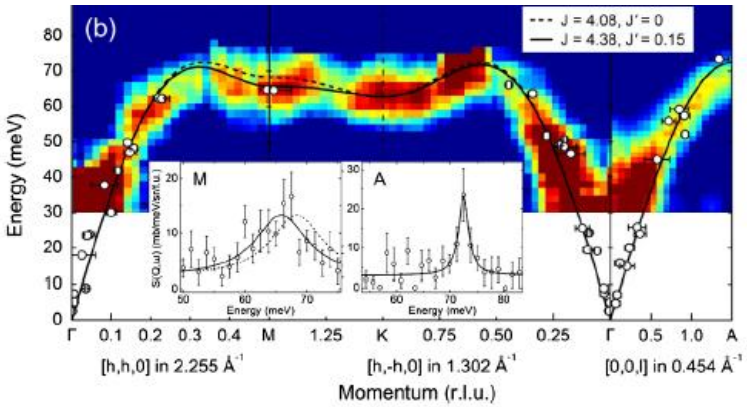

Figure 1. Spin waves in BFO. Solid lines show theoretical fits with nearest neighbor interaction J=4.38 meV, and next-nearest neighbor interaction J'=0.15 meV. Insets are momentum cuts at the M and A points of the Brillouin zone.[1]

Local weak ferromagnetism in BFO. For prospective applications, a multiferroic material should ideally exhibit large FE polarization coupled to ferromagnetic (FM) order at room temperature. Long ago, it has been predicted theoretically that BFO would possess the weak FM order if the long-range cycloidal modulation of its antiferromagnetic structure were absent. The FM order, however, is preserved locally. We have, for the first time, detected [2] this local ferromagnetism in single-crystalline BFO using small-angle neutron scattering, see Figure 2. Importantly, the observed magnitude of the FM moment is in the upper range of the theoretical predictions. This result is of high importance for future applied work on BFO thin films, in which the cycloidal modulation is suppressed. Presence of weak ferromagnetism in such films has so far been highly controversial. Our results show that synthesis of functional BFO films combining coupled FM and FE orders is highly probable, and provide a useful estimate for the magnitude of the expected ferromagnetic moment.

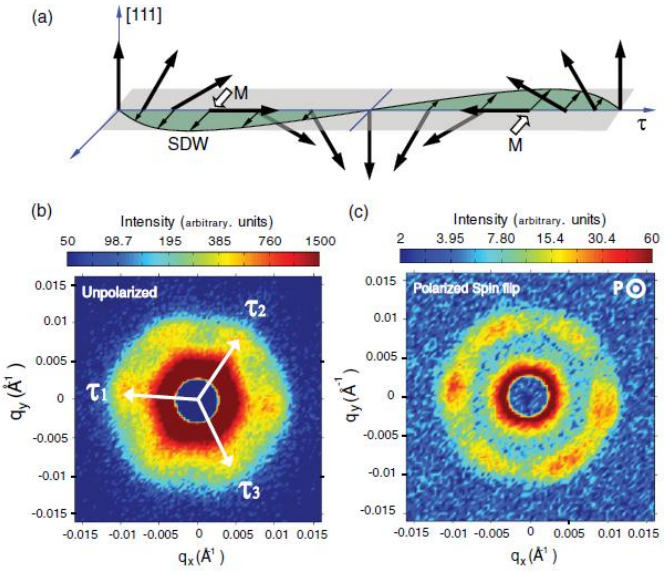

Figure 2. The SDW (thin arrows) produced by the tilt of the Fe spins out of the plane of the magnetic cycloid (thick arrows) in BFO. The amplitude of the SDW is exaggerated. Only a few representative spins are shown. Open arrows show local magnetization due to the SDW. (b) and (c): Images of the diffraction pattern in the (111) scattering plane with (b) unpolarized neutrons, (c) neutrons polarized with P|| k beam that scatter with spin flip.[2]

Magnons and crystal field transitions in hexagonal $RMnO_3$. Far-infrared optical transmission, reflection, and ellipsometry techniques have been used to study spectra of the antiferromagnetic resonances, or magnons, optical phonons, and crystal field transitions (CF) in hexagonal $R\mathrm{MnO_3}$ (R = Er, Tm, Yb, Lu) single crystals[3], see Figure 3. The magnon and CF frequencies, their oscillator strengths, and effective g-factors have been measured using external magnetic fields H

up to 9 T in the temperature range between 1.5 K and 100 K. The observed magnon frequencies increase systematically with the decrease of the *RE* ionic radius between Ho and Lu. The measured magnon frequencies allowed us to determine the product of exchange and anisotropy parameters J·D. At low temperatures below ~30 K the Mn-*R* interaction changes both the magnon *g*-factors and the magnon frequencies. Both trends are explained qualitatively by the changes of *R* magnetization with temperature and magnetic field: *M(H,T)~H/T*. Our data provide important input for understanding magnetoelectric excitations in these model compounds.

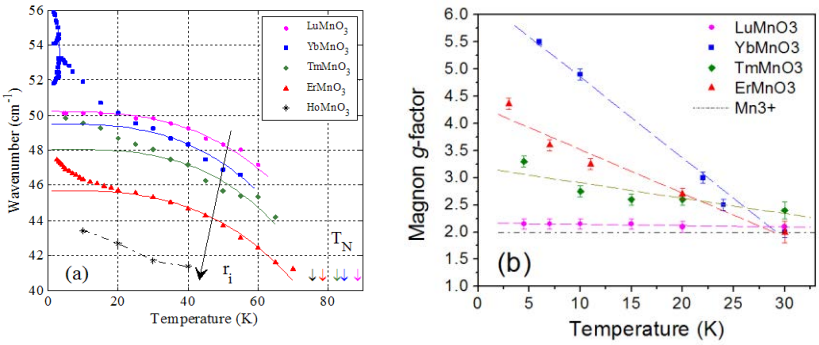

Figure 3. (a) Temperature dependence of the magnon frequency for five RMnO$_3$ samples at zero magnetic field. Solid curves for Lu, Yb, Tm, and Er samples show the fit results using $\Omega_M(0)-\Omega_M(T)\sim T^3$. The arrow labeled r_i indicates the increase of the *RE* ionic radius and the corresponding decrease of both, magnon frequency and T_N. At low temperatures, a single magnon in YbMnO$_3$ splits into several distinct absorption lines due to ordering of Yb spins at T=3.3 K. (b) Temperature dependence of the magnon g factor for RMnO$_3$. The horizontal line corresponds to the theoretical expectation for g factor of Mn3+: g_{Mn}=2. At higher temperatures above $T \approx 30 \pm 5$K, the magnon g factors approach g_{Mn}=2 in all RMnO$_3$. At low temperatures the magnon g-factors are enhanced due to R^{3+} magnetization.[3]

Future Plans

Detailed studies of the character (magnetic, electric, hybrid) of the excitations in the materials described above will be carried out. This will be achieved using polarized neutron scattering and far-IR ellipsometry (Muller matrix analysis). Several specific low-energy modes in BFO were predicted to be hybrid, and evidence exists for the hybrid character of certain magnon modes in hexagonal RMnO$_3$. These, as well as several other multiferroic materials, will be subject of further studies.

Publications (2010-2012)

[1] Spin Wave Measurements over the Full Brillouin Zone of Multiferroic BiFeO3 Jaehong Jeong, E. A. Goremychkin, T. Guidi, K. Nakajima, Gun Sang Jeon, Shin-Ae Kim, S. Furukawa, Yong Baek Kim, Seongsu Lee, V. Kiryukhin, S-W. Cheong, and Je-Geun Park, PRL 108, 077202 (2012).

[2] Local Weak Ferromagnetism in Single-Crystalline Ferroelectric BiFeO3 M. Ramazanoglu, M. Laver, W. Ratcliff, S. M. Watson, W. C. Chen, A. Jackson, K. Kothapalli, Seongsu Lee, S.-W. Cheong, and V. Kiryukhin, PRL 107, 207206 (2011).

[3] Magnons and crystal field transitions in hexagonal RMnO$_3$ (R = Er, Tm, Yb, Lu) *s*ingle crystals, E. C. Standard, T. Stanislavchuk, and A. A. Sirenko, N. Lee, and S.-W. Cheong, Phys. Rev. B **85**, 144422 (2012).

[4] Magnetic Excitations in the Low-Temperature Ferroelectric Phase of Multiferroic YMn2O5, J.-H. Kim, M. A. van der Vegte, A. Scaramucci, S. Artyukhin, J.-H. Chung, S. Park, S-W. Cheong, M. Mostovoy, and S.-H. Lee, PRL 107, 097401 (2011).
[5] Coupled Magnetic Cycloids in Multiferroic TbMnO3 and Eu3/4Y1/4MnO3, Hoyoung Jang, J.-S. Lee, K.-T. Ko, W.-S. Noh, T.Y. Koo, J.-Y. Kim, K.-B. Lee, J.-H. Park, C. L. Zhang, Sung Baek Kim, and S.-W. Cheong, PRL 106, 047203 (2011).
[6] Optical anisotropy and charge-transfer transition energies in BiFeO3 from 1.0 to 5.5 eV, S. G. Choi, H. T. Yi, S.-W. Cheong, J. N. Hilfiker, R. France, and A. G. Norman, PHYSICAL REVIEW B 83, 100101(R) (2011).
[7] Strong magnetoelastic effect on the magnetoelectric phenomena of TbMn2O5, Yoon Seok Oh, Byung-Gu Jeon, S. Y. Haam, S. Park, V. F. Correa, A. H. Lacerda, S.-W. Cheong, Gun Sang Jeon, and Kee Hoon Kim, PHYSICAL REVIEW B 83, 060405(R) (2011).
[8] Long-wavelength magnetic and magnetoelectric excitations in the ferroelectric antiferromagnet BiFeO3, D. Talbayev, S. A. Trugman, Seongsu Lee, Hee Taek Yi, S.-W. Cheong, and A. J. Taylor, PHYSICAL REVIEW B 83, 094403 (2011)
[9] Magnetic structure and electric field effects in multiferroic YMn2O5, R. A. de Souza, U. Staub, V. Scagnoli, M. Garganourakis, Y. Bodenthin, S.-W. Huang, M. Garc´ıa-Fern´andez, S. Ji, S.-H. Lee, S. Park, and S.-W. Cheong, PHYSICAL REVIEW B 84, 104416 (2011)
[10] High-pressure structural stability of multiferroic hexagonal *R*MnO3 (*R* = Y, Ho, Lu), P. Gao, Z. Chen, T. A. Tyson, T. Wu, K. H. Ahn, Z. Liu, R. Tappero, S. B. Kim, and S.-W. Cheong, PHYSICAL REVIEW B 83, 224113 (2011).
[11] Adjusted oscillator strength matching for hybrid magnetic and electric excitations in Dy3Fe5O12 garnet, P. D. Rogers, Y. J. Choi, E. C. Standard, T. D. Kang, K. H. Ahn, A. Dubroka, P. Marsik, C. Wang, C. Bernhard, S. Park, S-W. Cheong, M. Kotelyanskii, and A. A. Sirenko, Phys. Rev. B 83, 174407 (2011).
[12] Multiferroics: Past, present, and future, N. A. Spaldin, S-W. Cheong, R. Ramesh, Physics Today, 63, 38-43 (2010).
[13] Coupling between magnon and ligand-field excitations in magnetoelectric Tb3Fe5O12 garnet, T. D. Kang, E. Standard, K. H. Ahn, and A. A. Sirenko, G. L. Carr, S. Park, Y. J. Choi, M. Ramazanoglu, V. Kiryukhin, and S-W. Cheong, Phys. Rev. B **82**, 014414 (2010).
[14] Magnetic excitations and optical transitions in the multiferroic spin-1/2 system LiCu2O2, D. Hüvonen, U. Nagel, T. Rõõm, Y. J. Choi, C. L. Zhang, S. Park, and S.-W. Cheong, Phys. Rev. B **80**, 100402R (2009).
[15] Polar atomic displacements in multiferroics observed via anomalous x-ray diffraction, C. Azimonte, E. Granado, H. Terashita, S. Park, and S-W. Cheong, Phys. Rev. B **81**, 012103 (2010).
[16] Observation of anomalous phonons in orthorhombic rare-earth manganites, P. Gao, H. Y. Chen, T. A. Tyson,_ Z. X. Liu, J. M. Bai, L. P. Wang, Y. J. Choi, and S.-W. Cheong, Appl. Phys. Lett. **97**, 262905 (2010).
[17] Surface reconstruction of hexagonal Y-doped HoMnO3 and LuMnO3 studied using low-energy electron diffraction, R. Vasić, J. T. Sadowski, Y. J. Choi, H. D. Zhou, C. R. Wiebe, S. W. Cheong, J. E. Rowe, and M. D. Ulrich, Phys. Rev. Lett. **81**, 165417 (2010).
[18] Enhanced magnetic refrigeration capacity in phase separated manganites, L. Lima Sharma, P. A. Sharma, S. K. McCall, S.-B. Kim, and S.-W. Choeng, Appl. Phys. Lett. **95**, 092506 (2009).
[19] Crystal field excitations in the Raman spectra of FeSe1-x, Z. Qin, C. Zhang, S. O'Malley, K. Lo, T. Zhou, and S.-W. Cheong, Sol. Stat. Commun. **15**0, 768 (2010).
[20] Temperature-dependent local structure of LaFeAsO1−xFx: Probing the atomic correlations, T. A. Tyson, T. Wu, J. C. Woicik, B. Ravel, A. Ignatov, C. L. Zhang, T. Zhou, and S.-W. Cheong, J Appl. Phys. **108**, 123715 (2010).

Session VIII

Advanced Capabilities (II)

Polarized ^{3}He in Neutron Scattering

W.M. Snow (wsnow@indiana.edu), H. Yan
Center for the Exploration of Energy and Matter, Indiana University, 2401 Milo B. Sampson Lane, Bloomington, IN 47408

T.R. Gentile (thomas.gentile@nist.gov), Q. Ye
Stop 8461, NIST, Gaithersburg, MD 20899

Z. DeLand, B. Lancor, T.G. Walker
Dept. of Physics, University of Wisconsin, Madison, WI 53706

G.L. Jones
Physics Dept., Hamilton College, Clinton, NY 13323

Program scope

The goal of this program is to extend the technique of polarized neutron scattering into new domains by the development and application of polarized ^{3}He spin filters. This program is carried out by a collaboration that includes Indiana University, the National Institute of Standards and Technology (NIST), Hamilton College, and the Univ. of Wisconsin, along with collaborators at the Spallation Neutron Source (SNS) and the Indiana Low Energy Neutron Source (LENS). Our primary current goals include the application of polarized ^{3}He-based neutron spin filters to a spin echo small angle neutron scattering spectrometer (SESAME) and wide-angle polarization analysis. Spin-exchange optical pumping is employed to construct these spin filters. In this method, alkali vapor is polarized by optical pumping and the polarization is transferred to the ^{3}He nuclei during collisions. We have made significant progress in understanding the basic physics of SEOP. Built upon our past research and development, both the NCNR and the SNS have established spin filter programs. Connections between all of these ^{3}He spin filter programs is strong, with the interaction contributing to the development of technology and applications at all laboratories.

Recent progress

Indiana collaborated with Tony Tong at the SNS on cell development to help realize a ^{3}He polarizer on the powder diffractometer HB2A at the High Flux Isotope Reactor (HFIR). Indiana also contributed compressed air valve technology to the SNS for the ^{3}He polarization analyzer under development for the Hybrid Spectrometer (HYSPEC), which aims to employ SEOP combined with ^{3}He gas circulation and is a potential template for wide-angle polarization analysis at the SNS. We also worked toward implementation of a SEOP analyzer for the SESAME spin echo spectrometer at LENS. Postdoc Haiyang Yan assembled the system and performed electron paramagnetic resonance (EPR) measurements to estimate the ^{3}He polarization using a 1.1 bar, 7 cm long, 6.5 cm ID Rb/K SEOP cell made by SNS postdoc Peter Jiang. The ^{3}He polarization estimated in off-line tests from EPR measurements is 70%. We operated the SEOP system on the SESAME beamline at LENS and measured the ^{3}He cell transmission in August 2011.

At Wisconsin, we have concluded our direct experimental studies of circular dichroism and its effects on anomalous light consumption in SEOP cells. This included a measurement of

the potassium absorption cross section at the Rb optical pumping wavelength of 795 nm. This is a critical parameter for hybrid Rb/K spin-exchange optical pumping. Brian Lancor, who graduated in August 2011, incorporated all the new information we have obtained about circular dichroism into a comprehensive Mathematica model of the SEOP process. Last fall, he also incorporated our best understanding of the role of light-induced heating into the model. Thus we now have a model that to the best of our ability incorporates all the known physics of spin-exchange optical pumping. It is our intention to make this model publicly available via a server hosted at the UW Physics department. To further test the model, Zach DeLand has been making measurements of optical pumping wavefront velocities under SEOP conditions. Due to the great optical thickness of SEOP cells, under transient conditions the wavefronts can move quite slowly, meters/sec. We have developed a new method for making such measurements using AC magnetic fields instead of DC for the SEOP bias magnetic fields. Data is being obtained using this method and we are working on understanding how to interpret the results in terms of the SEOP model.

Hamilton's efforts have been divided between developing a fast, user friendly EPR system for diagnostic use at Indiana, NIST and the SNS, and gearing up to make measurements to understand the origin of the additional relaxation that currently limits the achievable ^{3}He polarization.

At NIST, we have focused on wide-angle polarization analysis. Just before the NCNR shutdown (4/11 to 4/12), an apparatus for wide-angle analysis was employed for the first experiment on the Multi-Axis Crystal Spectrometer (MACS). This apparatus consists of a large static field solenoid, a polarizer cell, one or two analyzer cells that can cover a total angular range of 240 degrees, a shielded radio frequency solenoid so that the polarization in the polarizer cell can be inverted without perturbing the analyzer cell, and an NMR method for monitoring the polarization in each cell. A key issue for this development is the analyzer cells. As of this first application we had not achieved high polarization in the quartz cells we had been pursuing, hence conventional blown cylindrical cells with restricted angular range were used. For the particular sample under study, FeSeTe, this restricted range was acceptable. In general the entire apparatus worked well.

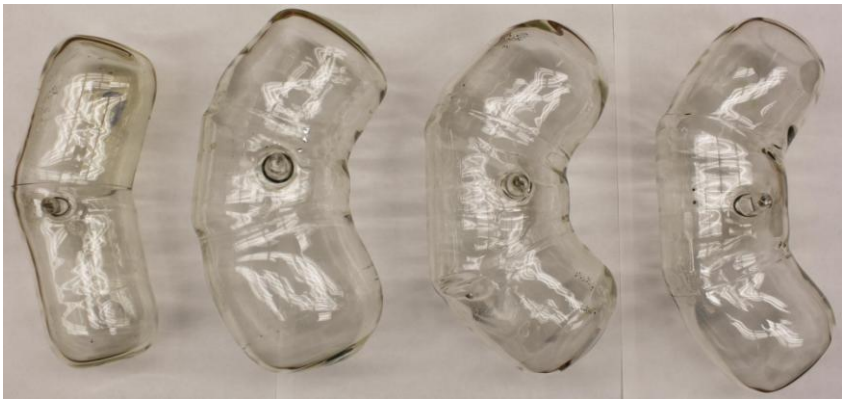

Fig. 1. SEOP spin filter cells for wide-angle polarization analysis.

We have recently succeeded in fabricating wide-angle cells from the boron-free, aluminosilicate glass (GE180) that has the best properties for SEOP-based spin filters. We have prepared four analyzer cells; three examples are shown in the figure along with an earlier

prototype cell. The relaxation times range from 100 to 200 hours. We have used both neutron transmission and EPR to determine that the achievable polarization in these cells is typically 75%. These results represent a significant improvement over the previously employed fused quartz cells, which only reached 45%. We have constructed an improved neutron-compatible solenoid so that the relaxation times of our cells will not be compromised. For NMR-based inversion of the ^{3}He polarization in the polarizer cell, we have reduced the polarization losses in both the polarizer and analyzer cells to < 0.1%. Finally we have conducted studies to better understand the limited polarization in quartz cells.

Future plans

Indiana intends to implement polarized ^{3}He on the SESAME spectrometer at LENS. The SESAME optical elements underwent a successful final tuning test at the Los Alamos Neutron Science Center (LANSCE) in late 2011 and have been reassembled at LENS. We plan to measure spin echo using the SEOP ^{3}He analyzer shortly after spin echo signals are observed on SESAME at LENS.

At Wisconsin, we are proceeding with upgrades to our apparatus to allow us to study larger cells as now commonly used in neutron experiments. We hope to soon do a test of an extremely large cell produced at the SNS by Tony Tong. Since the temperature-dependent relaxation (denoted by X) that limits the ^{3}He polarization is a surface phenomenon, it might be possible to circumvent it by the brute force method of polarizing much larger cells. We are also finalizing the ^{3}He SEOP model for public use by other researchers.

The primary goal at NIST is more extensive development and practice of wide-angle polarization analysis. Our apparatus will be employed sometime during MACS commissioning in early 2013. In addition, we will collaborate with the SNS on developing wide-angle analysis for a greater range of instruments.

2010 - 2012 Publications

1. *Method for deducing anisotropic spin-exchange rates*
   T.G. Walker, I.A. Nelson, S. Kadlecek
   Phys. Rev. A **81**, 032709 (2010)
2. *Breakdown of angular momentum selection rules in high pressure optical pumping experiments*
   B. Lancor, E. Babcock. R. Wyllie, and T.G. Walker
   Phys. Rev. Lett. **105**, 083003 (2010).
3. *Effects of nitrogen quenching gas on spin-exchange optical pumping of ^{3}He*
   B. Lancor and T.G. Walker
   Phys. Rev. A **82**, 043417 (2010).
4. *Circular dichroism of RbHe and RbN_2 molecules*
   B. Lancor, E. Babcock. R. Wyllie, and T.G. Walker
   Phys. Rev. A **82**, 043435 (2010).
5. *In-situ polarized ^{3}He-based neutron polarization analyzer for SNS magnetism reflectometer*
   W.-T. Lee, X. Tong, J. Pierce, M. Fleenor, A Ismaili, J.L. Robertson, W.C. Chen, T.R. Gentile, A. Hailemariam, R. Goyette, A. Parizzi, V. Lauter, F. Klose, H. Kaiser,

C. Lavelle, D.V. Baxter, G.L. Jones, J. Wexler, and L. McCollum
Journal of Physics: Conference Series **251**, 012086 (2010).

6. *Measurement of parity-violating γ-ray asymmetry in the capture of polarized cold neutrons on protons*
M.T. Gericke *et al.* (NPDGamma collaboration)
Phys. Rev. C **83**, 015505 (2011).
7. *Limits on possible new monopole-dipole interactions from the spin relaxation rate of polarized ^{3}He gas*
C.B. Fu, T.R. Gentile, and W.M. Snow
Phys. Rev. D **83**, 031504(R) (2011).
8. *Constraints on monopole-dipole interactions of WISPs from polarized gas relaxation time*
C. Fu, T.R. Gentile and W.M. Snow
Proceedings of the Fifth Meeting on CPT and Lorenz symmetry, Bloomington, Indiana, USA, June 28 - July 2, 2010, edited by A. Kostelecky (World Scientific (2011)), p. 244.
9. *A wide-angle neutron spin filter system using polarized ^{3}He*
C.B. Fu, T.R. Gentile, G.L. Jones, W.C. Chen, R. Erwin, S. Watson, C. Broholm, J.A. Rodriguez-Rivera
J. Scherschligt, Physica B **406**, 2419-2423 (2011).
10. *Fundamentals of spin-exchange optical pumping*
T.G. Walker
Journal of Physics: Conference Series **294**, 012011 (2011).
11. *Effects of high intensity neutron flux on in-situ spin-exchange optical pumping of ^{3}He*
E. Babcock, S. Boag, C. Beecham, T.E. Chupp, T.R. Gentile, G.L. Jones, A. Petoukhov and T.G. Walker
Journal of Physics: Conference Series **294**, 012001 (2011).
12. *Polarized ^{3}He cell development and application at NIST*
W.C. Chen, T.R. Gentile, C.B. Fu, S. Watson, G.L. Jones, J.W. McIver, and D.R. Rich
Journal of Physics: Conference Series **294**, 012003 (2011).
13. *Polarization limits in K-Rb spin-exchange mixtures*
B. Lancor and T.G. Walker
Phys. Rev. A **83**, 065401 (2011).
14. *Friedel-like Oscillations from Interstitial Iron in Superconducting $Fe_{1+y}Te_{0.62}Se_{0.38}$*
V. Thampy, J. Kang, J.A. Rodriguez-Rivera, W. Bao, A.T. Savici, J. Hu, T.J. Liu, B. Qian, D. Fobes, Z.Q. Mao, C.B. Fu, W.C. Chen, Q. Ye, R.W. Erwin, T.R. Gentile, Z. Tesanovic, and C. Broholm
Phys. Rev. Lett. **108**, 107002 (2012).
15. *Search for spin-dependent short-range force between nucleons using optically polarized He-3 gas*
W. Zheng, H. Gao, B. Lairemruata, Y. Zhang, G. Laskaris, W.M. Snow and C.B. Fu
Phys, Rev. D **85**, 031505 (2012)
16. *Comment on "Pressure dependence of wall relaxation in polarized ^{3}He gaseous cell"*
B. Saam, A.K. Petukhov, J. Chastagnier, T.R. Gentile, R. Golub and C.M. Swank, Phys. Rev. A **85**, 047401 (2012).

Development of New Methods for Studying Nanostructures using Neutron Scattering

Roger Pynn

Indiana University, Department of Physics, Swain Hall West, 3rd Street, Bloomington, IN 47405
rpynn@indiana.edu

Program Scope: The goal of this project is to develop and apply a new interferometric neutron scattering technique that extends and complements traditional neutron scattering methods in the study of nanostructures. The new method, dubbed Spin Echo Scattering Angle Measurement (SESAME), directly provides a measurement of a spatial correlation function in real space, automatically accounts for multiple neutron scattering and may be used to measure either bulk samples or surfaces.

Description of SESAME: About 200 years ago, a British chemist named William Wollaston showed that the two polarization states of light could be split by a pair of birefringent prisms that now bear his name. The action of Wollaston's device is shown in Figure 1a. Two Wollaston prisms, combined with an optical polarizer can be used to produce two, spatially-separated, polarized light rays which are coherent with one another and which have a well defined relative phase, ψ, as shown in Figure 1b. An equivalent device, such as those shown in Figures 2b and 2c can be built for neutrons by using triangular solenoids rather than calcite prisms.

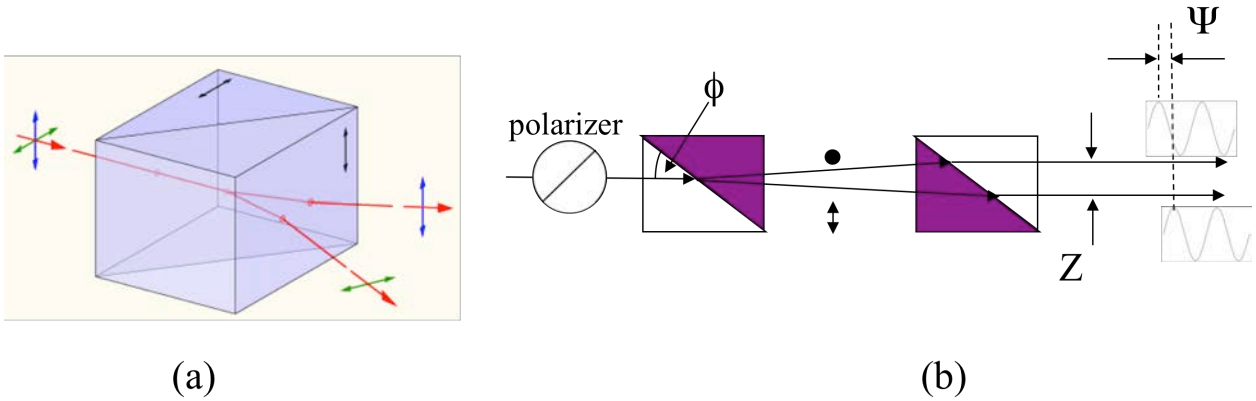

Figure 1: (a) A Wollaston prism made from two pieces of calcite with perpendicular optic axes; (b) A pair of such prisms produces two separated parallel rays with orthogonal polarizations. If the light incident on the first prism is plane polarized at 45° to the optic axis of either calcite crystal, as indicated by the circle with a 45° line to the left of the first Wollaston prism, the two parallel rays will be coherent and separated by the Larmor phase angle Ψ.

For SESAME, two neutron Wollaston prisms are used to spatially separate the spin eigenstates of a neutron and another pair of such prisms is used to bring those two states back together again, as shown in Figure 2a, to yield a spin echo. The distance probed in the sample (called the spin echo length) is equal to the separation of the spin states at the sample position and can range from a few tens of nanometers to several microns for reasonably achievable magnetic fields. The measured polarization of the spin echo is an Abel transform of the density-density correlation function of the sample.

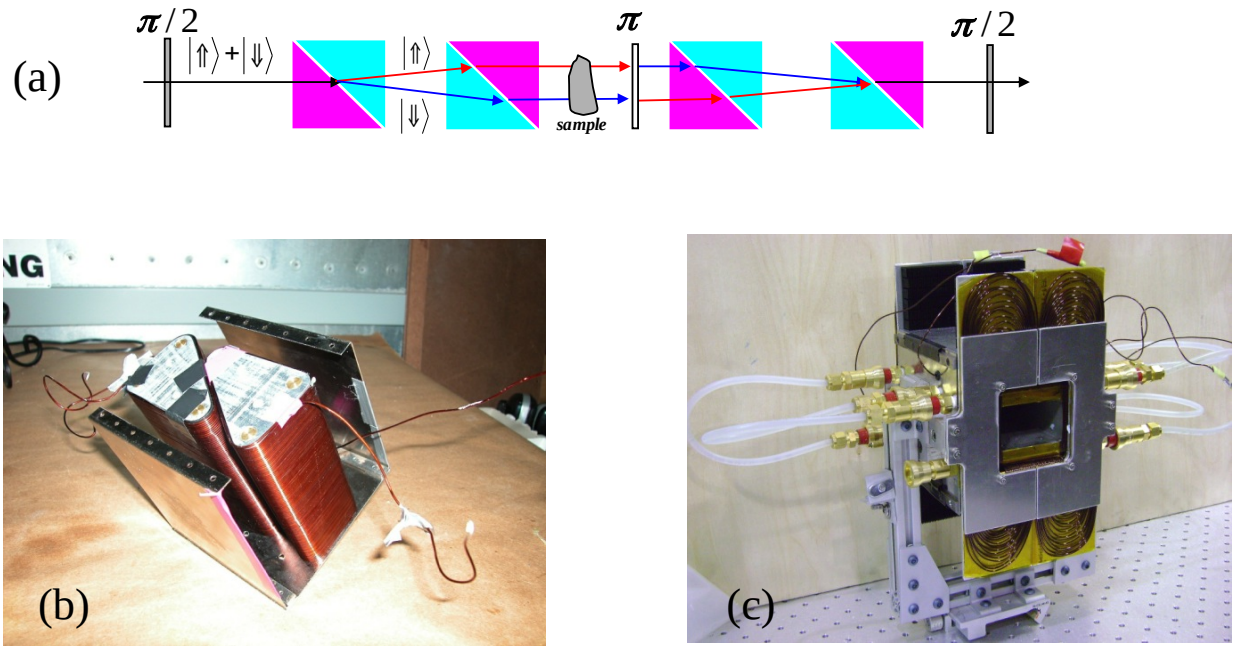

Figure 2: (a) the combination of neutron Wollaston prisms used in our experiments showing the separation of the two neutron spin eigenstates at the sample position; (b) an early version of a neutron Wollaston prism wound using aluminum wire (transparent to neutrons) showing the partially disassembled mu-metal magnetic flux return box; (c) a more recent neutron Wollaston device with water cooling and gaps in the entry and exit faces.

Recent Results (since 2010)

(a) *Development of a new generation of neutron Wollaston prisms*. We have carried out detailed magnetic field measurements and finite-element calculations to understand the performance of our first-generation neutron Wollaston prisms shown in Fig 2c. As a consequence, we have developed a simple but accurate model for the magnetic fields and calculated the Larmor phase accrued along multiple neutron trajectories. Using the model, we have optimized the dimensions of the new generation of neutron Wollaston prisms. These prisms have also been designed with improved cooling, including both air and water, so that we can increase the magnetic fields and reach a spin echo length (correlation distance) of 3 microns on the Asterix beam line at LANSCE. Numerical solution of the Bloch equation governing the evolution of a neutron spin in magnetic fields shows that the main source of neutron depolarization in our Wollaston prisms is at the boundary between the two current sheets the form the flipping plane in the prism. The magnetic field around individual wires causes this depolarization but simulations show that the effect can be overcome by careful design.

(b) *Development of a dynamical theory that reliably predicts neutron scattering from periodic nano-structured interfaces and allows quantitative evaluation of competing theories*. We have developed a dynamical scattering theory (DT) to describe neutron scattering from a periodic structure such as a diffraction grating. The computer code developed from our theory is stable to all orders that we have had the patience to test it, a feature not shared by any other similar code that we know about. Using a slicing method similar to the Parratt formalism, we have applied the theory to various surface profiles and compared the results

with SERGIS measurements obtained with the OFFSPEC instrument at ISIS (cf Fig 3b). In cases where the grating parameters are known (e.g. from SEM), the SERGIS measurements are well described by the DT, as Fig 3b demonstrates. We have tested the adequacy of other, approximate theories such as the Distorted Wave Born Approximation (DWBA) and the Phase Object Approximation (POA) (cf Fig 3b). We showed that the POA is inadequate to describe measurements in reflection geometry and that parameters (such a feature height) calculated by fitting the POA to data are often wildly inaccurate (by more than a factor of 2 in some cases). We did find that the POA generally gives a satisfactory account of the scattering in transmission geometry. Given the accuracy of the DT, we are now pursuing studies of soft-matter systems confined in the grooves of diffraction gratings.

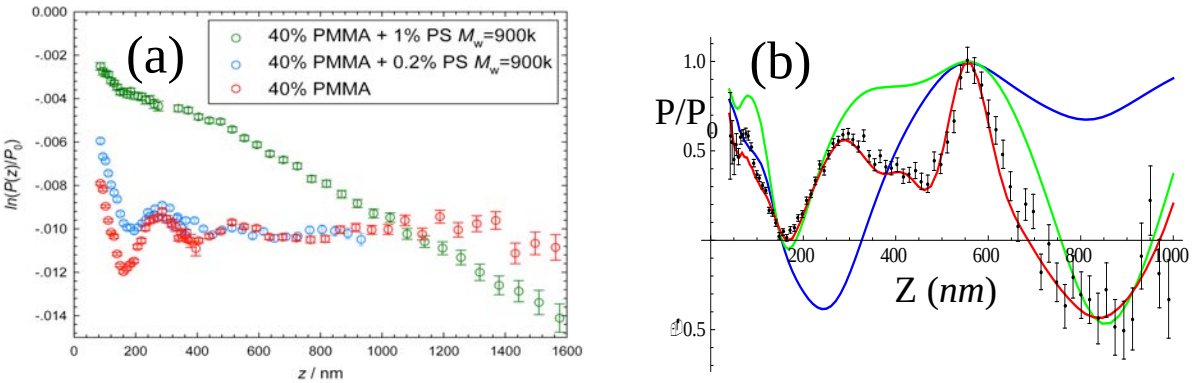

Figure 3: (a) Un-normalized SESANS correlation function for a system with 40% by volume of 260-nm-diameter PMMA spheres in decalin with various amounts of added polystyrene. (b) SERGIS signal obtained with a silicon diffraction grating with a 556 nm period. The red curve is the result from the dynamical theory with no adjustable parameters, the green curve is for the Phase Object Approximation and the blue for the DWBA.

(c) *Simultaneous measurement of short- and long-range inter-particle correlations in a colloidal fluid with controlled depletion interactions.* We have carried out a series of experiments to investigate the effects of adding polystyrene (PS) molecules to colloidal suspensions of mono-disperse PMMA spheres. In good solvents, PS causes a depletion attraction between the PMMA spheres and hence a change in the correlations between them. The principle results from these studies have been:

i. The Percus-Yevick (PY) approximation adequately describes correlations between PMMA particles up to volume fractions of ~40%.

ii. When small amounts of PS are added to suspensions of PMMA in dodecane (a poor solvent for PS), there is no change in the correlations between PMMA spheres. We suspect that, in this case, the PS plates out on the PMMA spheres.

iii. By contrast, when PS is added to suspensions of PMMA in decalin, which is roughly a theta solvent for PS, substantial changes are induced in the correlations between PMMA spheres. When small amounts of PS (0.1% of either 110 kDa or 900 kDa PS) are added, the short-range correlations are similar to those calculated from integral-equation theory applied to sticky hard spheres with an attractive potential of about 2kT (blue data in Fig 3a). For larger amounts of PS, PMMA aggregates develop with long-range correlations that can be described as fractal (green data in Fig 3a). These fractal-like

correlations extend down to inter-particle distances of about twice the diameter of the PMMA particles. Below that distance the inter-particle correlations are indistinguishable from those calculated for the 2kT sticky spheres. The size of aggregates varies with PS concentration and we have studied them with SESAME up to sizes of 18 microns using the SESANS instrument in Delft, Holland.

Publications 2010-2012:

Theoretical studies on the structure of interacting colloid suspensions by spin echo small angle scattering; X. Li, C-Y Shew, Y. Liu, R. Pynn, E. Liu, K. W. Herwig, G. S. Smith, J. L. Robinson, and W-R Chen; J. Chem. Phys., **132**, 174509 (2010)

Dynamical theory calculations of spin-echo resolved grazing-incidence scattering from a diffraction grating: R. Ashkar, P. Stonaha, A. L. Washington, V. R Shah, M. R. Fitzsimmons, B. Maranville, C. F. Majkrzak, W. T. Lee, W. L. Schaich, and R. Pynn; J. Appl. Cryst., **43**, 455 (2010)

Theoretical studies on the structure of interacting colloid suspensions by spin echo small angle scattering; X. Li, C-Y Shew, Y. Liu, R. Pynn, E. Liu, K. W. Herwig, G. S. Smith, J. L. Robinson, and W-R Chen, J. Chem; Phys., **132**, 174509 (2010)

Development of a beam line for spin echo scattering angle measurement at the Low Energy Neutron Source; A. L. Washington, P. Stonaha, R. Ashkar, R. Pynn, V. R. Shah; Proceedings of ICANS XIX (Grindelwald, Switzerland, 2010) ISSN-Nr. 1019-6447

Prospect for characterizing interacting soft colloidal structures using spin-echo small angle neutron scattering; Xin Li, Chwen-Yang Shew, Yun Liu, Roger Pynn, Emily Liu, Kenneth W. Herwig, Gregory S. Smith, J. Lee Robertson, and Wei-Ren Chen; J. Chem. Phys., **134**, 094504 (2011)

Scattering Functions of Platonic Solids; Xin Li, Chwen-Yang Shew, Lilin He, Flora Meilleur, Dan A. Myles, Emily Liu, Yang Zhang, Gregory S Smith, Kenneth W Herwig, Roger Pynn and Wei-Ren Chen; J. Appl. Cryst., **44**, 545, (2011)

Some recent results using spin echo resolved grazing incidence scattering (SERGIS); Roger Pynn, Rana Ashkar, P.Stonaha, A.L.Washington; presented at Polarized Neutrons in Condensed Matter Investigation (PNCMI), Delft, (2010); Physica **B406**, 2350 (2011)

Comparison of dynamical theory and the phase-object approximation for neutron scattering from periodic structures; Rana Ashkar, V. O. deHaan, A. A. VanWell, R. Dalgliesh, J. Plomp, M. R. Fitzsimmons, W. L. Schaich and Roger Pynn; J. Appl. Cryst., **44**, 958 (2011)

Dynamical Theory: Application to Spin-Echo Resolved Grazing Incidence Scattering from Periodic Structures; Rana Ashkar, W. L. Schaich, V. O deHaan, A. A. VanWell, R. Dalgliesh, J. Plomp, and Roger Pynn; presented at the Int. Conf. on Surface X-Ray and Neutron Scattering (SXNS11); J. Appl. Phys. **110**, 102201 (2011)

Contrast Variation in spin-echo small angle neutron scattering; Xin Li, Bin Wu, Roger Pynn, Chwen-Yang Shew, Gregory S. Smith, Kenneth W. Herwig, J. Lee Robertson, Wei-Ren Chen, and Li Liu; Journal of Physics: Condensed Matter, **24**, 064115 (2012)

Optimization of a solid state polarizing bender for cold neutrons; V. R Shah, A. L. Washington, P. Stonaha, R. Ashkar, H. Kaiser, T. Krist and Roger Pynn; Nucl. Instrum. and Methods (submitted)

Session IX

Frustrated Magnetism

A Unified Effort for Crystal Growth, Neutron Scattering, and X-ray Scattering Studies of Novel Correlated Electron Materials

Young Lee (younglee@mit.edu), Department of Physics, MIT, Cambridge, MA 02139

Research scope

Our research activities are focused on understanding the fundamental science of correlated electron materials. Much of the research involves performing neutron and x-ray scattering experiments on single crystal samples to investigate the spin, charge, and lattice dynamics which are central to the exotic physics in these systems. We have performed scattering experiments at the Spallation Neutron Source at Oak Ridge, the Advanced Photon Source at Argonne, the NIST Center for Neutron Research, and the ISIS facility at Rutherford Laboratory. We have also performed thermodynamic and transport measurements to provide a comprehensive picture of the microscopic behavior. Growing large single crystal samples for neutron scattering is a crucial aspect of this research.

New physics can emerge in systems where quantum fluctuations are enhanced due to reduced dimensionality and strong frustration. One long sought example is the resonating valence-bond (RVB) state, where the magnetic moments are strongly correlated but do not order or freeze even in the limit of $T \rightarrow 0$. The RVB state does not break conventional symmetries, such as lattice translation or spin-rotation. Such a quantum spin liquid in two-dimensions would represent a new state of matter. It is believed that spin liquid physics plays a role in the phenomenon of high-T_C superconductivity, and the topological properties of the spin liquid state may have applications in the field of quantum information. One of our main focuses has been on studying materials for which two-dimensional spin liquid physics may be at play. These include frustrated magnetic materials (such as the spin-1/2 kagome lattice) and the high temperature superconducting cuprates.

Recent progress

Fractionalized excitations in the spin liquid state of a S=1/2 kagome antiferromagnet

A hallmark feature of quantum spin liquids is the presence of deconfined spinons as the fundamental excitation from the ground state. Spinons are an example of fractionalized quantum excitations, where the conventional spin-wave excitation with quantum number S=1 is fractionalized into two S=1/2 spinons. In one dimensional systems, this phenomenon is well established for the spin-1/2 Heisenberg antiferromagnetic chain, where the spinons may be thought of magnetic domain boundaries which disrupt the Neel order. In two-dimensions, the character of the spinon excitations is less clear. First, the existence of the quantum spin-liquid as the ground state of two dimensional magnets is still a matter of great debate. Second, the various spin liquids states which are possible in theory give rise to a great variety of spinon excitations, such as having a spinon Fermi surface or having a Dirac quasiparticle spectrum.

The spin-1/2 kagome lattice Heisenberg antiferromagnet has long been recognized as a promising system in which to search for quantum spin liquid states, as the highly frustrated kagome network of corner-sharing triangles serves to destabilize long-range magnetic order. We have previously shown that the compound herbertsmithite, $ZnCu_3(OD)_6Cl_2$, is a particularly ideal S=1/2 kagome lattice antiferromagnet using powder samples. Our breakthrough in the past year

has been in growing a large single crystal sample and performing inelastic neutron scattering measurements of the spin excitation spectrum. A color contour plot of the differential cross section measured at three different energy transfers is shown in Figure 1. Figure 1(a) shows the excitations in reciprocal space with energy transfer ω = 6 meV at T = 1.6 K. A similar pattern of diffuse scattering is observed for ω = 2 meV shown in Fig. 1(b). Surprisingly, even at a temperature of 1.6 K, which is two orders of magnitude below the exchange energy scale of J ≃ 17 meV, the scattered intensity remains diffuse rather than concentrated at specific points in reciprocal space. In fact, the overall insensitivity of the pattern of the scattered intensity to the energy transfer is a remarkable feature of the data. Conventional spin-wave excitations take the form of sharp surfaces of dispersion in ($\boldsymbol{Q}$,ω)-space. No sharp surfaces of dispersion are observable in the data.

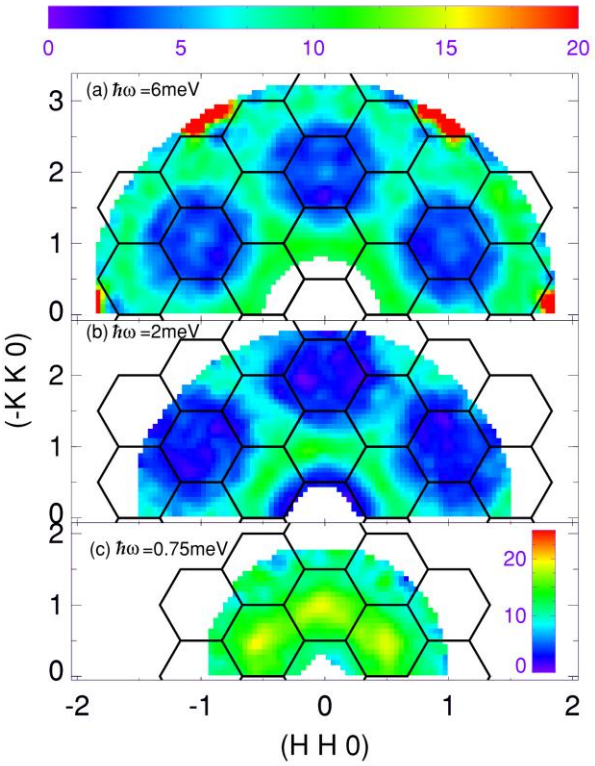

Figure 1. Intensity for inelastic neutron scattering from a single crystal sample of $ZnCu_3(OD)_6Cl_2$ measured at T = 1.6 K. The differential cross section $S_{tot}(\boldsymbol{Q}, \omega)$ is plotted for (a) ω = 6 meV, (b) ω = 2 meV, and (c) ω = 0.75 meV.

The $\boldsymbol{Q}$-dependence of the scattering provides important information about the spin correlations of the ground state. The energy integrated structure factor has been compared to a model of uncorrelated nearest neighbor singlets on a kagome lattice. To first approximation, the observed magnetic signal resembles this calculation. Therefore, the ground state wave function of herbertsmithite has a large component resembling randomly arranged nearest neighbor singlets. However, the calculation also shows that the spin correlations in herbertsmithite are longer ranged than just nearest neighbors. These neutron results are the first detailed look at the spin correlations in a two-dimensional spin-liquid.

Using phonons as a probe of electronic density wave order in superconducting Bi2201

In the high-temperature superconducting cuprates, there is an intriguing interplay between different types of electronic order which may compete and/or coexist with the superconductivity. It is now believed that the unusual pseudogap region of the phase diagram is characterized by a symmetry-breaking electronic state. A rich variety of broken-symmetries have been observed in different materials, including translation, time-reversal, four-fold rotation, and inversion. Understanding how these broken-symmetries relate to each other and which ones are universal is one of the key questions under current debate. Our x-ray scattering results on the superconductor $Bi_2Sr_{2-x}La_xCuO_{6+\delta}$ (Bi2201) reveal the coupling of low energy phonons to the electronic density wave order observed in prior scanning-tunneling microscopy studies.

Inelastic x-ray scattering data from the longitudinal acoustic phonon in single crystal $Bi_2Sr_{2-x}La_xCuO_{6+\delta}$ are shown in Figure 2. The sample shown is underdoped with a T_C of 31 K. The principal discovery is that an anomalous broadening of the longitudinal mode is observed for reduced wavevectors near (0.25, 0, 25, 0), which is not observed in the transverse mode. This behavior is consistent with coupling of the lattice to an electronic density wave with characteristic wavevector near (1/4,1/4, 0) as suggested by previous STM studies. This acoustic phonon anomaly is qualitatively different than the previously reported optical phonon anomalies in the high-T_C cuprates. The energy of the mode that we measure is about an order of magnitude smaller than that of the optical mode anomaly previously observed in Bi2201. This anomaly does not occur in the transverse mode. Since the longitudinal polarization corresponds to deformations of the bond lengths, while the transverse polarization does not strongly change bond lengths, the former should be much more strongly coupled to any density wave state. Also, the sample dependence of the anomaly (not shown) indicates that the more underdoped sample has a larger wavevector, consistent with the STM results, lending further credence to the close connection with the electronic density wave.

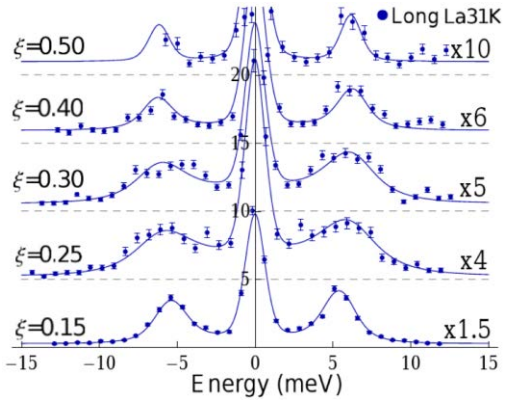

Figure 2. Inelastic x-ray scattering scans of the longitudinally polarized acoustic mode along the (ξ,ξ,0) direction. The energy-width of the phonon mode is dramatically broadened for reduced wavevectors near $\xi \approx 0.25$

Moreover, there is a surprising effect observed in the intensity of the phonons at low temperatures. We find a violation of the relation $S(-\boldsymbol{Q},\omega) = S(\boldsymbol{Q},\omega)$, which means that both inversion (I) and time-reversal (TR) symmetries are broken in the system. There is a statistically significant asymmetry in the intensity for the low temperature data at $\boldsymbol{Q}$=(2.25, 2.25, 0). This effect cannot solely arise from a possible non-centrosymmetric unit cell since TR must also be broken. The asymmetry of the intensity has a clear temperature dependence between T = 300 K and T = 100 K (which spans $T^* \approx 150$ K), showing that the broken symmetries exist in the pseudogap phase. The observation that more than one type of symmetry is broken prior to entering the superconducting state has profound implications for the theories explaining the physics of these systems. These measurements also reveal that the coupling to phonons provides an unexpectedly sensitive probe of the subtle electronic order in the cuprates. Our preprint is C.J. Bonnoit et al, cond-mat:1202-4994.

Future Plans

Using our high quality single crystal sample of $ZnCu_3(OD)_6Cl_2$, we plan to probe the spin correlations from mid- to high- energy transfers (up to ~60 meV). These measurements are crucial to determine the dispersion of the upper bound of the spin excitations of the spin liquid state. In addition, we wish to introduce mobile charge carriers into the S=1/2 kagomé lattice. Certain theories of the high-T_C superconductors based on the RVB picture predict that the addition of carriers to a spin liquid ground state should lead to superconductivity. Needless to say, this is a very exciting prediction to test. It would also be interesting to study quantum spin

systems with smaller exchange couplings, as theories suggest one can drive a zero-temperature quantum phase transition by applying modest magnetic fields. Our recent measurements on the organic-inorganic hybrid kagomé system Cu(1,3-bdc), suggest that this is a realization of an S=1/2 kagome *ferromagnet*. This material is characterized by having a flat band in the spin wave excitation spectrum. Such a ferromagnetic system can be used to probe theories regarding how the spin-orbit interaction creates a gap between the dispersive modes and the flat, non-dispersive mode. This has direct relevance to tight-binding models of electrons hopping on frustrated lattices, which may be a route to new topological states of matter. Finally, the acoustic phonon anomaly that we have discovered in single-layer Bi2201 superconductors must be following up in the related double-layer Bi2212 superconductors (and other cuprates) to test the universality of the observation. Also, it is important to determine how the temperature dependence of the symmetry breaking changes with the doping level.

Publications (last two years)

10) T.H. Han, S. Chu, and Y.S. Lee, Refining the spin Hamiltonian in the spin-1/2 kagome lattice antiferromagnet $ZnCu_3(OH)_6Cl_2$ using single crystals, Phys. Rev. Lett. 108, 157202 (2012).

9) D.E. Freedman, R. Chisnell, T.M. McQueen, Y.S. Lee, C. Payen, and D.G. Nocera, Frustrated magnetism in the S=1 kagome lattice $BaNi_3(OH)_2(VO_4)_2$, Chem. Comm. 48, 64-6 (2012).

8) T.M. McQueen, T.H. Han, D.E. Freedman, P.W. Stephens, Y.S. Lee, and D.G. Nocera, $CdCu_3(OH)_6Cl_2$: A New Layered Hydroxide Chloride, J. Sol. St. Chem. 184, 3319-23 (2011).

7) T. Imai, M. Fu, T.H. Han, and Y.S. Lee, Local Spin Susceptibility of the S=1/2 Kagome Lattice in $ZnCu_3(OD)_6Cl_2$, Phys. Rev. B 84, 020411 (2011).

6) S. Chu, P. Müller, D.G. Nocera, and Y.S. Lee, Hydrothermal growth of single crystals of the quantum magnets: Clinoatacamite, paratacamite, and herbertsmithite, Appl. Phys. Lett. **98**, 092508 (2011).

5) T.H. Han, S. Chu, J.S. Helton, A. Prodi, D.K. Singh, C. Mazzoli, P. Muller, D.G. Nocera, and Y.S. Lee, Synthesis and Characterization of Single Crystal Samples of Spin-1/2 Kagome Lattice Antiferromagnets in the Zn-Paratacamite Family $Zn_xCu_{4-x}(OH)_6Cl_2$, Phys. Rev. B 83, 100402(R) (2011).

4) D. Wulferding, P. Lemmens, P. Scheib, J. Roder, P. Mendels, S.Y. Chu, T.H. Han, Y.S. Lee, Interplay of thermal and quantum spin fluctuations in the kagome lattice compound herbertsmithite, Phys. Rev. B 82, 144412 (2010).

3) A. Prodi, J.S. Helton, Y. Feng, and Y.S. Lee, Pressure-induced spin-Peierls to incommensurate charge-density-wave transition in the ground state of TiOCl, Phys. Rev. B 81, 201103(R) (2010).

2) S. Chu, T. M. McQueen, R. Chisnell, D.E. Freedman,‡ P. Muller, Y.S. Lee, and D.G. Nocera, A Cu^{2+}(S= 1/2) Kagome Antiferromagnet: $Mg_xCu_{4-x}(OH)_6Cl_2$, J. Am. Chem. Soc. 132, 5570–5571 (2010).

1) J.S. Helton, K. Matan, M.P. Shores, E.A. Nytko, B.M. Bartlett, Y. Qiu, D.G. Nocera, and Y.S. Lee, Dynamic Scaling in the Susceptibility of the Spin- 1/2 Kagome Lattice Antiferromagnet Herbertsmithite, Phys. Rev. Lett. 104, 147201 (2010).

Neutron Scattering Study of Unconventional Superconductors

Seung-Hun Lee
Department of Physics, University of Virginia, Charlottesville, VA 22904

A. Research Scope

Strongly correlated electron systems provide myriad opportunities to study novel electronic, magnetic, and structural phenomena that emerge out of strong interactions between electrons. Some of these phenomena are high T_c superconductivity and novel magnetic states such as quantum spin liquid. Our group has been studying several exemplary systems to identify the novel states and to understand the microscopic mechanism for those phenomena. Particular systems of our current interest are geometrically frustrated magnets such as 2-dimensional kagome, 3-dimensional pyrochlore (spinels), and quasi-two-dimensional kagome-triangular-kagome trilayer system SCGO, magnetic molecules such as Ni_4 and Mn_6 and Fe-based superconductors. For this research our group utilizes elastic/inelastic neutron scattering techniques that directly probe static and dynamic properties of solid at the atomic length scale.

B. Recent Progress

As shown in the publication list (section D), our group has recently been studying three types of materials: geometrically frustrated magnets such as $Zn_xCo_{4-x}(OD)_6Cl_2$[2], $CdCr_2O_4$[6], $ZnCr_2O_4$, and $SrCr_{9p}Ga_{12-9p}O_{19}$ (SCGO) [4], magnetic molecules such as Ni_4 [1] and Mn_6 molecules, and unconventional superconductors, an ambipolar cuprate [7], and Fe pnictide $FeTe_{1-x}Se_x$ [8,9]

In this abstract, we will describe our recent work [4] that identified a topological spin glass state and its microscopic origin for the kagome-triangular-kagome trilayer system SCGO.

B.1. Topological spin glass state of a quasi-two-dimensional frustrated magnet [4]

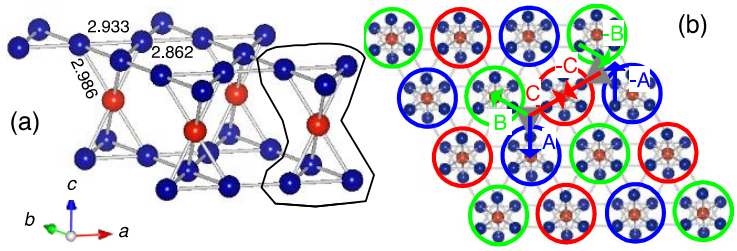

Fig. 1 (a) The (111)-slab of pyrochlore lattice made up by a kagome(blue spheres)-triangular(red spheres)-kagome tri-layer realized by the magnetic Cr^{3+} ions in SCGO. The numbers are the bond lengths in Å. The blue and red spheres represent kagome and triangular sites, respectively. (b) The lattice is projected on the ab-plane. The red, blue, green arrows represent the three spin directions of a 120° configuration, either (A,B,C) or (-A,-B,-C).

In ordinary magnets, when temperature is lowered, the spins freeze into a long-range ordered state or a spin solid. Some magnets however do not order even at low temperatures. The simplest examples are a triangle of three antiferromagnetic (AFM) spins and a

tetrahedron of four AFM spins. For both systems, any spin configuration with total zero spin can be a ground state. When such triangles (tetrahedra) are arranged in a two-dimensional (three-dimensional) corner-sharing network or kagome (pyrochlore) lattice, there is an infinite way of covering the entire lattice with the total-zero-spin building blocks. As a result, instead of ordering at low temperatures, the kagome and pyroclore antiferromagnets remain in a spin liquid state. A hallmark of the frustration-driven spin liquid is the existence of local zero energy excitation modes that continuously connect their degenerate ground states in the phase space of spin configuration and energy; the so-called weather-vane mode for the kagome and the hexagonal mode for the pyrochlore antiferromagnets.

Some frustrated magnets exhibit spin-glassy behaviors characterized by the field-cooled and zero-field-cooled hysteresis in the bulk susceptibility data and static short-range spin correlations in neutron scattering data. Among them, $SrCr_{9p}Ga_{12-9p}O_{19}$ [SCGO(p)] and $Ba_2Sn_2ZnGa_3Cr_7O_{22}$ (BSZGCO) are particularly interesting because in both systems the magnetic Cr^{3+} ($3d^3$; s = 3/2) ions form a <111> slab of pyrochlore lattice or a kagome-triangular-kagome tri-layer. The Cr^{3+} ions in the tri-layer are surrounded octahedrally by six oxygens, and the neighboring oxygen octahedra share an edge. Due to the direct overlap of the t_{2g} electrons of the neighboring Cr^{3+} ions, the antiferromagnetic nearest neighbor (NN) exchange interactions become dominant and further neighbor interactions become negligible:

$$\mathcal{H} = J\sum_{k} \vec{S}_i \cdot \vec{S}_j + J'\sum_{k-t} \vec{S}_i \cdot \vec{S}_j$$

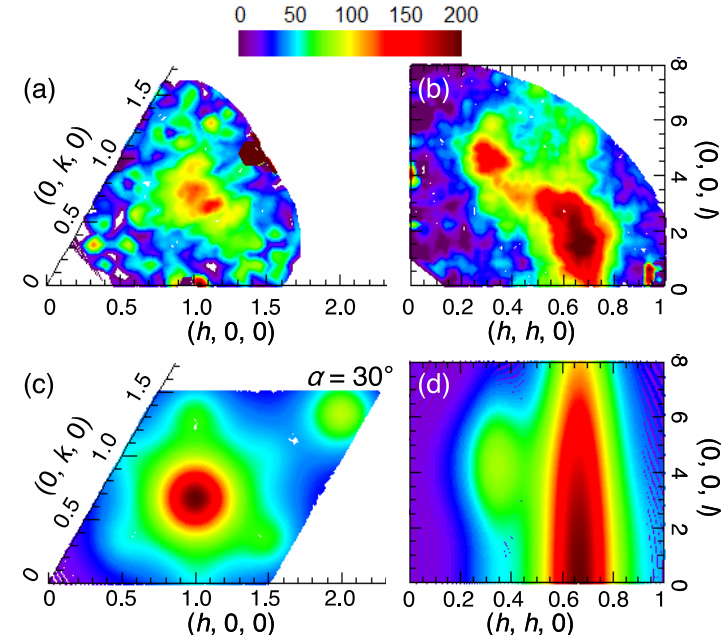

Fig. 2 (a),(b) The experimental magnetic neutron scattering intensities in the (hk0) and (hhl) planes obtained from single crystal measurements of SCGO. (c),(d) The calculated elastic magnetic scattering intensities.

where the first sum is over the NN bonds between the kagome spins and the second sum is over the bonds between the kagome and triangular spins [Fig. 1 (a)]. The different values of J and J' are due to their different bond lengths. The tri-layers are well separated from each other by non-magnetic layers which confine the magnetic interactions within each tri-layer. Since the discovery of SCGO more than two decades ago, understanding the origin of the spin glass behavior has been a challenging issue.

We view the quasi-two-dimensional lattice from a

different perspective. We consider two corner-sharing tetrahedra or a bi-pyramid with a triangular base circled by a solid line in Fig. 1 (a) as a "molecular" unit. As shown in Fig. 1 (b), the bi-pyramids form a triangular superlattice. This new perspective allows us to map the magnetic interaction problem onto a model with two independent degrees of freedom, tri-color and binary sign. The mapping leads us to a methodical way to construct the complex classical spin ground states with collinear and coplanar bi-pyramidal spins for uniform and nonuniform NN interactions. We also identify 'partial but extended' zero-energy excitations amongst the ground states that are qualitatively different from the 'local' zero-energy excitations found in spin liquid states of other frustrating magnets. By comparing the resulting theoretical magnetic scattering to the experimental neutron intensities obtained from single crystals of SCGO(p = 0.67), the ratio of J'/J ~ 0.70(15) was obtained, which is reasonable for SCGO. The unique properties of the degenerate ground state and of the extended zero-energy excitations provide a topological argument for the nonconventional spin glass state as the intrinsic ground state for this quasi-two-dimensional magnetic system.

C. Future Plans

C.1. Magnetic correlations in Fe(Te,Se)

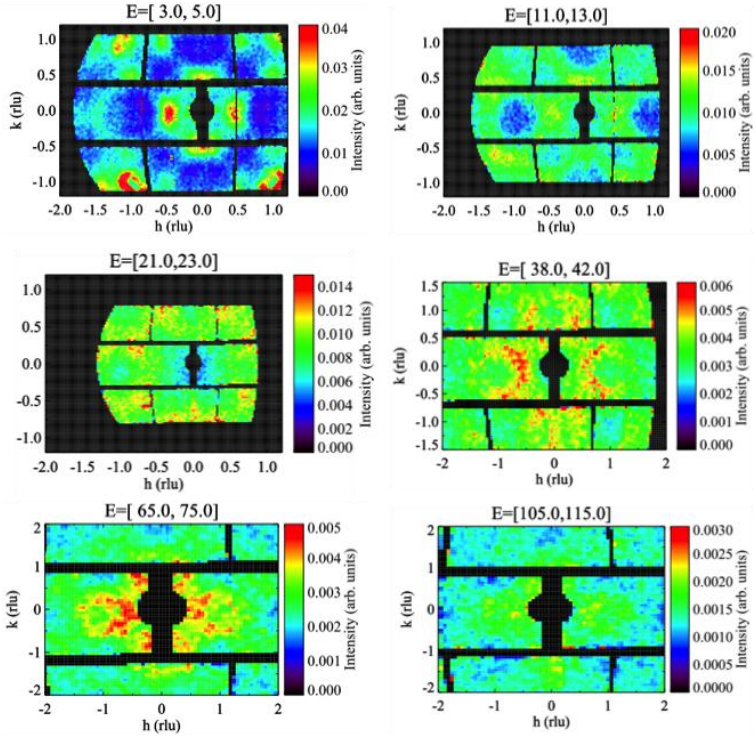

Fig. 3. Constant energy cut of inelastic neutron scattering data in the (hk) plane at energies around (a) 4meV, (b) 12meV, (c) 22meV (d) 40meV, (e) 70meV, and (f) 110meV. The data were taken at a time-of-flight spectrometer ARCS at SNS from single crystals of $FeTe_{0.85}Se_{0.15}$.

We have studied magnetic fluctuations in the insulating $FeTe_{0.85}Se_{0.15}$ using inelastic neutron scattering. Fig. 3 shows color contour maps of several constant energy cuts to see how the momentum dependence of the magnetic fluctuations evolves as energy increases. Low energy magnetic fluctuations exhibit anisotropic scattering that is centered at $(0.5 + \delta, 0)$ and elongated along the transverse direction. As the energy increases, at ~ 10 meV the fluctuations start dispersing to form a quartet around the zone boundary (1,0) at ~ 20 meV. With further increasing energies, the

quartet moves close to (1,0) forming a ring, and eventually for energies above 100 meV the ring collapses into (1,0), which indicates that the bandwidth of the magnetic excitations is about 120 meV. We are in the process of analyzing the data in terms of a J_1-J_2-J_3 Heisenberg model on the square lattice near the limit of maximum frustration.

C.2. Perform neutron scattering experiments on $AV_{10}O_{15}$ (A = Sr, Ba). We have recently been working on an orbitally degenerate system $AV_{10}O_{15}$ (A = Sr, Ba). In this system, the magnetic V^{3+} ions with orbital degeneracy form a complex hybrid lattice with coupled one-dimensional and tetrahedral motifs. We will perform inelastic neutron scattering on single crystals of $(Sr,Ba)V_{10}O_{15}$ to determine their effective spin Hamiltonians to understand the nature of the orbital and magnetic correlations in the complex oxides.

D. List of papers in which DOE support is acknowledged

Here list our papers that were supported by DOE and published/in press/submitted since June 1, 2010.

1. *Determination of spin Hamiltonian for the Ni_4 magnetic molecule*, K. Iida, S.-H. Lee, K. Matsubayashi, T. Onimaru, T. J. Sato, submitted to Phys. Rev. B (2012).
2. *Magnetic-field-induced instability of the cooperative paramagnetic state in $Zn_xCo_{4-x}(OD)_6Cl_2$*, S. E. Dissanayake, C. Chan, S. Ji, J. Lee, Y. Qiu, K. C. Rule, B. Lake, M. Green, M. Hagihala, X. G. Zheng, T. K. Ng, S.-H. Lee, Phys. Rev. B, in press (2012).
3. *Ferromagnetism in CuFeSb: Evidence of competing magnetic interactions in Fe-based superconductors*, B. Qian, J. Lee, J. Hu, G. C. Wang, P. Kumar, M. H. Fang, T. J. Liu, D. Fobes, H. Pham, L. Spinu, X. S. Wu, M. Green, S.-H. Lee, Z. Q. Mao, Phys. Rev. B, in press (2012).
4. *Coexisting order and disorder hidden in a quasi-two-dimensional frustrated magnet*, K. Iida, S.-H. Lee, S-W. Cheong, Phys. Rev. Lett., in press (2012).
5. *Conductivity and incommensurate antiferromagnetism of $Fe_{1.02}Se_{0.10}Te_{0.90}$ under pressure*, N. Katayama, K. Matsubayashi, Y. Nomura, S. Ji, J. Leao, M. Green, T. J. Sato, Y. Uwatoko, M. Fujita, K. Yamada, R. Arita, S.-H. Lee, Europhys. Lett., in press (2012).
6. *Synchrotron x-ray study of lattice vibrations in $CdCr_2O_4$*, J. Phys. Soc. Jpn, **80**, 073603 (2011).
7. *Zero-doping state and electron-hole asymmetry in an ambipolar cuprate*, K. Segawa, M. Kofu, S.-H. Lee, I. Tsukada, H. Hiraka, M. Fujita, S. Chang, K. Yamada, Y. Ando, Nature Physics **6**, 579-583 (2010).
8. *Investigation of the spin-glass regime between the antiferromagnetic and superconducting phases in $Fe_{1+y}Se_xTe_{1-x}$*, N. Katayama, S. Ji, D. Louca, S.-H. Lee, M. Fujita, T. J. Sato, J. S. Wen, Z. J. Xu, G. D. Gu, G. Xu, Z. W. Lin, M. Enoki, S. Chang, K. Yamada, J. M. Tranquada, J. Phys. Soc. Jpn, **79**, 113702 (2010).
9. *Coupling of spin and orbital excitations in an Fe-based superconductor*, S.-H. Lee, G. Xu, W. Ku, J. S. Wen, C. C. Lee, N. Katayama, Z. J. Xu, S. Ji, Z. W. Lin, G. D. Gu, H.-B. Yang, P. D. Johnson, Z.-H. Pan, T. Valla, M. Fujita, T. J. Sato, S. Chang, K. Yamada, J. M. Tranquada, Phys. Rev. B **81**, 220502 (2010).

ORBITAL SELECTIVE MAGNETISM IN THE SPIN-LADDER IRON SELENIDES $BA_{1-X}K_XFE_2SE_3$

T.M. McQueen[1,‡]

[1]Department of Chemistry, Department of Physics and Astronomy, Institute for Quantum Matter, The Johns Hopkins University, Baltimore, MD, USA

The “1-2-3” spin-ladder compounds $BaFe_2Se_3$ and KFe_2Se_3 are built of double-chains of edge-sharing [$FeSe_4$] tetrahedral, cut-outs of the full two-dimensional [Fe_2X_2] layers found in iron pnictide superconductors. Total neutron scattering of $BaFe_2Se_3$ reveal long-range ordered antiferromagnetism (AFM) built of ferromagnetic Fe_4 plaquettes that is coupled to local iron displacements. These local displacements are greatly reduced or absent in KFe_2Se_3, with a concomitant change to an AFM stripe order that is analogous to that found in the iron arsenide superconductors. Even for intermediate compositions, the spin-ladders remain insulating down to 1.8 K. Taken together, these results imply an orbital selection of magnetic order that is likely important in all iron-based materials. More generally, as with the copper oxide superconductors two decades ago, our results highlight the importance of reduced dimensionality spin-ladder compounds in the study of the coupling of spin, charge, and atom positions in superconducting materials.

‡ mcqueen@jhu.edu

Session X

Dynamics

Metastable Vortex Lattices - Properties and Applications

Morten R. Eskildsen (eskildsen@nd.edu)
Department of Physics, University of Notre Dame, Notre Dame, IN 46556

Research Scope

Vortices induced by a magnetic field in type-II superconductors naturally reflect the intrinsic nature and properties of the superconducting state in the host material. Studies of the vortex lattice (VL) by small-angle neutron scattering (SANS) can provide a wealth of otherwise unattainable information deep within the superconducting phase, and can, of course, also be used to study the physics of the vortices and the VL.

The present research project has two main objectives. The first is to investigate well-ordered, metastable vortex phases observed in the two-band/two-gap superconductor MgB_2. Metastable phases of matter are well known, with famous examples including supercooling and superheating of liquids and diamond which is one of the many allotropes of carbon. Metastability is almost exclusively observed in connection with first-order transitions, and is often found in frustrated systems where the energy difference between the states is small. The structure of the VL is known to be highly sensitive to changes in external parameters such as temperature and magnetic field and can therefore naively be expected to display metastability, for example, in connection with first-order transitions such as the VL melting or the reorientation transition of the rhombic VL found in most superconductors with a fourfold basal-plane anisotropy. The study of metastable VL phases will provide new insight into collective vortex behavior, and also explore analogies to other systems such as colloids or granular material. Finally, it will provide a reference for measurements on other superconductors where a field quenching technique has been used to explore the VL structure formed in high-temperature phases and imaged at low temperature.

The second objective is to study the VL in multiphase and/or unconventional superconductors, with special emphasis on materials where the spins of the Cooper pairs are believed to be in a triplet configuration. Among these materials one finds the heavy-fermion material UPt_3 which can be considered as a paradigm for unconventional superconductivity, having an *f*-wave triplet order parameter most likely of the E_{2u} orbital state. In addition, the superconductor Sr_2RuO_4 is widely accepted to be a *p*-wave triplet superconductor. Despite extensive research the detailed order parameter in both of these compounds is not well established, and in particular the chirality of ψ is unresolved with different experimental techniques yielding apparently conflicting results. Moreover, the relation between the spin and orbital angular momentum (conventionally described by the so-called *d*-vector) of the superconducting condensate, and in particular how this may be affected by a magnetic field, is unresolved in both of the abovementioned compounds. Furthermore, there are theoretical predictions of chiral domain formation and, in the case of UPt_3 for single to doubly quantized vortices across the so-called B to C transition. Creative use of different field-temperature histories can be applied to prepare metastable VL configurations, as well as to induce well-defined chiral states with different chiral direction relative to the applied magnetic field.

Recent Progress

Metastable vortex lattice phases in MgB_2: An unprecedented degree of VL metastability was found in MgB_2 with $\boldsymbol{H} \parallel \boldsymbol{c}$. Previous studies of this compound had revealed a continuous, field-driven 30¬ VL rotation, understood to arise from a competition between sixfold Fermi surface anisotropies with opposite signs on two different bands coupled with the suppression of superconductivity on one band by a modest magnetic field. Figure 1 shows VL configurations which clearly demonstrate that different, well-ordered phases can exist at the same place in the *HT*-phase diagram. Surprisingly, the metastability occurs in connection with second-order transitions rather than a first-order transition which is usually required for hysteretic behavior. In addition it was shown that longevity of the metastable phases cannot be understood solely from the free energy of a single VL domain. Moreover, careful studies of how the metastable VL phase transitions to the ground state during a slow field reduction showed a gradual rather than abrupt emergence of ground state domains. Furthermore, the vortex density in both the metastable and equilibrium domains decrease as the field is reduced, showing that the metastable phase is not due to vortex pinning. Rather, the results indicate a jamming of counter-rotated VL domains. This notion is supported by measurements of the VL subjected to an AC-drive which shows a logarithmic dependence of the ground state domain population on the number of applied field cycles.

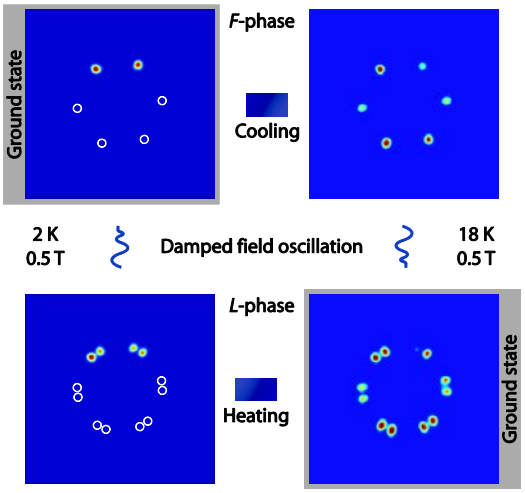

Figure 1 Diffraction patterns showing the triangular vortex lattice (VL) F (top) and L (bottom) phases in MgB_2. Heating or cooling across the critical temperature for the ground-state F-L rotation transition leaves the VL in a metastable configuration. At any field/temperature the ground state VL can be obtained by applying a damped small-amplitude field oscillation.

In summary our results present a new multi-scale model system for VL studies where both vortex-vortex and VL domain interactions are important. Moreover, the VL in MgB_2 exhibits many similarities to granular materials, including jamming and glassy dynamics.

Superconducting anisotropy of Sr_2RuO_4: Despite being widely considered a triplet *p*-wave superconductor, a number of details concerning the superconducting state in Sr_2RuO_4 remain unexplained. Among these is the anisotropy of the upper critical field as $\boldsymbol{H}$ is rotated from the *c*-axis to the basal plane [A. P. Peter Mackenzie and Y. Maeno, Rev. Mod. Phys. **75**, 657 (2003)]. Specifically, the upper critical field anisotropy ~20 is much smaller than what is expected from the Fermi surfaces (57 – 174). Furthermore, H_{c2} appear truncated when then field is applied within a few degrees of the basal plane.

To resolve this we investigated the VL for fields applied close to the basal plane as shown schematically in Figure 2(a). Such measurements are only possible because of the large anisotropy of Sr_2RuO_4 which leads to a significant transverse field modulation due to the VL when the field is close to, but not perfectly aligned with, the basal plane. This is demonstrated in Figure 2(b) which shows the scattered intensity at 3 fields as a function of the angle with respect

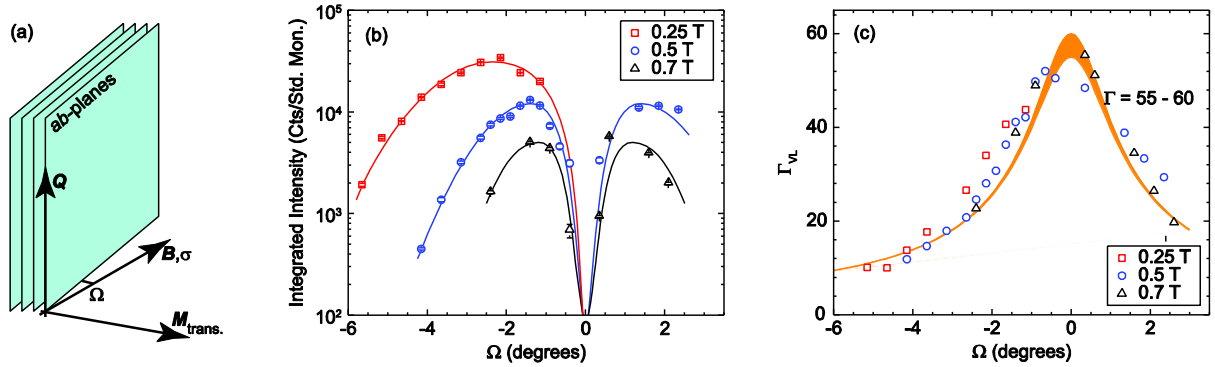

Figure 2 VL studies in Sr_2RuO_4 with $\boldsymbol{H}$ close to the basal plane. **(a)** Scattering geometry. The angle between the basal plane (*a*-axis) and the field is denoted by Ω. **(b)** Integrated scattered intensity as the field is rotate away from the basal plane. Lines are guides to the eye. **(c)** Vortex lattice anisotropy determined from the magnitude of the vertical scattering vector assuming singly-quantized vortices. The orange curve shows the calculated anisotropy.

to the basal plane. Assuming that the vortices carry a single flux quantum it is possible to extract the VL anisotropy as shown in Figure 2(c). This shows that the VL anisotropy is independent of field (over the measured range) and extrapolates to a value of 55 – 60 for $\boldsymbol{H} \parallel \boldsymbol{a}$. This is much greater than the upper critical field anisotropy which could be interpreted as an indication of Pauli limiting. If confirmed this present a significant challenge to the current theoretical understanding of equal spin pairing for $\boldsymbol{H} \perp \boldsymbol{c}$ ($\boldsymbol{d} \parallel \boldsymbol{H}$). A possible explanation for this discrepancy could be a *d*-vector which rotates with applied field.

In summary, we have measured the intrinsic anisotropy of the superconducting state in Sr_2RuO_4 which is found to be 3 times larger than that of H_{c2}. This raises a number of questions in relation to the current theoretical understanding of the superconducting state in this material.

Future Plans

Vortex lattice metastability in MgB_2: Further studies of the dynamics of the VL metastable to ground state transition under an AC drive will be carried out. This will explore the range over which logarithmic behavior and also explore any dependence on the frequency of the AC drive. The results will provide further insight into the physics of VL domain growth and the stability of VL domain boundaries. In addition it will allow us to study the analogies between the VL and the jamming of granular materials in more detail.

Anisotropy of Sr_2RuO_4: The measurements of the VL anisotropy will be extended to fully explore the superconducting phase diagram (both higher and lower fields as well as higher temperatures). Measurements at low fields will allow us to look for a rotation of the *d*-vector in this material; something which has been speculated could occur but have not yet been observed. For higher fields the scattered intensity from the VL decreases rapidly as seen in Figure 2(b). However, it is estimated that measurements should be possible up to fields close to H_{c2}. Finally, the upper critical field anisotropy is known to be strongly temperature dependent which renders studies of the *T*-dependence of the VL anisotropy desirable.

Study of chiral vortex lattice phases in UPt_3: The VL have been studied $\boldsymbol{H} \parallel \boldsymbol{a}^*$. For this field orientation the temperature dependence of the VL intensity was measured at 0.2 T and 0.4 T. In both cases an unconventional linear temperature dependence was observed. Moreover at the lower field the intensity goes to zero at the transition between the A- and B-phases, indicative of a "weak" superconducting state in the A-phase. For measurements at 0.4 T, corresponding to the A-, B- and C-phase tri-critical point, the VL intensity goes to zero at T_c, proving that the result at the lower field is not simply due to poor statistics.

Preliminary measurements with $\boldsymbol{H} \parallel \boldsymbol{c}$ have been carried out, successfully imaging the VL up to an unprecedented high field of 0.8 T with indications that these measurements can be extended even further. In the future we will perform systematic measurements of the VL in UPt_3 for this field orientation to search for effects of chiral superconducting phases. This includes field reversal experiments, where it has been proposed that vortices with a current circulation opposite chiral direction of the order parameter can lead to a change in the VL symmetry or even to vortices carrying multiple flux quanta. Furthermore, we will extend earlier measurements which used a temperature quenching technique to study the VL in the A-phase which exist immediately below T_c for fields ≤ 0.8 T. The latter measurements will be greatly facilitated by our studies of VL metastability in MgB_2.

Measurements of the bulk magnetization in UPt_3: The experimental case for equal spin pairing in UPt_3 hinges on a few crucial experiments, one of which is NMR measurements of the Knight shift which show no change in the electron susceptibility upon entering the superconducting phase. This result appears inconsistent with measurements of the upper critical field indicating Pauli limiting and thus raises concerns about the interpretation of the NMR results. We measured the bulk magnetization of UPt_3 with $\boldsymbol{H} \parallel \boldsymbol{a}$ using polarized-neutron scattering. As shown in Figure 3, no measurable change in the magnetization was observed upon entering the superconducting state, thus confirming the NMR results. To complement these results measurements of the magnetization with $\boldsymbol{H} \parallel \boldsymbol{c}$ are required. Another single crystal of UPt_3 is being grown and will be used to complete these measurements.

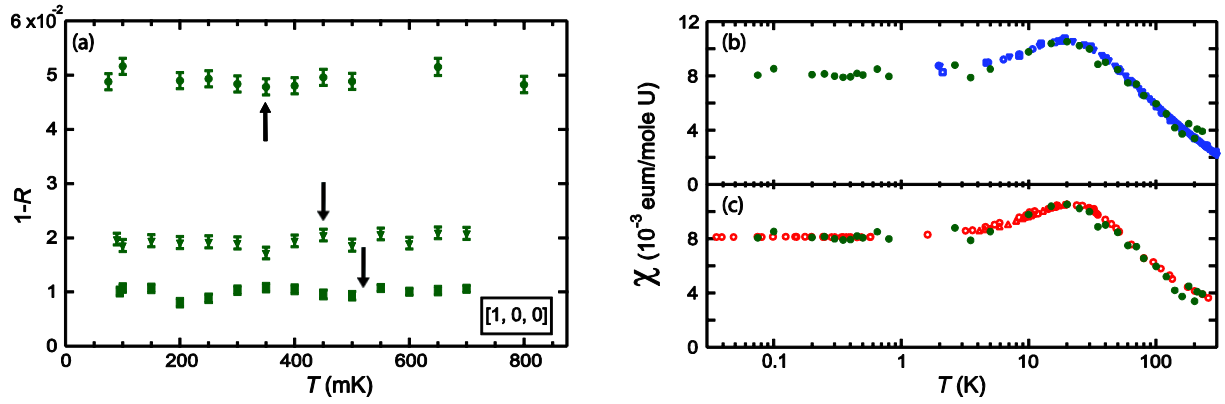

Figure 3 Measurements of the bulk magnetization in UPt_3 with $\boldsymbol{H} \parallel \boldsymbol{a}$ by polarized-neutron diffraction. **(a)** Flipping ration at three fields: 0.2 T (squares), 0.4 T (triangles) and 1.0 T (circles). The superconducting transition temperature, T_c, at each field is indicated by the arrows. **(b)** Magnetization measured by neutron scattering (green) compared magnetic susceptibility measurements obtained by SQUID measurements (blue). **(c)** Comparison of magnetization measured by neutron scattering (green) and the susceptibility calculated from Knight shift measurements (red).

Vortex lattice studies in other superconductors: Building on the results and experience with VL studies in UPt_3 and Sr_2RuO_4, the possibility of extending SANS measurements to other superconductors will be actively explored. A particular focus will be on materials with strong anisotropy and/or those with possible chiral superconducting phases.

Publications (FY10 – FY11)

1. *Observation of Well-Ordered Metastable Vortex Lattice Phases in Superconducting MgB_2 Using Small-Angle Neutron Scattering*
   P. Das, C. Rastovski, T. R. O'Brien, K. J. Schlesinger, C. D. Dewhurst, R. Cubitt, L. DeBeer-Schmitt, N. D. Zhigadlo, J. Karpinski and M. R. Eskildsen
   Phys. Rev. Lett. **108**, 167001 (2012).

Acknowledgements

Measurements on UPt_3 are been carried out in collaboration with Prof. W. P. Halperin from Northwestern University. Measurements of the bulk magnetization in UPt_3 are also in collaboration with Prof. P. Dai from the University of Tennessee.

Neutron Scattering Studies of Classical and Quantum Fluids in Porous Media

Henry Glyde (glyde@udel.edu)
Department of Physics and Astronomy, University of Delaware, Newark, DE 19716

Superflow, Supersolids and Bose-Einstein Condensation

Our goal is to measure Bose-Einstein Condensation (BEC) in solid helium and in liquid helium under pressure close to solidification. The aim is both to better understand BEC and to verify the existence of superflow in solid helium. Superflow and superconductivity are a consequence of BEC.

In 2004, Kim and Chan reported a superfluid fraction in solid helium, both in bulk helium and in helium confined in porous media. This remarkable result extended superflow to the solid phase (periodic long range order). It was previously limited (and believed to be limited) to gases and liquids. They observed solid helium in a torsional oscillator (TO). Below a critical temperature T_C ~ 200 mK, a fraction of the solid decouples and ceases to oscillate with the remainder of the solid. This fraction is identified as the superfluid fraction, ρ_s/ρ. The TO technique is the tried and tested method of determining the superfluid fraction in liquid helium where ρ_s/ρ -> 1 at T -> 0 K. The ρ_s/ρ is much smaller (1 %) in the solid, appears to be associated with defects, has dissipation associated with it at higher temperatures, but a ρ_s/ρ of varying size has been reported in many laboratories. Controversy as to whether it is genuinely superflow remains.

In fluids, superflow and superconductivity follow from BEC. A macroscopic fraction of the Bosons (Cooper pairs in the superconducting case) condense into the lowest energy single particle state which can create macroscopic coherence across the sample and an energy gap that enables superflow. If there is genuine superflow there should be associated enabling BEC.

Drawing on spallation neutron sources (e.g. ISIS and more recently SNS) and on the pioneering work of Woods, Svensson and Sears and of Sokol and collaborators, we have made the current state of the art determination of the atomic momentum distribution, n(p) and the BE condensate fraction in liquid ^{4}He, in liquid ^{3}He - ^{4}He mixtures and in liquid ^{4}He films (2D) [14]. Superflow in 2D is associated with observable algebraic coherence [14]. In response to the reports of superflow in the solid, we have searched for BEC in the solid but found none (Diallo et al. Phys. Rev. Lett. 98, 205301 (2007), [8, 11]). An upper limit n_0 < 0.3 % in hcp solid ^{4}He at 40 bars, was set [11].

More recently, we have turned to measuring the condensate fraction in liquid helium under pressure up to the solidification pressure (25.3 bar) [4,5]. This shows (see Figure 1) that n_0 drops from 7.5 % at p =0 to 3 % at the solidification pressure. Extrapolation into the solid phase (not very reliable) suggests that n_0 is indeed small (but perhaps still observable) in the solid. Most recently, we have measured the temperature dependence of n_0(T) in the liquid at 24 bar on ARCS at SNS [3]. As well as determining n_0(T), this measurement shows that atomic momentum distribution n(p) at for p > 0 narrows with the onset of BEC, an effect magnified at high pressure where interatomic interaction is especially strong. It also showed that increased precision is possible on ARCS.

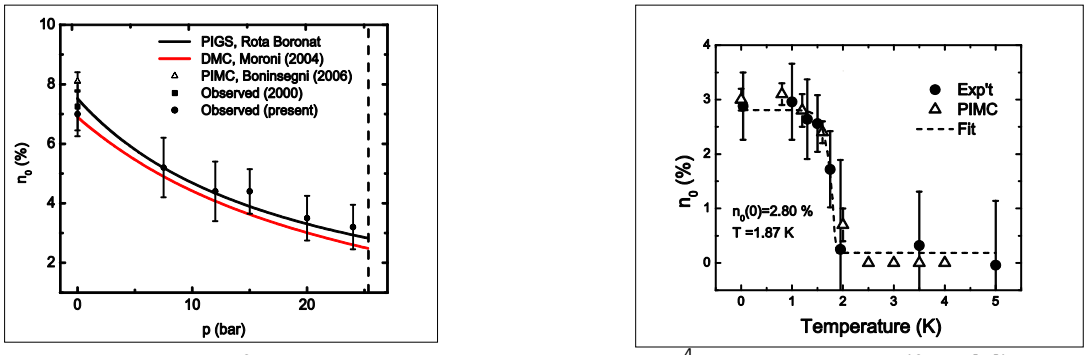

Figure 1. LHS: Condensate fraction, n_0, at low temperature in liquid ^{4}He versus pressure (from [5]). The solid circles are the present observed values. The lines are calculated values, PIGS by Rota and Boronat and DMC by Moroni and Boninsegni. RHS: Observed condensate fraction at p= 24 bar as a function of temperature (from [3]). The dashed line is a fit to the experimental data using $n_0(T) = n_0(0)[1 - (T/T_\lambda)^\gamma]$, where T_λ = 1.86 K that gives $n_0(0)$ = 2.8% and γ = 13.1. The open triangles are simulated PIMC results.

Our immediate goal now is to observe n_0 in liquid ^{4}He and then in solid ^{4}He confined in porous media (e.g. MCM-41). Firstly, in the liquid in porous media we find (see below) that the critical temperature for superflow, T_C, is separated from the onset temperature of BEC, T_{BEC} [13, 15, 16]. The T_C is suppressed below T_{BEC} by the disorder introduced by the porous media. There is a region of temperature ($T_C < T < T_{BEC}$) in which there is BEC but the BEC is localized or confined to patches or islands in the porous media [13, 15, 16]. We have islands of BEC (and local superflow) but no extended BEC or superflow across the sample as required for observable superflow in a TO. We infer the existence of BEC from the existence of well-defined phonon-roton modes. For example, in gelsil T_C appears to go to zero at 34 bar whereas measurements [13, 15] of phonon-roton modes suggest we have BEC up to T_{BEC} = 1.5 K. Our goal is to measure n_0 in the liquid directly as a function of temperature and pressure and compare $n_0(T)$ with the superfluid fraction and T_{BEC} obtained from $n_0(T)$ with the T_{BEC} inferred from P-R modes.

Secondly, a finite superfluid fraction (up to 20 %) and a finite BE condensate fraction (0.5 %) is predicted in amorphous solid helium. The same calculations predict that both ρ_s and n_0 are negligible in perfect crystalline solid helium. We have shown [9] that solid helium in smaller diameter porous media is all amorphous (no crystalline regions). A superfluid fraction is observed in solid helium in Vycor and gelsil (ρ_s/ρ = 1-1.5 %). Our goal is to observe a BE condensate fraction in amorphous solid helium in porous media (Vycor and MCM-41). Observation of BEC would be an unequivocal verification of superflow in solid helium.

Dynamics of liquid and Solid Helium in Porous Media

Both BEC and the intrinsic collective modes of liquid and solid helium are uniquely observed using neutrons. Our goal is to determine the modes and dynamics when liquid and solid helium are confined to nanoscales in porous media. Helium in porous media is clean example of Bosons in disorder. Our aim is to reveal the impact of disorder on the modes and dynamics. In the liquid it is also to determine the dependence of the P-R modes on BEC which is possible since, as noted above, T_C and T_{BEC} are separated

in porous media especially at higher pressure. In the solid the aim is to determine the dynamics of amorphous solid helium.

Phonon-roton modes and BEC in porous media: When liquid ^{4}He is confined in porous media (in disorder), T_C is suppressed to lower temperatures; for example from $T_C = T_\lambda = 2.17$ K in bulk liquid is suppressed to $T_C \approx 0.8$ -1.3 K in smaller diameter porous media at saturated vapor pressure (SVP) ($p \approx 0$). The liquid phase is also extended to higher pressure in porous media, from 25.3 bar in the bulk up to 38 bar in small pore diameter gelsils and MCM-41 (50 Å). These changes enable us to explore P-R modes to higher pressure and to determine separately the dependence of the modes on superflow and BEC.

At SVP ($p \approx 0$ bar), the P-R mode energies and widths in several porous media are found to be the same as in the bulk within precision. However, surprisingly, well-defined P-R modes are found to exist at temperatures well above T_C, up to temperatures close to T_λ. There are sound theoretical reasons why well defined P-R modes (e.g. the roton) exist only when there is BEC, but not without BEC [1]. The observation of well-defined modes up to T_λ indicates that there is BEC up to T_λ in these porous media, i.e. $T_{BEC} \approx T_\lambda$ in porous media at SVP.

More recently, we have observed [13, 15] the P-R modes as a function of pressure, up to solidification at 38 bars in gelsils and MCM-41. Above 25 bar the intensity in the P-R mode decreases with increasing pressure until there is no intensity in the mode (e.g. no roton) at solidification at 38 bar [1, 13, 15]. No rotons or other modes in that energy range are observed in the solid (amorphous) phase above 38 bar.

With new data on liquid ^{4}He under pressure p = 34 bar in MCM-41 we have shown that the P-R mode at higher wave vectors exists at low temperature only [1]. As the temperature is increased, there is a transfer of intensity from the P-R mode to new intensity at low energy. Above a specific temperature, denoted T_{BEC}, there is no longer an observable P-R mode. T_{BEC} is identified as the temperature at which P-R modes no longer exist in the liquid. Above T_{BEC}, all the intensity is at low energy which is interpreted as the response of the normal liquid (NL) where there is no BEC. A simple transfer of intensity from the P-R mode to NL response with no mode broadening is observed at 34 bar because, under pressure, (a) the P-R mode disappears at low temperature ($T_{BEC} \approx 1.5$ K) before thermal broadening of the mode becomes significant and (b) the normal liquid response lies at low energy ($E \approx 0$) that can be readily distinguished from the P-R mode. The P-R mode is therefore not simply a sharp density mode in a cold Bose liquid which broadens with increasing temperature. Rather it depends for its existence as a sharp mode on BEC. The transfer of intensity is not so clear in bulk liquid ^{4}He at lower pressure because there is mode broadening as well as intensity transfer and the P-R and NL intensities overlap in energy making it difficult to distinguish the NL response from the broadened PR mode. In the bulk liquid, the loss of BEC coincides with the loss of superflow ($T_{BEC} = T_\lambda$).

Density of States of Amorphous Solid Helium: Finally, we have measured the dynamics of amorphous solid helium in MCM-41. This shows that there are no well defined low energy modes suggestive of local or extended superflow, only a broad density of states that is similar to that observed in classical amorphous solids. A manuscript is in preparation and further measurements of the dynamics of amorphous and crystalline solid helium are in progress.

Publications (2008-12)

1. Phonon-Roton Modes in Liquid ^{4}He coincide with Bose-Einstein Condensation. J. Bossy, J. Ollivier, H. Schober, and H. R. Glyde. *Euro.Phys. Lett* (to appear June), (2012).
2. Intrinsic Mean Square Displacements of Hydrogen in Proteins. D. Vural and H. R. Glyde. *arXiv:1202.5591v1*. *Phys. Rev. E* (submitted) (2012).
3. Bose-Einstein Condensation in Liquid ^{4}He near the Liquid-Solid Line. S. O. Diallo, R. T. Azuah, D. L. Abernathy, R. Rota, J. Boronat, and H. R. Glyde. *Phys. Rev. B* **85**, 140505(R) (2012).
4. Atomic Momentum Distribution and Bose-Einstein Condensation in Liquid ^{4}He under Pressure. H. R. Glyde, S. O. Diallo, R. T. Azuah, O. Kirichek, and J. W. Taylor. *Phys. Rev. B* **84**, 184506 (2011).
5. Bose-Einstein Condensation in Liquid ^{4}He under Pressure. H. R. Glyde, S. O. Diallo, R. T. Azuah, O. Kirichek, and J. W. Taylor. *Phys. Rev. B* **83**, 100507(R) (2011). Editor's suggestion to read
6. Vibrational Dynamics of Hydrogen in Proteins. D. Vural and H. R. Glyde, *Phys. Rev. E* **83**, 031922 (2011).
7. Superflow in Amorphous Solid Helium. J. Bossy, H. R. Glyde and T. Hansen. *Research Highlight, Institut Laue Langevin Annual Report 2010*, p.74 (2011).
8. The Quest for Bose-Einstein Condensation in Solid ^{4}He. S. O. Diallo, R. T. Azuah, and H. R. Glyde. *J. Low Temp. Phys.***161**, 258 (2010).
9. Amorphous solid helium in porous media, J. Bossy, T. Hansen, and H. R. Glyde, *Phys. Rev. B* **81**, 184537 (2010) (Editor's suggestion to read).
10. Dynamics of one dimensional and two dimensional helium adsorbed on carbon nanotubes. S. O. Diallo, B. Fåk, M. A. Adams, O. E. Vilches, M. R. Johnson, H. Schober, and H. R. Glyde. *Euro Phys. Lett*. **88**, 56005 (2009).
11. Limits on Bose-Einstein condensation in confined solid ^{4}He. S. O. Diallo, R. T. Azuah, O. Kirichek, J. W. Taylor and H. R. *Glyde. Phys. Rev*. B **80**, 060504(R) (2009).
12. Superfluidity and BEC in optical lattices and porous media: A path integral Monte Carlo study. A. A. Shams and H. R. Glyde. *Phys. Rev B* **79**, 214508 (2009).
13. Excitations of nanoscale quantum liquids under pressure and the Bose glass phase. J. Bossy, J. V. Pearce, H. Schober, and H. R. Glyde. *Phys. Rev. B* **78**, 224507 (2008).

14. Bose-Einstein coherence in two-dimensional superfluid 4He. S. O. Diallo, J. V. Pearce, R. T. Azuah, J. W. Taylor and H. R. Glyde. *Phys. Rev. B* **78**, 024512 (2008).

15. Phonon-roton modes and localized Bose-Einstein condensation in liquid helium under pressure in nanoporous media. J. Bossy, J. V. Pearce, H. Schober, and H. R. Glyde. *Phys. Rev. Lett*. **101**, 025301 (2008).

16. Phonon-roton excitations and quantum phase transitions in liquid ^{4}He in nanoporous media. H. R. Glyde, J. V. Pearce, J. Bossy, and H. Schober. Recent Progress in Many Body Theories, Vol. 14, Eds. G. E. Astrakharchik, J. Boronat and F. Mazzanti, (World Scientific, Singapore, 2008) p. 411.

17. Condensate depletion in two-species Bose gases: A variational quantum Monte Carlo study. A. R. Sakhel, J. L. DuBois, and H. R. Glyde. *Phys. Rev. A* **77**, 043627 (2008).

Neutron and X-Ray Scattering Studies of the Liquid-Liquid Transition in Supercooled Confined Water and the Slow Dynamics in Biomolecular Assemblies

Sow-Hsin Chen (sowhsin@mit.edu) and Christopher E. Bertrand

Department of Nuclear Science & Engineering, Massachusetts Institute of Technology, Cambridge, MA 02139

Research Scope

We have extensively studied the thermodynamics and dynamics of supercooled water under confinement using elastic, quasi-elastic (QENS), and inelastic (INS) neutron scattering techniques. By confining water in the 1-D nano-porous silica material MCM-41-S, we can suppress the temperature of the homogenous nucleation process down to at least 150 K. We were thus able to study the anomalous properties of deeply supercooled water in the "no-man's land". We discovered the existence of a minimum in density of water (D_2O) at 210 K, which occurs in addition to the well-known density maximum at 284 K; we observed a Fragile-to-Strong dynamic crossover at T_L=225 K for the first time; we detected the appearance of boson peaks at and below the T_L. We are performing a series of measurements of the density of water as a function of temperatures along various isobars, i.e. to determine the equation of state of the confined water. This will be a decisive experiment that could prove the existence or non-existence of the liquid-liquid critical point (LLCP). We shall also use QENS and INS to further detect the crossover temperature at a series of high pressures. The objective is to map out the entire locus of the Widom line and to eventually determine the location of its end point, the LLCP.

We also plan to extend these methods to explore the slow dynamics of hydration water of the biopolymers and its relation to the so-called glass transition of the biopolymers.

We shall continue to explore the dynamics of hydration water in Portland cement paste as a function of additives and temperatures (especially at low temperatures), and establish the connection between its non-exponential relaxation behavior and the mechanical strength of the cement.

Molecular dynamics simulations, elastic neutron scattering experiments, and quasi-elastic neutron scattering experiments have shown that many hydrated protein powders undergo a "dynamic transition" at a temperature of $T_D \approx 220$ K. With increasing temperature, the onset of the dynamic transition is marked by a sharp increase in conformational flexibility, as characterized by the mean-squared displacement of the protein's constituent atoms. Below T_D, the biological function of the protein, such as enzymatic catalysis, is significantly diminished. This has lead to the suggestion that the protein dynamic transition may be closely linked to biological activity. It is notable that the dynamics of the protein hydration water also undergo a transition in the same temperature range. The enzymatic function of lysozyme also increases sharply for hydration levels above $H \approx$ 20% at the physiological temperature of 297 K. The nature and origin of the protein

dynamic transition have received significant attention in recent years, particularly in regards to the connection between the dynamic transition in the hydration water, the protein dynamic transition, and biological function.

Condensed matter systems generally exhibit collective propagating modes, which can be associated with collective vibrational, or phonon-like, excitations. The dispersion relation, damping and amplitude of these modes provide important information about the underlying dynamics of the system. Propagating modes in hydrated protein powders have received relatively little attention compared to the diffusive motion associated with the protein dynamic transition. Often times different dynamic modes coupled and interrelated. Thus, understanding the relationship between the dynamic transition and the behavior of phonon-like excitations in hydrated protein powders can provide insight into whether the high-frequency vibrational motions in the secondary structures of proteins have any bearing on biological function.

Recent Progress

Temperature dependence of the phonon dispersion relation: Phonon-like excitations in four different hydrated protein powders, lysozyme (LYS), bovine serum albumen, α-chymotrypsinogen A (CHT), and casein (Csn), have been studied using inelastic X-ray scattering at 30% hydration. Previous work on hydrated protein powders focused on the protein self-motion as probed by incoherent quasi-elastic neutron scattering. X-ray scattering is always coherent and can therefore be used to probe the collective motions in proteins. The phonon properties were extracted with a previously developed *generalized three effective eigenmode* theory. The Q-dependent intraprotein (high-Q) collective vibrational frequencies were found to exhibit a substantial softening for temperatures above T_D. Large amplitude motions with wavelengths corresponding to this Q range may be correlated with biological activity. CHT presents both secondary and tertiary structural arrangements, whereas Csn lacks tertiary structure. Both show similar phonon population levels indicating that the phonons are propagating between elements of the tertiary structure [6].

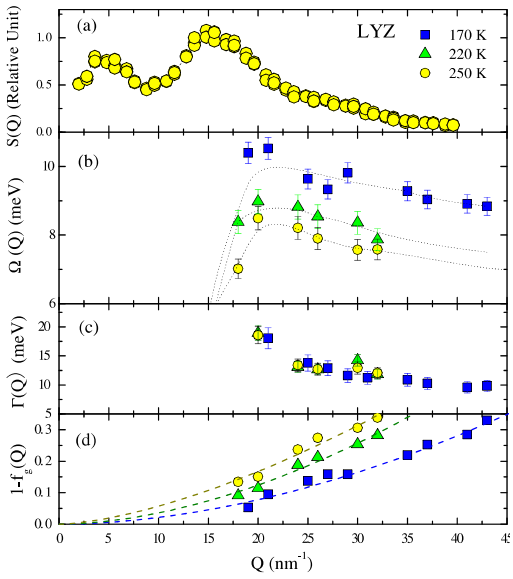

Figure 1: (a) Structure factor $S(Q)$ of LYS. We see two major peaks at Q = 5 nm^{-1} and 15 nm^{-1}. The second corresponds to the characteristic distances of the protein secondary structure. (b) Dispersion of the intraprotein phonon-like energy excitations of LYS as a function of Q, above the second major peak in the structure factor. (c) The phonon damping as a function of temperature. (d) Fractional area of the Brillouin peak (phonon population). [Liu et al. Phys. Rev. Lett. **101**, 135501 (2008)]

Hydration dependence of the phonon dispersion relation: Inelastic X-ray scattering (IXS) has also been used to investigate the intraprotein phonon-like collective excitation in

hydrated lysozyme powder at three different hydration levels H = 6%, 33% and 43% (T = 297 K). Significant softening of the phonon energy and its population enhancement are observed within the high Q, which corresponds to wavelengths in the range from 2 to 3 Å, when the threshold hydration level of H = 30% is crossed from below. This finding may give quantitative meaning to the so-called "motional flexibility" required for a globular protein to function as an enzyme.

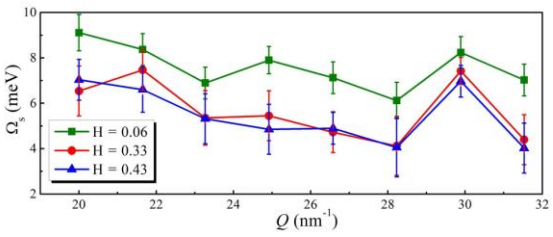

Figure 2: Measured dispersion relation of phonon-like excitations as a function of Q at three different hydration levels. Note that the phonon energies are softened significantly when crossing the minimum hydration level required for enzymatic function from H = 6% to H = 33%. This phenomenon indicates that the softening of phonon energy may be related to the onset of the enzymatic function of lysozyme [21].

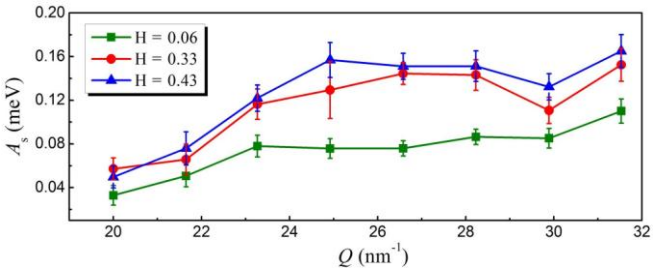

Figure 3: Fractional area of the Brillouin peaks A_s as a function of Q at three different hydration levels. The fractional area of the Brillouin peaks, which indicates the phonon population, are enhanced significantly when crossing the minimum hydration level required for enzymatic function of lysozyme from H = 6% to H = 33% [21].

Future plans

Molecular dynamics simulations: Both the hydrated protein and the protein hydration water contribute to the measured X-ray scattering. The individual contributions from the hydration water and protein dynamics cannot be resolved from these measurements; however, they are easily investigated via molecular dynamics simulations. Using a previously investigated model of hydrated lysozyme powder, we are in the process of fully investigating the connection between the phonon-like protein excitations and water dynamics as functions of both temperature and hydration level.

Publications

[1] *Microstructure determination of calcium-silicate-hydrate globules by small-angle neutron scattering*, W.-S. Chiang, E. Fratini, P. Baglioni, D. Liu, and S.-H. Chen, J. Phys. Chem. C **116**, 5055 (2012).
[2] *The dynamical crossover phenomenon in bulk water, confined water and protein hydration water*, F. Mallamace, C. Corsaro, P. Baglioni, E. Fratini, and S.-H. Chen, J. Phys.: Condens. Matter **24**, 064103 (2012).
[3] *Dyanmic crossover in hydration water of curing cement paste: the effect of superplasticizer*, H. Li, W.-S. Chiang, E. Fratini, F. Ridi, F. Bausi, P. Baglioni, M. Tyagi, and S.-H. Chen, J. Phys.: Condens. Matter **24**, 064108 (2012).

[4] *Quasi-elastic neutron scattering studies of the slow dynamics of supercooled and glassy aspirin*, Y. Zhang, M. Tyagi, E. Mamontov, and S.-H. Chen, J. Phys.: Condens. Matter **24**, 064112 (2012).
[5] *Water confined in MCM-41: a mode coupling theory analysis*, P. Gallo, M. Rovere, and S.-H. Chen J. Phys.: Condens. Matter **24**, 064109 (2012).
[6] *Phonon-like excitation in secondary and tertiary structure of hydrated protein powders*, M. Li, X.-Q. Chu, E. Fratini, P. Baglioni, A. Alatas, E. E. Alp, and Sow-Hsin Chen, Soft Matter **7**, 9848 (2011).
[7] *Density hysteresis of heavy water confined in a nanoporous silica matrix*, Y. Zhang, A. Faraone, W. A. Kamitakahara, K.-H. Liu, C.-Y. Mou, J. B. Leao, S. Chang, and S.-H. Chen, Proc. Nat. Acad. Sci. USA **108**, 12206 (2011).
[8] *Hydrogen spillover effect of Pt-doped activated carbon studied by inelastic neutron scattering*, C.-S. Tsao, Y. Liu, H.-Y. Chuang, H.-H. Tseng, T.-Y. Chen, C.-H. Chen, M.-S. Yu, Q. Li, A. Lueking, and S.-H. Chen, J. Phys. Chem. Lett. **2**, 2322 (2011).
[9] *The role of the dynamic crossover temperature and the arrest in glass-forming fluids*, F. Mallamace, C. Corsaro, H. E. Stanley, and S.-H. Chen, Eur. Phys. J. E **34**, 94 (2011).
[10] *Thermodynamical properties of glass forming systems: A nuclear magnetic resonance analysis*, F. Mallamace, C. Branca, C. Corsaro, J. Spooren, S.-H. Chen, and H. E. Stanley, J. Non-Cryst. Solids **357**, 286 (2011).
[11] *Transport properties of supercooled confined water*, F. Mallamace, P. Baglioni, C. Corsaro, J. Spooren, H. E. Stanley, and S.-H. Chen, Riv. Nuovo Cimento **34**, 253 (2011).
[12] *A possible role of water in the protein folding process*, F. Mallamace, C. Corsaro, D. Mallamace, P. Baglioni, H. E. Stanley, S.-H. Chen, J. Phys. Chem. B **115**, 14280 (2011).
[13] *Reply to Elmatad: Supercooled viscous liquids display a fragile-to-strong dynamic crossover*, F. Mallamace, C. Corsaro, S.-H. Chen, and H. E. Stanley, Proc. Nat. Acad. Sci. USA **108**, E231 (2011).
[14] *Reply to Soper: Density measurement of confined water with neutron scattering*, Y. Zhang, A. Faraone, W. A. Kamitakahara, K.-H. Liu, C.-Y. Mou, J. B. Leao, S. Chang, and S.-H. Chen, Proc. Nat. Acad. Sci. USA **108**, E1193 (2011).
[15] *Effect of catalyst size on hydrogen storage capacity of Pt-impregnated active carbon via spillover*, C.-S. Tsao, Y.-R. Tzeng, M.-S. Yu, C.-Y. Wang, H.-H. Tseng, T.-Y. Chung, H.-C. Wu, T. Yamamoto, K. Kaneko and S.-H. Chen, J. Phys. Chem. Lett. **1**, 1060 (2010)
[16] *Neutron scattering methodology for absolute measurement of room-temperature hydrogen storage capacity and evidence for spillover effect in a Pt-doped activated carbon*, C.-S. Tsao, Y. Liu, M. Li, Y. Zhang, J. B. Leao, H.-W. Chang, M.-S. Yu, and S.-H. Chen, J. Phys. Chem. Lett. **1**, 1569 (2010).
[17] *Probing the room temperature spatial distribution of hydrogen in nanoporous carbon by use of small-angle neutron scattering*, C.-S. Tsao, M. Li, Y. Zhang, J. B. Leao, W.-S. Chiang, T.-Y. Chung, Y.-R. Tzeng, M.-S. Yu, and S.-H. Chen, J. Phys. Chem. C **114**, 19895 (2010).
[18] *Transport properties of glass-forming liquids suggest that dynamic crossover temperature is as important as the glass transition temperature*, F. Mallamace, C. Branca, C. Corsaro, N. Leone, J. Spooren, S.-H. Chen, and H. E. Stanley, Proc. Nat. Acad. Sci. USA **107**, 22457 (2010).
[19] *Dynamic crossover phenomenon in confined water and its relation to the liquid-liquid critical point: experiments and MD simulations*, S.-H. Chen and Y. Zhang, Varenna lecture one presented at the International School of Physics "Enrico Fermi" on June 29th 2010 (published as a book chapter in 2012)
[20] *Dynamics of biopolymers and their hydration water studied by neutron scattering*, S.-H. Chen, X.-Q. Chu, and M. Lagi, Varenna lecture two presented at the International School of Physics "Enrico Fermi" on June 29th 2010 (published as a book chapter in 2012)
[21] *Softening and enhancement of the phonon-like excitation within certain Q range in lysozyme when crossing the minimum hydration level required for its enzymatic function*, Z. Wang, C. E. Bertrand, W.-S. Chiang, E. Fratini, P. Baglioni, A. Alatas and S.-H. Chen, (to be published)

Poster Sessions

Poster Session I

1. **Terahertz Excitations in the 1D Ising Chain Quantum Magnet $CoNb_2O_6$**
   N.P. Armitage, C.M. Morris, S. Koophayeh, R. Valdes Aguilar and C. Broholm, Johns Hopkins University

2. **Photoelectron Spectroscopy of Transuranics**
   John Joyce, T. Durakiewicz and K.S. Graham, Los Alamos National Laboratory

3. **Quantum Strings in Quantum Spin Ice**
   Yuan Wan and Oleg Tchernyshyov, Johns Hopkins University

4. **Emergent Phenomena in Novel Materials and Functionality Control: Characterization at Multiple Length and Time Scales**
   Shinichiro Yano and Despina Louca, University of Virginia

5. **Impurity Scattering, Reconstructed Nesting and Density Wave Diagnostics in Iron Pnictides**
   Zlatko Tesanovic, Johns Hopkins University

6. **Charge Stripe Order at High Pressure**
   Markus Huecker, G. D. Gu, and J. M. Tranquada, Brookhaven National Laboratory
   M. von Zimmermann, HASYLAB at DESY, 22603 Hamburg, Germany
   Wolf Schottenhamel, Leibniz Institute for Solid State and Materials Research, 01069 Dresden, Germany

7. **Understanding Pu- and Ce-Based "115s"**
   Marc Janoschek and Filip Ronning, Los Alamos National Laboratory

8. **ARCS – The Wide Angular-Range Chopper Spectrometer at the Spallation Neutron Source**
   D.L. Abernathy, M. B. Stone, Oak Ridge National Laboratory

9. **SEQUOIA: The Fine Resolution Thermal to Epithermal Neutron Spectrometer at the SNS**
   G. E. Granroth and A. I. Kolensnikov, Oak Ridge National Laboratory

10. **The Cold Neutron Chopper Spectrometer at the Spallation Neutron Source – Review of the first three years of User Operation**
    Andrey Podlesnyak and Georg Ehlers, Oak Ridge National Laboratory

11. **The Nanoscale Ordered MAterials Diffractometer (NOMAD) at the SNS: A Fast Neutron Diffractometer for Pair Distribution Function (PDF) Determinations**
    Jörg Neuefeind, Oak Ridge National Laboratory

12. **Recent Development of the HYSPEC Instrument at the SNS**
    A. Zaliznyak, S. M. Shapiro, D. Fobes and J. M. Tranquada, Brookhaven National Laboratory, M. Hagen, A. Savici, B. Winn, M. Graves-Brooks, M. Lumsden, Oak Ridge National Laboratory

13. Recent Development of the TOPAZ Single-Crystal Diffractometer at the SNS
Xiaoping Wang and Christina Hoffmann, Oak Ridge National Laboratory

14. Development of a High-Energy X-ray Precession Camera at the Advanced Photon Source
A. *I. Goldman, A. Kreyssig, D. K. Pratt and R. J. McQueeney, Ames Laboratory and Dept. of Physics and Astronomy, Iowa State University, Ames, Iowa*
D. S. Robinson and J. C. Lang, Advanced Photon Source, Argonne National Laboratory

Poster Session II

15. Neutron Compton Scattering as a Probe of Hydrogen Bonded (and Other) Systems
George Reiter, University of Houston

16. Novel Molecular Materials for Hydrogen Storage Applications
Maddury Somayazulu, Robert Potter, Timothy Strobel,Viktor Struzhkin and Russell J Hemley, Geophysical Laboratory, Carnegie Institution of Washington, Washington DC. Raja Chellappa, Los Alamos National Laboratory

17. Materials for Energy Applications
O. Chmaissem, S. Avci, B. Dabrowski, Northern Illinois University
S. Rosenkranz and, R. Osborn, Argonne National Laboratory

18. Polythiophene-Fullerene Phase Behavior and Effects on Organic Photovoltaic Device Performance
David Bucknall, Georgia Tech.Alamgir Karim, Jose Chapa Garza, Gurpreet Singh, Xiong Gong, University of Akron. Dharmaraj Raghavan, Praveen Pitliya, Shimelis Hailu, Paul Hudrlik, Anne Hudrlik, Howard University, Scott Sides, TECH-X Corporation, Boulder, CO and B Sumpter, Oak Ridge National Laboratory

19. Dynamics of Ionic Polymers at Interfaces: Key to Enhanced Longevity of Clean Energy Devices – Neutron Scattering and Molecular Dynamics Simulation Studies
Dvora Perahia, Naresh Osti, Thusitha Etampawala, Flint Pierce, Clemson Univeristy and Gary S. Grest, Sandia National Laboratory

20. Application of In Situ Neutron Diffraction to Understand the Mechanism of Phase Transitions during Electrochemical Cycling of High Capacity Mg/Si Nanostructured Electrodes
K. S. Ravi Chandran, University of Utah

21. Neutron and X-ray Scattering Group: Developments Enabling Science
S. Rosenkranz, R. Osborn, S.G.E. te Velthuis, U. Perez-Salas, G.P. Felcher, J.-P. Castellan and F. Weber, Argonne National Laboratory

22. Development of Grazing Incidence Optics for Neutron Imaging and Scattering
M. V. Gubarev, B. D. Ramsey, K. Kilaru, Marshall Space Flight Center, NASA, VP62, Huntsville, AL 35812,B. Khaykovich, D. Liu, D. E. Moncton, Nuclear Reactor Laboratory, Massachusetts Institute of Technology, 138 Albany St., Cambridge, MA 02139,V. E. Zavlin Universities Space Research Association, 320 Sparkman Drive, Huntsville, AL35805,S. Romaine, R. E. Rosati, R. Bruni, Harvard-Smithsonian Center for Astrophysics, 60 Garden Street, Cambridge, MA 02138

23. Small-Angle Neutron Scattering at Oak Ridge National Laboratory
William T. Heller, Kenneth C. Littrell, Changwoo Do, Christopher B. Stanley, Yuri B. Melnichenko, Lilin He, Carrie Y. Gao, Katherine Bailey, Neutron Sciences Directorate, Oak Ridge National Laboratory

24. Recent Advances in High Pressure Neutron Diffraction at Oak Ridge National Laboratory
Chris A. Tulk, A. M. dos Santos, J. J. Molaison, N. Pradhan, Oak Ridge National Laboratory

25. Neutron Reflectometry Capabilities and Research at the Spallation Neutron Source
John F. Ankner, Valeria Lauter, and James F. Browning, Neutron Sciences Directorate, Oak Ridge National Laboratory

26. National School on Neutron and X-ray Scattering
Suzanne G.E. te Velthuis, Jonathan C. Lang, Argonne National Laboratory
Bryan C. Chakoumakos, John D. Budai, Oak Ridge National Laboratory

27. Los Alamos Neutron Science Center (LANSCE) School on Neutron Scattering
James J. Rhyne, Lujan Center, Los Alamos National Laboratory, Los Alamos, NM 87545
Heinz Nakotte, Physics Department, New Mexico State University, Las Cruces, NM 88003

Poster Abstracts

TERAHERTZ EXCITATIONS IN THE 1D ISING CHAIN QUANTUM MAGNET $CoNb_2O_6$

N.P. Armitage,[‡] C.M. Morris, S. Koophayeh, R. Valdes Aguilar, C. Broholm
Department of Physics and Astronomy, Institute for Quantum Matter, The Johns Hopkins University, Baltimore, MD, USA

The one-dimensional magnet $CoNb_2O_6$ was recently demonstrated to be an excellent realization of a one-dimensional quantum Ising spin chain. It has been shown to undergo a quantum phase transition in a magnetic field oriented transverse to its ferromagnetically aligned spin chains by Coldea et al. Low energy spin-flip excitations in the chains were recently observed via inelastic neutron scattering and shown to have a interesting energy scaling governed by symmetries of the E8 exceptional Lie group. Here, time-domain terahertz spectroscopy (TDTS) is used to investigate optically active low energy excitations in $CoNb_2O_6$. We take advantage of the polarization sensitivity of this technique to characterize both electric and magnetic dipole active excitations in this compound. A connection is made from the q=0 response observed here to the excitations observed by neutron scattering. In addition, we will show results on the terahertz spectra of this material as it undergoes the magnetic field-tuned quantum phase transition and discuss its relevance to the symmetries of the E8 group.

[‡] npa@pha.jhu.edu

Photoelectron Spectroscopy of Transuranics

J.J. Joyce (jjoyce@lanl.gov), T. Durakiewicz and K.S. Graham
Los Alamos National Laboratory, Los Alamos, NM 87545

Program Scope

The goal of this program is to advance the understanding of actinide (An) materials through focused experiments on select actinides and to couple these experiments to innovative theories for electronic structure. In complex electronic materials, actinides straddle the middle ground between more itinerant transition metal materials and more localized rare-earth materials. There is a transition from Friedel-like bonding of the 5f electrons in the early actinide elements, to localized, rare-earth-like f-electron character in the actinides beyond Pu. The central focus in understanding An materials is a detailed knowledge of the 5f electrons. This program uses photoelectron spectroscopy (PES) techniques to isolate and quantify the role of 5f electrons in the electronic structure of actinide materials with an emphasis on Pu. The emphasis on Pu is driven by the nature of the 5f electrons in actinides. Plutonium is the transition point in the element series between localized and itinerant 5f electron character. Additionally, there is a wide range of strongly correlated electron properties in Pu compounds including; superconductivity in $PuCoGa_5$, $PuCoIn_5$, and $PuRhIn_5$, covalency in the Mott insulator PuO_2, as well as magnetic signatures in Pu intermetallic compounds. These Pu compounds have interesting counterparts in uranium as well as in some rare-earths, so we incorporate U, Yb and Ce compounds to elucidate the nature of 5f electronic structure. This program is a subtask of the larger and more broad-ranging Complex Electronic Materials program lead by Joe Thompson at LANL.

We draw on the unique transuranic single crystal growth capabilities available at Los Alamos (both intermetallic Pu compounds and Mott insulators) as well as theoretical research on actinides. Using a range of PES approaches, including angle-resolved photoelectron spectroscopy (ARPES), resonance photoemission (RESPES), temperature dependent PES and high energy PES, this program provides detailed spectroscopic information necessary for development and validation of electronic structure models beyond an independent particle approach. Models for these materials include the dynamical mean field theory (DMFT) and the hybrid functional model with recent work on a fluctuation exchange approximation (FEA) model. The transuranic ARPES capability within this program is the only such capability in the world and thus provides unique insight into the electronic structure of transuranic materials.

Recent Progress

Localization in $PuCoGa_5$ and $PuCoIn_5$: Our original angle-integrated PES research on the 18.5 K superconductor $PuCoGa_5$ published in 2003 indicated a dual nature to the 5f electrons with some 5f spectral weight localized 1 eV or more below the Fermi energy while a smaller fraction of 5f intensity was near the Fermi energy and presumed itinerant. With the discovery of isoelectronic $PuCoIn_5$ which has a 25% larger volume than $PuCoGa_5$, we are able to probe the localized/itinerant 5f boundary. New

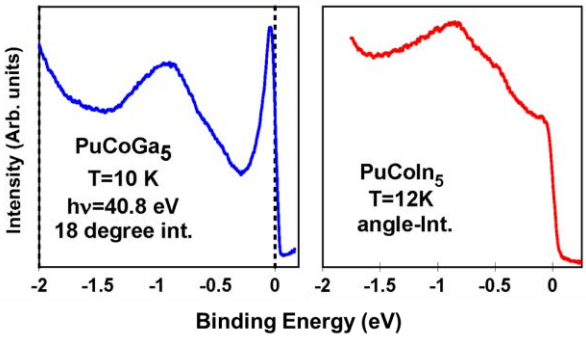

Figure 1: Valence band PES for $PuCoGa_5$ and $PuCoIn_5$ at 40.8 eV.

results on $PuCoGa_5$ along with first PES on $PuCoIn_5$ are presented in Figure 1 and show clear indication of 5f localization moving from $PuCoGa_5$ to $PuCoIn_5$. The 5f spectral intensity located at the Fermi surface (dashed line) in $PuCoGa_5$ is removed from the Fermi level in $PuCoIn_5$ and shifted to the localized manifold 1 eV below the Fermi energy. We have an ongoing collaboration which will provide DMFT and new FEA calculations for $PuCoM_5$ including energy vs. momentum dependence to be directly compared with our ARPES data.

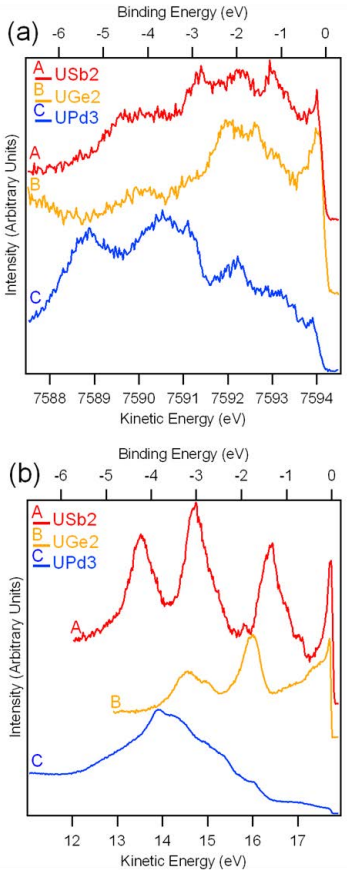

Figure 2: a) High energy PES (HAXPES) at 7.6 KeV, b) low energy ARPES at 22 eV.

ARPES and HAXPES for U systems: Spectroscopy on strongly correlated uranium materials include URu_2Si_2,USb_2, UGe_2 and the most localized uranium compound UPd_3. Research addresses the nature of 5f localization as well as magnetism and hidden order. Figure 2 shows HAXPES at 7.6 keV compared to PES at 22 eV. The same spectral features are seen in the valence band of the three materials through a photon energy range of 7600 eV. With the much greater mean-free-path of photoelectrons for 7.6 keV, the samples were introduced from air and measured without surface preparation. We have Pu analogs for many uranium materials in order to establish systematics across families of related materials. Access to the public synchrotrons for uranium research enables a broader range of spectroscopies with the full range of RESPES, ARPES and HAXPES. With high energy resolution and broad photon energy ranges we are able to determine the self-energy for some uranium systems providing a quantitative assessment of the electronic structure and motivating new developments for 5f theory including the FEA approach now being used for Pu and U intermetallic compounds.

Delta Pu electronic structure: There are two important concepts related to the electronic structure of intermetallic Pu materials. The first is a localization/delocalization boundary or dual nature for the 5*f* electrons in Pu materials while the second is valence fluctuation involving $5f^5$ and $5f^6$ configuration. Our new data for delta phase Pu (δ-Pu) show both the localization/delocalization boundary and the valence fluctuation involving $5f^5$ and $5f^6$ configuration. The temperature dependence for δ-Pu shown in Figure 3 demonstrates a link between the measured photoemission spectra and the ground state of material. The temperature dependence in δ-Pu between 20 and 210 K is completely consistent with the Fermi function acting on a spectral feature which is 100 meV wide and 20 meV below the Fermi energy (E_F) in the ground state of the system. We also observed a similar temperature dependence in 40.8 eV spectra favoring 5*f* orbital cross-sections. A range of simulations was run with peak widths ranging from 200 to 50 meV and binding energies ranging from -50 meV to +50 meV with respect to E_F.

The symmetric crossing point in the PES data as a function of temperature at E_F, gives a strong indication that there is little if any temperature dependence beyond that attributed to the Fermi function. Many-body resonances often exhibit energy shifts and exaggerated asymmetric broadening beyond the conventional Fermi function effects. This analysis doesn't account for phonon broadening which can have a substantial effect on peak height as opposed to integrated

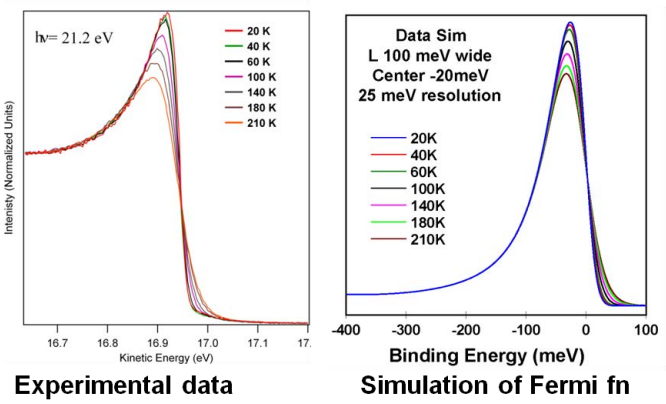

Figure 3: Left: PES as a function of temperature for delta Pu. Right: Temperature simulation using only the Fermi function on a narrow peak just below the Fermi energy.

spectral intensity. The results for Fig. 3 indicate a narrow quasiparticle peak for δ-Pu just below E_F with no substantive temperature dependence beyond that attributable to the Fermi function.

Actinide oxide ARPES and models: Photoemission was undertaken to quantify the electronic structure of key members of the AnO_2 family of Mott insulators and provide input to new computational schemes to address the Mott insulator problem in actinides. The An oxides are Mott insulators, thus density functional theory (DFT) fails to predict the insulating character of these materials since DFT does not account for the substantial Coulomb correlation of the 5f electrons.

Establishing a single crystal thin film capability at LANL for the AnO_2 system (not funded by this program) was essential since there are no bulk single crystals of PuO_2 available for ARPES (mm size) but it is now possible to grow large area single crystal thin (50nm) films of PuO_2 as well as UO_2. The agreement between model and our experiment is very good, showing the ionic character of UO_2 as well as the change in character to covalent bonding moving to PuO_2. In PuO_2, the separation between the An 5f states and the O 2p states has gone to zero and there is then strong intermixing between the 5f and 2p states. The angle-integrated PES largely substantiated this model but it was necessary to directly observe the 5f and 2p intermixing in order to validate the model predictions. Our ARPES data for PuO_2 provided the direct experimental evidence of this orbital state mixing. The unique ARPES in actinides has played a significant role in the development of an effective model for family of AnO_2 Mott insulators which span the range from ionic to covalent insulators.

Future Plans

Having established a transuranic ARPES capability, there are four groups of materials which require substantial experimental research over the next few years. The first category ripe for exploration is the $PuTM_5$ (T=Co, Rh, M=Ga, In) family. With new ARPES on $PuCoGa_5$ indicating itinerant character of the peak near the Fermi energy and preliminary data on $PuCoIn_5$, we need to map out the Fermi surface of $PuCoM_5$ materials and quantify the role of the 5f electrons in the Fermiology of this superconducting family. Additionally, we will begin a detailed investigation of the superconductors $PuRhGa_5$ and $PuRhIn_5$. The $PuTM_5$ family of materials will be compared against DMFT as well as new FEA model calculations. Second, the actinide oxides will require a sustained effort to quantify the electronic structure and validate theoretical efforts using the hybrid functional approach. The ARPES data for PuO_2 show good agreement with hybrid functional calculations, details for quenching magnetic solutions in the calculations are the only impediment to major publications. A broader range of ARPES experiments including a range of photon energies will complete work on PuO_2. Research on Pu_2O_3 and NpO_2 as cross-over materials will be undertaken using both ARPES and XPS to follow the transition from ionic (UO_2) to covalent (PuO_2) character in the series of the actinide oxides. The third system is PuTe, where we will conduct temperature dependent PES studies and

compare the results with recent dynamical mean field theory predictions of a strong temperature dependence to the three-peak structure near E_F [Yee, *et. al*, PRB, **81**, 035105 (2010)]. We will also explore the recent prediction of a topological insulator state in PuTe [Zhang, *et. al*, Science **335**, 1464 (2012)]. PuTe is a starting point for the interesting actinide chalcogenides which, in the Pu monochalcogenides, exhibit a three peak structure associated with the most localized 5f electron configurations. The fourth group of materials for study is Pu metal, both in the alpha phase and the cubic delta phase. For the Pu metal research we will focus on temperature dependent PES using the new capability of our transuranic system, exploring details of electron-phonon coupling requiring higher energy resolution than current results. A stretch goal would be determining the electronic structure of δ-Pu through ARPES but we still don't have single crystals of δ-Pu of sufficient size for ARPES. Preliminary temperature dependent results on δ-Pu look promising and we now have access to our first alpha Pu sample in over twelve years.

Publications (2011-2012)

1. Tanmoy Das, Tomasz Durakiewcz, Jian-Xin Zhu, John J. Joyce, John L. Sarrao, Matthias J. Graf, " Imaging the formation of high-energy dispersion anomaly in the actinide $UCoGa_5$", Physical Review-X, *re-submitted* (2012).
2. Tanmoy Das, Jian-Xin Zhu, Tomasz Durakiewicz, John J. Joyce, and Matthias J. Graf, "Materials specific electronic correlation effects and spectral weight 'hot spots' in intermetallic actinides **",** Mat. Res. Soc. Symp. Proc. *accepted* (2012).
3. Miles Beaux II, John Joyce, Tomasz Durakiewicz, Kevin Graham, Eric D. Bauer, Jeremy Mitchell, Paul Tobash, and Scott Richmond, "Electronic Structure, Localization and 5*f* Occupancy in Pu Materials", Mat. Res. Soc. Symp. Proc. *accepted* (2012).
4. Eve Bauer, Tony Burrell, Mark McCleskey, Brian Scott, Quanxi Jia, Tomasz Durakiewicz, John Joyce, Kevin Graham, Stosh Kozimor, Steve Conradson, and Richard Martin, Lindsay Roy, Gustavo E. Scuseria, "The Localization-Delocalization Dilemma: The Electronic Structure of *f*-Element Oxides", Actinide Research Quarterly, *accepted* (2012).
5. T. Klimczuk, C.H. Wang, J.M. Lawrence, Q. Xu, T. Durakiewicz, F. Ronning, A. Llobet, F. Trouw, N. Kurita, Y. Tokiwa, Han-oh Lee, C. H. Booth, J.S. Gardner, E.D. Bauer, J.J. Joyce, R. Movshovich, R.J. Cava, and J.D. Thompson, "Crystal fields, disorder, and antiferromagnetic short-range order in $(Yb_{0.24}Sn_{0.76})Ru$," Phys. Rev. B **84**, 075152 (2011).
6. C.H. Booth, T. Durakiewicz, C. Capan, D. Hurt, A.D. Bianchi, J.J. Joyce, and Z. Fisk, "Electronic structure and *f*-orbital occupancy in Yb-substituted $CeCoIn_5$", Phys. Rev. B, **83**, 235117 (2011).
7. M.F. Beaux II, T. Durakiewicz, L. Moreschini, M. Grioni, F. Offi, G. Monaco, G. Panaccione, J.J. Joyce, E.D. Bauer, J.L. Sarrao, M.T. Butterfield, E. Guziewicz, " Electronic structure of single crystal UPd_3, UGe_2, and USb_2 from hard X-ray and angle-resolved photoelectron spectroscopy", J. Electr. Spectr. Rel. Phenom., **184**, 517 (2011).
8. J.J. Joyce, T. Durakiewicz, K.S. Graham, E.D. Bauer, D.P. Moore, J.N. Mitchell, J.A. Kennison, R.L. Martin, L.E. Roy, and G.E. Scuseria, "Pu Electronic Structure and Photoelectron Spectroscopy"**,** J. of Phys. Conf. Ser., **273**, 012023 (2011).
9. T. Durakiewicz, J.J. Joyce, Y. Li, P.S. Riseborough, P.M. Oppeneer, E.D. Bauer, K.S. Graham, "Band renormalization effects in correlated f-electron systems", J. of Phys. Conf. Ser., **273**, 012029 (2011).

Quantum strings in quantum spin ice

Yuan Wan and Oleg Tchernyshyov
Johns Hopkins Institute for Quantum Matter

Spin ice is a highly frustrated ferromagnet displaying rich emergent phenomena. In its ground states, magnetization of spin ice satisfies a zero-divergence constraint leading to an effective cancellation of the internal magnetic field. Spin excitations violate this constraint and thus behave as magnetic monopoles.

Strong quantum fluctuations in spin-ice materials such as $Tb_2Ti_2O_7$ [1] and $Yb_2Ti_2O_7$ [2] may produce qualitatively new physics. I will discuss the nature of low-energy excitations in quantum spin ice in the presence of spontaneous magnetization or an external magnetic field along the $\langle 100 \rangle$ direction [3,4]. When monopoles are confined by the magnetic field or the effective molecular field, elementary excitations are Dirac strings connecting pairs of monopoles (Fig.1) [5]. In contrast to classical spin ice, where string dynamics are driven by thermal fluctuations, strings in quantum spin ice possess inherent quantum dynamics that can be described by an emergent quantum string theory. When quantum fluctuations are weak, the vibrational modes of quantum string are manifested as multiple resonances in the dynamical structure factor. Strong fluctuations make the string tension negative and destabilize the polarized ground state. As the external field is increased, the strings gradually evolve to magnons, and the effective theory reduces to conventional spin wave theory [6].

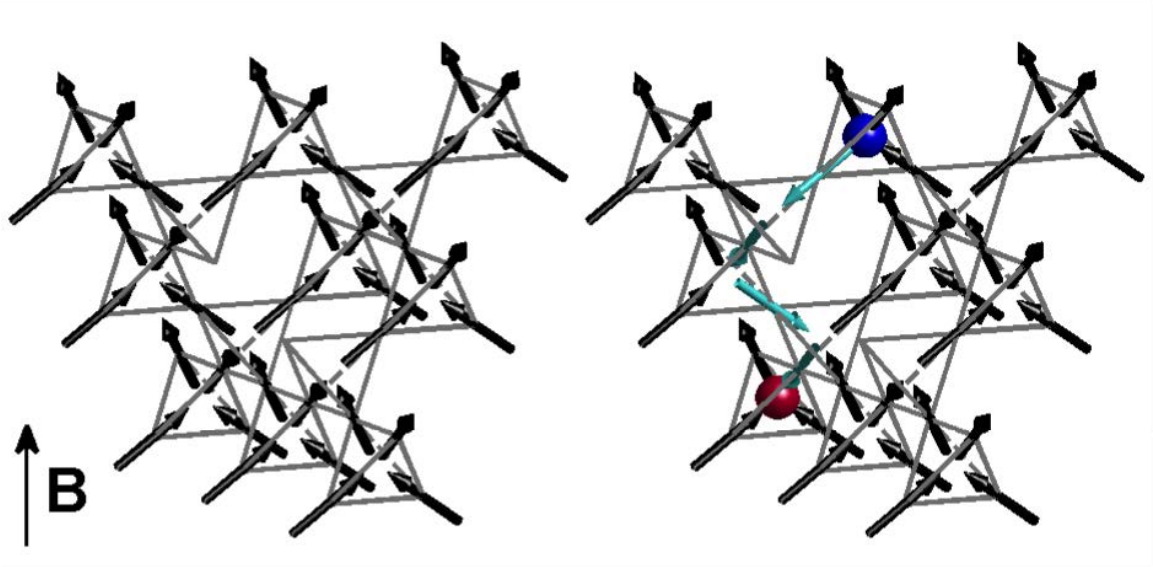

[1] H. R. Molavian, M. J. P. Gingras and B. Canals, Phys. Rev. Lett. **98**, 157204 (2007).
[2] K. A. Ross, L. Savary, B. D. Gaulin, and L. Balents, Phys. Rev. X **1**, 021002 (2011).
[3] L.-J. Chang, S. Onoda, Y. Su, Y.-J. Kao et al, arXiv:1111.5406.
[4] R. Applegate, N. R. Hayre, R. R. P. Singh, T. Lin et al, arXiv:1203.4569.
[5] L. D. C. Jaubert, J. T. Chalker, P. C. W. Holdsworth, and R. Moessner, Phys. Rev. Lett. **100**, 067207 (2008).
[6] Y. Wan and O. Tchernyshyov, arXiv:1201.5314.

Emergent Phenomena in Novel Materials and Functionality Control: Characterization at Multiple Length and Time Scales

Despina Louca
University of Virginia

1) Program scope:

The emergence of exotic states arising from the intricate coupling of the electronic and lattice degrees of freedom is a unique feature in strongly correlated electron systems. Such states cannot be readily characterized with traditional means used for probing single electron behavior. This is because their behavior is a collective effect, in response to strong interactions, and unless new methodologies are implemented to describe such novel phenomena, the predictive capabilities of our theoretical tools will fail. A well-known example is that of a Mott insulator for which band theory predicts it to be a metal but is instead insulating. We now know that a combination of *d-d* correlations, charge transfer and hybridization is what makes most transition metal oxides insulating. The goal of the proposed program is to explore such states of matter that appear to be endemic to oxide and intermetallic compounds.

In this program, we have focused on experimentally identifying the local microstructure, the distortions invoked by magnetic interactions, the effects of orbital hybridization and crystal phase transitions, local and global distortions and of their role in materials functionality and phase transitions in a wide class of materials. In this approach, we identify the nature of spin correlations and of their role in spin-charge and -lattice interactions by varying temperature, magnetic field, pressure and magnetic ion doping, and characterize magnetic incommensurabilities by altering the chemistry of the material in question. Furthermore, we attempt to develop an understanding into how different electronic, magnetic and structural order parameters compete and co-exist and how they can lead to phase separation. In doing so, we implement both neutron and X-ray scattering techniques at national and international facilities that allow us to probe structures and dynamics at different length and time scales.

2) Recent progress:

Magnetopolaron formation and field-induced melting in $LaCo_{1-y}Ni_yO_3$

Dilute magnetic ion doping in $LaCo_{1-y}Ni_yO_3$ with $y \leq 1\%$ leads to the formation of isotropic magnetic clusters that exhibit intra-cluster interactions with ferromagnetic character, in an analogous way to dilute magnetic semiconductors and molecular magnets. The clusters are comprised of Ni ions surrounded by six magnetically polarized Co ions. The Ni spin is delocalized from the Ni^{3+} ion but is confined in the vicinity of the six coordinated environment forming small magnetopolarons. The cluster ground state is estimated from bulk magnetization to be about $gS \sim 10$, in contrast to $LaCoO_3$ which is not magnetic. Using neutron spectroscopy, we observed two new transitions between the lowest energy levels indicating that the ground state is split (Fig. 1). Under a magnetic

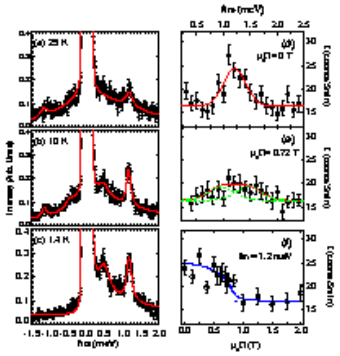

Fig. 1: (a-c) The temperature dependence from a single crystal of LCNO (y=0.005) measured at CNCS. Field dependence of the inelastic intensity from a powder sample of LCNO (y=0.01) at Q=1.65 $Å^{-1}$ measured at SPINS under is shown in (d) at 0 T, (e) at 0.72 T and (f) as a function of field. The data were integrated over $0.4 < L < 1.0$ r.l.u. and a limited range of H (varying from about a -0.1 to 0.3).

field of 1 Tesla, the transitions are suppressed possibly in response to the increase in the Zeeman splitting (Fig. 1). With increasing temperature, the intra-cluster transitions are overshadowed by the activation of Co^{3+} ions to the intermediate spin state.

Possible link of a structurally-driven spin flip with the insulator-metal transition in the perovskite $La_{1-x}Ba_xCoO_3$

The nature of the magnetic ground state near the insulator-metal transition (IMT) in $La_{1-x}Ba_xCoO_3$ was investigated via neutron diffraction. Below the critical concentration, $x_c \sim 0.22$, a commensurate antiferromagnetic (AFM) phase appears initially. Upon approaching x_c, the AFM component weakens and a ferromagnetic (FM) ordered phase sets in while in the rhombohedral lattice. At x_c, a spin flip to a new FM structure occurs at the same time as the crystal symmetry transforms to orthorhombic (Pnma). The Pnma phase may be the driving force for the IMT. In Fig. 3, the three different magnetic phases are shown while in Fig. 4, the phase diagram reveals the complexity of this system arising from Ba doping.

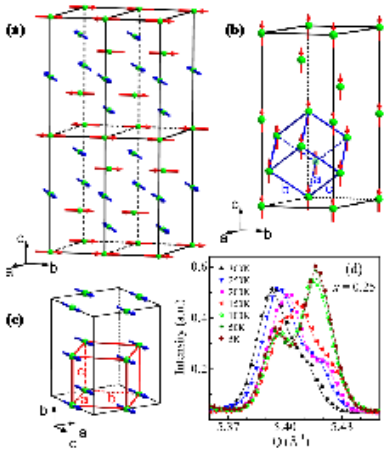

Fig. 3: (a) The AFM cell in the R3c phase. The moments are in the $(001)_R$ plane. The moment on Co_1 is along $(010)_R$, while the moment on Co_2 is either along $(110)_R$ or $(1\bar{1}0)_R$. (b) The FM cell in the R3c phase. The moments on both Co sites are along $(001)_R$. (c) The new FM cell in the Pnma phase. The Co moments are along the $(001)_O$. (d) The temperature dependence of the diffraction pattern at x=0.25.

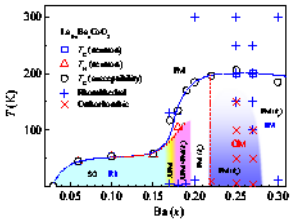

Fig. 4: The phase diagram of $La_{1-x}Ba_xCoO_3$ ($0.03 \leq x \leq 0.50$) was constructed from neutron and bulk susceptibility measurements. When $x \geq 0.17$, the FM and AFM magnetic phases become long-range. For $x \geq 0.2$, only FM order exists. The nuclear symmetry is R3c for $x \leq 0.20$. The R3c to Pnma transition is observed in x = 0.22, 0.25 and 0.27.

Evidence of local disorder in the overdoped regime of $Ba(Fe_{1-x}Co_x)_2As_2$

The appearance of superconductivity in $BaFe_2As_2$ with Co doping coincides with a phase transition from an orthorhombic to a tetragonal structure where coexistence of the two is observed near the phase boundary. Overdoping brings suppression of T_C near x=0.12 that is not accompanied by a transition back to the orthorhombic phase. Using pulsed neutron powder diffraction, the relation of superconductivity to the atomic structure in the overdoped regime has been investigated. The suppression of superconductivity is accompanied by a structural local distortion around Co. The distortion, described as a breathing mode with alternating two or four Fe ions displaced towards Co in the ab-plane, sets in above T_C and remains in place below (see Fig. 5).

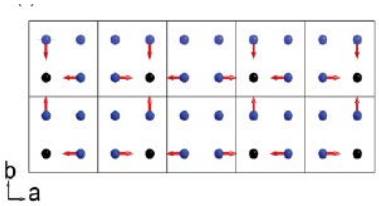

Fig. 5: Only the Fe/Co atoms are shown for simplicity in the ab-plane. The black spheres correspond to Co atoms, and the blue ones correspond to Fe atoms. Arrows indicate the direction of displacement of the Fe atoms

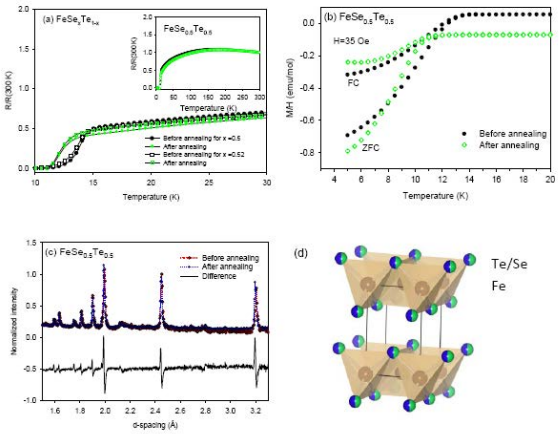

Fig. 6: (a) A plot of the resistance normalized to the room temperature value for two of the samples, the x = 0.5 and 0.52. A reduction in T_C is observed for both samples. (b) The M/H curve for the annealed and as prepared sample of x = 0.5 sample shows the same transitions as the resistance plot. (c) The diffraction patterns compared before and after annealing in the x = 0.5 composition. The peaks become sharper and shift to the left after annealing. d) The crystal structure shown with the Se and Te sharing the same site.

Suppression of superconductivity in Fe chalcogenides by annealing: a reverse effect to pressure

Superconductivity in $FeTe_{1-x}Se_x$ can be controlled by annealing, in the absence of extrinsic influences. Using neutron diffraction, we show that T_C sensitively depends on the atomic configurations of the Te and Se ions. Low temperature annealing not only homogenizes the Te and Se ion distribution, it suppresses T_C because of changes in the chalcogen ions' z-parameter (Fig. 6). In particular, the height of Te from the Fe basal plane is much reduced while that for Se shows a modest increase. These trends are reverse of the effects induced by pressure. Previous studies on the Fe-based superconductors have focused on the effects of the z-parameter early on. However, no study has been performed on a single composition to monitor the evolution of the physical properties while changing the z-parameters, without introducing foreign atoms or applying pressure. All studies have focused on different compositions. In our study, we annealed to homogenize the sample without any external influences. The small compositional fluctuation resulting from the homogenization should raise T_C according to the well developed phase diagrams. But this is not what is happening. The change of the Se ion coordinates (i.e. height and angle) is small, while the change of the Te ion coordinates is large and is the dominant factor that changes the physical properties. Our results clearly demonstrate the effect of the Te-height on the properties

Dynamics of the local structure of $FeSe_xTe_{1-x}$ determined by inelastic neutron scattering

The dynamics of the local atomic correlations in the local structure of $FeSe_xTe_{1-x}$ (x = 0.1, 0.5, and 0.9) were investigated using the dynamic pair density function analysis. Superconducting and non-superconducting compositions were measured above and below the superconducting transition temperature using an E_i of 242 meV which allowed us to reach a momentum transfer of 22 $Å^{-1}$. The dynamics in the local structure of the three compositions change in the way shown in Fig. 8. The six panels depict the energy integrated ρ(r,E) in increments of 12 meV and plotted up to 40 meV and 5 Å. In the non-superconducting Te-rich x = 0.1 composition, the first nearest Fe-Fe correlations are enhanced with cooling. This may in turn be related to the enhanced magnetism observed in this part of the phase diagram. On the other end, in the Se-rich x = 0.9 superconducting composi-

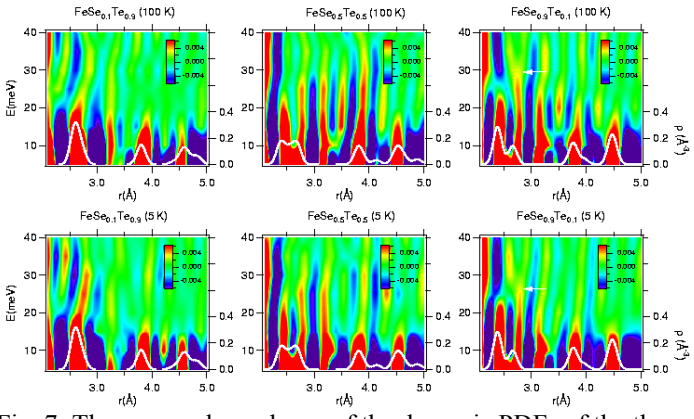

Fig. 7: The energy dependence of the dynamic PDFs of the three $FeSe_xTe_{1-x}$ samples at 5 and 100 K. Also shown in white lines are the model PDFs calculated from the static structures.

tion, the intensity in the dynamics involving the second Fe-Fe correlations are somewhat suppressed, followed by a less obvious suppression in the first Fe-Fe correlation. In the optimally doped composition, very strong suppression in the intensity is observed involving the second nearest Fe-Fe correlations around 3.8 Å. While above T_C, these correlations extend up to 40 meV, below T_C, the intensity dies out beyond 15 meV.

3) Future Plans:

Our future work will focus on continuing with the Fe-based superconductors. We succeeded in making the $K_xFe_{2+y}Se_2$ compound and are now studying the local structure. We will continue with the $LuMnO_3$ multiferroic using a single crystal to determine the nature of the incommensurate phases that were detected by our previous diffraction experiments. We will continue with our efforts to understand the SrFeO2 magnetism and the effects of electron and hole doping and with the GMR anti-perovskite systems of $GaCMn_{3-x}Ni_x$ and $Cu_{1-x}Sn_xNMn_3$. We are also working on the $Bi_2(Se_{1-x}Te_x)_3$ topological insulators.

4) List of Papers:

1. "*Oxygen displacements and magneto-electric coupling in $LuMnO_3$*", P. Tong, D. Louca, N. Lee and S.-W. Cheong, submitted to Phys. Rev. B (2012).
2. "*Dynamics of local bond correlations in $FeSe_xTe_{1-x}$ by inelastic neutron scattering*", K. Park, J. W. Taylor, and D. Louca, submitted to Phys. Rev. B (2012).
3. *"Suppression of magnetic coupling by in-plane buckling in $SrFeO_2$*", K. Horigane, A. Llobet, and D. Louca, submitted to J. Supercond. Novel Magn. (2012).
4. "*Site selection and ordering of the topological insulator $Bi_2Se_{3-x}Te_x$*", K. Park, A. Llobet, Y. Nomura, R. Arita, and D. Louca, submitted to Phys. Rev. B (2012).
5. "*Dilute magnetism and magnetopolaron melting in $LaCo_{1-y}Ni_yO_3$*", by J. Yu, D. Phelan, J. A. Rodriguez-Rivera, D. Louca, submitted to Phys. Rev. B (2011).
6. "*Possible Link of a Structurally Driven Spin Flip Transition and the Insulator-Metal Transition in the Perovskite $La_{1-x}Ba_xCoO_3$*", P. Tong, J. Yu, Q. Huang, K. Yamada, and D. Louca, Phys. Rev. Lett. **106**, 156407 (2011).
7. "*Spin-state transitions in $PrCoO_3$ investigated by neutron scattering*", J. Yu, D. Phelan, and Despina Louca, Phys. Rev. B **84**, 132410 (2011).
8. "*Effects of local disorder in the overdoped regime of $Ba(Fe_{1-x}Co_x)_2As_2$*", K. Park, A. Llobet, J. Yan and D. Louca, Phys. Rev. B **84**, 024512 (2011).
9. *"Suppression of superconductivity in Fe chalcogenides by annealing: a reverse effect to pressure",* D. Louca, J. Yan, A. Llobet, R. Arita, Phys. Rev. B **84**, 054522 (2011).
10. *"Local atomic structure of superconducting $FeSe_{1-x}Te_x$"*, D. Louca, K. Horigane, A. Llobet, R. Arita, S. Ji, N. Katayama, S. Konbu, K. Nakamura, T.-Y. Koo, P. Tong, and K. Yamada, Phys. Rev. B **81**, 134524 (2010).
11. "*Nature of magnetoelastic coupling with the isovalent substitution at the B-site in $LaCo_{1-y}B_yO_3$*", J. Yu, K. Kamazawa, and D. Louca, Phys. Rev. B 82, 224101 (2010).
12. *"Investigation of the spin-glass regime between the antiferromagnetic and superconducting phases in $Fe_{1+y}Se_xTe_{1-x}$*", N. Katayama, S. Ji, D. Louca, S.-H. Lee, M. Fujita, T. J. Sato, J. S. Wen, Z. J. Xu, G. D. Gu, G. Xu, Z. W. Lin, M. Enoki, S. Chang, K. Yamada, and J. M. Tranquada, J. Phys. Soc. Jpn **79**, 113702 (2010).
13. *"Frustrated magnetism and cooperative phase transitions in spinels"*, S.-H. Lee, H. Takagi, D. Louca, M. Matsuda, S. Ji, H. Ueda, Y. Ueda, T. Katsufuji, J.-H. Chung, S. Park, S.-W. Cheong and C. Broholm, J. Phys. Soc. Jpn 79, 011004 (2010).

IMPURITY SCATTERING, RECONSTRUCTED NESTING AND DENSITY WAVE DIAGNOSTICS IN IRON PNICTIDES

Zlatko Tesanovic[*,‡]
[*]Department of Physics and Astronomy and Institute for Quantum Matter, Johns Hopkins University, Baltimore, Maryland, USA

While the impurity-induced nanoscale electronic disorder has been extensively reported in the underdoped iron pnictides, its microscopic origins remain elusive. Recent STM measurements reveal a dimer-type resonant structure induced by cobalt doping. These dimers are randomly distributed but uniformly *aligned* with the antiferromagnetic *a*-axis. Theory of the impurity-induced quasiparticle interference patterns is presented[1] that shows the local density of states developing an oscillatory pattern characterized by both geometry and orbital content of the *reconstructed* Fermi pockets, occasioned by the pocket density wave (PoDW) order along the *b*-axis. This pattern breaks the C_4 symmetry and its size and orientation compare well with the dimer resonances found in the STM experiments, hinting at the presence of ``hidden" PoDW order.[1] More broadly, our theory spotlights such nanoscale structures as a useful diagnostic tool for various forms of order in iron pnictides.

‡ zbt@pha.jhu.edu

[1]J. Kang and Z. Tesanovic, http://arxiv.org/abs/1205.5280, to appear in Phys. Rev. B; J. Kang and Z. Tesanovic, Phys. Rev. B **83**, 020505(R) (2011).

Charge Stripe Order at High Pressure

Markus Huecker (huecker@bnl.gov), G. D. Gu, and J. M. Tranquada
Condensed Matter Physics & Materials Science Department
Brookhaven National Laboratory, Upton, NY 11973-5000

M. von Zimmermann
HASYLAB at DESY, 22603 Hamburg, Germany

Wolf Schottenhamel
Leibniz Institute for Solid State and Materials Research, 01069 Dresden, Germany

Our studies of *charge stripe order at high pressures* in the cuprates is one segment of our overall program of *stripe order at extreme conditions* which we have pursued in recent years, where the other extreme environments are high electric and magnetic fields. The goal is to study the actual physical properties of charge stripes, such as their coupling to the crystal lattice and their competition with superconductivity, which goes far beyond a basic characterization.

We have successfully studied charge stripes in $La_{2-x}Ba_xCuO_4$ at high pressure and high magnetic fields (and in an earlier experiment the stripe order in nickelates at high electric fields). Until recently the X-ray studies of the charge stripe order in $La_{2-x}Ba_xCuO_4$ were performed either at high pressure or at high magnetic field. In our most recent experiment we have been able to combine these two extreme environments. This is an important step forward to fully decipher the competing nature of stripe order and superconductivity. Pressure reduces the structural pinning potential for the charge stripes and enhances the superconductivity. A simultaneously applied magnetic field then suppresses the superconductivity which can cause a recovery of the stripe order.

Our key technique is high energy X-ray diffraction with 100 keV photons; similar experiments with neutrons would be significantly more difficult if not impossible. The challenge is related to the fact that the charge stripe reflections are 10^7 to 10^9 weaker than a strong Bragg. Therefore, the beamline requirements are high photon flux, single crystal diffraction, point detector, low temperatures, and finally the extreme environments.

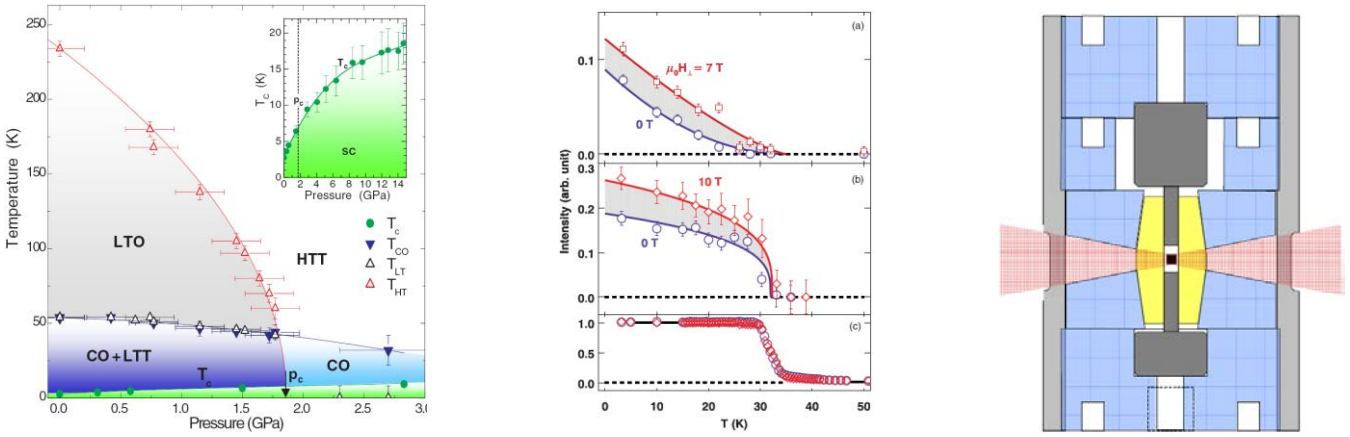

Fig. 1: Stripe order in $La_{2-x}Ba_xCuO_4$ under extreme conditions. Left: Temperature versus pressure phase diagram of $La_{1.875}Ba_{0.125}CuO_4$. Middle: Enhancement of the charge and spin stripe order parameter in $La_{1.905}Ba_{0.095}CuO_4$. Right: New miniature McWhan pressure cell for high energy X-ray diffraction experiments. The red region indicates the aperture.

The specific needs for this type of experiments have led to the development of three different types of pressure cells, all of which allow to probe the bulk properties of cubic millimeter sized single crystals. The latest design is a miniaturized McWhan type pressure cell (in its original large version used for neutron scattering). The central pressure chamber is replaceable, which is ideal to test new high strength materials such as highly transparent (to X-rays) carbon-based materials.

In addition to the high pressure X-ray diffraction experiments, we are developing a highly sensitive pressure cell for magnetization measurements. While this pressure cell is also able to determine the superconducting $T_c(p)$, its key application will be studies of the magnetization in the normal state that often contains crucial information about why the system eventually becomes superconducting. The device will be especially useful in cases where magnetic and structural transitions have only been accessible by high pressure neutron or x-ray diffraction. With pressure cells available so far, only strongly magnetic materials can be studied in the normal state, such as ferromagnets. The new cell allows studies of materials orders of magnitude less magnetic, as is often the case in correlated electron materials as for example cuprates, nickelates, heavy fermions, and iron pnictide superconductors.

References:

[1] *Uniaxial linear resistivity of superconducting La1.905Ba0.095CuO4 induced by an external magnetic field,*
J. S. Wen, Q. Jie, Q. Li, M. Hücker, M. v. Zimmermann, Z. J. Xu, D. K. Singh, L. Zhang, G. D. Gu, and J. M. Tranquada, Phys. Rev. B **85**, 134513 (2012)

[2] *Stripe order in superconducting La(2-x)Ba(x)CuO(4) for 0.095 <= x <= 0.155,*
M. Hücker, M. v. Zimmermann, G. D. Gu, Z. J. Xu, J. S. Wen, G. Y. Xu, H. J. Kang, A. Zheludev, and J. M. Tranquada, Phys. Rev. B 83, 104506 (2011)

[3] Zn *doping dependence of stripe order in La(1.905)Ba(0.095)CuO(4),*
M. Hücker, M. v. Zimmermann, Z. J. Xu, J. S. Wen, G. D. Gu, W. Tian, J. Zarestky, and J. M. Tranquada, J. Supercond. Nov. Magn. 24, 1229 (2011)

[4] *Spontaneous symmetry breaking by charge stripes in the high pressure phase of superconducting La(1.875)Ba(0.125)CuO(4),*
M. Hücker, M. v. Zimmermann, M. Debessai, J. S. Schilling, J. M. Tranquada, and G. D. Gu, Phys. Rev. Lett. 104, 057004 (2010).

Understanding Pu- and Ce-based "115s"

Marc Janoschek and Filip Ronning
Los Alamos National Laboratory

The so-called 115 superconductors are prototypical strongly correlated unconventional superconductors. Impurity studies have proven to be a very valuable method to understanding both conventional and unconventional superconductors. Here we show that the electronic tuning - with respect to an underlying quantum critical point in the d-wave superconductors $CeCoIn_5$ and $CeIrIn_5$ - is reversible with electron and hole doping. Though neither dopant in $CeCoIn_5$ can be fully understood in terms of the theory of Abrikosov and Gorkov; we show that electron doping has twice the pair breaking effect on superconductivity as hole doping does. These effects can be qualitatively understood from band structure calculations. In addition, the recent discovery of several new Pu-based superconductors has cast some doubt on the electron-hole analogy between the Ce- and Pu-based 115s, and opens the possibility that $PuCoGa_5$ is a valence-fluctuating mediated superconductor. We report here on our preliminary results to understand the spin response in the superconducting state of the Pu-based superconductors.

2012 Neutron Scattering Principal Investigators' Meeting
DOE Division of Materials Sciences and Engineering
Gaithersburg Marriott Washingtonian Center, Gaithersburg, Maryland. July 22-25, 2012

ARCS – the wide Angular-Range Chopper Spectrometer at the Spallation Neutron Source

D.L. Abernathy, M. B. Stone

Quantum Condensed Matter Division, Neutron Sciences Directorate, Oak Ridge National Laboratory, Oak Ridge TN 37831

Abstract:

The wide angular-range chopper spectrometer ARCS at the Spallation Neutron Source (SNS) is optimized to provide a high neutron flux at the sample position with a large solid angle of detector coverage [1]. The instrument incorporates modern neutron instrumentation, such as an elliptically focused neutron guide, high speed magnetic bearing choppers, and a massive array of ^{3}He linear position sensitive detectors. ARCS views the SNS decoupled ambient temperature water moderator, using neutrons with incident energy typically in the range from 15 to 1500 meV. This range, coupled with the large detector coverage, allows a wide variety of studies of excitations in condensed matter, such as lattice dynamics and magnetism, in both powder and single-crystal samples. Because of the high flux available, parametric studies across broad ranges in temperature or sample composition can address thermodynamics in alloys or explore anharmonic effects through phonon density of states measurements. Single crystal studies of magnetic or lattice excitations across large volumes of reciprocal space provide new insights into local dynamical structures and electron-phonon coupling, for example. The highly efficient data collection at ARCS enables more detailed studies of quantum liquids and solids. Recent results will be presented to highlight the contributions of ARCS to these areas.

[1] D. L. Abernathy, M. B. Stone, M. J. Loguillo, M. S. Lucas, O. Delaire, X. Tang, J. Y. Y. Lin, and B. Fultz, "Design and operation of the wide angular-range chopper spectrometer ARCS at the Spallation Neutron Source," Review of Scientific Instruments **83**, 15114 (2012)

SEQUOIA: The fine resolution thermal to epithermal neutron spectrometer at the SNS

G. E. Granroth[1] and A. I. Kolensnikov[2]

[1] Quantum Condensed Matter Division
[2] Chemical and Engineering Materials Division
Oak Ridge National Laboratory, Oak Ridge, TN

SEQUOIA is a direct geometry time-of-flight chopper spectrometer with fine energy transfer (ω) and wave-vector (**Q**) resolution. The instrument is used to conduct forefront research on dynamical processes in materials. In particular, SEQUOIA is enabling high-resolution thermal to epithermal inelastic neutron scattering studies of magnetic excitations and fluctuations and lattice vibrations. The impact on Condensed Matter Physics, Materials Science, and Geology is demonstrated by several recent results. For Condensed Matter Physics, magnetic excitations in a powder of the dimerized spin system TiOBr, magnetic excitations in Mn doped $BaAs_2Fe_2$, and a study of the structure factor of the magnetic excitations in Gd are shown. For Materials Science and Geology, studies of the Hydrogen potentials in several phases of MgH_2 and mica are given, respectively. Finally observation of the H recoil in water and a multi energy study on KCuF3 reveal other operating conditions for SEQUOIA.

Title: The Cold Neutron Chopper Spectrometer at the Spallation Neutron Source – Review of the first three years of User Operation

Andrey Podlesnyak and Georg Ehlers, Oak Ridge National Laboratory

The Cold Neutron Chopper Spectrometer (CNCS) at the Spallation Neutron Source (SNS) in Oak Ridge is a very flexible and versatile direct-geometry multi-chopper inelastic time-of-flight (TOF) spectrometer that provides both good energy and momentum transfer resolution at low incident neutron energies (1-50 meV). The CNCS is located at SNS beam line 5 with a cold coupled moderator, and features a source to sample distance of 36.25 meters. Two high-speed choppers, one to shape the neutron pulse from the moderator and a second to cut down the pulse length at the sample position, provide an adjustable energy resolution, ranging from ~1.2% to ~10% of the incident energy. The secondary flight path, with a length of 3.5 meters, has a highly pixilated detector covering scattering angles between -50° and +135° in the scattering plane and ±16° perpendicular to the scattering plane. The detector array with a total solid angle of 1.7 sr consists of 400 two meter long tubes filled with ^{3}He gas at 6 atm. CNCS has been operating since May 2009 (more than 110 peer-reviewed user experiments to date) with external facility users. This contribution reviews some of the user experiments performed during this time.

The Nanoscale Ordered MAterials Diffractometer (NOMAD) at the SNS: A fast neutron diffractometer for Pair Distribution Function (PDF) determinations

Jörg Neuefeind
Neutron Scattering Science Directorate, Oak Ridge National Laboratory, Oak Ridge, TN 37831

The Nanoscale Ordered MAterials Diffractometer (NOMAD) is neutron time-of-flight diffractometer designed to determine pair distribution functions of a wide range of materials ranging from short range ordered liquids to long range ordered crystals. Due to a large neutron flux provided by the Spallation Neutron Source SNS and a large detector coverage neutron count-rates exceed comparable instruments by one to two orders of magnitude. This is achieved while maintaining a relatively high momentum transfer resolution of a $\delta Q/Q$ ~ 0.8% FWHM (typical), and a possible $\delta Q/Q$ of 0.24% FWHM (best). The real space resolution is related to the maximum momentum transfer; a maximum momentum transfer of 50Å^{-1} can be obtained routinely and the maximum momentum transfer given by the detector configuration and the incident neutron spectrum is 125Å^{-1}. High stability of the source and the detector allow small contrast isotope experiments to be performed. A detailed description of the instrument has been given in[1].

An increase in neutron count rate by two orders of magnitude provides a lot of flexibility for unprecedented experiments. An obvious desire is to follow a structural evolution in situ. Figure 1 shows the structure factor and the pair distribution function of diamond as a function of data collection time. It is apparent that for is a strong scatterer and about 1g of sample neutron experiments on a second time scale become feasible.

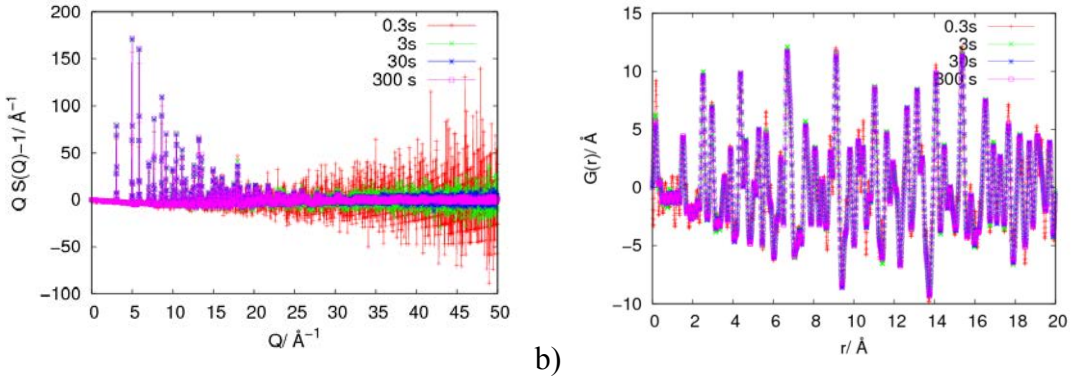

a) b)

Figure 1: The scattering function (a) and the pair distribution function (b) in the representation G(r)= r [g(r)-1] of diamond as a function of measurement time. Short measurement times are achieved by taking into account only a limited number of neutron events. All Fourier transforms have a Q_{max}=30Å^{-1}

Experiments with small samples are another frontier. Experience shows that many experiments run at NOMAD now work with about 50mg of sample. That is not an absolute the lower limit, but it is often a reasonable compromise between the difficulty to

produce larger samples and considerations about measuring time and signal to background ratio.

Examples of recent experiments at NOMAD include the characterization of local atomic structure of high-strength lightweight amorphous and semi-amorphous Al alloys, studies of phase change materials used for high density optical data storage applications, a number of studies of Li compounds for use in energy storage applications, investigations of aerodynamically levitated silicate melts at very high temperature, structural characterization of fast acting amorphous drugs and studies of oxynitrides with possible application to use visible light to split water into H_2 and O_2.

In summary, NOMAD is the fastest neutron diffractometer in its class. Stability and precision are commensurate and it is a valuable tool for the determination of both disordered materials and crystalline structures.

References

1 J. Neuefeind et al. Nucl. Instr. Meth. B (2012) in press
http://dx.doi.org/10.1016/j.nimb.2012.05.037

Recent Development of the HYSPEC instrument at SNS

I. A. Zaliznyak (zaliznyak@bnl.gov), S. M. Shapiro, D. Fobes and J. M. Tranquada
Condensed Matter Physics & Materials Science Department
Brookhaven National Laboratory, Upton, NY 11973-5000

M. Hagen, A. Savici, B. Winn, M. Graves-Brooks and M. Lumsden
Neutron Sciences Directorate, Oak Ridge National Laboratory, Oak Ridge, TN 37831-6477

Program Scope

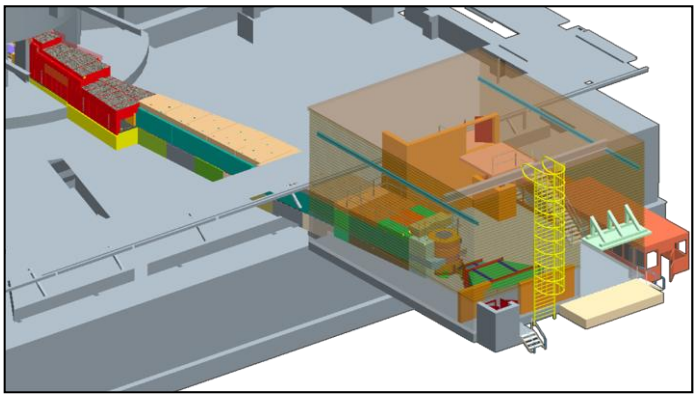

Figure 1. Schematics of the HYSPEC layout on the beamline 14B. The secondary spectrometer is located in a separate satellite building, adjacent to the target hall.

The Hybrid Spectrometer (HYSPEC) is a new high-intensity, direct-geometry instrument at the ORNL's Spallation Neutron Source, which is optimized for measurement of dynamical properties of small single-crystal samples [1-3]. HYSPEC has been proposed by the Instrument Development Team (IDT) lead by scientists from the BNL Neutron Scattering Group and which joins experts in neutron scattering studies of condensed matter from leading US Universities, National Laboratories, and from abroad.

HYSPEC provides a next-generation platform for neutron scattering studies of low-energy dynamical properties of hard and soft matter, which dramatically extends the range of capabilities offered by the traditional thermal neutron spectrometers. It is a unique instrument, whose concept combines advantages of the time-of-flight (TOF) technique traditionally used at the pulsed sources, with those of crystal spectrometers, which use continuous neutron beams [2]. The incident neutron beam on HYSPEC is monochromated using a Fermi chopper with short, straight blades, and is then focused onto the sample using Bragg scattering optics. Either full or partial neutron polarization analysis can be deployed on HYSPEC by using a Heusler crystal array to polarize the incident beam and either a ^{3}He spin filter or supermirror wide-angle polarization analyzers for the scattered beam [4,5]. The combination of TOF techniques and crystal optics offers an unprecedented flexibility in choosing the wave vector and the energy resolution, which are intrinsically decoupled. Among other advantages offered by the HYSPEC design is a capability to accept complex and bulky sample environment, which is needed for studies of physics in extreme environment of high magnetic fields, extreme pressures, temperatures, etc.

HYSPEC construction has been completed in 2011, and now the instrument is undergoing testing and commissioning. Now the IDT took a lead in conducting the first scientific experiments, which will lead to establishing and developing the IDT's HYSPEC science program.

Recent Progress

HYSPEC construction has been completed in FY 2011 and since then it is undergoing commissioning studies. A number of hardware and software issues have been identified and resolved. Overall, the instrument was found to conform to most of the design parameters. No problems significantly limiting its performance and which could not be remedied during the commissioning period were found. Among the issues which still remain of some concern are the longer than expected from the early neutronics simulations used in the original HYSPEC conceptual design neutron pulse, and a time-structured background arising from neutrons leaking from the target. The latter is identified on HYSPEC more easily than on the other instruments due to the extremely low intrinsic background. The latter, as well as the performance of the Bragg focusing optics, have positively met the design expectations.

Figure 2. Photograph of the HYSPEC secondary spectrometer – the focusing crystal drum shield, the sample stage and the detector vessel – in the satellite building.

Engaging expertise and experience of the IDT is extremely important for the instrument to be successful. In 2012, HYSPEC IDT members have begun conducting test experiments in the framework of their scientific programs, which will lead to establishing the science program of the HYSPEC IDT. Among these are measurements of the low-energy magnetic excitations in lightly doped cuprate $La_{2-x}Ba_xCuO_4$ (x=0.025) led by K. Fritsch of B. Gaulin's group from McMaster University shown in Fig. 3, anomalous phonons in $FeSb_2$ led by I. Zaliznyak from Brookhaven group shown in Fig. 4, magnetic response of NiO nanoparticles by M. Feygenson from ORNL (formerly at BNL), and others.

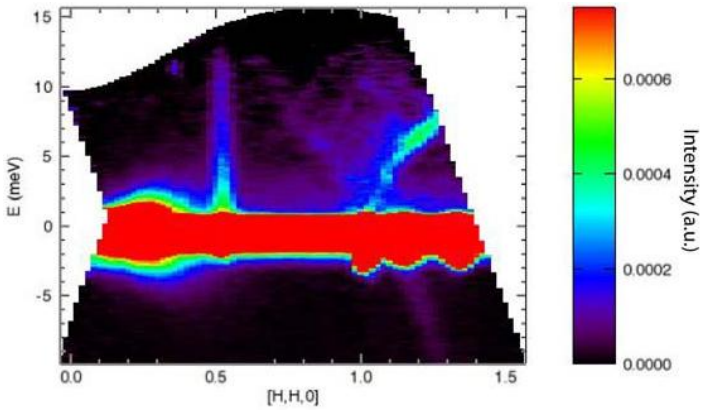

Figure 3. Gapless magnetic excitations in quantum magnet $La_{2-x}Ba_xCuO_4$ (x=0.025) emanating out of ~ 1/2 1/2 L. These particular data were taken with HYSPEC at T=4 K and integrate over much of the direction normal to the two-dimensional copper-oxide planes.

An important goal of these initial studies is to accumulate the experience and establish the experimental procedures on how to conduct measurements using this entirely new type of spectrometer. The experience gained in these studies is communicated between the IDT and the

SNS HYSPEC team (instrument scientist, instrument associate, and others) in part via HYSPEC memos, which provide an important mechanism for interaction and information sharing between the IDT and the SNS HYSPEC team. To date, memos on the standard sample design for Vanadium calibration, on avoiding the prompt pulse background, on TOF-specific inelastic spurions from multiple scattering events, and others, have been written. Not only these provide descriptions for the identified problems, they also describe experimental procedures and solutions to problems based on the expertise and experience of the IDT and the local HYSPEC team members.

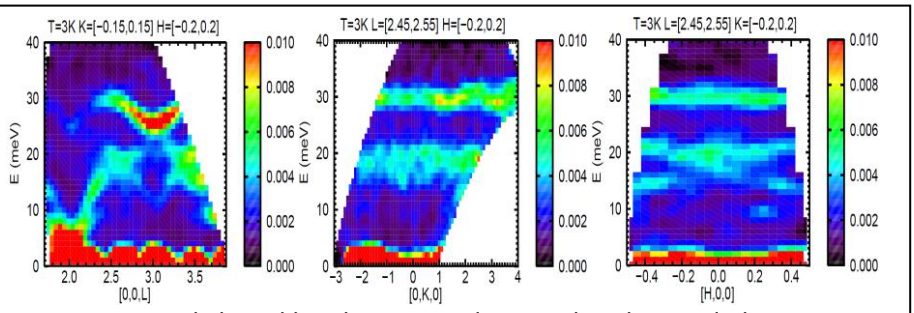

Figure 4. Unusual chain-like phonon mode in $FeSb_2$. This mode has anomalously strong temperature dependence, concomitant with the appearance of temperature-induced electronic paramagnetism.

Future Plans

A limited beam time on HYSPEC will be offered for users already in the next SNS proposal round. We plan to take full advantage of this opportunity and conduct large part of our scientific program using the unique capabilities of HYSPEC. The proposed studies include further investigations of phonons and electronic magnetic scattering in $FeSb_2$ and $Fe_{1-x}Cr_xSb_2$, where magnetism emerges upon Cr doping, unusual low-energy dynamics of iron chalcogenides, including the temperature-induced magnetism and the unusual low-Q excitation, which leverage the unique small-angle inelastic scattering capability of HYSPEC, magnetic excitations in doped cuprates, and others. Meanwhile, we also plan to actively participate in further commissioning and test studies, investing our time and effort in improving and extending HYSPEC capabilities. In particular, we plan to participate in the first inelastic polarized beam experiments on a TOF instrument – first tests of the polarized beam on HYSPEC have already begun in June, 2012.

References

1. I. A. Zaliznyak and S. M. Shapiro.” HYSPEC: A Crystal-Time-of-Flight Hybrid Spectrometer for the Spallation Neutron Source”, BNL Technical Report BNL-52677 (2002); Proposal submitted to the US DOE, http://neutrons.phy.bnl.gov/HYSPEC/documents/HYSPEC_DOEproposal.pdf (2002).
2. I. A. Zaliznyak and S. M. Shapiro. “HYSPEC Top Level Specificaitons”, http://neutrons.phy.bnl.gov/HYSPEC/documents/HYSPEC_TLS_revision_A.pdf (2002).
3. S. M. Shapiro, I. Zaliznyak, L. Passell, V. Ghosh. ”HYSPEC: a Crystal Time-of-Flight Hybrid Spectrometer for the Spallation Neutron Source”, in: G. Mank, H. Conrad (Eds.), Proceedings of ICANS-XVI, Julich, 2003, p. 191.
4. I. Zaliznyak, V. Ghosh, S. M. Shapiro, L. Passell. ”Polarized beam operation of the Hybrid Spectrometer at the pulsed Spallation Neutron Source”, cond-mat/0410040; Physica B 356, 150-155 (2005).
5. S. M. Shapiro, I. Zaliznyak, L. Passell, V. J. Ghosh, V. J. Leonhardt, M. Hagen. ”HYSPEC: a Crystal Time-of-Flight Hybrid Spectrometer for the Spallation Neutron Source with Polarization Capabilities”, Physica B 385, 1107-1109 (2006).

Recent Development of the TOPAZ Single-Crystal Diffractometer at the SNS

Xiaoping Wang (wangx@ornl.gov) and Christina Hoffmann

Chemical & Engineering Materials Division
Oak Ridge National Laboratory, Oak Ridge, TN 37831

Single crystal neutron diffraction provides detailed three-dimensional structural information at atomic level about the position, displacement and site occupancy of all atoms, including hydrogen in a structure. Although it would be advantageous to determine a neutron structure, only a very small fraction (< 0.3%) of structures reported in the Cambridge Structural Database were measured with neutrons, due to both the very limited availability of neutron diffraction instruments, and the inability to measure small crystal samples in existing neutron facilities. The need for a multipurpose and high throughput neutron single crystal instrument has been addressed with the design and construction of a neutron wavelength-resolved single-crystal diffractometer (TOPAZ) at the Spallation Neutron Source, Oak Ridge National Laboratory. Success in commissioning of the TOPAZ instrument will expand greatly the range of materials explored using neutrons in chemistry, biology, condensed matter physics and materials science.

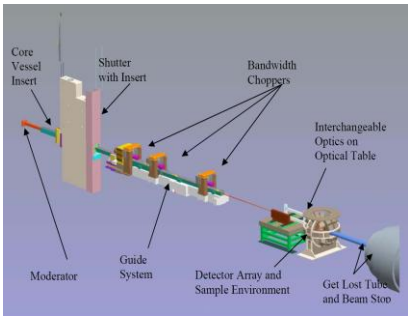

Figure 1a.
Layout of the TOPAZ beamline

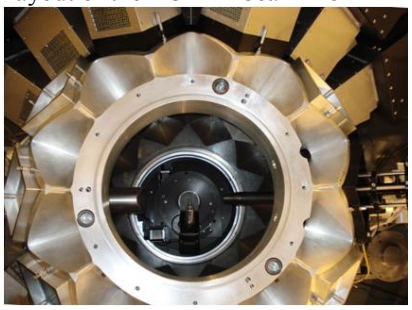

Figure 1b.
TOPAZ with 11 Detector modules installed for commissioning test

The layout of the TOPAZ beamline at the SNS is shown in Figure 1a. It uses a curved guide to achieve high neutron beam flux at the sample position, while discriminating against unusable, background enhancing fast neutrons and gamma rays, and an extended array of area detectors for high throughput data collection (Figure 1b). Each detector module has an active 150 ×150 mm^2 area that is divided into 256 × 256 pixels. Crystals are mounted on a two-circle goniometer. A data set can be measured in wavelength-resolved time-of-flight Laue mode at ambient conditions or in controlled sample environments. A nitrogen cold stream provides sample temperature control in the range of 100 K to 450 K. Single crystals of 1 - 10 mm^3 in sizes, with a maximum length of 3 mm on an edge, preferably isometric, are best suited for TOPAZ. Unit cell

dimensions up to 50 Å are appropriate for high resolution data collection. Two tunable neutron wavelength bands are available: the first frame with a wavelength in the range 0.5 Å to 3.5 Å for high resolution structure determination; and the second frame in the range 4.0 Å to 7.0 Å for large unit cell sample and magnetic structural analysis. Raw data are recorded in event mode in time-of-flight intervals of 1μs. During data collection, the neutron event data are saved and broadcasted to a listening server to a local EventViewer program for live viewing of the measured diffraction pattern in 3*D* reciprocal space. The EventViewer program can be used for indexing peaks, generating an orientation matrix and carrying out data integration in real time. The Bragg peaks from each angular setting can be integrated in event mode in 3*D* *q*-space or processed offline as image frames. Currently, 11 of 48 detector locations are populated with Anger camera modules covering a scattering angle of 16° - 158° in 2θ matching 1.4 sr solid angle around the sample. To have sufficient data for a reliable structure refinement, an experimenter will typically want to measure > 90 % of the unique reflections within a certain range of d spacing. The CrystalPlan program,[1] a highly efficient experiment-planning software for data collection strategy optimization, has been developed to maximize the use of available beam time for each experiment according to sample symmetry.

TOPAZ is well suited to determine atomic positions and displacement parameters of light elements, such as hydrogen, lithium and oxygen next to heavy metals. During initial commissioning of TOPAZ, the feasibility of extending the resolution of the coenzyme cob(II)alamin structure to ultrahigh resolution was investigated by collecting a wavelength-resolved neutron crystallographic data set in two days versus 28 days of neutron beam time used on D19 at ILL.[2] The result showed that neutron diffraction data measured at TOPAZ can provide hydrogen-bonding parameters for the hydration of biomacromolecules with high accuracy while reducing data acquisition time by a factor of 14 compared to a monochromatic instrument. Recently, significant gains have also been made in the signal-to-noise ratio of data collected on TOPAZ by reducing the instrument scattering background. This will

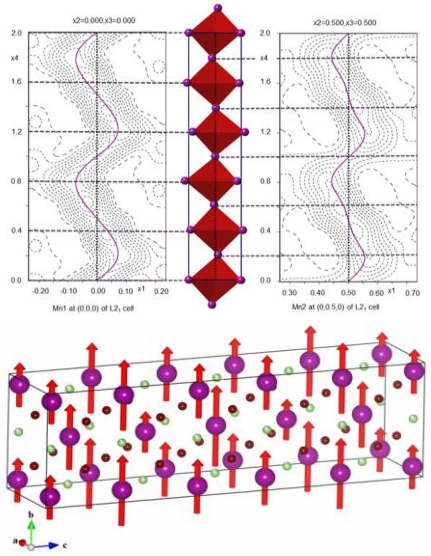

Figure2. Atomic displacements and magnetic modulation in 5M $Ni_2Mn_{1.14}Ga_{0.86}$ [3]

allow data collection for samples of smaller sizes and with low scattering power. The extensive area detector coverage makes it possible for three dimensional reciprocal or *q*-space mapping of Bragg peaks, measuring magnetic and diffuse scattering patterns from a stationary crystal at multiple setting angles for a wide range of materials, including functional inorganic materials to study the interplay of nuclear and magnetic structure and phase transitions. Figure 2 shows the structural and magnetic modulations of an off-stoichiometric Ni-Mn-Ga magnetic shape memory alloy that displays large magnetic-shape memory (MSM) effect at ambient temperature.[3] The crystallographic and magnetic structural details of an off-stoichiometric $Ni_2Mn_{1.14}Ga_{0.86}$ alloy were obtained from the refinement of high-resolution single crystal neutron diffraction data measured at TOPAZ, following a (3+1)-dimensional superspace formalism. It was observed that the modulation of the magnetic moments over subsequent atomic planes in a martensitic 5M structure correlate with the variations of the individual local atomic environments.

Much of the current effort is concentrating on improving the Anger camera neutron detector used at TOPAZ, and fine tuning the neutron guide to achieve high signal-to-noise ratio and optimal spectrum shape at both the sample and detector positions, which is of critical importance for accurate intensity measurement of Bragg peaks from a small (< 1 mm^3) single crystal sample. Future upgrades will be expanding the instrument measurement capability to diffuse scattering and polarized neutron studies. New sample environment capability developments are ongoing, including a displex cooled 2-axis cryogenic sample positioner for data collection down to 5 K in vacuum or He gas environment that will be available to general users after successful testing.

Publications

[1] Zikovsky, J.; Peterson, P. F.; Wang, X. P.; Frost, M.; Hoffmann, C. "CrystalPlan: an experiment-planning tool for crystallography" *Journal of Applied Crystallography* **2011,** 44, 418-423.

[2] Jogl, G.; Wang, X. P.; Mason, S. A.; Kovalevsky, A.; Mustyakimov, M.; Fisher, Z.; Hoffman, C.; Kratky, C.; Langan, P. "High-resolution neutron crystallographic studies of the hydration of the coenzyme cob(II)alamin" *Acta Crystallographica D* **2011,** 67, 584-591.

[3] Pramanick, A.; Wang, X. P.; An, K.; Stoica, A. D.; Yi, J. ; Gai, Z.; Hoffmann, C.; and Wang, X.-L. "Structural modulations and magnetic properties of off-stoichiometric Ni-Mn-Ga magnetic shape memory alloys" *Physical Review B* **2012**, *85*, 1444412.

Development of a high-energy x-ray precession camera at the Advanced Photon Source

A. I. Goldman (goldman@ameslab.gov), A. Kreyssig, D. K. Pratt and R. J. McQueeney
Ames Laboratory and Dept. of Physics and Astronomy, Iowa State University, Ames, IA 50011

D. S. Robinson and J. C. Lang
Advanced Photon Source, Argonne National Laboratory, 9700 S. Cass Avenue, Argonne, IL 60439

A key distinguishing feature of the Advanced Photon Source (APS) is the capability for high-energy scattering, which has been exploited for numerous applications including pair distribution function studies, high pressure studies, and investigations of the mechanical behavior of materials. High-energy x-rays offer several advantages for these measurements: (1) absorption effects are minimized and the entire bulk of the sample is probed and; (2) a large range of reciprocal space can be imaged when used together with even a modestly sized area detector since the scattering angles are strongly reduced for 100 keV x-rays as compared to standard 8 keV laboratory sources (e.g. Cu K_α radiation). Coupled with the new generation of two-dimensional area detectors, high-energy diffraction studies of powder samples provide an important and complementary path to conventional powder diffraction measurements. The capabilities for high-energy single-crystal diffraction measurements at the APS, however, remain underdeveloped and there is an emerging need for this technique. We have developed a high-energy x-ray precession camera (HEXPC) on beam line 6-ID-D for imaging reciprocal-space planes from single-crystal samples. The ability to visualize an entire reciprocal lattice plane can provide key insight into the nature of structural or magnetic phase transitions driven by temperature, pressure, or electromagnetic field.

In our realization of the HEXPC, the axis normal to the reciprocal lattice planes of interest is set at a small, but finite, half-cone angle with respect to the incident beam direction and rotated stepwise about it. This motion is common to both the high-energy precession method and the standard Buerger precession camera. A timed exposure of the area detector (MAR 3450), set at a well-defined distance from the sample, together with the known orientation matrix of the sample at each rotation step, allows a unique assignment of the 3-dimensional reciprocal space coordinates (Q_x and Q_y perpendicular to the incident beam and Q_z parallel to the beam) to each pixel of the area detector. Binning the data from each exposure and defining a finite integration range over Q_z, serves the function of the traditional layer screen and allows each level of reciprocal space to be isolated for study.

Over the past few years our group has employed a closely related crystal oscillation technique using high-energy x-rays to image planes of reciprocal space. This method has been applied, to a variety of systems including the new iron arsenide superconductors[1,2], quasicrystals[3,4], and crystallographic phase transitions[5]. We will describe our efforts over the last year using the HEXPC for investigations of order and disorder in quasicrystalline systems, including a newly discovered quasicrystal in a Na-Au-Ga alloy and diffuse scattering in decagonal Al-Ni-Co (see Figure 1), as well as ongoing studies of the relationship between strain and the novel tetragonal-to-collapsed tetragonal phase transition in $CaFe_2As_2$.

[1] M.A. Tanatar *et al., Phys. Rev. B* **79**, 180508 (2009).
[2] M.Prozorov *et al., Phys. Rev. B* **80**, 174517 (2009).
[3] P.C. Canfield *et al., Phys. Rev. B* **81**, 020201 (2010).
[4] A. I. Goldman *et al., Phil. Mag.* **91,** 2427 (2011).
[5] A. Kreyssig *et al., Phys. Rev. B* **76**, 054421 (2007).

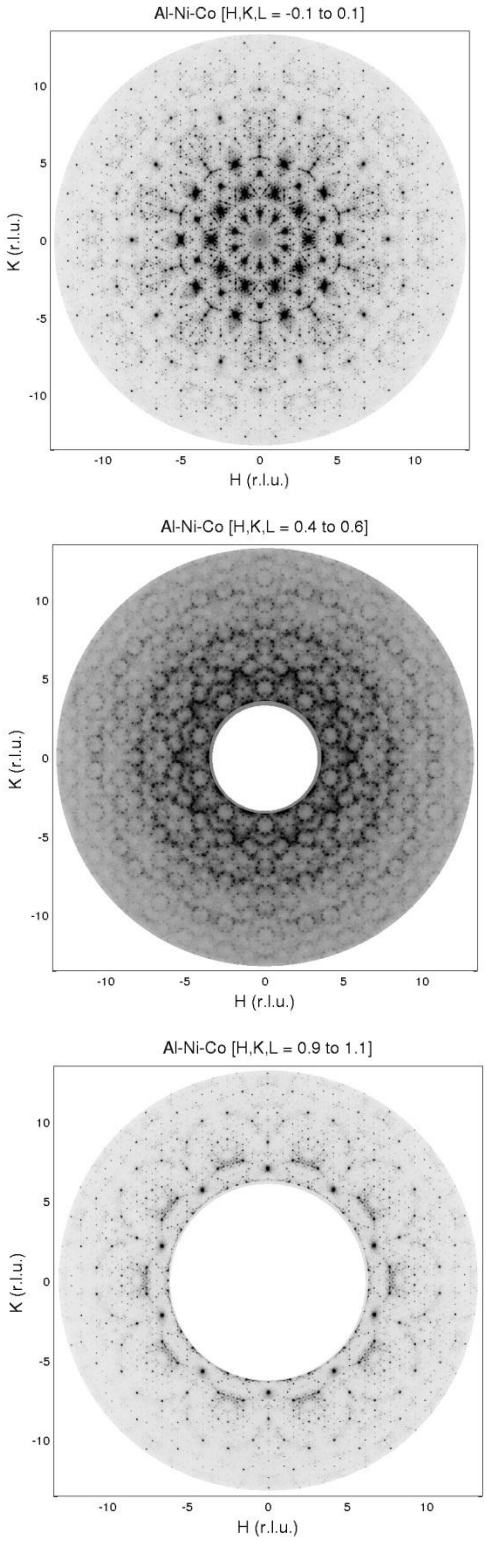

Figure 1.

The zero-, half- and first- layer levels of decagonal $Al_{70}Co_{15}Ni_{15}$ derived from the HEXPC data taken on Station 6ID-D at the Advanced Photon Source using an incident beam energy of 100 keV. For this quasicrystal, reciprocal lattice units (r.l.u) are in units of $Å^{-1}$.

Note the tenfold symmetry of the diffraction patterns for all three layers, the large range of Q_H and Q_K covered in each layer and, particularly, the strong diffuse scattering in the intermediate half-level.

Neutron Compton Scattering as a Probe of Hydrogen Bonded (and other) Systems

George Reiter
Physics Department
University of Houston
Houston Tx 77204-5506
greiter@uh.edu

Research Scope:
Neutron Compton Scattering, also called Deep Inelastic Neutron Scattering, makes use of incident neutrons in the range 2-100eV, and scattered wavevectors in the range of 30 to 100 $Å^{-1}$ to measure the momentum distribution of light ions, protons in these experiments. In nearly all cases, the momentum distribution is determined by the ground vibrational state of the protons, and hence provides a probe of the effective potential the proton experiences in its local environment. It is uniquely sensitive to quantum coherence, readily distinguishing between protons statistically distributed over two locations and those that are coherently "in two places at once". The focus has been on using this new probe to study hydrogen bonded systems, including water, on surfaces, in bulk and confined, ferroelectrics such as KDP, superprotonic conductors of both the solid acid(CsH_2PO_4) and hydrated ionomer varieties(Nafion), and the effects of changes in the zero point motion in the binding of water to DNA.
Recent Progress: Earlier work on water confined in single walled carbon nanotubes[1,2] (SWNT), 14Å diameter, demonstrated that the large Debye Waller factors observed with INS were due to the quantum delocalization of the protons in the water over distances on the order of .2 Å , about twice the localization width of the protons in bulk water. The momentum distribution at T<230K was nearly temperature independent, and showed a pronounced narrowing, with a mean kinetic energy/proton of 110meV, compared to 148meV in bulk water. This is in dramatic contrast to the recent results for slightly larger double wall carbon nanotubes(DWNT), 16Å inside diameter.[3] The momentum distribution in the DWNT is temperature dependent, broader at all temperatures than that of bulk water, and shows that the protons are coherently distributed over two sites .2-.3 Å apart.

We show in Fig. [1] the measured Compton profile for bulk water(ice) at 170K, compared with that for both the SWNT and DWNT. The relative changes in the kinetic energy of the two systems, proportional to the second moment of the Compton profile, are apparent from the figure. In Fig.[2], we show the temperature dependent momentum distributions, easily derivable from the Compton profiles, for the DWNT. The oscillations apparent in all but the room temperature result are the signature of protons being coherently distributed over double wells. The position of the minimum gives the separation of the wells, .2-.3Å.

The enhanced width of the DWNT profile at 170K corresponds to an increase in kinetic energy of 70meV over that of bulk water. At room temperature the increase is less, 24meV. This is, however,
enough to be thermodynamically significant for biological systems, and indeed, the changes in the kinetic energy of the protons in water binding to DNA has been shown to be entirely responsible for the binding at concentrations of 6water molecules/base pair. [4]. Earlier experiments on xerogel[5] have shown that the effects of confinement on the momentum distribution persist up to at least ~20Å, which is the typical distance between the elements of a biological cell. The distinctive quantum state of localized water that has been revealed by the NCS measurements would appear to be the relevant quantum background for the dynamics of life.

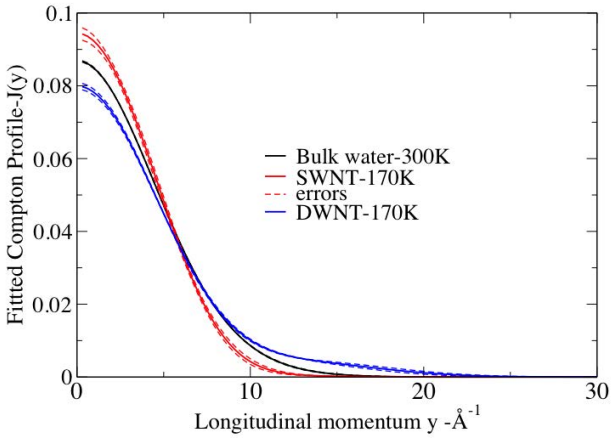

Fig. 1 Comparison of the Compton profile of SWNT(14Å), DWNT(16Å) and bulk water at 170K. The second moment of the profile determines the zero point kinetic energy. The DWNT K.E/proton. is larger by 70meV, the SWNT smaller by 40meV than that of bulk water

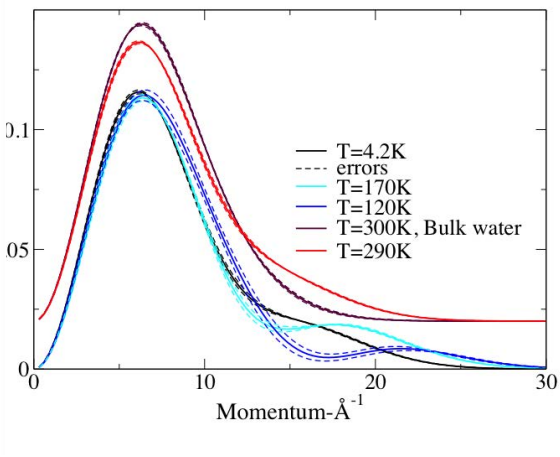

Fig. 2 The momentum distribution in the DWNT compared to that of bulk water. The upper curves have been displaced for clarity. The oscillation signifies coherent motion in a double well potential with a separation of the wells, determined by the minimum, of .2-.3Å

This state is also evident in other confined watersystems. Nafion is a sulfonated tetrafluorethyene copolymer used as an electrolyte in commercial fuel cells. The hydrophobic backbones of the polymer enclose the water in a spongelike matrix, with the hydrophilic side chains containing the sulphonyl groups. A typical separation of the polymers is 30Å. Conductivity in the material is due to protons donated from the sulphonyl groups of the polymer to the enclosed water matrix. Recently, a class of similar materials, with shorter side chains(DOW 858, DOW 840, DOW 1084)[6] have been shown to have improved electrical and structural properties with regard to Nafion. The conductivity is a function of the fraction λ of water molecules to sulfonyl groups. Fig.[3] shows the momentum distribution for the two materials at a value of λ of 14, where the Dow 858 has a conductivity nearly twice that of Nafion[6].

Momentum distribution measurements were made at room temperature on Nafion 1120, the commercial material, and Dow 858 at a water concentration in both cases of λ=14. Fig. 3 below, shows the comparison of these two measurements with each other and that of bulk water. It is evident that the quantum state of the protons in the Nafion materials is dramatically different from that of bulk water. The covalent bond has been replaced by a double well effective potential with, in both cases, a separation of the wells of ~.2 Angstroms. There are more such delocalized protons in the Dow 858 material. Since there is only one free proton for 14 water molecules, it must be that the hydrogen bond network itself is strongly distorted by the confinement in the polymer interstices to produce momentum distributions such as those above. An attractive hypothesis is that the difference in conductivity is due to the difference in the quantum state of the proton. Intuitively, if the proton is coherently delocalized, "in two places at once", it has a greater probability of transition to new locations than if it was only in one site.

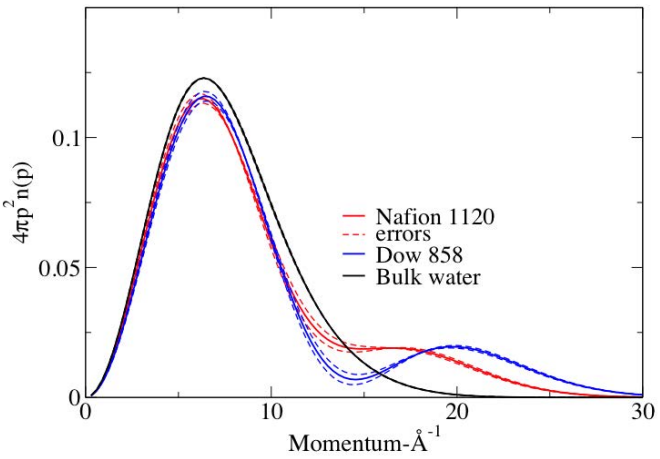

Fig.3 The momentum distribution for the protons in room temperature Nafion and Dow 858 samples. compared with bulk water. The greater number of bimodally coherently distributed protons in the Dow 858 material is correlated with the conductivity of these materials.

The broadening of the momentum distribution of the electrons is consistent with the increased kinetic energy seen in Fig. 3, and hence localization, of the protons. The observation of changes in the electron distribution corresponding to the changes seen in the proton momentum distribution is strong confirmation that we are seeing a distinct quantum state of water in confined geometries.

The change in the momentum distribution of the proton is associated with a change in the Born-Oppenheimer potential of the proton, and hence there should be a signature of that in the distribution of electrons in the vicinity of the proton. This has been observed using electron Compton scattering, in conjunction with Aniruddha Deb. We show in Fig.4 the electron Compton profile of the water in the Nafion and Dow 858 samples.

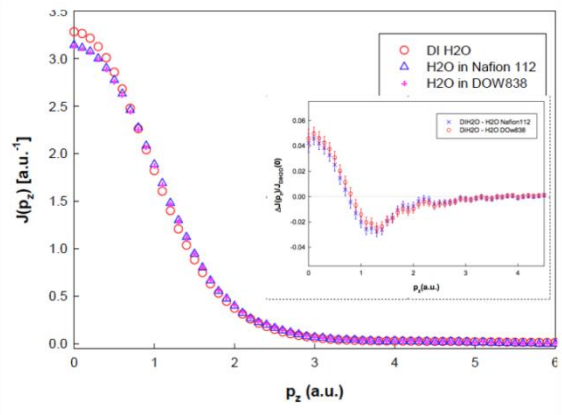

Fig. 4 Valence **Electron** Compton profile for water in Nafion and Dow 858 at room temperature, λ=14. The greater localization of the electrons is consistent with the greater kinetic energy of the protons seen in the neutron Compton scattering. The insert shows the difference between bulk water and the localized water, normalized to the bulk water value at P_z=0.

Future plans:

The conjecture that quantum coherence seen in the momentum distribution is responsible for the higher conductivity of Dow 858 relative to Nafion can be explored by measuring the momentum distribution at more values of λ and of using other variants of Nafion, such as Dow 1084 to determine if a pattern exists correlating the conductivity and the degree of. There are other candidates for improved fuel cell electrolytes that involve polymers contributing a proton to water confined by the polymer. In particular, SPS, sulfonated poly(p-phenylene sulfone has a higher conductivity than Nafion at the same values of λ, with somewhat smaller cavities for the water. [7] We will measure the momentum distribution in this material at two values of λ.

Our primary goal is to understand the nature of the quantum state of localized water. The evidence is that it is a many body state, involving the interaction of the protons. We will redo the measurements of the water in the carbon nanotubes using D2O, where correlated motion of the deuterons should be suppressed relative to that of the protons. The concomitant measurements of the electron Compton profile will be done as well for H2O in the nanotubes. We will be interested in seeing how the systematics of the variation in the electron distribution track with the variations with temperature and nanotube diameter seen in the momentum distribution.

Ab initio simulations of water confined in the carbon naonotubes are under way in collaboration with others to attempt to associate the observations with a definite electronic state and spatial configuration of the hydrogen bond network.

References

1. A. I. Kolesnikov et al, PRL **93**, 35503 (2004)
2. G. Reiter et al,PRL **97**, 247801 (2006)
3. G. Reiter et al, PRB **85**, 045403 (2012)
4. G. Reiter, R. Senesi, J.Mayers PRL **105**, 148101 (2012)
5. V. Garbuio et al, J. Chem. Phys. **127**, 154501 (2007)
6. K-D. Kreuer et al, Journal of Power Sources, **178**, 499 (2008)
7. C. C. de Araujo et al, PCCP **11**, 3305 (2009)

Published papers-2010-2012

1. *Changes in the Zero-Point Energy of the Protons as the Source of the Binding Energy of Water to A-Phase DNA***,** G. Reiter, R. Senesi, J. Mayers, Phys. Rev. Letts. **105**, 148101 (2010)

2. Comment on "High-energy neutron scattering from hydrogen using a direct geometry spectrometer" Mayers J.; Gidopoulos N. I.; Adams M. A.; et al., Phys. Rev. B **84,** 056301 (2011)

3. The proton momentum distribution in strongly H-bonded phases of water: A critical test of electrostatic models , Burnham C. J.; Hayashi T.; Napoleon R. L.; et al, J. Chem. Phys **135** , 144502 (2011)

4. *Evidence for an anomalous quantum state of protons in nanoconfined water* , Reiter G. F.; Kolesnikov A. I.; Paddison S. J.; et al. Phys. Rev. B Volume: **85** 045403 (2012)

5. The VESUVIO electron volt neutron spectrometer, J Mayers and G Reiter , Meas. Sci. Technol. **23** ,045902 (2012)

Novel Molecular Materials for Hydrogen Storage Applications

Maddury Somayazulu (zulu@gl.ciw.edu), Robert Potter, Timothy Strobel,
Viktor Struzhkin and Russell J Hemley
Geophysical Laboratory, Carnegie Institution of Washington, Washington DC, 20015

Raja Chellappa
Los Alamos National Laboratory, Los Alamos, NM, 87545

Research Scope

The technology of using hydrogen as an environmentally clean and efficient fuel is an active research area worldwide[1-3]. The key to emergence of a viable global hydrogen economy is the availability of light weight transport and safe storage of hydrogen as a fuel. Major factors that dictate this include high volumetric and gravimetric density of the storage media, optimal thermodynamics and kinetics of hydrogenation and re-hydrogenation, ease of handling, and small environmental footprint. The effort to develop new materials and investigate their thermo-physical tunability is outpaced by the growing world energy consumption [4]. There are currently four leading methods to store hydrogen: physical means, sorbents, metal hydrides (classical and complex), and so-called chemical hydrides. At the heart of the issue is the fact that hydrogen is a gas at standard pressure and temperature and therefore low volumetric density.

On other hand, hydrogen molecules can bind to the surface of any material either through weak dispersive interactions (physisorption) or through stronger chemical bonding (chemisorption). Storage via physisorption in metal-organic or covalent-organic frameworks and activated carbons is a field that has received a lot of experimental and theoretical attention [5-9]. While both these routes to hydrogen storage show a high degree of reversibility (rehydrogenation), they suffer from poor retention and low gravimetric capacity limiting their storage capability to low temperatures (typically below 77 K) and off-board applications.

Hydrogen clathrates and molecular (van der Waal) compounds of H_2 and other simple molecules such as CH_4, NH_3, CO_2, N_2 have been known to form under high pressures and some of them can be recovered at ambient pressure and low temperatures[10-11]. The hydrogen storage potential of such clathrates and molecular compounds has received much attention not only because of their superior gravimetric capacity (the compound $CH_4(H_2)_4$ has 33.4 wt% of stored hydrogen and is found stable at ambient pressure and 77 K), but potentially small environmental footprint and high degree of reversibility[12].

Progress Report

Progress Report

We have discovered a new structure type in the H_2-H_2O system at low pressure-temperature conditions. The structure of the new phase is consistent with a water framework similar to α-quartz; the structure could also be related to the tetragonal clathrate phase reported previously for nitrogen and argon guests.

Raman spectroscopy and synchrotron X-ray diffraction are used to examine the high-pressure behavior of tetramethylammonium borohydride (TMAB) to 40 GPa at room temperature. The measurements reveal weak pressure-induced structural transitions around 5 and 20 GPa. Rietveld analysis and Le Bail fits of the powder diffraction data based on known structures of tetramethylammonium salts indicate that the transitions are mediated by orientational ordering of the BH_4- tetrahedra followed by tilting of the $(CH_3)_4N$+ groups.

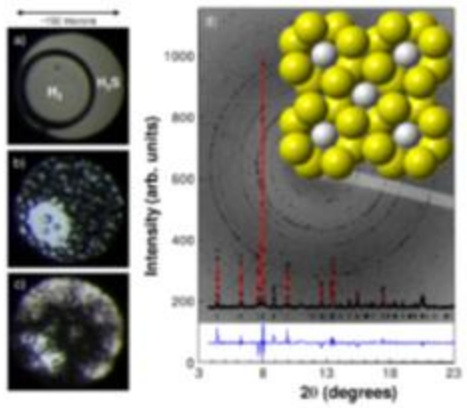

Fig. 1: Photomicrographs of H_2S + H_2 mixtures at room temperature (a) 0.2 GPa: fluid H_2S and fluid H_2 (b) 1.0 GPa: fluid H_2 and solid H_2S (c) 3.5 GPa: fluid H_2 and the compound (dark areas) (d) Experimental diffraction pattern (λ = 0.40548 A) at 4.5 GPa (points) along with the Rietveld refinement (red curve). The difference is shown in the lower panel for a fit with R_f = 3.5%. The 2D image is shown with the white spheres (H_2S) and yellow spheres (H_2) representing disordered molecules viewed along the c axis.

Hydrogen sulfide (H_2S) and hydrogen (H_2) crystallize into a 'guest-host' structure at 3.5 GPa and, at the initial formation pressure, the rotationally disordered component molecules exhibit weak van der Waals type interactions. With increasing pressure, hydrogen bonding develops and strengthens between neighboring H_2S molecules, reflected in a pronounced drop in S-H vibrational stretching frequency and also observed in first-principles calculations. At 17 GPa, an ordering process occurs where H_2S molecules orient themselves to maximize hydrogen bonding and H_2 molecules simultaneously occupy a chemically distinct lattice site. Intermolecular forces in the H_2S+H_2 system may be tuned with pressure from the weak hydrogen-bonding limit to the ordered hydrogen-bonding regime, resulting in a novel clathrate structure stabilized by cooperative interactions.

Previous efforts had focused on the NH_3BH_3/H_2 system and its polymeric analogs which were found to form van der Waals compounds at elevated pressures. In order to address questions regarding rehydrogenation of spent BN materials, compounds of the series $NR_xH_{(3-x)}BH_3$ were analyzed using gas phase G3MP2 calculations previously shown to reproduce BN and BH bond forming reactions to within 1.0 and 1.8 kcal/mol, respectively. Me_2NHBH_3 was down selected from the series due to the inability of the compound to lose multiple equivalents of H_2 and the modest enthalpy associated with the hydrogen release reaction as compared to other compounds of the series. Me_2NHBH_3/H_2 mixtures were found to hydrogenate ethylene and carbon dioxide at room temperature and pressures above 0.5 GPa. Control cells with no Me_2NHBH_3 showed no reaction after several weeks. The reaction with CO_2 was found to consistently produce CH_4 as the only product, but due to the multiple phases present, rates of the reaction have difficult to measure.

As a continuation of our high pressure studies of metal-rich hydrides, we continued to pursue synthesis, characterization and high pressure studies on this unique class of hydrides. The structural behavior of Na_2ReH_9 and K_2ReH_9 at high pressure was studied using *in-situ* Raman

spectroscopic and x-ray diffraction studies at high-pressure. The measurements reveal new phase transformation above 9 GPa and 18 GPa for both Na_2ReH_9 and K_2ReH_9 due to compression. The deuterated analogues have been synthesized and characterized. These samples were used to obtain in-situ diffraction patterns at high pressures using the Paris-Edinburgh cell at SNS.

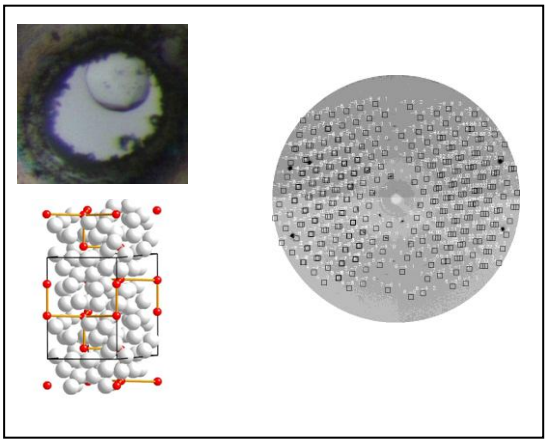

Fig 2: Photomicrograph of $Xe(H_2)_{24}$ in a diamond cell. The diffraction pattern could be indexed to a hexagonal unit cell and the structure of the xenon sublattice is shown in red. The hydrogen molecules are shown in gray.

The solid phase that occurs at 4.2 GPa and 300 K in the Xe-H_2 system has been identified as $Xe(H_2)_{24}$. The stoichiometry has been deduced from a determination of the overall xenon stoichiometry based on direct method solution of the crystal structure. The volume of the unit cell and the known molar volume of xenon at this pressure is then used to determine the lower bound on the hydrogen stoichiometry. Refinement of crystal structure indicates higher hydrogen content based on the fact that the xenon site occupancy is lower than unity for one of the three sites. Raman spectroscopy and x-ray diffraction studies show that this phase can be retrieved at 90 K and at atmospheric pressure.

References

1. Graetz, J., *New Approaches to hydrogen storage.* Chem. Soc. Rev., 2009. **38**: p. 73-82.
2. Tromp, T.K., et al., *Potential Environmental Impact of a Hydrogen Economy on the Stratosphere.* Science, 2003. **300**(5626): p. 1740-1742.
3. Dresselhaus, M.S. and I.L. Thomas, *Alternative energy technologies.* Nature, 2001. **414**: p. 332 - 337.
4. *Basic Research Needs for Electrical Energy Storage - a report of Basic Energy Sciences Workshop on Electrical Energy Storage*, U.S.D.o. Energy, Editor. 2007.
5. Murray, L.J., M. Dinca, and J.R. Long, *Hydrogen storage in metal-organic frameworks.* Chem. Soc. Rev., 2009. **38**: p. 1294-1314.
6. Rosi, N.L., et al., *Hydrogen Storage in Microporous Metal-Organic Frameworks.* Science, 2003. **300**(5622): p. 1127-1129.
7. Ward, M.D., *MATERIALS SCIENCE: Enhanced: Molecular Fuel Tanks.* Science, 2003. **300**(5622): p. 1104-1105.
8. Yang, Z., Y. Xia, and R. Mokaya, *Enhanced Hydrogen Storage Capacity of High Surface Area Zeolite-like Carbon Materials.* Journal of the American Chemical Society, 2007. **129**(6): p. 1673-1679.
9. Yaghi, O.M., *Organic Molecular Solids: Properties and Applications Edited by William Jones. CRC Press: Boca Raton, FL. 1998. 441 pp. $145.00. ISBN 0-8493-9428-7.* Journal of the American Chemical Society, 1999. **121**(51): p. 12214-12215.
10. Vos, W.L., et al., *Novel H_2-H_2O clathrates at high pressures.* Phys. Rev. Lett., 1993. **71**: p. 3150-3153.
11. Somayazulu, M.S., et al., *New high-pressure compounds in methane-hydrogen mixtures.* Science, 1996. **271**: p. 1400-1402.
12. Mao, W.L. and H.K. Mao, Hydrogen storage in molecular compounds. Proc. Nat. Acad. Sci., 2004. 101: p. 708-710.

Publication list acknowledging the DOE grant or contract

1."Novel Cooperative interactions and structural ordering in H_2S-H_2" Timothy Strobel, P. Ganesh, Maddury Somayazulu, P. R. C. Kent and Russell J Hemley, Phys. Rev. Lett. **107**, 255503 (2011)

2. "Static Compression of Tetramethylammonium Borohydride" Douglas Allen Dalton, M. Somayazulu, Alexander F. Goncharov, and Russell J. Hemley. Jl. Phys. Chem A, **115**, 11033 (2011)

3."High-pressure study of silane to 150 GPa" Timothy A. Strobel, Alexander F. Goncharov, Christopher T. Seagle, Zhenxian Liu, M. Somayazulu, Viktor V. Struzhkin, and Russell J. Hemley, Phys. Rev **B83,** 144102 (2011).

4."Phase Behavior of H_2 - H_2O at High Pressures and Low Temperatures" Timothy A. Strobel, Maddury Somayazulu, and Russell J. Hemley, J. Phys. Chem. C, **115**, 4898-4903 (2011).

5."High-Pressure Hydrogen interactions with polyaminoborane and polyiminoborane" Raja. S. Chellappa, Thomas Autrey, M. Somayazulu, V. V. Struzhkni and R. J. Hemley, ChemPhysChem, **11**, 93 (2010)

6. "Vibrational dynamics, intermolecular interactions, and compound formation in GeH_4-H_2 under pressure" Timothy A Strobel, X-J Chen, M. Somayazulu and R. J. Hemley, J. Chem. Phys., **133**, 164512 (2010)

7. "Pressure-induced bonding and compound formation in xenon-hydrogen solids" M. Somayazulu, P. Dera, A. F. Goncharov, S. A. Gramsch, P. Liermann, W. Yang, Z. Liu, H.K. Mao and R. J. Hemley, Nature Chemistry, **2**, 50 (2009)

Materials for Energy Applications

O. Chmaissem (chmaissem@anl.gov)*, S. Avci, B. Dabrowski*, S. Rosenkranz, R. Osborn
Materials Science Division, Argonne National Laboratory, Argonne, IL 60439
**and the Physics Department, Northern Illinois University, DeKalb, IL 60115*

Research Scope

With the beginning of the twenty-first century, the world finds itself on the brink of a large scale energy crisis and in a dire need for the discovery of novel materials for energy applications in addition to the ongoing search for previously untapped renewable energy. In the last decade, a few promising discoveries were made that propelled the fields of thermoelectrics, multiferroics, and rechargeable lithium ion batteries to the forefront of current research interests.

Research conducted in our labs led to the development of a set of well understood rules that allow for the design of new materials with tailored properties. The synthesis of high quality stoichiometric samples often requires the precise control of oxygen excess and/or vacancies at elevated temperatures where the tolerance factor magnitudes can be monitored to favor the formation of phases with diverse structures. For example, choosing the right temperature and oxygen partial pressure allows for the stabilization of either perovskite type or hexagonal $A\mathrm{MnO}_{3+d}$ phases. While the perovskite phases belong to the well known family of colossal magnetoresistance materials, the hexagonal ones were discovered to exhibit excellent oxygen storage capabilities. On the other hand, proper chemical substitutions at the *A*-site of the perovskite phase can lead to excessive strains and bond stretching to the point where the structure must buckle to release the strains. This structural behavior led to the recent discovery of true multiferroic properties in $\mathrm{Sr}_{1-x}\mathrm{Ba}_x\mathrm{MnO}_3$.

On another front, electrifying the transportation sector is necessary for increased implementation of renewable green energy technologies. Cathodes for rechargeable batteries have been under intense investigation since the development of Li-ion batteries. LiCoO_2 is the first reported layered oxide used as cathode and is currently commercially used in Li-ion batteries. However, this material still suffers from many drawbacks such as high costs and the relative toxicity of Co. To overcome some of these shortfalls, $\mathrm{LiMn}_2\mathrm{O}_4$, LiMnO_2 and LiNiO_2 were proposed as alternative cathode materials due to their chemical stability, low cost, environmental compatibility and relatively high operating voltage. However, these cathodes too present a set of new challenges that inhibit their use in rechargeable batteries. All these challenges, including high cost and the limited availability of Li, encouraged scientists to look for alternative cheaper and more abundant solid solutions. Our collaborators at Argonne led by Chris Johnson and Mike Thackery (CSE) have successfully synthesized several series of $(\mathrm{Na,Li})(\mathrm{Ni,Mn})\mathrm{O}_\delta$ that can be reliably used as cathodes at ambient temperatures in novel Na-ion battery cells. It is our goal to use neutron and x-ray diffraction to understand the functioning of these new materials when operated in *in-situ* and *ex-situ* environments.

Recent Progress

Materials for oxygen storage

We recently discovered that a special class of hexagonal manganites can be readily oxygen loaded to unusual high content levels that make the materials suitable for oxygen storage applications. Oxygen intake and release take place at relatively low temperatures of ~ 300 ^{o}C. High resolution x-ray (APS 11BM-B) and neutron powder diffraction (SNS-POWGEN) data collected from the $A_{1-x}\mathrm{Y}_x\mathrm{MnO}_{3+\delta}$ materials (where *A* = Dy, Er, and Ho) show large reversible oxygen storage/release capacities at atmospheric conditions. Diffraction and thermogravimetric measurements confirmed the high quality of the hexagonal $\mathrm{P6}_3\mathrm{cm}$ stoichiometric samples (δ=0)

and the formation of two new phases Hex_2 and Hex_3 at $\delta = 0.25$ and $\delta > 0.40$, respectively, as demonstrated by the behavior of the Bragg peaks shown in Fig. 1. The in-situ data shown in Fig. 1 were collected while heating $DyMnO_{3.45}$ in vacuum to 350 ^{o}C. Neutron data demonstrated the formation of disordered hexagonal (P6_3cm) structures for relatively low oxygen contents (e.g., $ErMnO_{3.25}$ and $YMnO_{3.25}$) and ordered (R-$3c$) superstructures for $DyMnO_{3.45}$ and $HoMnO_{3.4}$.

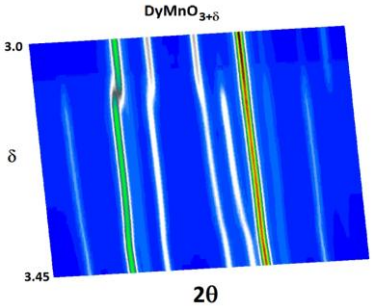

Fig. 1 X-ray data collected at beamline 11BM-B (APS)

Multiferroic $Sr_{1-x}Ba_xMnO_3$

Search for multiferroic materials, where magnetism and ferroelectricity are strongly coupled, is of fundamental technological and theoretical importance. Room temperature magnetic ferroelectricity, showing unique sensitivity to applied magnetic fields could lead to several new revolutionary magneto-electronic devices. Typically, both phenomena tend to be mutually exclusive because ferroelectricity is usually present for d^0 (for example M=Ti^{4+}, V^{5+}, Nb^{5+}) and magnetism for non-d^0 (for example, M=Cr^{4+}, Mn^{3+}, Mn^{4+}, Fe^{3+}, Co^{3+}) transition metals. Coupling between post-transition metal's (for example, Pb^{2+}, Bi^{3+}) ferroelectricity of *s*- and *p*-electrons and transition metal's *d*-electrons magnetism is known (for example, $Bi^{3+}Fe^{3+}O^3$), but it is weak and not of practical usage.

Recently, the Tokura group managed to grow $Sr_{1-x}Ba_xMnO_3$ single crystals with large Ba content (e.g., x = 0.45 and 0.50) in non-equilibrium conditions and observed spectacular multiferroic properties with $T_F \sim 400$ K and $T_N \sim 180$ K. Their extrapolated spontaneous polarization of ~25 $\mu C/cm^2$ is similar to typical ferroelectric $Ba^{2+}Ti^{4+}O_3$, thus, promising a real breakthrough for technological applications.

Very recently, we were able to overcome the synthesis challenges of thermodynamically stable bulk samples with x = 0.43 – 0.55 (see Fig. 3). Temperature-dependent data collected at the SNS (POWGEN) proved the formation of a non-centrosymmetrical structure P$4mm$ between T_N and T_F. In this space group, the positive Mn and negative oxygen octahedra have their center of mass shifted by a finite distance to create the polarization vector of the ferroelectric phase. Preliminary analysis of the structural results at 10 K suggested the magnitude of the polarization vector to be as large as 4.2 $\mu C/cm^2$. Below the magnetic transition temperature of ~200 K, the ferroelectric induced tetragonal distortion is largely suppressed and the material becomes G-type antiferromagnetic. The magnetic structure can be refined using the magnetic space group P$4/m'm'm$. The process is reversible as we recover the tetragonal P$4mm$ distortion after reheating the material to room temperature. Fig. 2 shows neutron refinements for x = 0.45 at room temperature using the space group P$4mm$.

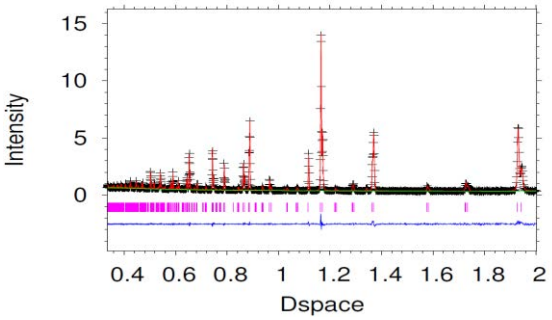

Fig. 2 Best-fit Rietveld refinements for $Sr_{0.55}Ba_{0.45}MnO_3$. Data collected at POWGEN proves the P$4mm$ structure.

Layered transition metal oxide battery cathodes

Layered transition metal (TM) oxides fall in the most successful category of cathodes with the formula of $LiMO_2$ (where M: Mn, Co, Ni, etc). The layered structure of these oxides provides very effective diffusion pathways for the Li ions during the charging and discharging processes of the battery. $LiCoO_2$ is the first reported layered oxide used as cathode and is currently commercially used in Li-ion batteries. Its energy is relatively low (0.5 e^- per Co) despite its high voltage of 4.2 V.

The low cost alternative electrodes $LiMn_2O_4$ and $LiMnO_2$ are chemically stable with a relatively high operating voltage of 4.1 V. However, due to irreversible processes, $LiMn_2O_4$ dies very quickly especially at temperatures over 50 ^oC due to dissolution by the electrolyte while $LiMnO_2$ experiences an irreversible structural transition due to Jahn-Teller distortion. $LiNiO_2$ cathodes are cheaper, safer and exhibit a higher reversible capacity (200mA h g^{-1}) than that of $LiCoO_2$. However, they form a disordered structure during charging because of the Ni^{+3} ions transformation into larger Ni^{+2} ions with comparable ionic size with Li; thus, preferring to move into the emptied Li locations. Replacing Li with Na in $(Na,Li)(Ni,Mn)O_\delta$ not only reduces the cost of the proposed batteries but also prevents the Na/TM disorder due to the large ionic size of Na. The average voltage of the Na-cell is determined as 3.4 V with a very stable capacity of 95-100 mA h g^{-1} over 50 cycles. The electroactivity, stable capacity, ambient temperature operation capability and wide availability of Na make these oxides promising candidates for Na-ion batteries.

To understand the underlying physical and chemical properties in these materials, unique structural dynamic measurements as a function of Li insertion/extraction composition must be conducted and analyzed. However, preliminary neutron diffraction data are needed to determine the diverse phases that may form before, during, and after cycling of the battery. For this purpose, eighteen samples were prepared and measured on HRPD-ISIS from which we were able to demonstrate the formation of the layered structure in addition to other intermediate phases (Fig. 3). Detailed analysis of the data is currently underway.

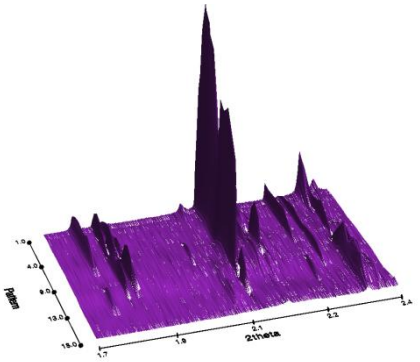

Fig. 3 Raw neutron diffraction data showing the evolution of diverse phases in $(Na_xLi_y)(Ni_{1-z}Mn_z)O_\delta$

Future Plans

Thermoelectrics

$CsBi_4Te_6$ has been known as a leading thermoelectric material at low temperature for over ten years since its discovery by the group of Mercouri Kanatzidis. Stoichiometric $CsBi_4Te_6$ is a narrow gap semiconductor and has an electrical conductivity of 2000 $\Omega^{-1}cm^{-1}$ and a thermoelectric figure of merit, ZT, of 0.82 at 225 K with *p*-type doping. Because it can also be doped with *n*-type carriers, this compound is particularly suitable for low temperature cooling applications. Recently it was found that this compound becomes superconducting upon both *p*-type and *n*-type doping. The origin of superconductivity in doped semiconductors is not yet understood although resonant scattering from the dopant virtual bound state or an excitonic mechanism, as proposed in intercalated $TiSe_2$ are candidates. We will utilize inelastic neutron scattering in order to obtain detailed investigations of the phonon density-of-states in this and related compounds. This will provide insights into why this material is such a good thermoelectric compound and this will also allow us to determine the strength of electron-phonon coupling and whether it is sufficient and responsible for inducing superconductivity.

Sodium based ionic batteries

Neutron diffraction experiments on the $Na_xLi_yNi_{1-z}Mn_zO_\delta$ system will enable us to pinpoint the locations of the Na and Li ions in diverse environments and to determine subtle and systematic changes in the nuclear structures. The most effective way to gain insight into these processes is to perform *in situ* experiments. While such experiments on Li-ion batteries and cathodes have been performed extensively utilizing x-ray synchrotron sources, relatively few have been performed using neutron sources, and in particular, none have involved analysis of composite 'layered-layered' cathodes. *In situ* neutron scattering has the advantage of being more sensitive to subtle structural changes involving lighter atoms, such as Li and O, during the charging and discharging cycle. These cathode materials undergo a unique oxygen loss process and structural

rearrangement on the first battery charge that is largely unknown due to limitations of x-ray – based measurements in analysis of movement of Li and O. *In situ* neutron scattering techniques and measurements will be integrated into the ongoing Li-ion battery development and improvement programs. Solutions and insights for optimizing the composite cathode will be gained with these new measurements. Innovative approaches to the design of battery cells for neutron scattering coupled with recent advances in neutron data acquisition methods are key to overcoming the typical challenges posed by *in situ* diffraction experiments. Ultimately, our goal is to establish leadership in neutron scattering sciences for Li-ion batteries, including new systems such as Li-air batteries.

$Sr_{1-x}Ba_xMnO_3$: pressure and magnetic field dependent measurements

We plan to perform in-depth studies as a function of extreme pressures (7.5-25 GPa) and high magnetic fields (up 14.5 T) at 300 K (below T_F) and base temperature (below T_N). We speculate that both the pressure and/or magnetic fields would force the cations and anions to move off their equilibrium positions and change the electric polarization vector. It is very likely that the antiferromagnetically aligned magnetic moments would be forced to cant; thus, inducing ferromagnetism that would coexist with ferroelectricity. Moreover, it's likely that the pressure and magnetic fields would induce structural and magnetic transitions which, in turn, would affect the electric polarization vector direction and magnitude. We will use the neutron data to determine the magneto-ferroelectric correlations with the structure. Structural data under pressure and temperature will also enable us to determine the optimum buckling angles (e.g., Mn-O-Mn (T, constant P or H)) and bond-lengths which will guide our efforts to synthesize newer versions of this multiferroic system in which both ferroelectricity and ferromagnetism coexist near or at room temperature.

Publications

1- Kinetic control of structural and magnetic states in $LuBaCo_4O_7$, S. Avci, O. Chmaissem, H. Zheng, A. Huq, D. Khalyavin, P.W. Stephens, M.R. Suchomel, P. Manuel, J.F. Mitchell, Phys. Rev. B 85, 094414 (2012)

2- Structural and physical properties of Re substituted B-site ordered and disordered $SrCo_{1-x}Re_xO_{3-d}$ (x=0.1, 0.25, 0.5), A. Baszczuk, B. Dabrowski, S. Kolesnik, O. Chmaissem, M. Avdeev, Journal of Solid State Chemistry 186, 240–246 (2012)

3- Comparison of magnetic and thermoelectric properties of $(Nd,Ca)BaCo_2O_{5.5}$ and $(Nd,Ca)CoO_3$, S. Kolesnik, B. Dabrowski, O. Chmaissem, K. Wojciechowski, and K. Swierczek, Journal of Applied Physics 111, 07D727 (2012)

4- Synthesis and oxygen content dependent properties of hexagonal $DyMnO_{3+\delta}$, S. Remsen, B. Dabrowski, O. Chmaissem, J. Mais, A.Szewczyk, Journal of Solid State Chemistry 184, 2306–2314 (2011)

5- Parameters controlling magnetic interactions in perovskite manganites, B Dabrowski, J Mais, S Kolesnik and O. Chmaissem, Journal of Physics 303 (2011) 012057

6- Superconductivity and oxygen ordering correlations in the homologous Series of $(Cu,Mo)Sr_2(Ce,Y)sCu_2O_{5+2s}$, O. Chmaissem, I. Grigoraviciute, H. Yamauchi, and M. Karppinen, and M. Marezio, Phys. Rev. B 82, 104507 (2010)

7- Competing magnetic ground states in A-Site layer ordered manganite $La_{1-x}Ba_{1+x}Mn_2O_6$, O. Chmaissem, D. E. Brown, Y. Ren, S. Kolesnik, J. Mais, B. Dabrowski, Physical Review B 81, 012407 (2010)

8- Electronic structures, hole-doping and superconductivity of the s = 1, 2, 3 and 4 members of (Cu,Mo)-12s2 homologous series of superconductive copper oxides, Inga Grigoraviciute, Maarit Karppinen, Ting-Shan Chan, Ru-Shi Liu, Jin-Ming, Chen, Omar Chmaissem, and Hisao Yamauchi, Journal of the American Chemical Society 132, 838-841 (2010)

Polythiophene-Fullerene Phase Behavior and Effects on Organic Photovoltaic Device Performance

David Bucknall, N Deb, School of Materials Science and Engineering, Georgia Institute of Technology, Atlanta, GA
Alamgir Karim, Jose Chapa Garza, Gurpreet Singh, Xiong Gong, Department of Polymer Engineering, University of Akron, Akron, OH
Dharmaraj Raghavan, Praveen Pitliya, Shimelis Hailu, Paul Hudrlik, Anne Hudrlik, Department of Chemistry, Howard University, Washington D.C.
Scott Sides, Tech-X Corporation, Boulder, CO
Bobby Sumpter, Oak Ridge National Lab, Oak Ridge, TN

We are conducting studies to try to understand polymer-fullerene interactions and the effect that ligands on the fullerene play in the phase behavior with polymers and ultimately how this affects device performance. We have therefore been studying both a homopolymer homologous semicrystalline polythiophenes (poly(3-butyl thiophene) (P3BT), poly(3-hexyl thiophene) (P3HT) and poly(3-octyl thiophene) (P3OT)) blended with the fullerenes C_{60}, PCBM and bis-PCBM, and in parallel work blends of PS-P3HT block copolymers mixed with N-methyl fulleropyrrolidine with various sides group (R) (see Figure 1 below). Evaluation of their miscibility and morphology in thin films has been made for all systems and for the polythiophene-fullerene mixtures also compared to organic photovoltaic (OPV) device performance.

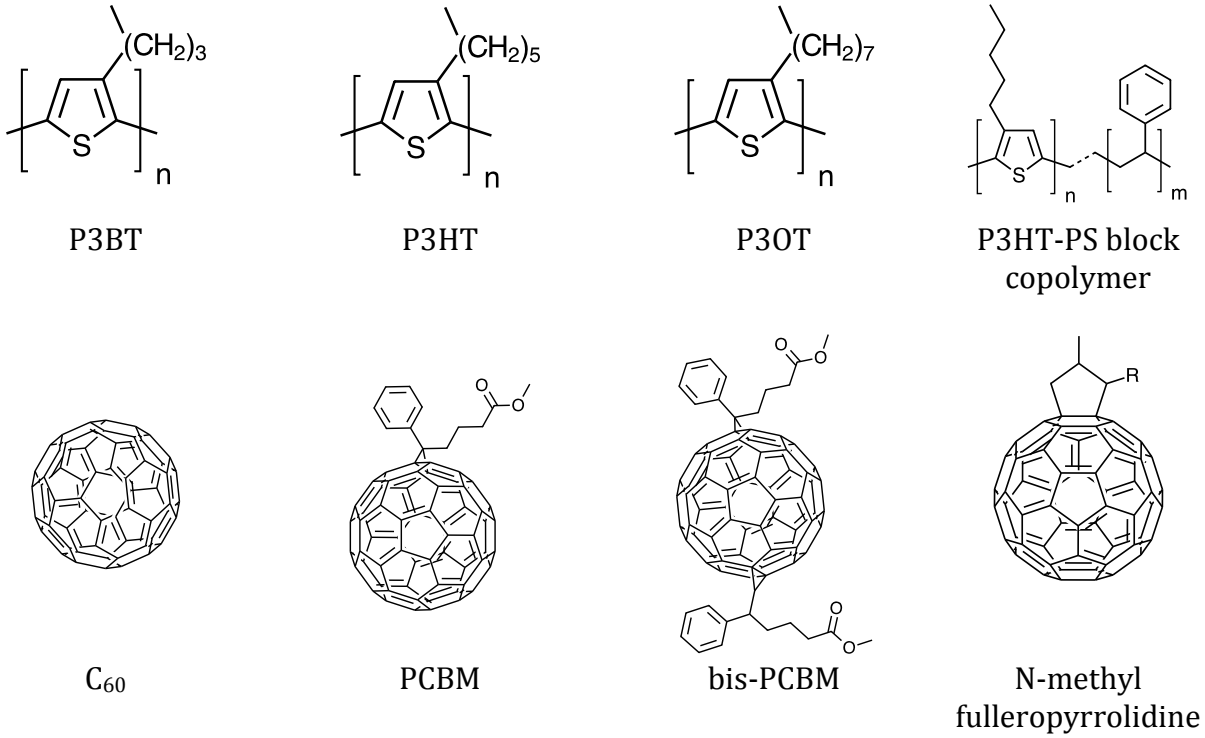

Figure 1: *Chemical formulae of polymers and fullerenes being studied. The R groups in the N-methyl fulleropyrrolidine are described in the text.*

Polythiophene-fullerene phase morphology:
The morphology of the three polythiophenes and three fullerenes has been explored predominantly in thin film device geometry allowing us to compare directly to device performance. The morphology of the thin films has been measured using neutron reflectivity (NR) to give the composition profile normal to the film thickness. The bulk heterojunction (BHJ) blends of each polythiophene and fullerene combination were all prepared from solution and included in a standard device configuration consisting of PEDOT:PSS/polythiophene:fullerene BHJ/Al. For the NR measurements the samples were prepared on Si substrates (because of their superior flatness required for these types of measurements), but exactly the same thicknesses of films were used in the devices prepared on ITO instead of Si in order to provide the bottom electrical contact.
NR data show that even in the as spun films there is a non-homogenous composition profile in the BHJ layer. After annealing using a standard time and temperature for these materials (30 mins at 150°C) the NR shows that for all the systems the BHJ are composed of three distinct components. At the Al interface there is an excess of fullerene and there is additionally a depletion of fullerene (an excess of polythiophene) at the PEDOT:PSS interface. In between the composition at least in the normal direction is constant. This model can be summarized as shown in Figure 2 for the example of the P3HT series.

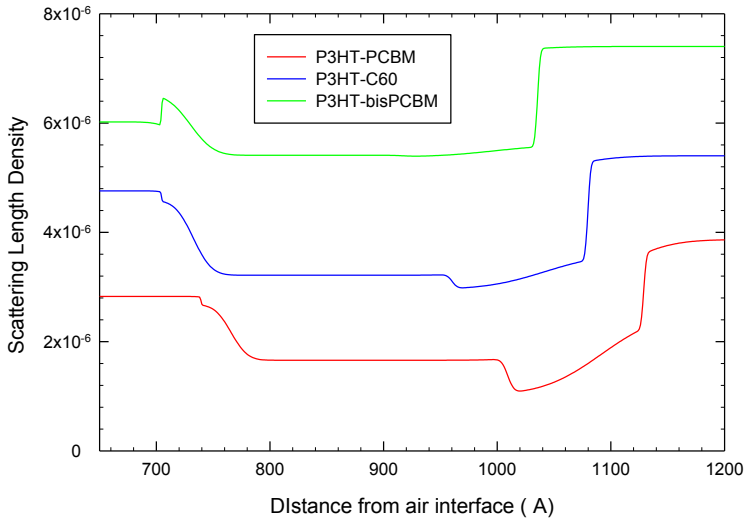

Figure 2: *Neutron scattering length density versus distance profiles for P3HT for different fullerenes, showing enrichment of the fullerene at the Al interface (LHS of plot) and depletion at the PEDOT:PSS interface (RHS of plot).*

Comparing the characteristic features of the morphology of the BHJ films to the device performance (PCE% measurements) it would appear that the depletion of the fullerenes from the PEDOT:PSS interface is the dominant factor increasing the PCE%, with little correlation to the excess fullerene observed at the Al interface. The efficiency of the fullerene-polythiophene systems is non-linear with alkyl chain length for all fullerenes,

with a maximum observed for the P3HT BHJs. This is consistent with the NR data showing a maximum depletion of the fullerene from the PEDOT:PSS interface. While this factor is obvious from the data, future studies will examine the exact mechanism of depletion and whether it is the only contributing factor.
The relationship between device performance and the polythiophene-fullerene interaction behavior is still not fully understood, but on-going DFT calculations coupled with detailed on-going neutron scattering studies are beginning to reveal important correlations.

Block Copolymer-Fullerene Phase Behavior
To control the morphology we are exploiting the use of block copolymers nanophase separation into which the fullerenes are incorporated. We have synthesized PS-P3HT block copolymer by combining atom transfer radical polymerization (ATRP) and Grignard metathesis (GRIM) polymerization, using a modified method of McCullough *et* al.[1] The synthesized final compound was characterized by NMR and GPC. ^{1}H NMR spectrum of PS-P3HT shows the appearance of new peaks indicating the formation of diblock copolymer. GPC established the weight average molecular weight and polydispersity of the PS-P3HT to be 11389 and 1.47, respectively.
A homologous series of novel fulleropyrrolidine derivatives were synthesized by exploiting the Prato reaction.[2] The synthesis of N-methyl fulleropyrrolidine (NMFP) analogues was based on 1, 3-dipolar cycloaddition of azomethine ylides to C_{60}. The compounds synthesized are *R* = 4-nitro phenyl, 4-cyano phenyl, 4-formyl phenyl, phenyl, pyridinyl, and 4-fluoro, 3-nitro phenyl. The functionalized fulleropyrrolidines were characterized by ^{1}H NMR, ^{13}C NMR, FT-IR, MALDI-TOFMS, UV-Vis, and fluorescence spectroscopy. A characteristic quasi molecular ion (M+H) peak for the synthesized compounds was observed by MALDI-TOFMS. Functionalization of C_{60} causes a hypsochromic shift of the peak at 329 nm to lower wavelengths in the UV-Vis spectra and an enhancement in the fluorescence intensity (see Table 1). In addition there is a hypsochromic shift in toluene solutions with the introduction of highly electronegative groups on N-methyl fulleropyrrolidines (NMFP). The fluorescence bands are furthermore sensitive to the solvent media in which they are dispersed as well.

Table 1: Absorbance and Fluorescence parameter of C60 and its derivatives

Compounds	Absorbance band/nm (Cyclohexane)	Fluorescence band/nm	
		Toluene	Benzonitrile
C60	329,405,622	689	-
1	255,306,328,433,705	711	714
2	257,313,326,433,701	707	710
3	257,313,326,433,702	707	709
4	255,310,326,430	708,	710
5	256,309,326,430,701	710	712
6	258,310,326,431,702	708	710
7	255,318,430,657,699	706	710

We noticed an increase in anodic shift of the first reduction potential of functionalized fulleropyrrolidine with respect to the electron withdrawing ability of the *R*-group attached to NMFP. The first reduction potential of N-methyl-2-(4-fluoro, 3-nitro phenyl) fulleropyrrolidine (NO_2-F-NMFP) and N-methyl-2-(4-nitro phenyl) fulleropyrrolidine (*p*-NO_2-NMFP) and N-methyl-2-(4-cyano phenyl) fulleropyrrolidine (*p*-CN-NMFP) was found to be comparable to that of widely used PCBM. Thermal analysis of functionalized fulleropyrrolidines indicated that the novel NMFP compounds were stable up to 340 ^{o} C.

To understand the polymer-fullerene interactions and explore the effect of functional groups on the phase behavior with block copolymers and ultimately how this affects device performance, solution blended films were prepared by casting on a silicon substrate. A systematic study was performed in order to investigate the effect of thermal treatment with or without fullerene on the morphology of PS-P3HT film. AFM results of PCBM: PS-P3HT blends show that dispersion of PCBM in PS-P3HT is sensitive to the mode of annealing. Significant variation in surface topography of this blend was observed comparing as cast, oven annealed and zone annealed samples. Zone annealed (T_{max}=150 ^{o}C with 40^{o}C/mm gradient and 40 □m/s zone speed) films of PS-P3HT in Figure 3 shows a lamellar structure, which is in agreement with previously reported data.[3]

The zone annealed sample of PCBM: PS-P3HT shows that the 40% PCBM which is typical for solar cell devices is well dispersed in the PS-P3HT system, but it drastically changes the scale and nature of the lamellar ordering. Future scattering studies will investigate the nanoscale phase morphology of these synthesized novel functionalized NMFP/PS-P3HT systems, and compare it with PCBM:PS-P3HT system under different annealing conditions of oven versus zone annealing. These structural and morphological studies are being correlated to device studies currently underway as well. Finally, we plan to perform extensive device characterization studies with these promising ordered BHJ systems.

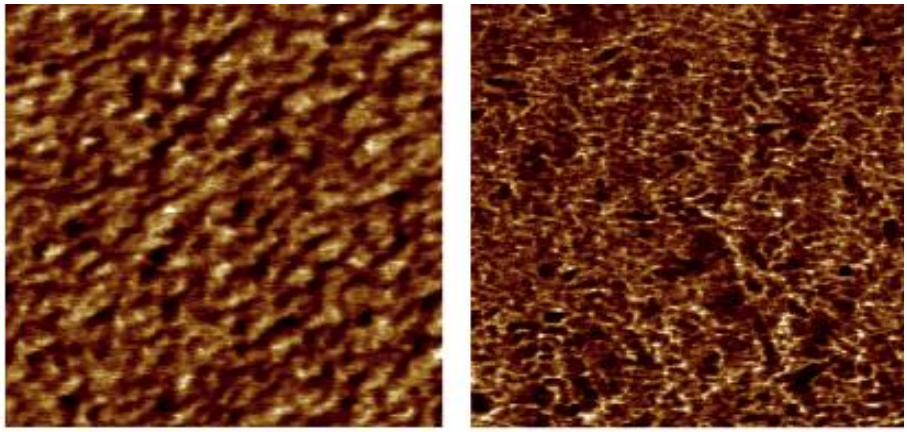

Figure 3: *Atomic Force Microscopy adhesion images (2mm X 2 mm) of zone annealed samples of synthesized PS-P3HT without (left image) and with typical 40 % PCBM (right image) as in organic solar cells.*

References:

[1]. Iovu, M.C., *et al. J Macromol Sci A: Pure & Appl Chem*, (2006) 43, 1991-2000.

[2]. Maggini, M., Sccorano, G., Prato, M. *J. Am. Chem. Soc. (1993)* 115:, 9798- 9799.

[3]. Yu, X., et al *ACS NANO,* (2011) 5, 3559-3567.

Acknowledgements

This work was funded under DOE Contract No. SC0005364

Dynamics of Ionic Polymers at Interfaces: Key to Enhanced Longevity of Clean Energy Devices Neutron Scattering and Molecular Dynamics Simulation Studies

Dvora Perahia (dperahi@clemsoon.edu), Naresh Osti, Thusitha Etampawala, Flint Pierce[1]

Chemistry Department Clemson University, Clemson SC 29634-0973

Gary S. Grest

Sandia National Laboratories, Albuquerque, NM 87185

1-Current address Sandia National Laboratory, Albuquerque, NM 87185

Scope of Research

Polymers serve as key components in fuel cells, flexible solar cells and polymer-based batteries, where instabilities that develop in the membranes during operation affect their efficiencies and mechanical integrity. Controlling the ability of polymers to move and rearrange to compensate for changes that take place during operation will enhance the efficiency and longevity of polymer based clean energy devices.

Examining closely the role of polymers in energy applications it becomes apparent that the macromolecules reside at interfaces with additional components such as electrodes, nanoparticles or non-active polymer layers. The advantage of polymers for clean energy applications lies in their flexibility, optional control over their chemistries as well as their low cost. One of the most profound challenges for using macromolecules however remains that under the conditions where transport of light, electrons, ions, or guest molecules is optimized the interfacial regions within the complex system are compromised. With ion transport being in the core of fuel cells and batteries, the current research probes the dynamics of complex ionic rigid polymers that consist of a hydrophobic part and hydrophilic ionizable group at interfaces with a working hypothesis that the rigidness of the polymer will enhances the mechanical stability of the membranes.

The dynamics of polymers in bulk and interfaces has been at the center of numerous studies and is only partially resolved. Confining ionic polymers to an interface results in a multifaceted problem where process including transport of ions and guest molecules, dynamics of the hydrophobic part of the polymer and that of the ionizable part of the chain take place. Our studies are distinctive in their focus on the dynamics at the interfacial regions on multiple time scales, accounting for the multifaceted nature of the interfaces.

The study consists of two components, experimental investigations and computational efforts. The experimental component was designed to derive empirical trends that will be correlated with

a molecular parameters that characterize the polymers with a focus on a rigid family of ionic materials. The computational study was designed to provide molecular insight into the ensemble averages provided by the experimental neutron studies. The interfacial regions were probed on multiple length scales from molecular dimensions, to the nanometer lengths to a macroscopic understanding of recovery process of membranes, where the polymer molecules have to migrate across an interface to heal.

Resent Progress

Neutron studies including neutron reflectometery and neutron back scattering have shown that hierarchal bundle structures formed by highly rigid polymer sulfonated polyphenylene (SPP) ionomer, provide a sturdy immobile network that allows dynamics of ions and guest molecules while the mesh is retained. The solvent dynamics takes place at the interface of the bundles. Figure 1-a demonstrates the rigidity of the polymer, where the patterns remain as rigid as a solid vanadium reference sample across a broad temperature range from *-100 to 250 ^{o}C* and across a large energy scale that corresponds to characteristic energies associated with diffusion of polymers. While the polymer forms a rigid network, water and methanol remain dynamic as demonstrated Figure 1-b. At low temperatures water molecules hop between different sites. With increasing temperature, the solvent molecules are less confined and their dynamics become that of a constraint though continuous diffusion.

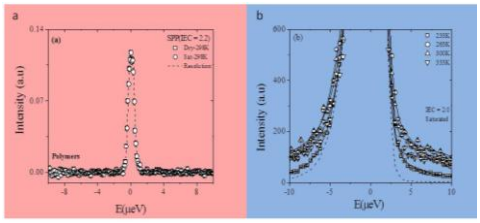

Figure 1: a-Quasi-elastic neutron scattering pattern of a SPP membrane with a 33.3 mol% sulfonation a-The polymer is protonated in 99.9% D_2O; b-in H_2O.

On a macroscopic level, interface mediated diffusion water diffusion into ultrathin SPP films was investigated by neutron reflectometry. Measurements were carried out as a function of time, ionic strength and film thickness. The dry film profiles were often affected by the spin coating procedure. When annealed in presence of room humidity, the films become rather homogenous. Exposure to vapor resulted in water accumulation at the air interface. The water diffusion into the film occurs in two stages. The water first wets the surface and then penetrates into the film. Initial water diffusion into SPP is characterized as Fickian diffusion, which transitioned to an anomalous diffusion with extended exposure time to water. Our results have shown that water diffusion depends on ionic strength and film thickness.

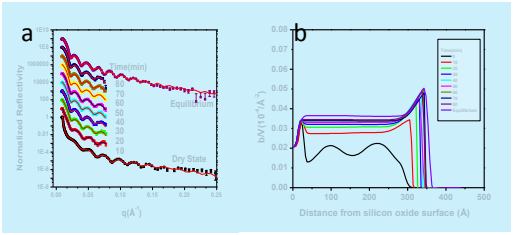

Figure 2: a-Neutron reflectivity data (symbols) with fitted profiles (solid lines) in contact with D_2O vapor, from bottom to top as a function of increasing exposure time; b-Polymer profiles extracted from the data.

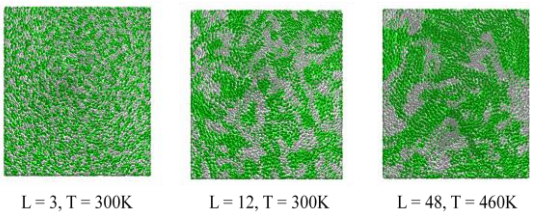

Figure 3: Top view of a liquid of multiblocks that consist of 96 mers at the indicated block length L and temperature. For L=48, a diblock co-polymer, an elevated temperature projection is shown to retain the liquid phase.

Computational Studies have resolved for the first time the complex nature of interfaces of a polymer that consists of highly incompatible segments well as identified pathways for migration across an interface. At the onset of our study with the available computational tools, we could atomistically probe processes up to 10 nsec and with course-grain models up to ~100 nsec. We therefore studied model systems. The chemical composition of an interface defines much of the interfacial behavior of a polymer including its stability, adhesion as well as interfacial mediated transport. Using model semifluorinated multiple block co-polymers, we have shown that the interface is complex and consists of both fluorinated and protonated segments as observed in Figure 3. This complex structure affects the diffusion across the interface. The next step would be to incorporate ionic groups in one of the blocks.

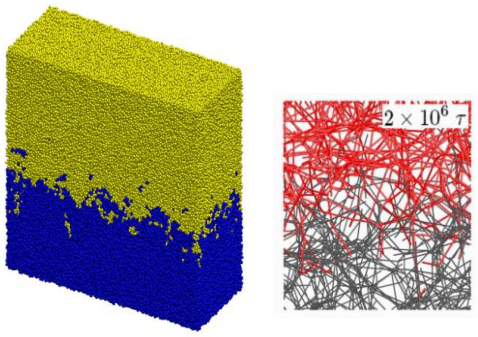

Figure 4: Left: A snapshot of the interfacial region for two entangled liquid polymer films of length N=500 after interpenetrating for $2x10^6$ τ and a primitive path representation of the same interface.

In order to heal damaged regions, polymer molecules have to migrate across an interface and regain the original structure. Using coarse grain molecular dynamics simulations we identified the pathways of polymer dynamics across interfaces. Shown in Figure 4 is a snapshot of the interface between two interpenetrating polymers and a primitive path analysis of the entanglements between the two films after a specified time. This is the first time where the onset of formation of entanglements has been observed.

Future Plans

Neutron Studies: Our future work will focus on elastic and inelastic neutron studies of controlled geometries at interfaces and in bulk membranes. Using well defined anionic polymerization we will tailor the hydrophilic and hydrophobic parts of the polymers and the number of ionizable groups. The model polymers will incorporate an ionomer block, a block that will allow mobility and rearrangements and a block that will enhance mechanical stability. The working hypothesis is that the well defined conditions will allow tailoring the structure of the polymer and therefore its interfacial behavior, leading to a significantly improved mechanical stability and ionic transport simultaneously.

Computational Studies: The computational component will initially track the experimental studies. With the development of computational tools and enhanced resources, we will study the same systems probed experimentally. The neutron techniques will provide ensemble averages of the interfacial structure and dynamics whereas the computational studies will provide molecular insight and resolve the interactions that control the systems. Combined they will provide unprecedented insight into the dynamics at the interfacial boundaries of ionic polymers.

Publications (FY09-FY011)

1. Pierce, F; Tsige, M.; Borodin, O.; Perahia, D.; Grest, G. S**., Interfacial properties of semifluorinated alkanes,** J. Chem. Phys. (2008) 128, 214903-1– 214903-14.
2. Pierce, F.; Tsige, M.; Perahia, D.; Grest, G. S., **Liquid-liquid interfaces of semifluorinated alkane diblock copolymers with water, alkanes, and perfluorinated Alkanes**, J. Phys. Chem. B (2008) 112, 16012-16120.
3. Pierce, F.; Perahia, D.; Grest, G. S.*,* **Interdiffusion of short chain pligomers into an entangled polymer film,** Macromolecules (2009) 42, 7969-7973.
4. Pierce, F.; Perahia, D.; Grest, G. S., **Spreading of liquid droplets on permeable polymeric surfaces,** EPL (2009) 86, 64004/1-64004/5.
5. He, L.; Smith, H. L.; Majewski, J.; Fujimoto, C. H.; Cornelius, C. J.; Perahia, D., **Interfacial effects on water penetration into ultrathin ionomer films: An in situ study using neutron reflectometry,** Macromolecules (2009) 42, 5745-5751.
6. He, L.; Fujimoto, C. H.; Cornelius, C. J.; Perahia, D., **From solutions to membranes: structure studies of sulfonated polyphenylene ionomers,** Macromolecules (2009) 42, 7084-7090.
7. Pierce, F.; Perahia, D.; Grest, G. S., **Interfacial effects of nanometer fluorinated segments on energy controlled responsive polymeric films: molecular dynamic simulations** Polymer Preprints (American Chemical Society, Division of Polymer Chemistry) (2009) 50, 150-151.
8. Pierce, F.; Perahia, D.; Grest, G. S., **Dynamics of polymers across an interface**, EPL (2011) 95, 46001.
9. Maskey, S; Pierce, F.; Perahia, D.; Grest, G. S., **Structure and dynamics of a single conjugated polymer molecule in solution**, J. Chem. Phys. (2011), 134, 244906/1-244906/8.
10. Perahia, D.; Ratnaweera, D. R.; Shrestha, U. M.; Iacono, S. T.; Smith, D. W.; Mabry, J.; Majewski, J., **Semi-fluorinated polymer/POSS thin film nanocomposites: response to water,** ACS Book Series (2012, accepted)

Application of *in situ* Neutron Diffraction to Understand the Mechanism of Phase Transitions During Electrochemical Cycling of High Capacity Mg/Si Nanostructured Electrodes

K. S. Ravi Chandran
Department of Metallurgical Engineering
135 South 1460 East Rm. 412, The University of Utah, Salt Lake City, UT 84112
email: ravi.chandran@utah.edu

Abstract

The fundamental process governing charging and discharging in energy storing battery electrodes is phase transition. For increased cyclic capacity, efficiency and durability, electrodes for Li-cells must show fully reversible phase transformations upon Li extraction and insertion. Progress in this direction is therefore depends on understanding the factors that enable or prevent such transformations under battery cycling conditions.

The primary objective of this research is to perform *in situ* neutron diffraction experiments under electrochemical conditions to understand the fundamental nature of phase transitions during Li insertion/extraction in Mg/Si nanostructured high capacity electrodes. A novel electrochemical cell, that enables time-averaged in situ observations of bulk phase transitions, will be constructed and optimized for this research. The cell will be used to understand the phase transitions in electrodes made with different nanoparticle sizes and embedded in a conductive medium. The key objective is to discover the particle sizes and compositions at which electrochemically reversible transformations would occur. Mg/Si nanomaterials are the most suited for this study because they (i) can provide very high energy-storage capacity, (ii) offer many phase transition paths (solid solution, intermetallic, displacement reactions and ordering) representing most anode materials and (iii) present the greatest challenge in anode material science. In particular, the research will investigate (i) how the changes in particle size and composition of the electrodes affect/limit the phase transitions and cell degradation and (ii) how the potential windows and rate of charge/discharge rates affect the kinetics of phase transitions and (iii) the kinetics of formation of SEI layer in electrode-electrolyte interface. The research will be performed in collaboration with SNS facility (collaboration with Dr. Xun-Li) at Oak Ridge National Laboratory where the in situ neutron diffraction experiments will be conducted.

The understanding of phase transitions in Mg/Si electrodes can lead to breakthroughs in electrode chemistry and design for high energy-storage capacity Li-Mg and Li-Si cells. The research can have a large impact in battery materials science. The lack of reversible phase transformations in electrodes based on these materials, over a large number of cycles, has been the bottleneck that is preventing the realization of high capacity battery systems. Nanoparticle electrodes have a high-density of nanoscale interfaces and the research can lead to the discovery of optimum particle size, structure and composition that yield highly reversible electrode. The research will also enable the education and training of two graduate students in the new frontiers of battery material science.

Neutron and X-ray Scattering Group: Developments Enabling Science

S. Rosenkranz (srosenkranz@anl.gov), R. Osborn, S.G.E. te Velthuis,
U. Perez-Salas, G.P. Felcher, J.-P. Castellan, F. Weber
Materials Science Division, Argonne National Laboratory, Argonne, IL 60439

Research Scope

Members of the Neutron and X-ray Scattering Group have a long tradition of advancing the field of both neutron and x-ray scattering through instrument and technique development when it is necessary to overcome limitations of existing techniques that hinder the goals of our scientific programs. As a direct consequence of the needs our scientific programs, members of our group were responsible for the conceptual design and proposal of *Corelli*, an instrument under construction at SNS dedicated to single crystal diffuse scattering measurements with efficient energy discrimination obtained by utilizing the cross correlation method. To further enhance our capabilities to utilize diffuse scattering to study complex disorder due to frustration and phase competition, we are also exploiting the latest developments of fast x-ray area detectors in order to optimize high-energy x-ray diffuse scattering measurements. Members of the group also proposed developing an instrument, *SERGIS*, based on combining spin echo methods with grazing-incidence small angle scattering for efficient studies of the structure and kinetics of soft interfaces, and they were involved in the first successful demonstration of this technique. This technique is now available on *OFFSPEC* at ISIS, U.K., but the capabilities and strengths of this technique and data analysis methods are still in the process of being defined and developed.

In order to fully utilize the capabilities of current instrumentation, we have developed a novel technique of measuring single crystal inelastic neutron scattering at pulsed sources. This *Sweep* mode exploits the event-mode data acquisition system at SNS in combination with continuous sample rotation to allow almost instantaneous measurements over complete four-dimensional volumes of ($\mathbf{Q}$,ω)-space, which has tremendous advantages over the traditional step-and-stop measurements at discrete rotation angles. Members of the group are also supervising the development of a flexible toolbox for the simultaneous analysis of both neutron and x-ray data.

Recent Progress

Corelli: The development of efficient tools for single crystal diffuse scattering arose from our scientific projects to study the influence of complex disorder in the form of stripes, checkerboards, phase separation, and other short-range order motifs, that underlie many unusual physical properties, such as colossal magnetoresistance or high temperature superconductivity. In order to obtain a realistic model on how a material self organizes on the nanoscale, diffuse scattering measurements must be made over large volumes of reciprocal space with high momentum and energy resolution. These conflicting requirements cannot currently be met with existing instrumentation. In order to overcome these limitations, we proposed to build a dedicated instrument, *Corelli*, which utilizes cross correlation to obtain sufficient energy discrimination while retaining the efficiency of a white-beam Laue diffractometer for covering large volumes. This instrument is now under construction at SNS and is projected for user operation by 2014. In preparation to fully utilize this instrument when it becomes operational, we have carried out final tests of the capabilities of this technique for providing energy

discrimination and for measuring diffuse scattering from single crystal samples utilizing a prototype instrument installed on flight path 12 of the Lujan Neutron Scattering Center in Los Alamos. From measurements performed on a powder sample of $PrAl_3$, which has a well-known, sharp crystal-field transition at 4meV, we were able to successfully reconstruct the scattering function and show that the cross correlation can achieve the desired energy discrimination. We have also obtained data on a variety of single crystal samples with strongly enhanced diffuse scattering, such as the Huang scattering in the polaronic phase of manganites.

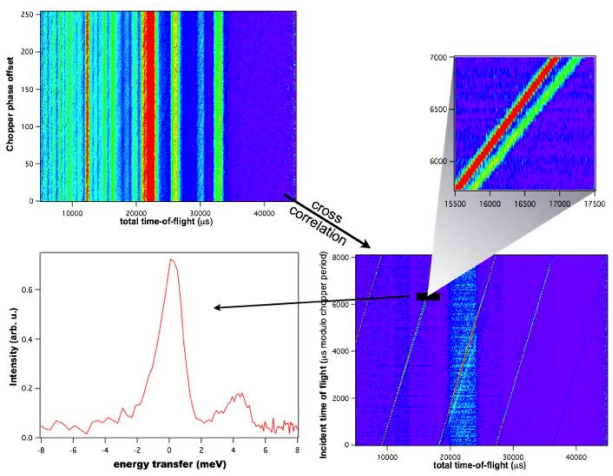

Fig. 1: Raw data (top left) and reconstructed scattering function (bottom right) from the test experiments performed on PrAl3. The cut (bottom left) through part of the data shows the clearly resolved elastic line and the crystal field excitation.

SERGIS: Following our previous successful SERGIS studies of thin dewetted polymer films, we have started to explore the feasibility of studying biological systems with this novel technique. Specifically, we have used the OFFSPEC beamline at ISIS to do SERGIS experiments scientifically aimed at understanding the role of Phospho-L-Serine (PS) in the organization of cholesterol containing model lipid membranes. We performed experiments on a single lipid membrane (a 1:1 DPPC:DLPC mixture) floating on D_2O or a D_2O/H_2O subphase using a Langmuir-Blodgett trough. At low temperatures these experiments showed a small decrease in the neutron spin polarization (i.e. depolarization) of about 10% at a spin echo length consistent with the size of the domains previous observed in microscopy studies. With temperature, the depolarization changed, but in a somewhat unexpected way. Measurements on two spin-coated lipid multi-stack samples (one supported on a hydrophilic surface and another on a hydrophobic surface) showed a maximal variation in the polarization. For the membrane deposited on a hydrophilic surface this signal changed significantly and reproducibly with cycling of the temperature. Although the analysis of the data is underway, the results are promising.

Sweep mode: We have developed a novel method to measure the full four-dimensional scattering function $S(\mathbf{Q},\boldsymbol{\omega})$ from single crystals utilizing continuous sample rotation in combination with an event-based data acquisition system. In contrast to the traditional method, whereby data is taken sequentially at a predetermined fixed number of angles and the full data can only be reconstructed *a posteriori*, the sweep method allows the complete result to be monitored immediately, and to adjust the experimental conditions based on scattering features and measurement statistics. We have successfully performed *sweep* mode measurements on samples with a variety of different scattering features, such as high-energy phonons in boron carbide superconductors, phonons in bilayer manganites, scattering from coupled dimers, and broad magnetic scattering in $CePd_3$.

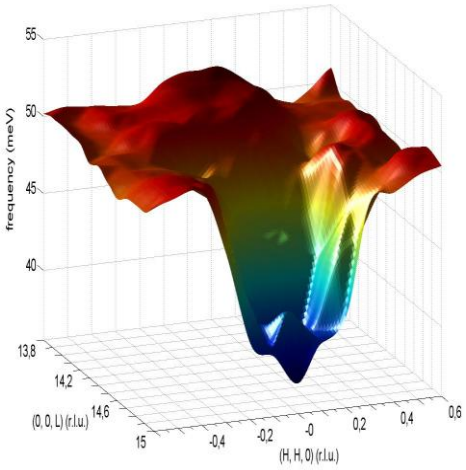

Fig. 2: Phonon dispersion surface of the superconductor YNi_2B_2C determined from *Sweep* mode measurements on ARCS.

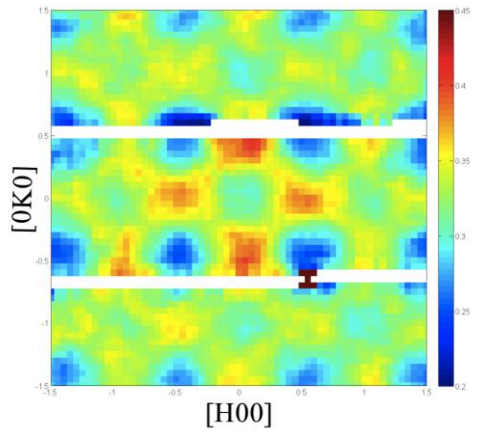

Fig. 3: Magnetic scattering in the intermediate valence compound $CePd_3$ measured using the *Sweep* method on ARCS.

NeXpy – A Python Interface to Neutron and X-ray Data: In collaboration with Argonne's Mathematics and Computing Science Division, we have developed a Python API and a GUI interface to data stored in the NeXus data format allowing new data structures of arbitrary rank to be defined interactively by an intuitive syntax, visualized, manipulated, scaled, and combined through a variety of mathematical operations. This is designed to be a simple analysis toolbox that gives scientists access to both raw and analyzed data from any major facility including the Advanced Photon Source and the Spallation Neutron Source. It is therefore complementary to more complex data analysis frameworks such as the Mantid framework being implemented at the SNS, but is much more flexible and convenient for customizing the analysis to novel experimental configurations.

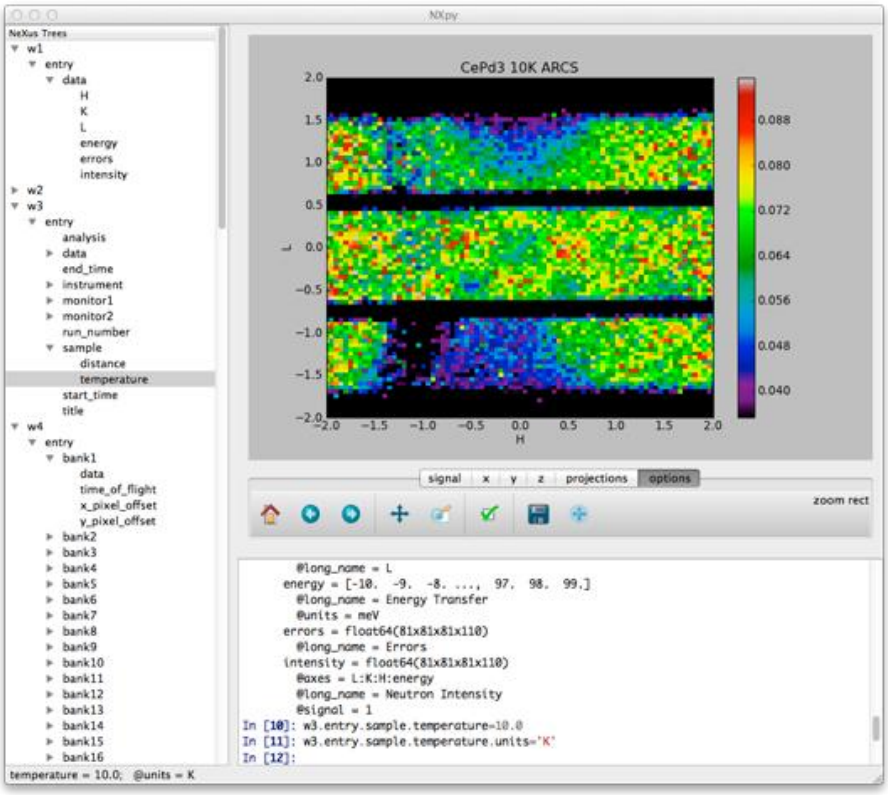

Fig. 4: Screenshot of the NeXpy interface showing the data panel (left), command-line interface to the data (bottom), and a display of inelastic data from $CePd_3$ measured using the *Sweep* mode on ARCS.

Future Plans

Diffuse Scattering at SNS and APS: Following the completion of taking data on the prototype instrument, we will analyze the single crystal data in detail and compare it to model simulations in order to asses the degree of elastic discrimination and the momentum resolution obtained. We will then shift our focus to prepare for utilizing *Corelli* when it comes online in 2014. In particular, we will collaborate with the *Corelli* instrument scientist and the SNS data analysis group and utilize our experience gained with the prototype experiments for developing the tools necessary to be able to perform such experiments and we will devise the proper protocols for calibration and normalizations in order to be ready to perform the first experiments during commissioning of *Corelli*. To advance our capabilities to use high-energy synchrotron diffuse scattering, we recently started to develop python based software tools, with a first successful application for analyzing diffuse scattering measurements utilizing the crystal rotation method. With these new tools, we can utilize various types of 2D detectors available at the APS, including using several detectors with arbitrary orientation simultaneously, and reconstruct and visualize the measured data in physical space during the experiment. Members of our group are also involved in a collaboration with members of the synchrotron radiation group in first measurements of X-ray coherent speckles from atomic disorder in liquids and glasses. This is in preparation for future applications of this technique, in particular the use of speckle spectroscopy to study the structure and dynamics of short-range order and its influence on physical properties in strongly correlated systems.

Fig. 5: Installation of the sample and detector tank of *Corelli*.

NeXpy – A Python Interface to Neutron and X-ray Data: We plan to use the NeXpy interface to develop software for both single crystal x-ray diffuse scattering at the APS and neutron diffuse scattering in preparation for the commissioning of *Corelli* at the SNS. This will require implementing the cross correlation analysis within the Python framework and the development of methods for the joint optimization of neutron and x-ray scattering data. If proposals to stream X-ray data to remote clusters are funded, we will use NeXpy as a portal to the remote data storage.

Publications

1. A. Vorobiev, J. Major, H. Dosch, P. Müller-Buschbaum, P. Falus, G.P. Felcher, S.G.E. te Velthuis, "Phase and microphase separation of polymer thin films dewetted from silicon – a spin-echo resolved grazing incidence neutron scattering study"
J. Phys. Chem. B **115**, 5754 (2011).

Development of grazing incidence optics for neutron imaging and scattering

M. V. Gubarev[1,a], B. Khaykovich[2] , D. Liu[2], B. D. Ramsey[1], V. E. Zavlin[3], K. Kilaru[1], S. Romaine[4], R. E. Rosati[4], R. Bruni[4] and D. E. Moncton[2]

[1]Marshall Space Flight Center, NASA, VP62, Huntsville, AL 35812, USA

[2]Nuclear Reactor Laboratory, Massachusetts Institute of Technology, 138 Albany St., Cambridge, MA 02139, USA

[3] Universities Space Research Association, 320 Sparkman Drive, Huntsville, AL35805;

[4] Harvard-Smithsonian Center for Astrophysics, 60 Garden Street, Cambridge, MA 02138;

I. Program scope

Because of their wave nature, thermal and cold neutrons can be reflected from smooth surfaces at grazing incidence angles, be reflected by multilayer coatings or be refracted at boundaries of different materials. The optical properties of materials are characterized by their refractive indices which are slightly less than unity for most elements and their isotopes in the case of cold and thermal neutrons as well as for x-rays. The motivation for the optics use for neutrons as well as for x-rays is to increase the signal rate and, by virtue of the optic's angular resolution, to improve the signal-to-noise level by reducing the background so the efficiency of the existing neutron sources use can be significantly enhanced.

Both refractive and reflective optical techniques developed for x-ray applications can be applied to focus neutron beams. Typically neutron sources have lower brilliance compared to conventional x-ray sources so in order to increase the beam throughput the neutron optics has to be capable of capturing large solid angles. Because of this, the replicated optics techniques developed for x-ray astronomy applications would be a perfect match for neutron applications, so the electroformed nickel optics under development at the Marshall Space Flight Center (MSFC) can be applied to focus neutron beams. In this technique, nickel mirror shells are electroformed onto a figured and superpolished nickel-plated aluminum cylindrical mandrel from which they are later released by differential thermal contraction. Cylindrical mirrors with different diameters, but the same focal length, can be nested together to increase the system throughput. The throughput can be increased further with the use of the multilayer coatings deposited on the reflectivr surface of the mirror shells. While the electroformed nickel replication technique needs to be adopted for neutron focusing, the technology to coat the inside of cylindrical mirrors with neutron multilayers has to be developed. The availability of these technologies would bring new capabilities to neutron instrumentation and, hence, lead to new scientific breakthroughs. We have established a program to adopt the electroformed nickel replication optics

Fig. 1: *Pure nickel mirrors electroformed using pulse plating technique*

[a] Mikhail.V.Gubarev@nasa.gov

technique for neutron applications and to develop the neutron multilayer replication technology.

II. Recent progress

a. Pure nickel replication technique development

Modern electroformed nickel mirrors for astrophysical applications are made from a high-strength nickel-cobalt alloy. This is done because the pure nickel tends to crystallize during conventional electroform plating leading to an optical surface with higher micro-roughness, and because pure nickel has higher stresses that can potentially distort the axial figure profile of a mirror. Both the potential figure degradation and the higher surface micro-roughness can lead to a lower optical performance of neutron mirrors. On other hand, the large amount of cobalt in the mirror material is not acceptable for neutron applications. Therefore, the pure nickel plating process needs to be enhanced in order to control the material stress and to suppress the crystallization of the nickel on the mirror surface.

To address these issues we have applied an innovative pulse plating technique to mirror electroforming. In this, an alternating current, instead of the usual direct current, is utilized so that the plating of the nickel is followed by an etching of the material which removes misplaced nickel atoms. The technique results in a layered nickel structure which makes the material more amorphous-like and suppresses the nickel crystallization. To optimize this, the pulse plating parameters were studied using flat replica samples with the goal to lower the stress and to obtain a good surface roughness. The flat nickel replicas have demonstrated a surface roughness below 6A, the acceptable level for the pure nickel neutron mirrors. Then the process was transferred to cylindrical mandrels. Three nickel mirrors fabricated using the pulse plating technique were nested and assembled into microscope system with magnification factor of four. Figure 1 shows one of the shell mirrors fabricated using the pulse plating technique. The microscope system was tested using the microfocus x-ray source. For comparison we used the similar microscope system fabricated previously using the conventional (non-pulsed) electroformed nickel plating technique. The results are shown in table 1. Please note, the improved optical performance is a result of several factors: improved axial figure of the mandrel, reduced scattering due to surface microroughness and less deformation of the mirrors in the microscope housing due to reduced azimuthal mirror deformations. The microscope system assembled from the pulse-plated pure nickel mirrors is intended for imaging experiments planned to be performed at the National Institute of Standards and Technology's Center for Neutron Research in July 2012.

Table 1. Focal spot size for the four fold magnified image of microfocus x-ray source

Focal spot size	Half Power Diameter, mm	Full width on Half Maximum, mm
Conventional technique	1.48	0.39
Pulse plating	0.89	0.18

b. Neutron multilayer replication technique development

We are developing neutron supermirror multilayers suitable for direct replication from nickel masters to produce axisymmetric neutron supermirrors. This work is performed in collaboration with the Massachusetts Institute of Technology (MIT) and the Smithsonian Astrophysical Observatory (SAO). The research is focused on two tasks. First, the development of a separation layer applicable for direct replication of multilayers from a master, second, the development of a multilayer coating suitable for nickel replicated mirrors as the substrates.

Fig. 2: *Two conical mandrels used for replication tests (shown in background); three un-coated conical shells, replicated from these (foreground).*

Experiments have been carried out with flat mandrels using thin TiN layers vacuum deposited on to the mandrel followed by the multilayer and the subsequent nickel shell. TiN provides just enough adhesion to support multilayer growth but not enough to inhibit removal. Extensive testing has shown that an 80 A layer of TiN is optimal; the release layer preserves the micro-roughness of the substrate surface, while multilayers replicated from this release layer exhibit no loss of performance, as quantified by x-ray reflectivity measurements. To verify the release mechanism on cylindrical shells, and to tune the plating bath parameters for optimal coatings, replication tests were performed using straight cone mandrels. In these tests, the TiN layer was coated onto cone mandrels and nickel replicas were fabricated from these. Figure 2 shows a selection of mandrels and replicas produced from them. Surface figure measurements were used to compare the figure of the replicated cone with the figure of the mandrel. The samples show clean separation of the replica and mandrel. We are preparing to perform next step in the development program, the direct replication of the neutron supermirror from a mandrel fabricated in accordance with two reflections optical prescription.

A NiC/Ti graded-d-spacing deposition process suitable for direct replication was also developed. First, the experiments were carried with perfectly flat and exceptionally smooth super-polished fused silica substrates with the goal to set the deposition parameters. X-ray reflectivity data were obtained for all samples to assess the quality of the coatings. Figure 3 is an example of the X-ray reflectivity data collected for a fused silica substrate sample coated with m=1.9 multilayers and the model fit. X-ray reflectivity measurements are an excellent means of providing snapshots of the multilayer quality in preparation for more detailed neutron reflectivity measurements that cover larger sample areas and probe the multilayer more deeply.

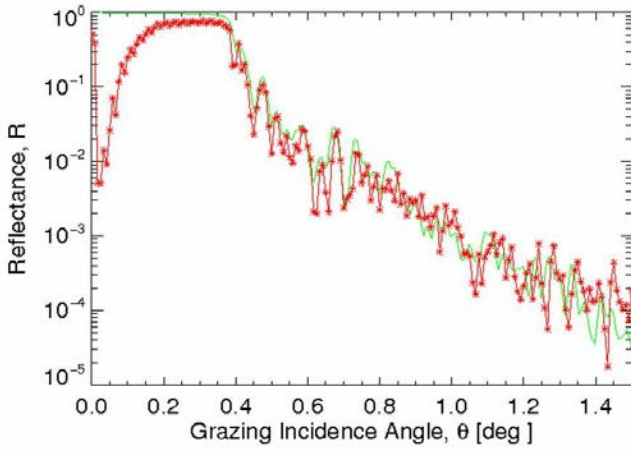

Fig. 3: *Cu K-α (1.54Å) X-ray reflectivity of a NiC/Ti supermirror deposited on superpolished fused silica substrate (red) with model fit (green).*

Using the x-ray measurements, the deposition parameters were tuned so that the microroughness of the interface layers obtained from the fit data was found to be from 7 to 8 A for the fused silica substrate samples, meeting the requirements for the neutron supermirrors. Then, the tuned deposition process was used to deposit films on the flat nickel mandrels which had been polished to have the surface microroughness of 3-4A the level that we expect for the nickel cylindrical

mandrels to be used to replicate the neutron supermirrors. X-ray data from these confirmed that the interface microroughness was in the same range, this time between 7.5 to 8.5 A. The multilayer films were also deposited on flat mandrels coated with TiN release layer. The films were over-plated with nickel and released from the mandrels. After x-ray testing confirmed the quality of the multilayer coating, several samples were tested in neutron beams at the MAGICS Reflectometer at SNS. The goal of this test was to verify the quality of the multilayer coatings for neutron reflection and to fine tune the deposition rate parameters. Reflectivity data along with model fit for one of the flat nickel master samples, with 19 layer pairs, m=1.9 and theoretical reflectivity of 97%, are shown in Figure 4 which is a plot of specular reflectivity vs. Qz. The microroughness of the interfaces obtained from the neutron reflectivity data is in good agreement with those obtained from the x-ray reflectivity data for these samples, confirming the value of the quick-look x-ray data. Below the critical angle the measured neutron reflectivity matches the theoretical value very well making the developed process applicable to neutron optics.

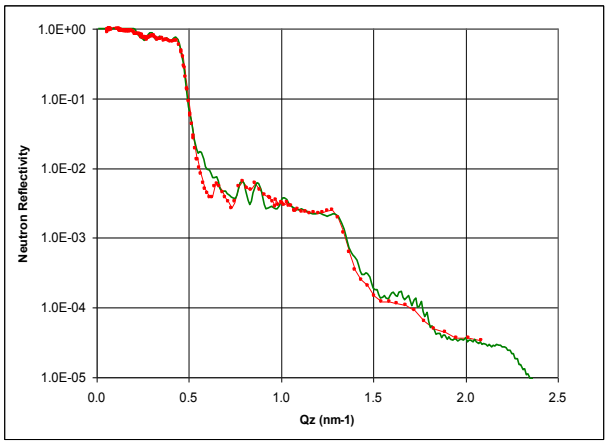

Fig. 4: *Neutron specular reflectivity of a NiC/Ti supermirror (flat nickel mandrel #G09) on Ni substrate (red) and the model fit (green).*

III. Future plans

Pure nickel multilayer-coated mirrors replicated from mandrels fabricated in accordance with two reflections optical prescription will be demonstrated in the near future. A three-mirror pure nickel optic fabricated using a pulse plating technique will be soon tested at the HFIR (ORNL) to demonstrate SANS applications for the developed technology.

Research supported by the U.S. Department of Energy, Office of Basic Energy Sciences, under Awards # DE-FG02-09ER46556 and DE-FG02-09ER46557.

IV. Publication resulting from work supported by the DOE project over the last two years

[1] B. Khaykovich, M. V. Gubarev, Y. Bagdasarova, B. D. Ramsey, and D. E. Moncton, "From x-ray telescopes to neutron scattering: Using axisymmetric mirrors to focus a neutron beam." Nucl. Instrum. Methods Phys. Res. Sect. A: Accel. Spectrom. Det. Ass. Equip. 631 (2011), 98.
[2] D. Liu, M. V. Gubarev, G. Resta, B. D. Ramsey, D. E. Moncton, and B. Khaykovich, "Axisymmetric Grazing-Incidence Focusing Optics for Small-Angle Neutron Scattering", Nucl. Instrum. Methods Phys. Res. Sect. A: Accel. Spectrom. Det. Ass. Equip. To be published (2012); doi:10.1016/j.nima.2012.05.056; arxiv:1205.0524v1
[3] M. V. Gubarev, B. Khaykovich, B. D. Ramsey, *et al*, "From x-ray telescopes to neutron focusing", Proc. SPIE 8147 (2011), 81470B-1.
[4] B. Khaykovich, M. V. Gubarev, V. E. Zavlin, *et al*, "Novel neutron focusing mirrors for compact neutron sources", Physics Procedia 26 (2012), 299.

Small-Angle Neutron Scattering at Oak Ridge National Laboratory

William T. Heller[1], Kenneth C. Littrell[2], Changwoo Do[1], Christopher B. Stanley[1], Yuri B. Melnichenko[1], Lilin He[1], Carrie Y. Gao[3], Katherine Bailey[4]
[1]Biology and Soft Matter Division, [2]Chemical & Engineering Materials Division, [3]Research Accelerator Division, [4]Research Reactors Division, Oak Ridge National Laboratory, Oak Ridge, TN 37831.

Oak Ridge National Laboratory is home to two of the world's most powerful neutron sources, the Spallation Neutron Source (SNS) and the High Flux Isotope Reactor (HFIR). These facilities serve a broad suite of instruments. Among these are two world-class small-angle neutron scattering instruments, the General Purpose SANS (GP-SANS) instrument at the HFIR and the Extended Q-Range SANS (EQ-SANS) instrument at the SNS. The GP-SANS is a highly versatile, high flux SANS instrument capable of probing structure and interactions in materials over length scales ranging from 0.5-200 nm. The EQ-SANS is a time-of-flight SANS instrument that provides a wide q-range coverage at a single instrument configuration that is ideal for a wide variety of materials studies. The high flux available on both instruments makes them well-suited to studies of weakly scattering systems and kinetic processes *in situ*. The capabilities of the GP-SANS and EQ-SANS, including available sample environments, will be summarized. Recent research highlights from the user programs of both instruments will also be presented.

This research at Oak Ridge National Laboratory's Spallation Neutron Source and High Flux Isotope Reactor was sponsored by the Scientific User Facilities Division, Office of Basic Energy Sciences, U.S. Department of Energy. Oak Ridge National Laboratory is managed by UT-Battelle, LLC for the U.S. Department of Energy under Contract DE-AC05-00OR22725.

Recent Advances in High Pressure Neutron Diffraction at Oak Ridge National Laboratory

Chris A. Tulk,[1] A. M. dos Santos,[2] J. J. Molaison[3] and N. Pradhan[3]

1) Chemical and Engineering Materials Division, Neutron Sciences Directorate, Oak Ridge National Laboratory; 2) Quantum Condensed Matter Division, Neutron Sciences Directorate, Oak Ridge National Laboratory; 3) Instrument Support group, Research Accelerators Division, Neutron Sciences Directorate, Oak Ridge National Laboratory

Research Scope: Over the past 2 years there have been significant advances in high pressure neutron scattering capabilities at the high pressure instrument at the SNS. A scientific base has been built around the well known Paris – Edinburgh press design and this versatile tool has been used for the initial scientific output from the instrument. However, our biggest advances utilize a new pressure cell design based on a modified diamond anvil cell and have experimentally demonstrate ultra-high pressure neutron *powder* diffraction well above ½ Mbar, and approaching the 1 Mbar threshold (the design goal if the diffractometer). Note that 1Mbar = 1000 kbar ~ 100 GPa ~ 15 million PSI. As a diffractometer, SNAP has shown itself to be highly versatile and capable of measuring diffraction data from minute powdered samples, even those held within a diamond anvil cells, and for total diffraction studies of liquid and amorphous samples where S(Q) functions are measured and Fourier inverted into radial distribution functions. A 'slice' of scientific and technical projects carried out using the SNAP instrument are given.

Recent Progress (scientific):

Hydrocarbon and Anthropogenic Greenhouse Gas Interactions with Water, C.A. Tulk, D. D. Klug, S. Machida, A. M. dos Santos

CO_2 hydrate has been shown to transform at 0.77 GPa from the well-known strucuture I into an unidentified high pressure phase, Hirai et al 2010. Recently the high pressure diffractometer, SNAP, has been used to collect high quality neutron data that show the structure to be a filled ice form with CO_2 molecules filling the water channels in such a way that the molecular orientation mimicked the corrugated zig-zag pattern of the channel side-walls. A model of this structure, showing the location of the CO_2 in the ice, is shown in the figure to the right.

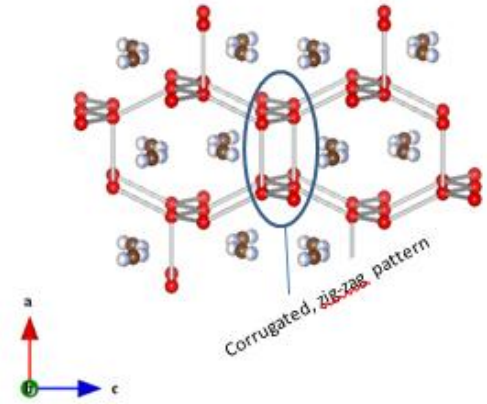

In a process similar to the formation of high density amorphous ice, amorphous methane hydrate was formed by the pressure induced collapse of crystalline methane clathrate at 32 kbar and 100 K. Whereas the very high density amorphous form of pure water undergoes a glass transition near 130 K at low pressure and crystallizes over a broad pressure range at ~ 160 K, the amorphous network of the water - methane binary system exhibits a region of meta-stability that persists up to 220 K between 15 and 40 kbar. It appears that in this system the connectivity of the water network exhibits sufficiently low mobility so as to inhibit the diffusion and phase separation of the constituents until 220 K, where the high pressure ice VIII crystallization can occur. The figures below show neutron data from the crystalline starting and final products (left) and amorphous forms (right) collected on SNAP.

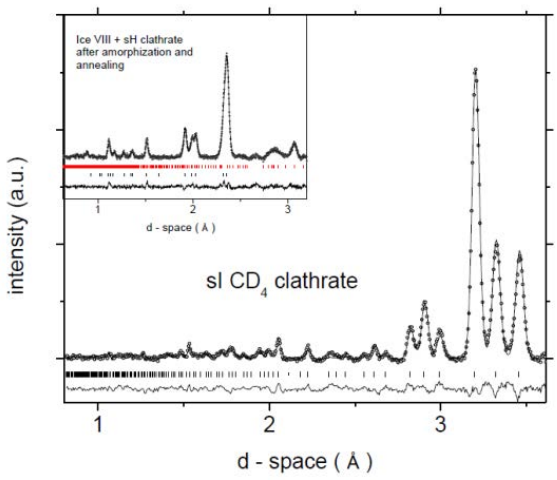

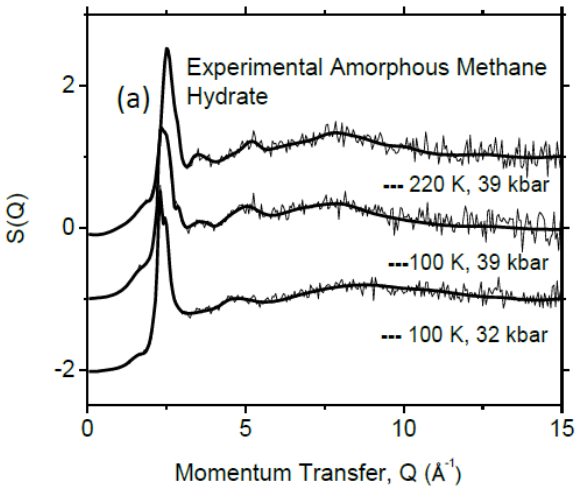

Liquid structures of small molecules under high pressure, M. Guthrie, C. A. Tulk, S. Machida

Total pair-distribution functions of pure ammonia, determined by Fourier analysis of the static structure factor, are used to examine the structural changes from the first neighbors to extended ranges of ~30 °A in both the liquid and solid state. In the proton-disordered crystalline phase III, the first coordination shell is almost identical to that of the higher-pressure, ordered phase IV. The H-bond correlation is observed as a distinct shoulder at 2.5 A° . A similar local structure is seen in the liquid at a pressure just below freezing, and, in particular, a pronounced H-bond correlation is observed in the liquid across the pressure range studied. A substantial increase in the ordering length scale of the liquid is observed at high pressure with correlations extending to at least 25 °A compared to ~12 °A at ambient.

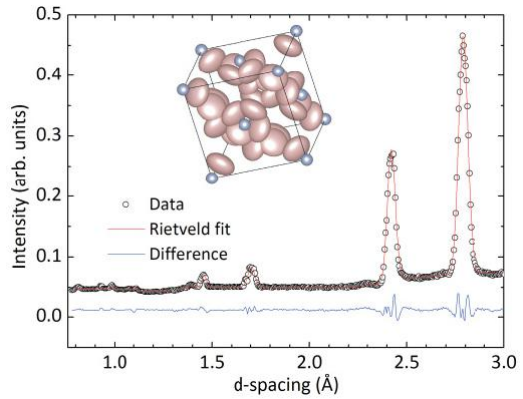

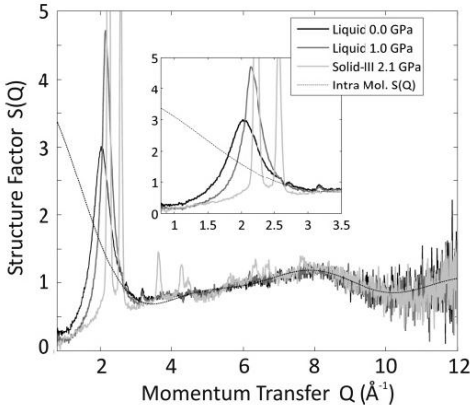

Magnetic Systems under Pressure, M. Baldini, A. M. dos Santos, C. A. Tulk

X-ray magnetic circular dichroism and neutron diffraction measurements were conducted *in-situ* at high pressure and low temperature to investigate the evolution of the magnetic properties of Nd0*:*53Sr0*:*47MnO3 (NSMO47). The neutron diffraction data provide the first experimental evidence for the presence of antiferromagnetic domains within the conducting ferromagnetic host at ambient pressure. The antiferromagnetic phase becomes dominant above 3 GPa while the long range ferromagnetic order is strongly reduced at approximately 8 GPa. This finding indicates that the magnetic ground state of NSMO47 is more complex than previously reported, confirming the coexistence of

competing phases over the doping range in which Colossal Magnetoresistance is observed. We also find that magnetic phase separation in the form of domains appears to be an intrinsic phenomenon at high pressure.

Fundamental hydrogen bond interactions in water ice, M. Guthrie, C. A. Tulk, R. Boehler

Experiments are underway to investigate the form of the hydrogen bond in water ice up to 1 Mbar. Data from an experiment up to 53 GPa are shown on the left, further refinements in background measurment/modeling and modification to the anvil seat design have recently resulted refinable data collected from powdered samples **up to 63 GPa**. The density distribution of the hydrogen along the hydrogen bond is expected to become symmetric in this pressure range.

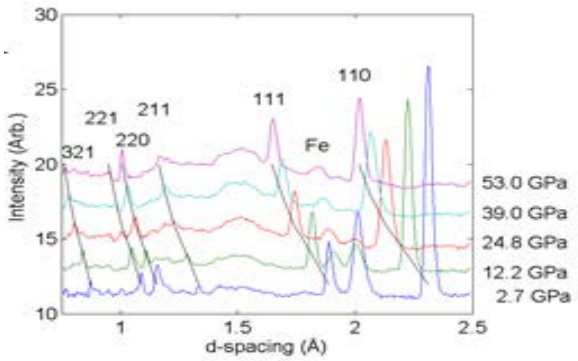

D_2O up to 53 Gpa [Guthrie, Boehler, Li, Machida, Tulk, Dos Santos, Molaison]

Recent Progress (technical):

Development of ultra-high pressure neutron powder diffraction cells for mega-bar pressure experiments, M. Guthrie, R. Boehler, C. A. Tulk, A. M. dos Santos, H.-k Mao

On the way to reaching 63 GPa with neutron powder diffraction: from top left, clockwise: early prototype with PCD anvil and gold sample. Early design has upstream single-crystal diamond and downstream PCD, early collimation and laser alignment are shown. Current micro-collimator, 400um aperture, defines the beam (powder surrounding collimator is the remains of diamond that failed at around 60 GPa). Current design with single-crystal diamond anvils on both the incident and exiting beam paths, WC and steel supports are custom designed and built by Carnegie. WC seat after anvil failure indicating that current limit (60 GPa) is due to seat, not anvil, failure. Next iteration will use a PCD-core seat (shown), which is predicted to facilitate neutron diffraction at >100 GPa.

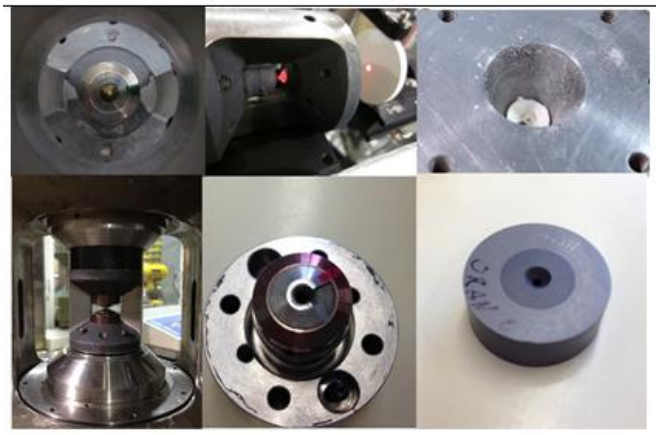

Background Reduction to enable Diamond Anvil Cell work on SNAP, C. A. Tulk, A. M. dos Santos, J. J. Molaison, N. Pradhan, M. Guthrie

(A) shows the first attempt to measure a ~1.0 mm^3 ice VII sample in an early prototype DAC ca. November 2010. (B) shows current data quality from samples of ~0.06mm^3 measured in March 2012 in the latest (Carnegie-designed) prototype diamond cell and collimation. The Bragg peak at 2 Å marked Fe is due to the steel gasket, but all other peaks are from the ice VII sample. The red line is a Rietveld fit.

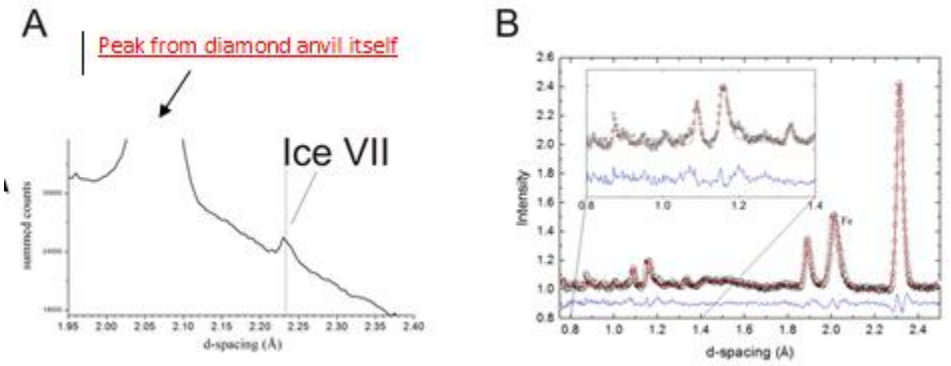

Resulting Publications

1) M. Baldini, Y. Ding, S. Wang, Y. Lin, C. A. Tulk, A. M. dos Santos, J. F. Mitchell, D. Haskel, and W. L. Mao, Pressure induced stabilization of antiferromagnetic phase in Nd0*.*53Sr0*.*47MnO3, Submitted to **Phys. Rev. Lett.** (2012).

2) K. Marty, A. D. Christianson, A. M. dos Santos, B. Sipos, K. Matsubayashi, Y. Uwatoko, J. A. Fernandez-Baca, C. A. Tulk, T. A. Maier, B. C. Sales & M. D. Lumsden, Unconventional energy scaling in superconductor $FeTe_{0.6}Se_{0.4}$ under pressure, Submitted to **Phys. Rev. Lett.** (2012).

3) 3) C. A. Tulk, D. D. Klug, J. J. Molaison, A. M. dos Santos, and N. Pradhan, The Structure and Stability of an Amorphous Water + Methane Mixture Produced by Cold Compression of Methane hydrate, **In Press, Phys. Rev. B.** (2012)**.**

4) Sarah A. Thomas, Georgiy M. Tsoi, Lowell E. Wenger, Yogesh K. Vohra Gary N. Chesnut, Samuel T. Weir, C. A. Tulk and Antonio F. Moreira Dos Santos, Neutron Diffraction Studies on Paramagnetic-to-Helical Antiferromagnetic Transition in Holmium at High Pressures, **Journal of Physics: Condensed Matter.** 24, 216003 (2012).

5) M. Guthrie, C.A. Tulk, J. Molaison & A.M.F. Dos Santos, Local structural motifs and extended-range order in liquid and solid ammonia under pressure, **Phys. Rev. B.,** 85 184205 (2012).

6) C. A. Tulk, D. D. Klug, A. M. dos Santos, G. Karotis, M. Guthrie, J. J. Molaison, and N. Pradhan Cage occupancies in the high pressure structure H methane hydrate: A neutron diffraction study, **J. Chem. Phys.** 136, 054502 (2012).

7) J.S. Tse, L. Yang, S.J. Zhang, C.Q. Jin, J.Z. Jiang, S. Yamanaka and C.A. Tulk, Pressure induced Electronic and Structural Transformations in Ba-doped Si Clathrates, **Phys. Rev. B. 84** 184105 (2011).

8) D. D. Klug, J. S. Tse, J. Y. Zhao, W. Sturhahn, E. E. Alp and C. A. Tulk, Dynamics of Kr in dense clathrate hydrates, **Phys. Rev. B.,** 83 184116 (2011).

9) O. Delaire, M. S. Lucas, A.M. dos Santos, A. Subedi, A.S. Sefat, M.A. McGuire, L. Mauger, J.A. Mu˜noz, C.A. Tulk, Y. Xiao, M. Somayazulu, J.Y. Zhao, W. Sturhahn, E.E. Alp, D.J. Singh, B.C. Sales, D. Mandrus, and T. Egami, Temperature and pressure dependence of the Fe-specific phonon density of states in Ba(Fe 1-xCo x) 2As 2, In Press **Phys. Rev. B** (2010).

10) Horita J., dos Santos A. M., Tulk C. A.,; et al. High-pressure neutron diffraction study on H-D isotope effects in brucite, Phys. Chem. of Minerals, **37,** 741-749 (2010).

11) Author(s): Ice G. E.; Choi J. -Y.; Takacs P. Z. C. A. Tulk; et al. Nested neutron microfocusing optics on SNAP, Appl. Phys. A. **99** 635-639 (2010).

12) Delaire O. Lucas M. S. dos Santos A. M. C. A. Tulk et al. Temperature and pressure dependence of the Fe-specific phonon density of states in Ba(Fe1-xCox)(2)As-2 , Phys. Rev. B. **81,** 094504 (2010).

13) Yang L.; Tulk C. A.; Klug D. D.; et al. Guest disorder and high pressure behavior of argon hydrates, Chem. Phys. Lett. **485,** 104-109 (2010).

Neutron Reflectometry Capabilities and Research at the Spallation Neutron Source

John F. Ankner, Valeria Lauter, and James F. Browning

Neutron Sciences Directorate
Oak Ridge National Laboratory

Neutron reflectivity is a powerful tool for the study of thin films, particularly those containing hydrogen and/or magnetic atoms. Two of the initial instruments constructed at the Spallation Neutron Source were reflectometers: a horizontal-surface instrument devoted to soft matter studies (Liquids Reflectometer) and a vertical-surface instrument optimized for studies of magnetic films (Magnetism Reflectometer). After nearly six years of commissioning and operation, these instruments are mature and serve a growing user community. We will describe the instruments, their capabilities and associated sample environments, and recent science highlights.

National School on Neutron and X-ray Scattering

Suzanne G.E. te Velthuis (tevelthuis@anl.gov)
Materials Science Division, Argonne National Laboratory

Bryan C. Chakoumakos
Quantum Condensed Matter Division, Oak Ridge National Laboratory

Jonathan C. Lang
Advanced Photon Source, Argonne National Laboratory

John D. Budai
Materials Science and Technology Division, Oak Ridge National Laboratory

Scope

Since 1999, the National School on Neutron and X-ray Scattering has provided a comprehensive introduction to the underlying theory of neutron and x-ray scattering and related experimental techniques that are available. The school plays an important strategic role in educating the United States scientific community in the capabilities of its national neutron and x-ray user facilities. While the two-week school was initially held at Argonne National Laboratory, in 2008 ANL partnered with Oak Ridge National Laboratory, and now participants spend equal time at both sites. The program includes both classroom lectures from experts in the field and hands-on experiments.

Recent Progress

The 12th and 13th National School on Neutron and X-ray Scattering held June 12th-26th in 2010 and June 11th-25th in 2011, respectively. Interest from the scientific community in the school is strong as the school has been consistently oversubscribed, by over a factor of 3.3 in the most recent years. During the school, the participants (63 in 2010, 65 in 2011) each performed a total of three neutron scattering experiments using Oak Ridge National Laboratory's Spallation Neutron Source and High Flux Isotope Reactor beamlines. They also performed at least three x-ray experiments at Argonne National

Laboratory's Advanced Photon Source. On the last day of the school as small groups the students give a short presentation on one of the experiments they participated in. The feedback from the students is positive each year, and many of the students subsequently apply for postdoctoral positions at Argonne and other neutron and X-ray scattering facilities, or continue to use the facilities for their research.

Impact

To date, 765 participants have attended the school. The national character of the school is reflected in the wide geographic distribution of the participants that have attended as is shown in Fig. 1. Participating students have represented over 141 unique colleges and universities, from 46 different states, Washington DC and Puerto Rico. About 19% of the participants attended schools in EPSCoR states. The distribution of the participants over the different states or territories generally tracks the distribution of the applicants.

Figure 1: Geographic distribution of school participants 1999-2011.

Many of the participants utilize these continued to past their sources well studies in graduate doctoral their post- positions research In fact, 70% and beyond. participants of the the school in who attended (1999) are the first year active currently while facility users, over 1999- averaged percentage 2006 this 44% (see is at least Figure 2).

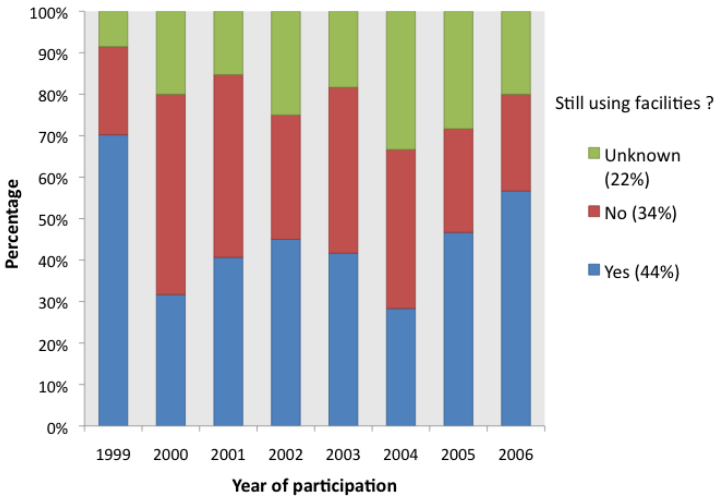

Figure 4: Percentages of 1999-2006 participants that are still using Neutron and or X-ray facilities[1].

Future Plans

The 14th National School on Neutron and X-ray Scattering will be held from August 12th - 25th, 2012. The participants will spend the first week at Argonne National Laboratory and then transfer to Oak Ridge Laboratory on August 18th for the remaining period. Besides receiving a comprehensive course in the fundamentals of neutron and x-ray scattering theory and the associated techniques though lectures, each student will perform three synchrotron x-ray and three neutron scattering experiments for a total of six hands-on experiments. Out of 222 applicants, 65 have been selected to attend the school this year.

[1] *As determined by searches of the internet and facility user records within the last two years.*

Los Alamos Neutron Science Center (LANSCE) School on Neutron Scattering

James J. Rhyne (rhyne@lanl.gov)
Lujan Center, Los Alamos National Laboratory, Los Alamos, NM 87545
Heinz Nakotte (hnakotte@nmsu.edu)
Physics Department, New Mexico State University, Las Crucas, NM 88003

i. PROGRAM SCOPE

The LANSCE Neuron Scattering school was established in 2004 and is held yearly at the Lujan Neutron Scattering Center at Los Alamos. It is a discipline-oriented school focusing each year on a specific topic to which neutron scattering makes a critical impact. The LANSCE School is thus distinct from other U.S. neutron scattering schools (e.g., the *National Laboratory National School on Neutron and X-ray Scattering* held at Argonne National Laboratory and at Oak Ridge National Laboratory, and the NIST Center for Neutron Research Summer School) that provide a general overview of scattering or that have an instrumentation focus. The main goal of the LANSCE is to provide in-depth neutron-scattering training for each of the selected topics, predominantly to graduate students in their early stage of thesis research. A particular emphasis is put on selecting a diverse student body in order to foster cross-institutional, cross-disciplinary and multicultural learning environment. An implied goal is to grow a diverse user community in different areas of neutron scattering. The topics of the seven schools held to date have been: *2004: Magnetism, 2005: Structural Materials, 2006: Soft Condensed Matter and Structural Biology, 2007: Hydrogen in Materials, 2008: Nanomaterials and Magnetism, 2009: Phase Transformations, 2010: Structural Materials. 2011: Energy and Environment, and 2012 (to be held in September) Application of Neutron Scatering to Soft Matter Research*

The school continues to enjoy strong demand from students from across the U.S. and even foreign countries as evidenced by the 2011 school that had a total of 74 applicants for the 30 available positions. The student evaluations of all components of the past Schools (lectures, experiments, organization, etc.) were very positive. Moreover, there is evidence that the school had a significant impact for graduate research and post-graduate careers for many of the past participants. Many of the students (> 30%) have returned to the Lujan Center as users with others doing scattering research at other neutron facilities. The schools are funded jointly by DOE-BES and by the NSF (through New Mexico State University.)

The general format of the school consists of 3 to 4 lectures each day (except 6 on the first), followed by an intense afternoon of conducting experiments on the Lujan Center neutron scattering instruments that are appropriate to the topic of the school. Typically five experiments are available for student participation and thus the experimental groups are of a manageable 6-7 person size. The students analyze the results of data taken on the instruments under the guidance of the instrument scientist. Strong emphasis is placed on the physical meaning of the experiments and how neutron techniques provide complementary information to other types of experiments. The lectures are primarily by

outside experts in the topic of the school (see list of 2011 lecturers in Section ii). One day during the school is an organized excursion to Bandelier National Monument or to the museums in Santa Fe.

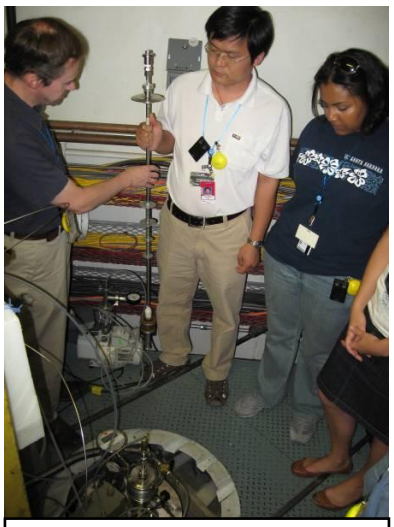

Figure 1 – Students learn about mounting samples in the FDS spectrometer from scientist Luc Daemen.

The number of accepted students is limited to 30. The applicants have come from a broad cross-section of the US and a number of foreign countries. A diverse student population has been represented including about 30% women. Only about 1/3 are US citizens. Many of the students (typically more than 1/3) have not previously used neutron scattering techniques, and thus the school is providing a valuable outreach function to enhance the general research knowledge base of neutron techniques.

The final morning of the school is devoted to talks by the students based on their laboratory experience. Our experience has been that these are excellent talks, worthy of any scientific meeting, and again reflect the high motivation level of the students. At the end of the 9-day school, students are asked to evaluate in detail components of the school including the lectures, the scattering laboratory experiments, and other aspects of the school program and organization. In addition written comments on the school are solicited and have proved very useful in improving the programs of subsequent schools.

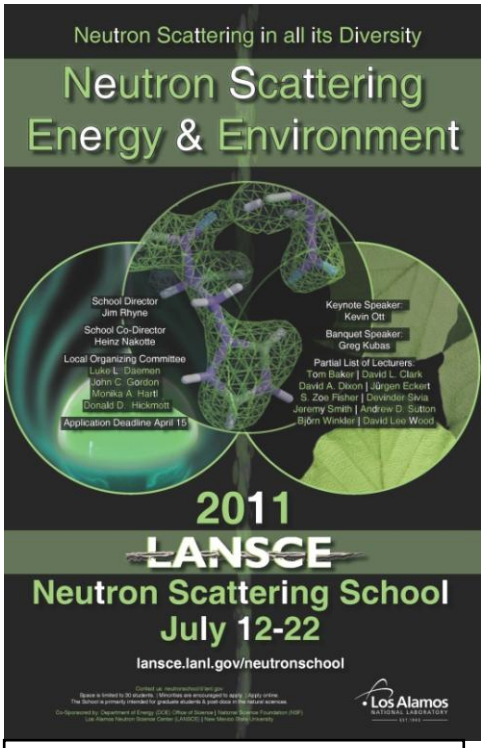

Figure 2 – Poster advertising 2011 LANSCE school.

An **External Advisory Board**, consisting of university faculty and staff from national laboratories, all of whom have neutron scattering interests[i] is charged with *suggesting and refining the topics* for each of the annual schools, as well as the *coordination and evaluation* of the school in light of national needs. The advisory board is consulted intermittently on any policy issues regarding the school and its interaction with other educational activities in neutron scattering.

Information on the school is posted on a web site http://lansce.lanl.gov/neutronschool maintained by LANSCE. Posters advertising the school are also distributed by e-mail to approximately 200 universities and laboratories in the U.S. A limited set of lecture slides are posted before the beginning of the school and the students are given an archival CD containing all lecture materials.

i. RECENT PROGRESS

The 2011 school was the 8th in the series and was held July 12-22, 2011. It focused on neutron scattering in ***Energy and Environmental Problems***, a topic that is widely considered as a large potential area for neutron scattering in the future. The organization of the 2011 *LANSCE School* was faced with unexpected challenges due to a major wildfire, which ravaged much of the area surrounding Los Alamos just prior to the 2011 school and led to the evacuation of the town of Los Alamos and a closure of Los Alamos National Laboratory for about 2 weeks.

Lecturers[ii] for the school are typically world-recognized experts in neutron scattering as applied to the specific topic of the school, or experts in more general theoretical and experimental investigation aligned with the school topic. As given in the partial list in reference (ii) the 2011 topics included catalysis, energy storage, nanoscale fluid dynamics, neutron radiography, fundamental concepts of crystallography, elastic and inelastic neutron scattering concepts, etc.

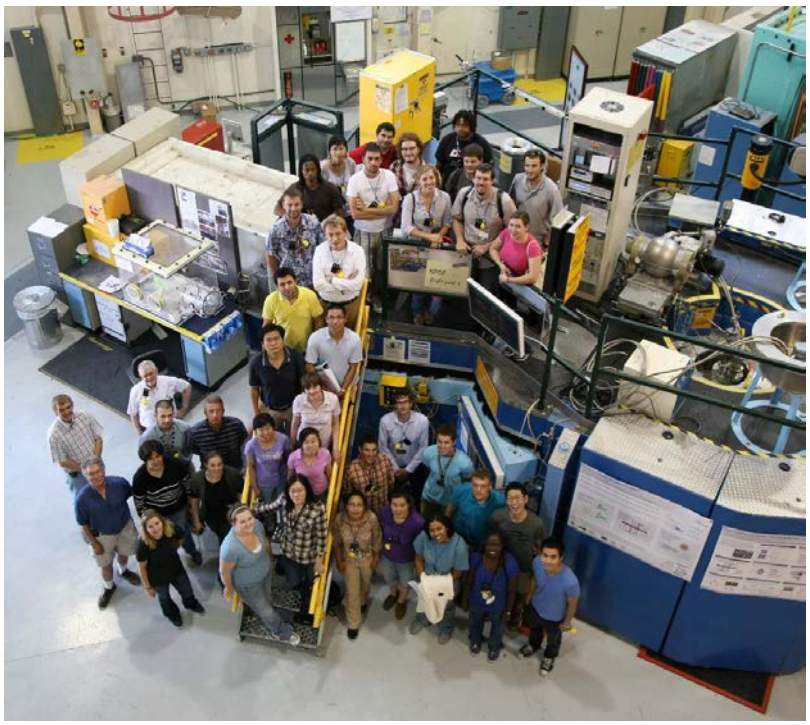

Figure 3 - 2011 *LANSCE Neutron Scattering School* participants (students, lecturers and organizers) at the Neutron Pair Distribution Function diffractometer.

ii. Future Plans

The topics proposed by the *External Advisory Board* for future schools are: ***Complex Fluids, Polymers and Membranes*** in 2012, ***Geosciences and Materials in Extreme Environments*** in 2013, and ***Thin Films and Mulilayers – Properties at Surfaces and Interfaces*** in 2014.

The 9th *LANSCE Neutron Scattering School* on *Soft Matter* is in the final planning stage. The school is co-chaired by Rex Hjelm and Jarek Majewski (both at LANL, LANSCE). The school will cover a broad range of soft-condensed-matter sciences, including emulsions, polymers and self assembly. Instruments that will participate in the hands-on experiments will be the small-angle scattering instrument LQD, the reflectometer SPEAR, the diffractometer NPDF, the inelastic spectrometer FDS and the neutron radiography station FP-5.

The proposed 10th *LANSCE School on Neutron Scattering* in 2013 will focus on *Geosciences and Materials in Extreme Environments*. This school will tentatively be co-chaired by Sven Vogel (LANL, LANSCE) and Don Hickmott (LANL, Earth and Environmental Sciences Group). The Lujan Neutron Scattering Center has unique sample-environment capabilities for the studies of materials at high temperatures and/or high pressures, which is instrumental for the understanding of materials behavior in the earth's interior. Topics can include phase and/or void evolution measurements measured by small-angle scattering, development of texture and residual strains measured by diffraction techniques, determination of porosity and crack evolution using radiography, and evolution of defects and phase transformations using total scattering experiments.

The 11th *LANSCE School on Neutron Scattering* in 2014 will focus on *Thin Films and Mulilayers – Properties at Surfaces and Interfaces*. This school will tentatively be chaired by Mike Fitzsimmons (LANL, LANSCE). This school is intended to emphasize the use of neutron (and complementary X-ray) techniques as a depth-dependent probe of composition, roughness and (structural and/or magnetic) correlations in thin films and multilayers. The main technique utilized in this school will be reflectometry utilizing the two neutron reflectometers (SPEAR and Asterix) and the X-ray reflectometer available at the Lujan Center. Additional hands-on studies may use the small-angle neutron diffractometer LQD (domains in thin films) and the inelastic neutron spectrometer FDS (vibrational spectroscopy in thin films).

iii. References

[i] The current membership of the External Advisory Board includes *R. Pynn* (Univ. of Indiana), *Thomas Proffen* (Oak Ridge National Laboratory), *S. teVelthuis* (Argonne National Laboratory), *Tonya Kuhl* (Uc-Davis), *S. K. Sinha* (UC San Diego), and *A. Shreve* (Univ. of New Mexico).

[ii] Some of the external 2011 lecturers and titles were: T. Baker (University of Ottowa, Canada) *Amine-Borane Fuel Blends for Chemical Hydrogen Storag,,* D. Cole (Ohio State University) *Structure and Dynamics of Fluids at Nanoscale Interfaces*, .J. Eckert (University of South Florida) *Neutrons as Microsopic Probes in Heterogeneous Catalysis,* M. Schlaf (University of Gueph, Canada) *Transition-Metal Catalyzed Deoxygenation of Bimass to Petrochemicals and Fuels – Strategies, Challenges and Some Successes,* A. Tremsin (University of California, Berkeley) *Introduction to neutron radiography and tomography at continuous and pulsed neutron sources,* Jeremy Smith (New Mexico State Univ.) *Catalysis as applied to materials for energy production/storage,* D. L. Wood (Oak Ridge Natl. Lab.) *Neutron Reflectometry Applied to Electrochemical Energy Storage and Conversion*, and Mike Kent (Sandia Natl. Lab.*) Neutron reflectometry and QCM-D study of the interaction of cellulases with films of amorphous cellulose*

Author Index

Participant List

Neutron Scattering Principal Investigators' Meeting
Participant Listing

Name	Organization	E-Mail
Doug Abernathy	Oak Ridge National Laboratory	abernathydl@ornl.gov
John Ankner	Oak Ridge National Laboratory	anknerjf@ornl.gov
Peter Armitage	The Johns Hopkins University	npa@pha.jhu.edu
Christopher Bertrand	Massachusetts Institute of Technology	cbertran@mit.edu
David Bucknall	Georgia Institute of Technology	bucknall@gatech.edu
Ravi Chandran	University of Utah	ravi.chandran@utah.edu
Wei-Ren Chen	Oak Ridge National Laboratory	chenw@ornl.gov
Omar Chmaissem	Argonne National Laboratory	chmaissem@anl.gov
Hans Christen	Oak Ridge National Laboratory	christenhm@ornl.gov
Pengcheng Dai	The University of Tennessee	pdai@utk.edu
Olivier Delaire	Oak Ridge National Laboratory	delaireoa@ornl.gov
Takeshi Egami	Univ. of Tennessee & Oak Ridge National Laboratory	egami@utk.edu
Morten Eskildsen	University of Notre Dame	eskildsen@nd.edu
Eric Fullerton	University of California, San Diego	efullerton@ucsd.edu
Brent Fultz	California Institute of Technology	btf@caltech.edu
Thomas Gentile	National Institute of Standards & Technology	thomas.gentile@nist.gov
Bonnie Gersten	U.S. Department of Energy	bonnie.gersten@science.doe.gov
Henry Glyde	University of Delaware	glyde@udel.edu
Alan Goldman	Ames Laboratory and Iowa State University	goldman@ameslab.gov
Garrett Granroth	Oak Ridge National Laboratory	granrothge@ornl.gov
Martin Greven	University of Minnesota	greven@physics.umn.edu
Genda Gu	Brookhaven National Laboratory	ggu@bnl.gov
Mikhail Gubarev	NASA-Marshall Space Flight Center	Mikhail.V.Gubarev@nasa.gov
William Heller	Oak Ridge National Laboratory	hellerwt@ornl.gov
Markus Huecker	Brookhaven National Laboratory	huecker@bnl.gov
Marc Janoschek	Los Alamos National Laboratory	mjanoschek@lanl.gov
John Joyce	Los Alamos National Laboratory	jjoyce@lanl.gov
Alamgir Karim	University of Akron	alamgir@uakron.edu
Helen Kerch	U.S. Department of Energy	helen.kerch@science.doe.gov
Boris Khaykovich	Massachusetts Institute of Technology	bkh@mit.edu
Valery Kiryukhin	Rutgers University	vkir@physics.rutgers.edu
Lee-Ann Kiser	Oak Ridge Institute for Science and Education	lee-ann.talley@orise.orau.gov
Andreas Kreyssig	Ames Laboratory	kreyssig@ameslab.gov
Peter Lee	U.S. Department of Energy	peter.lee@science.doe.gov
Seung-Hun Lee	University of Virginia	shlee@virginia.edu
Young Lee	Massachusetts Institute of Technology	younglee@mit.edu

Chris Leighton	University of Minnesota	leighton@umn.edu
Eliane Lessner	U.S. Department of Energy	eliane.lessner@science.doe.gov
Despina Louca	University of Virginia	louca@virginia.edu
Robert McGreevy	Oak Ridge National Laboratory	mcgreevyrl@ornl.gov
Tyrel McQueen	Johns Hopkins University	mcqueen@jhu.edu
Robert McQueeney	Ames Laboratory	mcqueeney@ameslab.gov
Joerg Neuefeind	Oak Ridge National Laboratory	neuefeindjc@ornl.gov
Dan Neumann	National Institute of Standards & Technology	dan@nist.gov
Bradley Olsen	Massachusetts Institute of Technology	bdolsen@mit.edu
Raymond Osborn	Argonne National Laboratory	ROsborn@anl.gov
Dvora Perahia	Clemson University	dperahi@clemson.edu
Andrey Podlesnyak	Oak Ridge National Laboratory	podlesnyakaa@ornl.gov
Danilo Pozzo	University of Washington	dpozzo@u.washington.edu
Roger Pynn	Indiana University	rpynn@indiana.edu
Dharmaraj Raghavan	Howard University	draghavan@howard.edu
Larry Rahn	U.S. Department of Energy	larry.rahn@science.doe.gov
George Reiter	University of Houston	greiter@uh.edu
Dmitry Reznik	University of Colorado-Boulder	dmitry.reznik@colorado.edu
James Rhyne	Los Alamos National Laboratory	rhyne@lanl.gov
Filip Ronning	Los Alamos National Laboratory	fronning@lanl.gov
Stephan Rosenkranz	Argonne National Laboratory	srosenkranz@anl.gov
John Sarrao	Los Alamos National Laboratory	sarrao@lanl.gov
Sunil Sinha	University of California, San Diego	ssinha@physics.ucsd.edu
Andrei Sirenko	New Jersey Institute of Technology	sirenko@njit.edu
William Snow	Indiana University	wsnow@indiana.edu
Maddury Somayazulu	Carnegie Institution of Washington	zulu@gl.ciw.edu
Robert Stack	U.S. Department of Energy	robert.stack@science.doe.gov
Oleg Tchernyshyov	Johns Hopkins University	olegt@jhu.edu
Suzanne te Velthuis	Argonne National Laboratory	tevelthuis@anl.gov
Zlatko Tesanovic	Johns Hopkins University	zbt@pha.jhu.edu
Pappannan Thiyagarajan	U.S. Department of Energy	p.thiyagarajan@science.doe.gov
Joe Thompson	Los Alamos National Laboratory	jdt@lanl.gov
John Tranquada	Brookhaven National Laboratory	jtran@bnl.gov
Chris Tulk	Oak Ridge National Laboratory	tulkca@ornl.gov
Dhandapani Venkataraman	University of Massachusetts, Amherst	dv@chem.umass.edu
Xiaoping Wang	Oak Ridge National Laboratory	wangx@ornl.gov
Lane Wilson	U.S. Department of Energy	lane.wilson@science.doe.gov
Guangyong Xu	Brookhaven National Laboratory	gxu@bnl.gov
Shinichiro Yano	University of Virginia	sy3a@virginia.edu
Taner Yildirim	National Institute of Standards and Technology & University of Pennsylvania	taner@seas.upenn.edu
Igor Zaliznyak	Brookhaven National Laboratory	zaliznyak@bnl.gov
Jane Zhu	U.S. Department of Energy	jane.zhu@science.doe.gov